Single molecule studies of ligand-DNA interactions using atomic force microscopy

Benjamin D. Rackham

February 2014

A dissertation submitted in partial fulfilment of the requirements for the degree of Doctor of Philosophy at the School of Pharmacy, University of East Anglia.

Abstract

This thesis describes the results of experiments into the intra and inter-molecular binding of various ligands with dsDNA via the mechanism of intercalation, principally using the technique of atomic force microscopy (AFM). Since the description of the first AFM in the mid 1980's, AFM has emerged as a sensitive and versatile analytical tool, capable both of detecting and manipulating artefacts at picometer resolutions.

In these studies, AFM imaging, supported by circular dichroism, reveals unusual conformational changes in DNA that occur as a result of the binding of ligands that incorporate the acridine chromophore. These changes are distinct from those observed following the binding of other intercalators such as doxorubicin and echinomycin. Direct measurement of the length of linear DNA strands bound to acridine based ligands reveals a shortening of the DNA at very low ligand concentrations. This observation suggests that the structural changes that occur in DNA following the intercalation of the acridine chromophore are more wide ranging than previously thought and support molecular modeling studies that have proposed that the intercalated DNA duplex exhibits characteristics of both B and A form DNA. Variations in the conformational changes that occur in DNA as a result of intercalation may have implications for the application of new intercalating ligands as chemotherapeutic agents.

In addition, single molecule force spectroscopy has been used to examine the capacity of bisintercalators to bind to DNA in an inter-molecular fashion. By stretching individual strands of dsDNA, acridine dimers are shown to bind to separate strands of DNA. Inter-molecular binding of this kind remains an unexplored cytotoxic mechanism that may yet find an application *in vivo*. This observation is supported by a novel assay that utilises the controlled aggregation of gold nanoparticles. These nanoparticles, functionalised with DNA, are shown to aggregate on addition of a bisintercalator. The aggregation is fully reversible with the addition of sodium dodecylsulphate.

These force spectroscopy experiments have also uncovered a previously unobserved, inter-molecular binding mode of the peptide antibiotics echinomycin and TANDEM. In certain circumstances, these ligands are revealed to bind exclusively to the termini of separate DNA strands in a sequence dependent fashion. This finding may have implications for the employment of these ligands in the nanosciences, as a tool for joining short pieces of DNA or improving the efficiency of the enzymatic, blunt-end ligation of DNA.

Declarations

The work described in this thesis was conducted in the School of Pharmacy, University of East Anglia between July 2010 and June 2013 under the supervision of Dr. A. N. Round and Prof. M. Searcey. Parts of this work have been published or presented elsewhere and are detailed below.

Journals

M. J. Marin, B. D. Rackham, A. N. Round, L. A. Howell, D. A. Russell, M. Searcey, 'A rapid screen for molecules that form duplex to duplex crosslinks in DNA' *Chem. Commun.,* **2013**, 49, 9113 – 5 (Appendix 1)

B. D. Rackham, L. A. Howell, A. N. Round, M. Searcey, 'Non-covalent duplex to duplex crosslinking of DNA in solution revealed by single molecule force spectroscopy' *Org. Biomol. Chem.,* **2013**, 11, 8340 – 7 (Appendix 1)

Conferences

B. D. Rackham, L. A. Howell, M. Searcey, A. N. Round, 'Single molecule studies of ligand-DNA interactions using atomic force microscopy' *UK Scanning Probe Microscopy (SPM),* **2011**, (oral presentation)

B. D. Rackham, L. A. Howell, M. Searcey, A. N. Round, 'An insight into the interaction between acridine derivatives and dsDNA using atomic force microscopy and circular dichroism' *8th UK Nucleic Acids Forum,* **2012**, (poster presentation)

B. D. Rackham, L. A. Howell, A. N. Round, M. Searcey, 'Non-enzymatic, blunt-end ligation of DNA; uncovering a novel binding mode of peptide antibiotics' *American Chemical Society (ACS),* **2013**, (poster presentation)

Acknowledgements

This work would not have been possible without the support of a number of people and institutions. In no particular order, the author would like to convey his gratitude to these people and acknowledge their contribution to this work. All are, or have been, members of various Schools of the University of East Anglia, unless otherwise stated.

The author would like to express his gratitude to both of his supervisors, Dr. Andrew Round and Professor Mark Searcey, without whose expertise, support and guidance this work would not have been possible. The author would also like to express his gratitude to Dr. Lesley Howell not only for the loan of a range of acridine ligands that she had synthesized during earlier work, but also guidance and support with many aspects of this project. The author would like to thank the School of Pharmacy at the University of East Anglia for providing funding for this project, and both the School of Pharmacy and the Institute of Food Research (Norwich Research Park) for providing equipment and facilities.

For practical assistance and guidance with techniques associated with force spectroscopy, the author would like to thank Dr. Kate Bowman of the School of Pharmacy. The author would also like to thank Prof. Phil Williams of the University of Nottingham for thoughts and advice on the interpretation and presentation of force spectroscopy data.

The circular dichroism work presented in this project would not have been possible without the use of instrumentation provided by Dr. Myles Cheesman from the School of Chemistry. The author is indebted to Dr. Zoë Waller of the School of Pharmacy for practical assistance in this technique and guidance on the presentation and interpretation of data.

The author would like to express his gratitude to Prof. David Russell and Dr. Maria Marin-Altaba of the School of Chemistry for their collaboration in those experiments involving gold nanoparticles. At the same time, the author wishes to thank both Dr. Richard Bowater of the School of Biological Sciences and Dr. Anja Mueller of the School of Pharmacy for advice and practical guidance in respect of enzyme manipulation and the technique of gel electrophoresis.

Finally, the author would like to convey his gratitude to Dr. Jonathan Moffat of University College London, for advice in the application of FTIR, Mr. John Wood (formerly of the School of Pharmacy) for advice on the employment of statistical analyses and Mr. Richard Steel of the School of Pharmacy for practical assistance in preparing Figure 74.

List of abbreviations

AFM	atomic force microscopy
cAuNP	citrate-gold nanoparticles
CD	circular dichroism
CT-DNA	calf-thymus deoxyribonucleic acid
DCM	dichloromethane
DMF	dimethylformamide
DFS	dynamic force spectroscopy
DLS	dynamic light scattering
DMSO	dimethylsulfoxide
dsDNA	double stranded deoxyribonucleic acid
EFJC	extensible freely-jointed chain
EWLC	extensible worm-like chain
FJC	freely-jointed chain
FTIR	fourier transform infra-red spectroscopy
GPC	gel permeation chromatography
HJ	Holliday junction
IC-AFM	intermittent-contact atomic force microcopy
NC-AFM	non-contact atomic force microscopy
NMR	nuclear magnetic resonance
PEG	polyethylene glycol
SDS	sodium dodecyl sulphate
SE	standard error (of the mean)
SEM	scanning electron microscopy
ssDNA	single stranded deoxyribonucleic acid
STM	scanning tunneling microscopy
TAE	tris-acetate ethylenediaminetetraacetic acid
TBE	tris-borate ethylenediaminetetraacetic acid
TNM	tris-NaCl-$MgCl_2$ buffer
UV	ultra-violet
WLC	worm-like chain

Contents

Chapter 1 – Introduction

Background

Despite significant advances in the understanding of cancer as a disease state, it remains one of the leading global causes of death in the human population. Essentially, cancers constitute a malfunction of endogenous biological mechanisms, whereby cell division proceeds unchecked, leading to the growth of a tumour. In the initial stages of tumour development, a tumour may be localised, or one of several spread through an area of tissue. Unresolved, the majority of tumours will eventually metastasize, spreading to other tissues and organs within the body. The development of cancers in this fashion is classified according to the particular developmental stage, from stage I, where a tumour is localized, to stage IV, where metastasis occurs.

Early identification of the disease is essential to successful resolution. A national screening programme in the UK for breast cancer has been successful in signposting women with the early signs of tumour development for treatment.[1] In stage I cancers, surgery is usually the most effective option, with removal of cancerous tissue often sufficient to prevent relapse. During the later stages of cancer, where tumour development is sufficiently advanced to prohibit surgery, techniques are employed to either destroy the cancer or reduce it in size sufficiently for surgery to proceed.

Non-surgical options for treating cancer typically fall into one of two categories, those being either radiotherapy or chemotherapy. Significant technological advances in the controlled administration of radiotherapeutics, and sophisticated, non-invasive imaging technologies such as magnetic resonance imaging, have ensured that radiotherapy may be administered with a high degree of precision to a tumour.[2-3] Although multiple treatments are generally required before a cancer can be said to be in remission, the technique is associated with a high degree of patient compliance, since administration is controlled exclusively by a medical practitioner.

Chemotherapy remains an important treatment option, especially in those cases where neither surgery nor radiotherapy are viable options.[4-5] Many chemotherapeutic agents are employed in an adjunctive fashion, improving patient outcomes even where surgery or radiotherapy have also been employed. This is particularly true in later stage cancers, where the controlled administration of cytotoxics such as methotrexate and vincristine may slow the progression of metastasis and prolong a patient's life, if only for a short period of time.

Existing chemotherapies employ many different mechanisms of action. The *anti*-metabolite methotrexate inhibits the enzyme dihydrofolate reductase, preventing the synthesis of the

nucleoside thymidine and thereby inducing cellular apoptosis. By contrast, the monoclonal antibody, trastuzumab, binds to an extracellular portion of the HER2 receptor, a cell-regulatory protein that is overexpressed in some breast cancers.[6-7]

Compounds that bind to DNA have been of interest for a considerable period of time, primarily due to their application as chemotherapeutic agents. Two commonly used *anti*-cancer agents, amsacrine and cisplatin (Figure 1), both exert a cytotoxic effect on dividing cells by binding directly to DNA in the nucleus. Compounds that share this fundamental mechanism of action have been extensively studied,[8-11] and new agents have been subjected to clinical trials.[12] However, for a variety of reasons, few new agents of this kind have been employed in a clinical environment since the introduction of amsacrine (Figure 1) in the early 1980s.

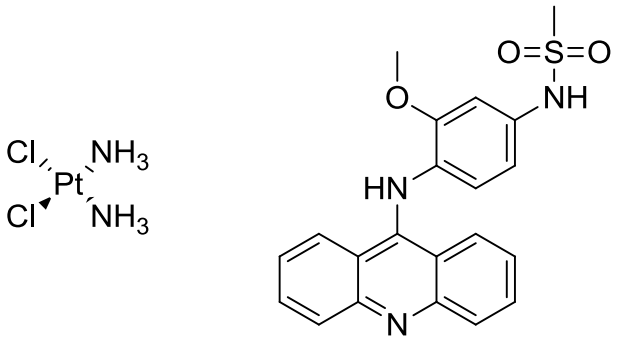

Figure 1 Structural formulae of the DNA platinating agent cisplatin (left) and the DNA intercalator amsacrine (right).

Amsacrine belongs to a class of DNA binding ligands referred to as intercalators. First described by Lerman in 1961,[13-14] these compounds bind directly to DNA. Despite having been in clinical use for several decades, amsacrine and other intercalating agents, such as doxorubicin and actinomycin, remain important adjunctive therapies, especially where other treatment options have failed.

At present, all clinically utilised intercalating agents are monointercalators. Derivatives of these compounds that incorporate multiple intercalating moieties have been shown *in vitro* to afford a greater degree of cytotoxicity. Attempts to introduce a bisintercalator into the clinic have not proved successful. The peptide antibiotic, echinomycin, did not deliver any improvement in patient outcomes *in vivo* relative to existing treatment options.[15-16]

Despite this, efforts to rationalise intercalator design have continued.[10, 17-19] In theory at least, an improved understanding of the molecular mechanics that surround the intercalation of

DNA with certain compounds may facilitate the design of new DNA-intercalators that find clinical application.

The structure of DNA

First described in the 1950s by James Watson and Frances Crick,[20] the helical structure of DNA is widely understood and accepted. Not only the structure, but the processes with which DNA is involved have also been extensively studied. Essentially a repository for genetic information, the successful transcription of DNA is essential to successful cell division. As such, DNA constitutes a viable target for disrupting the kinds of uncontrolled cell-division that are associated with tumour development.

DNA consists of a linear series of deoxyribonucleotides each coupled to another by a phosphodiester linkage. The basic repeating unit of DNA, β-2'-deoxy-D-ribofuranose, is illustrated in Figure 2.

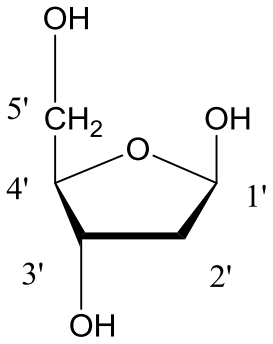

Figure 2 The chemical structure of β-2'-deoxy-D-ribofuranose. The numerals, from 1 to 5, refer to the carbon atoms at those positions.

Each preceding and subsequent ribose is connected at the 5' and 3' positions respectively. This arrangement is illustrated in Figure 3. Due to the constraints imposed by the cyclic ribose group, the bond between positions 3' and 4' of the ribose is not free to rotate in the same manner as the other components of the phosphodiester linkage. As such, the ribose group may exist in any of four different conformations, a phenomenon known as sugar pucker (Figure 4). Structural variations of this kind have important implications for the overall conformation of the DNA molecule.

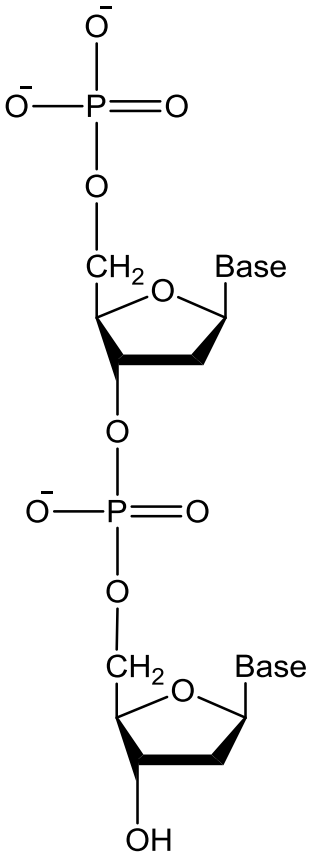

Figure 3 An illustration of the coupling of the structure of the DNA phosphate backbone. Adjoining ribose groups are coupled via a phosphodiester linkage at the 5' and 3' positions of the sugar. DNA sequences of this kind can contain many thousands of bases in such a linear sequence.

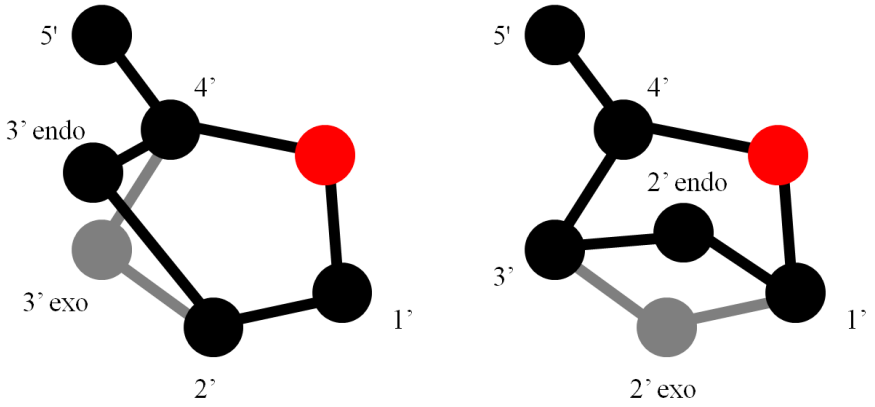

Figure 4 A Schematic illustration of the different conformations of the ribose ring that are observed in DNA. The red circle denotes the oxygen atom. Both the 2' and the 3' position may be in the same plane as the 5' position (endo) or in the opposite plane (exo).[21]

Original work on the structure of DNA utilised X-ray crystallography to define the spatial arrangement of the nucleobases and the phosphate/deoxyribose backbone of the molecule.[22] The primary structure of DNA consists of four distinct nucleobases, the purines adenine and guanine, and the pyrimidines, cytosine and thymine.

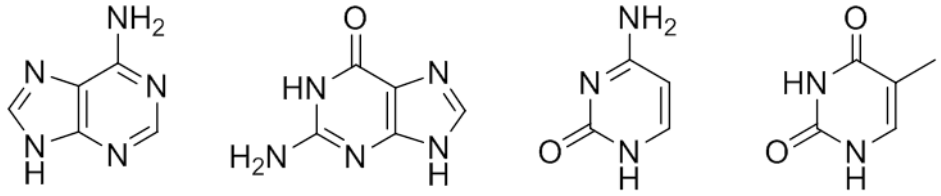

Figure 5 Chemical formulae of the four common nucleobases present in DNA, from left to right, adenine, guanine, cytosine and thymine.

In the classic Watson-Crick arrangement (referred to as the B form), these bases form pairs within the duplex, adenine to thymine and guanine to cytosine. Each base pair within the DNA primary sequence forms a step, separated from the next pair of nucleobases by a distance of 3.4 Å (0.34 nm).

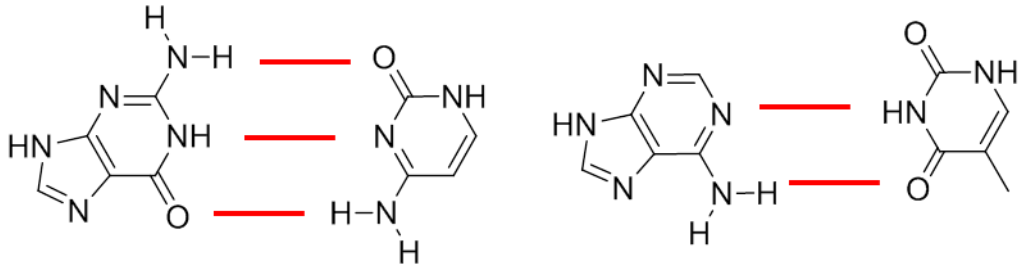

Figure 6 An illustration of the Hydrogen bonding arrangements of the two DNA base pairs, guanine and cytosine (left) and adenine and thymine (right).

Table 1 The common physical characteristics of the three most commonly known DNA conformations.[21]

Parameter	A Form	B Form	Z Form
Helical sense	Right	Right	Left
Diameter / nm	2.6	2.0	1.8
Base pairs / turn	11	10.5	12
Helical rise / nm	0.24	0.34	0.37
Sugar pucker	C3'-endo	C2'-endo	C2'-endo / C2'-exo
Tilt v. helix axis / °	20	6	7

Continued research into DNA structure revealed the existence of another form of DNA, that of the A form, often associated with DNA outside of an aqueous environment.[23] Although in this arrangement the pairing of the nucleobases is maintained, the distance between each base pair (helical rise) is reduced to only 2.4 Å. Another form of DNA that has been identified is that of the Z form.[24] While A and B form DNA maintain a right handed spiral, in Z-DNA the duplex is orientated in the other direction, a left hand spiral, while the bases are

separated by a rise of. 3.7 Å. These three forms of DNA, A, B and Z, are frequently referred to in the literature (Table 1 and Figure 7).

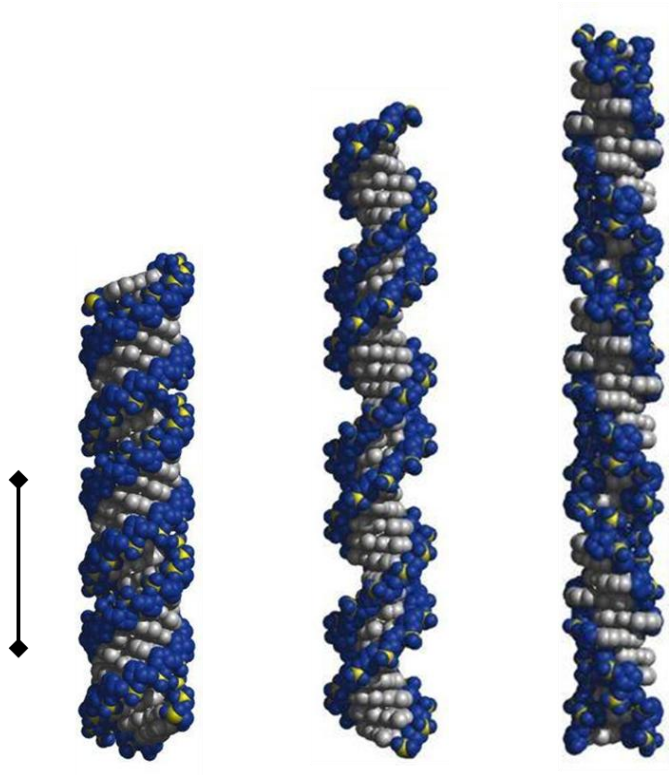

Figure 7 Graphical illustrations of the three common forms of DNA; from left to right, A, B, and Z forms.[21] The phosphate backbones of each of the two strands of DNA in the duplex are highlighted in blue. The scale bar represents one helical turn of A form DNA, approximately 2.6 nm. The models highlight two important features of the DNA helix, the major and minor grooves, coloured in grey. The major groove is shown to be wider in the B form model than the more compact A form.

However, numerous conformational isomers of the basic DNA duplex are now known to exist and the classical description of DNA constitutes something of an over-simplification. [25] Subtypes of the B conformation, referred to as B-I and B-II have been isolated, along with an alternative conformation, that of the C form that is structurally very similar to that of the B-II subtype. These isomers vary not only in the direction of the helix spiral, or sugar pucker, but also in the spatial positioning of the base pairs relative to one another. Subtle variations in the degree of tilting, or twist, between each base pair relative to the perpendicular helix axis can induce significant changes in the physical characteristics of the DNA helix as a whole.

Arguably, the picture that has emerged is that, far from adopting a particular, rigid, conformation, the DNA duplex demonstrates a high degree of conformational versatility, switching between conformations according to its environment. Such transitions need not affect the entire length of the DNA duplex, and may be localized while other regions remain

in a different conformation altogether. Importantly, it has been suggested that both A and Z form DNA are associated with the regulation of gene expression and DNA transcription, disruption of which may offer a means of controlling cell division.[21]

Intercalation of DNA

Originally defined by Lerman in 1961[13], intercalation involves the insertion of a planar, aromatic moiety into the space between the base pairs in the DNA duplex. Typically, the intercalating ligand approaches the DNA from the minor groove, forming several short-range interactions that widen the inter-base pair spacing sufficiently for intercalation to occur. Base stacking of this kind is a non-covalent interaction, distinct from the binding mechanism of other small DNA binding ligands such as nitrogen mustards and cisplatin where the process of attachment is irreversible. An illustration of this mechanism is provided in Figure 8.

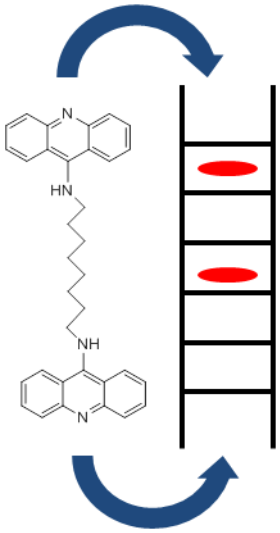

Figure 8 Graphical illustration of the binding of a bisacridine to a strand of DNA. The red sections denote the location of the ligand's chromophores between the DNA base pairs after binding.

The clinically employed DNA intercalators exert their cytotoxic effects in two different ways. The anthracycline doxorubicin and the acridine derivative amsacrine (Figure 1) incorporate additional chemical functionalities. Once the molecule is anchored in the DNA, these additional groups bind to the enzyme topoisomerase II during intra-cellular processing of the DNA, trapping the enzyme/DNA complex.[26] This enzyme relaxes DNA prior to transcription by inducing double strand breaks in the DNA duplex. Trapped in the intercalator/DNA/enzyme complex, usual re-attachment of the separated DNA strands by topoisomerase II is not possible, leading to cellular apoptosis.

Another clinically employed intercalator, actinomycin-D, employs a different mechanism of action to the anthracyclines. In this case, the ligand interferes with the activity of the enzyme RNA-polymerase, preventing the elongation of the RNA chain along the DNA template and thereby causing cell death.

Studies of the intercalation of a variety of ligands have suggested that the process of intercalation may distort the duplex to a greater degree than was originally supposed.[27] Separation of the base pairs in the duplex by an intercalator causes an unwinding of the DNA helix and a lengthening of the DNA strand.[14] This has been observed using a number of techniques, notably flow viscometry with intercalated DNA rods.[14, 28] Substantial amounts of data, such as the helix unwinding angle, have been published for an array of intercalating agents, including ethidium bromide, proflavin and YOYO-1.[9] Despite some similarities, these studies reveal that the precise nature of any structural changes in the DNA is unique to any given ligand.

Separation of the base pairs in the DNA sequence may also be accompanied by a reorientation of the base pairs relative to one another. In both A and B form DNA, the base pairs are arranged, relative to the phosphate backbone, according to the *anti*-configuration (Figure 9).

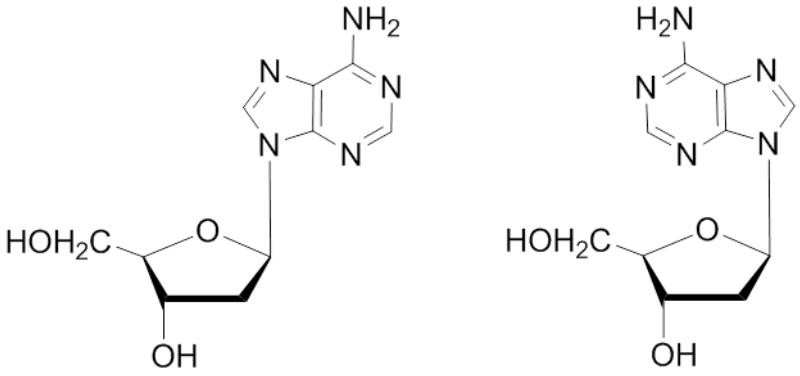

Figure 9 An illustration of the *anti*-configuration of the nucleobase adenine, left, and the alternative *syn*-configuration, right.

Rotation of the base about the glycosidic bond between itself and the ribose sugar causes a conformational change referred to as the *syn*-configuration, illustrated in Figure 9. The latter is characteristic of Z form DNA, but does not usually appear in A or B forms of DNA. However, some studies of intercalation have suggested that a distortion of this kind is induced by ligand binding, leading to a non Watson-Crick arrangement of the base pairs referred to as Hoogsteen base pairing (Figure 10).[29-31] The biological significance of this

change (if any) is not yet understood, but it has been suggested that this arrangement may occur during the binding of some intracellular enzymes to DNA.

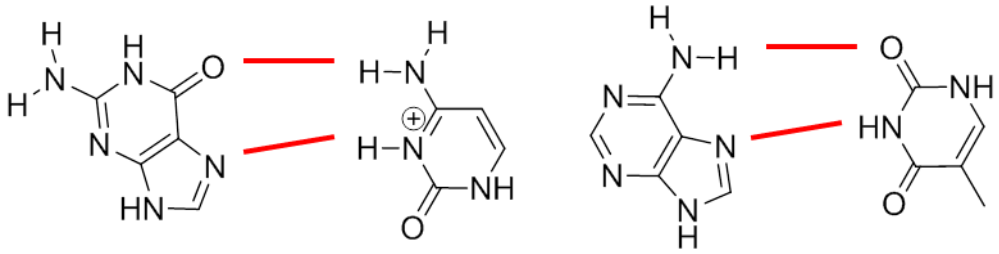

Figure 10 Illustrations of the alternative Hoogsteen arrangement of CG (left) and AT (right) base pairs that are observed in DNA. The red lines denote the hydrogen bonds between each base. The Hoogsteen arrangement requires the protonation of the cytosine base (left).

The existence of another class of intercalating agents, the bisintercalators, has already been discussed. In essence, a bisintercalator consists of two monointercalators that have been linked together. The synthesis of even larger compounds (even an *octakis* intercalator) has also been reported, but none of these compounds have been suggested for clinical use.[32] In the simple example of two acridine chromophores joined by a methylene chain, early studies revealed a transition from mono to bisintercalation when the length of the alkyl chain exceeded six methylene groups.[9] On average, both the helix unwinding angles of these bisintercalators and their helix extension parameters are roughly double those of the parent monomers.[9]

Bisintercalators are known to demonstrate greater cytotoxicity than monointercalators, even where the binding chromophores are structurally identical. However, the reasons behind this greater degree of cytotoxicity are complex. To an extent, the binding of each chromophore within the bisintercalator is synergistic, with binding of the first chromophore facilitating that of the second. However, equilibrium dialysis studies of the binding of bisacridines to CT-DNA revealed only a 10 to 15-fold increase in the binding affinities of bisacridines relative to 9-aminoacridine, as opposed to an expected increase of 10^4.[9] This discrepancy was attributed to unfavourable enthalpies and entropies associated with solvent rearrangements and distortions to the DNA duplex that occur with intercalation of an acridine.[9]

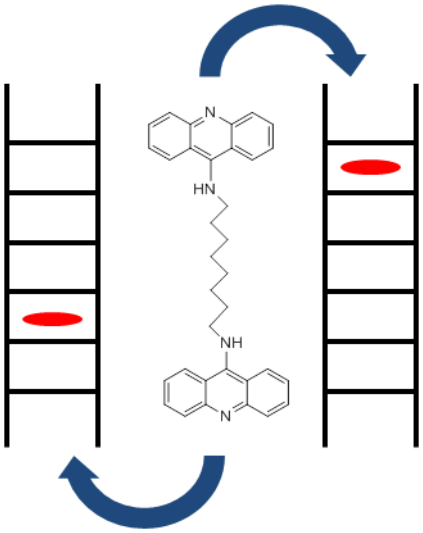

Figure 11 Graphical illustration of a bisacridine binding to two separate DNA strands (Type II intercalation). The red sections in the DNA strands demonstrate the position of the ligand chromophores.

As well as binding to the same strand of DNA, in the manner of a monointercalator, bisintercalators, notably luzopeptin[33] and some acridine analogues[34-35], have been observed to bind to separate DNA strands in an inter-molecular fashion (Figure 11). Though not commonly utilised, a nomenclature for these different modes of intercalation has been previously suggested, with Type I intercalation referring to intra-molecular binding, and Type II intercalation referring to inter-molecular binding.[33]

9-aminoacridine, doxorubicin and ethidium bromide

The chemical structures of the three monointercalators that were utilised during the course of these studies are provided below (Figure 12). For reference, the chemical structures of all ligands used during these studies are provided in Appendix 2 (*insert*).

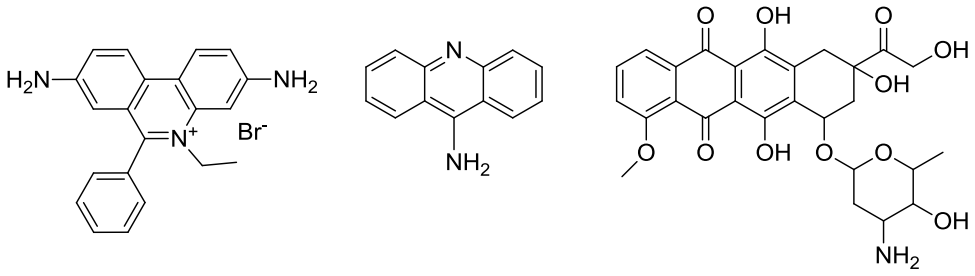

Figure 12 Chemical structures of the three monointercalators from left to right, ethidium bromide, 9-aminoacridine and doxorubicin.

Doxorubicin is commonly used in the treatment of many cancers, including acute leukaemias, Hodgkin's lymphoma and some breast cancers. The compound is administered

via infusion. Side effects are common with doxorubicin, and range from diarrhoea to permanent kidney damage. Higher doses are associated with an increased risk of heart failure, limiting the courses of treatment that may be administered and reducing the potential range of patients by excluding those with pre-existing cardiac disorders.[36] Like amsacrine, doxorubicin does not exert its cytotoxic effects via intercalation but by interaction with the enzyme topoisomerase II. The aglycone portion of the ligand stacks between nucleotides in the primary DNA sequence, the daunosamine residue remaining in the minor groove of the DNA. Doxorubicin is commonly believed to have a slight preference for intercalating into 5'-CpG steps,[37] although it has been suggested that the ligand exhibits a greater affinity for AT rich regions, specifically ApA.[38] Doxorubicin utilised in these studies was purchased from Sigma (UK). Solutions of this ligand (aqueous solubility 50 mg/ml) were prepared as required and stored at -20°C until use.

9-aminoacridine is an important precursor to many acridine based compounds that incorporate the acridine chromophore. The compound itself is a known cytotoxic and mutagen, and the potential utilization of this compound as a chemotherapeutic was suggested as early as 1948,[39] before its mode of action had been characterised. Despite the simplicity and small size of this ligand, sequence specificity has been suggested, the ligand appearing to bind more tightly to regions of high GC content, especially the GpC step.[40] Although 9-aminoacridine itself is not clinically utilised, the monointercalator amsacrine that incorporates the acridine chromophore is successfully used *in vivo*. 9-aminoacridine used in these studies was purchased from Sigma (UK). The compound is water soluble, and stocks were prepared as required and stored at -20°C until use.

Another DNA monointercalator, ethidium bromide is used as a dye, fluorescing when bound to DNA. This compound is commonly used as a DNA marker, especially in gel electrophoresis, and, like 9-aminoacridine, is a known mutagen. The compound was synthesized specifically to function as an *anti*-trypanosomal agent,[41] but has never been employed in humans due to concerns about carcinogenicity. As may be discerned from Figure 12, the arrangement of the intercalating moiety within ethidium bromide is slightly different from the linear arrangement of the aromatic groups within doxorubicin and 9-aminoacridine, the central aromatic ring being offset from the flanking pairs. Like doxorubicin and 9-aminoacridine, ethidium bromide is believed to exhibit a preference for GC rich regions of DNA.[42] Ethidium bromide was purchased from Fisher Scientific (UK), and used as received.

Echinomycin and TANDEM

Echinomycin (Figure 13) was, and so far remains, the only bisintercalator to enter phase II clinical trials.[12] To date there is no published synthesis of this compound. The sequence specificities, and precise mechanism of action of this compound, have been studied extensively in the literature. The ligand is known to bind preferentially to regions of high GC content, although binding has been observed to occur in areas of AT sequences.[43] DNAse footprinting and NMR have identified that echinomycin binds with the greatest degree of affinity to 5'-CpG steps within the DNA duplex,[44-45] hydrogen bonding between the 2-amino group of guanine and the peptide component of the bisintercalator essential to the stabilisation of the complex.[46] Precisely, the quinoxaline rings of the ligand flank the 2 nucleotide base pairs, whilst the peptide ring remains in the minor grove of the DNA. Three hydrogen bonds are formed between the alanine groups of the peptide ring and the bases of the minor groove at CpG steps; the N3's of both of the guanines at the binding site and the 2-amino group of one of the guanines.[46]

Echinomycin was purchased from Sigma (UK), and stock solutions in DMSO were prepared and stored at -20°C until use. The aqueous solubility of echinomycin is poor (approximately 5 μM), and solutions were prepared freshly in aqueous media when required.

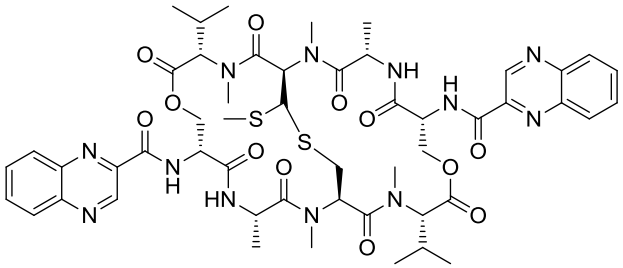

Figure 13 The structure of the peptide antibiotic echinomycin.

TANDEM (Figure 14), a synthetic analogue of Triostin-A, has also been extensively studied *in vitro*.[47] Triostin-A is a bisintercalator with similar binding behaviour to echinomycin, favouring GC rich regions of DNA. By contrast, TANDEM favours AT rich regions of DNA, attributed to the removal of the methyl groups from the inter-chromophore linker and the disulfide bridge.[48] These structural modifications disrupt the usual binding of the ligand to GC areas within the minor groove of the DNA strand. This is due to the formation of intra-molecular hydrogen bonds between the alanine residues of the peptide ring, prohibiting the formation of the necessary hydrogen bonds with the 2-amino group of guanine, the interaction that affords the specificity of echinomycin for CpG steps. By contrast, TANDEM has been shown to bind with high affinity to 5'-TpA steps.[49] However, binding of the

compound is strongly dependent not only on the base pairs sandwiched by the quinoxaline chromophores, but also the composition of the flanking base pairs, since binding does not always occur even at the preferred 5'-TpA steps.[48]

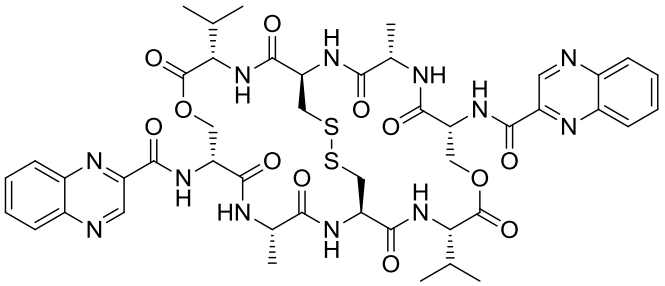

Figure 14 The chemical structure of the triostin-A analogue, TANDEM.

The complete solid-phase synthesis of TANDEM was published in 2005.[47] A supply of this compound was provided by Prof. M. Searcey (University of East Anglia). Stock solutions were prepared in DMSO, and diluted in aqueous media as required.

Bisacridines with flexible linkers

A simple acridine dimer (Figure 15), comprised of an alkyl linker between two acridine chromophores, was synthesized as part of this project. The other three bisacridines used in these studies were provided by Dr. L. A. Howell (University of East Anglia).[50] All were stored at -20°C in aqueous media until used.

Many similar linked acridines have been synthesized and biologically evaluated as *anti*-tumour agents. [51] Although the individual specificity of bisacridine 1 for DNA sequences has not been determined, it has been suggested that bisacridines have a slight preference for GC regions of DNA.[52-53] However, the reasons for this slight selectivity are not immediately clear, and importantly 9-aminoacridine is not known to exhibit any such preference. Incorporation of basic nitrogen atoms into the linker of bisacridines has been shown to either enhance or eliminate the alternative preference for ApT steps in DNA, suggesting that slight variations in sequence selectivity between different bisacridines are dictated by the chemistry of the linker and not the intercalating chromophore.

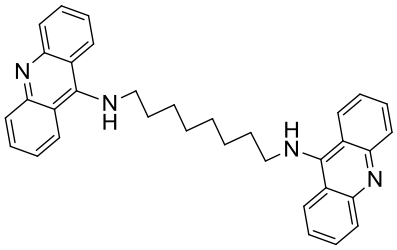

Figure 15 The chemical structure of the bisacridine, bis(acridine) N-(6-(acridin-9-ylamino)hexyl)acridine-9-amine (bisacridine 1)

Though structurally very similar, bisacridine 2 (Figure 16) incorporates additional functionalities that enhance the affinity of this compound for DNA.[54] While the inter-chromophore linker resides in the minor groove of the DNA, the carboxamide side-chains form hydrogen bond contacts with the O6 and N7 atoms of guanine in the major-groove, reducing dissociation of the ligand from the DNA and thereby enhancing its cytotoxic potential.

This variation on classical intercalation is referred to as 'threading', since it necessitates the insertion of the carboxamide substituent through the DNA duplex from the minor groove, between the base pairs and into the major groove. This mode of action is very sensitive to the precise arrangement of the carboxamide substituent on the chromophore, and may be prevented at a pH greater than 9. Under physiological conditions at pH 7, the nitrogen of the central aromatic group of the acridine chromophore is protonated, forming a hydrogen bond with the carbonyl of the carboxamide that maintains a planar arrangement between the acridine and the 4' substituent.

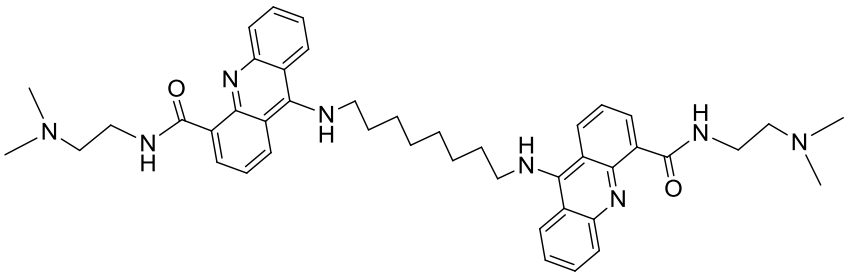

Figure 16 The chemical structure of a derivative of bis(acridine) N-(6-(acridin-9-ylamino)hexyl)acridine-9-amine, incorporating two carboxamide substituents at the 4' position of each acridine chromophore (bisacridine 2)

Both of these compounds bind to DNA via bisintercalation in a manner similar to echinomycin and TANDEM. The length of the flexible alkyl chain between the chromophores of 11.3 Å is sufficient to accommodate the required two base pairs, forming a sandwich between the acridine chromophores.[19]

Bisacridines with rigid linkers

By varying the structure of the inter-chromophore linker, some degree of control over the binding activity of a bisacridine may be afforded. While the flexible, alkyl linked bisacridines are ideal Type I bisintercalators, compounds comprising a rigid inter-chromophore linker are less able to bind to DNA in an intra-molecular fashion. Rigidly linked bisacridines, such as those illustrated in Figure 17 and Figure 18, have been evaluated for their capacity to adopt the Type II, inter-molecular mechanism of intercalation.[35] It has been suggested that cross-linking strands of DNA in this fashion offers another means of inducing cellular apoptosis.[34, 55]

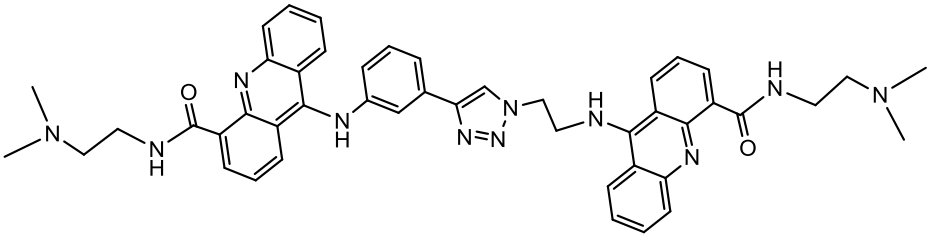

Figure 17 The chemical structure of N-(2-(dimethylamino)ethyl)-9-(3-(1-(2-(4-(2-(dimethylamino)ethylcarbamoyl)acridin-9-ylamino)ethyl)-1H-1,2,3-triazol-4-yl)phenylamino)acridine-4-carboxamide, a bisacridine incorporating a rigid linker (bisacridine 3)

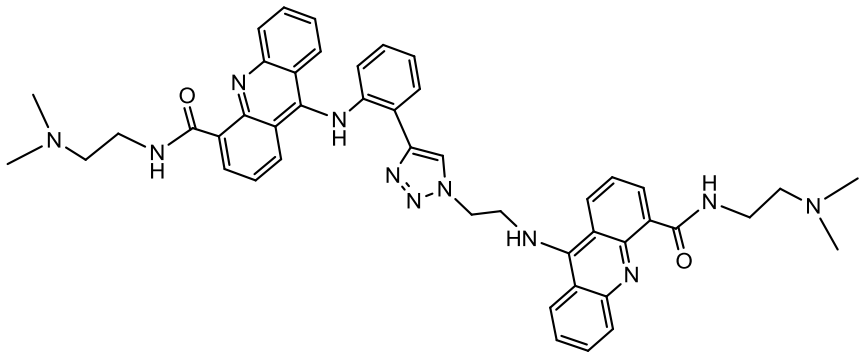

Figure 18 The chemical structure of N-(2-(dimethylamino)ethyl)-9-(2-(4-(3-(4-(2-(dimethylamino)ethylcarbamoyl)acridin-9-ylamino)ethyl)-1H-1,2,3-triazol-4-yl)phenylamino)acridine-4-carboxamide (bisacridine 4)

Chapter 2 – The method and application of atomic force microscopy

The method and application of atomic force microscopy

These studies make extensive use of two experimental techniques: intermittent contact mode atomic force microscopy; and single molecule force spectroscopy. Both of these techniques may be conducted using the same apparatus, commonly referred to as an atomic force microscope.

Techniques for obtaining information at near atomic resolution have been in existence for some time. The first studies using electron microscopy were reported during the 1930's, and demonstrated resolutions as high as 10 nm.[56] The technology of electron microscopy has developed considerably in this time, giving way to systems that permit not only the observation of artefacts at picometer resolutions, but even their manipulation. Using the concept of quantum tunneling, the scanning tunneling microscope was the first such instrument to permit analysis of this kind.[57] However, experimentation using this apparatus is restricted to conductive substrates.

Effectively a combination of the principles of the scanning tunneling microscope and the stylus profilometer, atomic force microscopy permits the analysis and manipulation of non-conductive substrates at very high resolutions (Figure 19). Early studies indicated that such apparatus was capable of demonstrating a lateral resolution of 3 nm and a vertical resolution of 0.1 nm.[58] Instrumental sensitivity of this kind permits the analysis of individual molecules at an atomic level comparable to that established by STM, and even the testing of individual chemical bonds.[59]

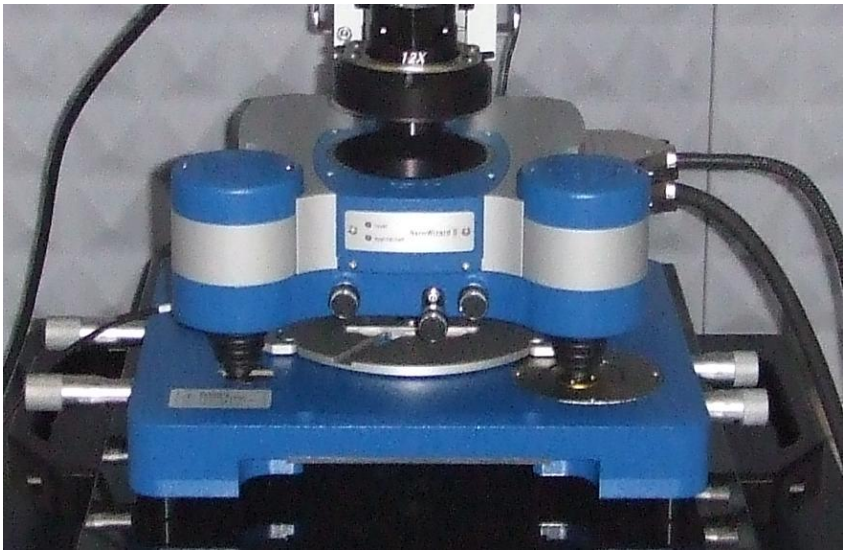

Figure 19 A Photograph of a JPK NanoWizard II™ atomic force microscope. Visible, from top to bottom, are the optical microscope, AFM scanning head, and the sample stage.

The concept of imaging a surface using the principles of AFM is relatively straightforward. A probe (Figure 20), typically made of silicon, is placed in contact with the surface to be analysed. As the probe is moved across the surface of the substrate, changes in the forces required to maintain a consistent contact between the probe and the substrate are monitored by the AFM instrumentation. These changes in force are translated into a digital computer image, representative of the topography of the region over which the AFM probe has passed.

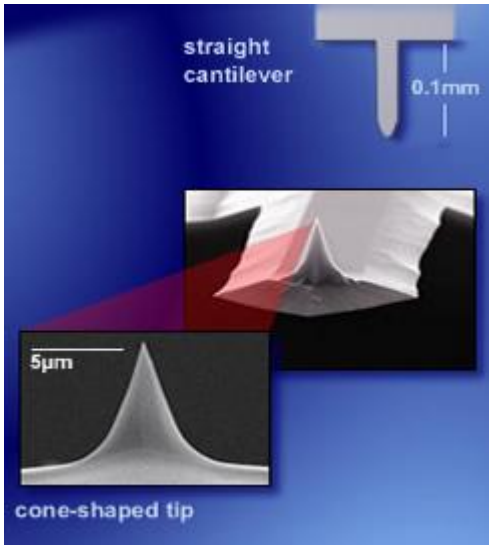

Figure 20 A SEM picture of a typical silicon AFM cantilever of the kind used in imaging experiments.[60] The schematic, top right, shows the length of the cantilever to which the probe is attached. The AFM probe is mounted within the scanning head of the apparatus.

Although an AFM image reflects the physical topography of the sample beneath the AFM cantilever, the AFM instrumentation itself actually measures changes in the electrical signal within a closed feedback loop. The position of the cantilever is controlled electrically via three piezo crystals, one each for the *x*, *y* and *z* axes. Piezoelectric material deforms in a reproducible manner proportional to the strength of an applied electric current. This permits the physical degree of movement of the cantilever to be controlled by varying the applied electrical force. Movement of the cantilever in the *x* and *y* axes can be carefully controlled in this way.

Unlike scanning electron, or even optical microscopy, where pictures of whole regions may be obtained immediately, AFM images are assembled from a series of lines across the *x* axis of the scanning region, the probe moving sequentially through the *y* axis until the entire region has been analysed. AFM imaging can therefore be slow, with a typical scan of a 5 x 5 micron region at a rate of 2 Hz typically taking several minutes. Technological developments are permitting faster scan rates, but this is often dependent on the nature of the sample that is being imaged.[61]

Image contrast, changes in surface topography, is provided by the movement of the AFM cantilever in the *z* axis. The precise deflection of the cantilever is determined by following the movement of a laser that is deflected from the back of the AFM cantilever onto a photodiode (Figure 21). The position of the reflected laser beam on the photodiode is transduced into an electrical signal. By measuring the changes in voltage required to maintain a constant degree of deflection in the cantilever (a concept referred to as the 'set-point') a representation of the surface topography may be determined.

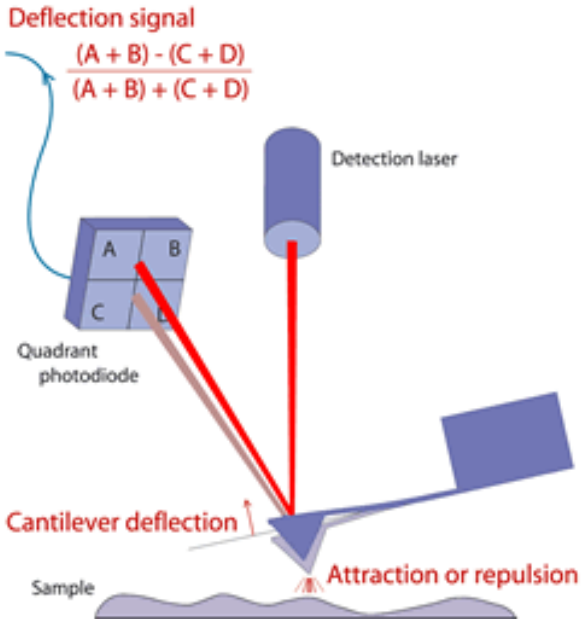

Figure 21 An illustration of the movement of the AFM cantilever in the *z* axis and how this is translated into the movement of the reflected laser beam on the photodiode.[60] The deflection signal is determined by measuring the differences in the electrical signal produced by each quadrant of the photodiode relative to one another.

One of the particular advantages with respect to AFM imaging is that, provided a sample is flat, any material may be analysed (Figure 22). Cantilevers are available in a number of different shapes and cover a range of different mechanical stiffness. While hard, well defined material such as silicon can be imaged at very high resolutions using a stiffer cantilever, images of softer material are best obtained using a more flexible cantilever that will follow the surface topography more closely. This is particularly useful for the analysis of biological material. AFM images of individual strands of DNA were first published in the early 1990's.[62]

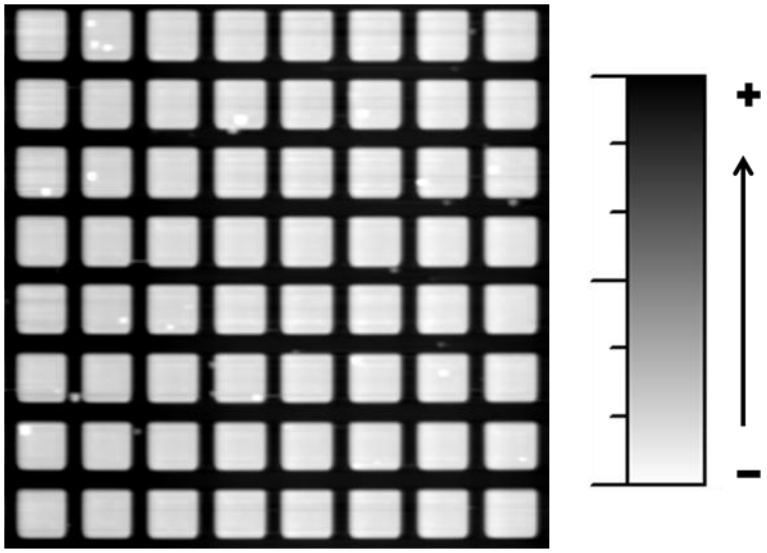

Figure 22 A typical AFM image, taken in contact mode, of a test grid (Bruker APCS-0099). The image is 72 x 72 µm in the *x* and *y* axes and the pitch of each repeating unit in the image is 9 µm. The scale bar to the right of the image denotes the *z* axis, indicating that the darker areas of the scan represent the higher regions.

Hitherto, the discussion has described a form of AFM imaging referred to as 'contact mode', where the AFM probe is held in continuous contact with the substrate (Figure 23). This form of imaging is ideal for hard samples, and has been used to analyse the surface of electrical components and solid-dose pharmaceutical products such as tablets.[63-64] However, initial efforts to obtain images of biological materials via AFM were hampered, despite the availability of softer cantilevers, by the delicacy of these substrates.[65] Given the constant force between the AFM probe and the cantilever, questions remained as to whether or not the AFM probe was distorting the substrate, yielding a defective image.[62]

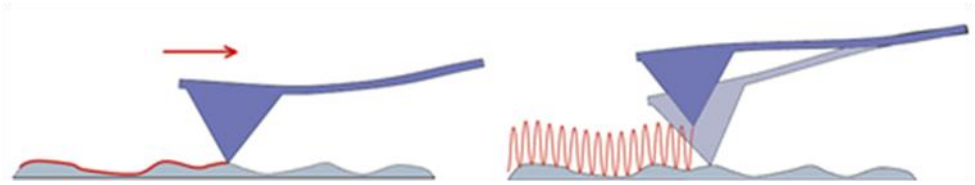

Figure 23 An illustration of two different types of AFM imaging, contact mode (left) and intermittent-contact (IC) mode (right).[60] In contact mode the cantilever remains on the surface of the sample, whereas in IC mode the cantilever oscillates above the sample.

The solution to this problem is to reduce the force applied by the cantilever to the substrate, and even minimize physical contact between the surface and the probe. In 'tapping mode' (or intermittent contact mode), an oscillating AFM cantilever is held above the surface of the substrate.[66] Changes in the amplitude of the oscillation of the cantilever are monitored as the cantilever moves across the surface of a sample, yielding a representation of the sample in the same manner as 'contact mode'. Not only, given the reduced contact between the AFM probe and the sample', is such an approach non-destructive, but other problems associated

with contact mode imaging, such as 'drag' (where the probe adheres to the substrate), are eliminated.[67]

Recent studies have highlighted the capacity of what is essentially a physical analytical technique to deliver remarkable insights into molecular interactions at an atomic scale. The publication of an AFM image of a series of benzene rings has been followed by work that provides images of the various stages of a chemical reaction at a molecular level.[68-69]

Studies that utilize AFM imaging are not limited, however, simply to obtaining pictures of a given sample. Quantitative information may also be obtained. With the assistance of appropriate computer software, the physical dimensions of features that appear within an image may be measured in a number of different ways. For example, by knowing the physical dimensions of a particular AFM image, it is possible to determine the area of that region that is occupied by an object of interest (Figure 24). By analyzing the relative fractions of protein monomers and dimers that were apparent in a series of AFM images, Ratcliff et al. were able to determine a dissociation constant for the DNA helicase UvrD.[70]

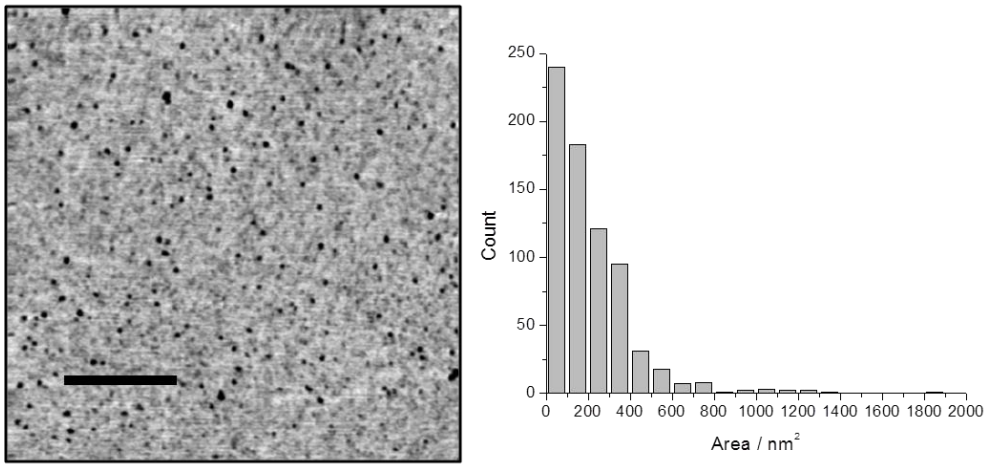

Figure 24 AFM image, taken in intermittent contact mode, of 33 base pair fragments of DNA that have been deposited on mica. The scale bar denotes 500 nm. The histogram provides the size distribution of the dark features, in nm^2, collected from a series of similar images. Each individual piece of DNA would have a theoretical area of approximately 22 nm^2. The area of the total AFM scan of 2 x 2 μm is 4 million nm^2.

The activity of a helicase enzyme, and of DNA intercalators, has also been investigated by observing the capacity of these agents to unwind supercoiled plasmid DNA. Agarose gel electrophoresis has been used for some time to demonstrate the unwinding of a plasmid, and can reveal information about the helix unwinding parameters of a ligand.[19] The same information may be taken from AFM images that also provide a direct visualization of the process itself, as the DNA progresses from a compact to a relaxed state.[71-72]

Not only may changes in the tertiary structure of DNA be observed, but also the physical dimensions of the secondary structure may be measured. By measuring linear sections of DNA (Figure 25), Coury et al. suggested that a diamidine, 2,5-bis(4-amidinophenyl) furan (APF), did not bind to DNA via an intercalative mechanism since no increase in the length of the DNA strands, a classical indication of intercalation, could be identified.[73] More recently, the activity of luzopeptin and echinomycin have also been studied in the same manner.[74] Using measurements of DNA contour lengths, Tseng et al. examined the sequence specificities of the DNA bisintercalator echinomycin.[75] This study confirmed the preference of this ligand for CpG steps in DNA by measuring the changes in the length of DNA strands relative to the adenine/thymine and guanine/cytosine composition of the DNA.[12, 46] Similar experiments with the bisintercalator luzopeptin also confirmed that AFM was capable of distinguishing between DNA before and after binding of a known intercalator.[74] The study with luzopeptin also revealed the formation of complex DNA morphologies at higher concentrations of the ligand. The authors attributed these structures to inter-molecular binding of the bisintercalator between adjacent DNA strands (Type II intercalation).[33]

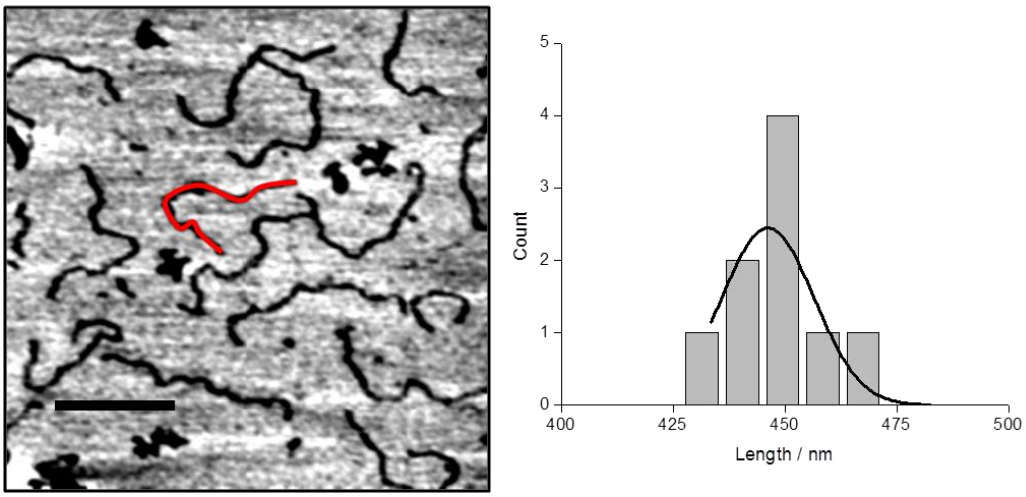

Figure 25 AFM image, taken in intermittent contact mode, of 1341 base pair, linear fragments of DNA deposited on mica. The scale bar denotes 500 nm. The histogram demonstrates the lengths of 9 fragments within the image that have been measured, yielding an experimental contour length of 447.9 nm (SE 0.95 nm). The theoretical length of these fragments, assuming 0.34 nm per base pair, is 455.9 nm.

Data derived from AFM images of a material are not restricted to the physical dimensions of features within the *x* and *y* axes of the scan region. The AFM cantilever may also be used to provide information about the nature of the material that is being examined. By pressing the AFM cantilever into an article of interest within a scan region, it is possible to determine the mechanical stiffness of the artefact as a function of the degree to which it resists the applied force.[76] Since an AFM cantilever is effectively a spring, there is a relationship between the

force (*F*) applied to it and the degree to which the spring will extend (*x)*. According to Hooke's law, where k is the spring constant of the cantilever:

$$F = k * x$$

This technique has been applied to cancerous cell lines, providing information about the structure of cells in a diseased state relative to healthy tissue.[77] Such information provides not only a means of distinguishing between cancerous and healthy cell lines, but also informs research into how changes in the regulation of processes within a cell may affect cellular structure at a global level. Colonies of bacteria have also been studied in this fashion, providing information that may be of use in the development of new antibiotics.[78-79]

Technological developments are now permitting data collected in this fashion to be incorporated into the imaging mode of the AFM, a technique referred to as quantitative imaging.[80] By controlling the movement of the AFM in the *x* and *y* axes, multiple depressions of the cantilever, conducted in series, can be assembled into an image. This technique provides a more comprehensive view of the mechanical properties of an entire region of a sample, as opposed to the area immediately beneath the AFM probe alone. A recent study has utilised this particular form of AFM imaging to study living cells in aqueous conditions resembling the cells' natural environment.[81]

Modification of the AFM probe permits different kinds of information to be analysed, not only the physical topography of a sample. Essentially a refinement of scanning tunnelling microscopy, the use of conductive AFM probes can be used to explore the electrical characteristics of a material. Using a gold coated cantilever, differences in the electrical conductivity of ferritin proteins have been explored, revealing holoferritin, where the protein is bound to high levels of iron, to be 5 to 10 times more conductive than apoferritin, the protein in its unbound state.[82]

Cantilevers may also be modified to conduct thermal energy. By measuring the energy required to maintain a constant temperature within the cantilever, the thermal conductivity of a material may be ascertained, although this technique requires careful maintenance of the environment surrounding the cantilever.[83] By applying an increasing temperature to the AFM probe, the melting temperature of a material may also be defined.[84] This technique is particularly useful for studying distinct regions within supposedly homogenous materials, and has been used to identify different crystalline states of pharmaceutical reagents.[85] This would not be possible, even with sensitive thermal analysis techniques such as modulated

differential scanning calorimetry, since information applies to all the material within a bulk sample.

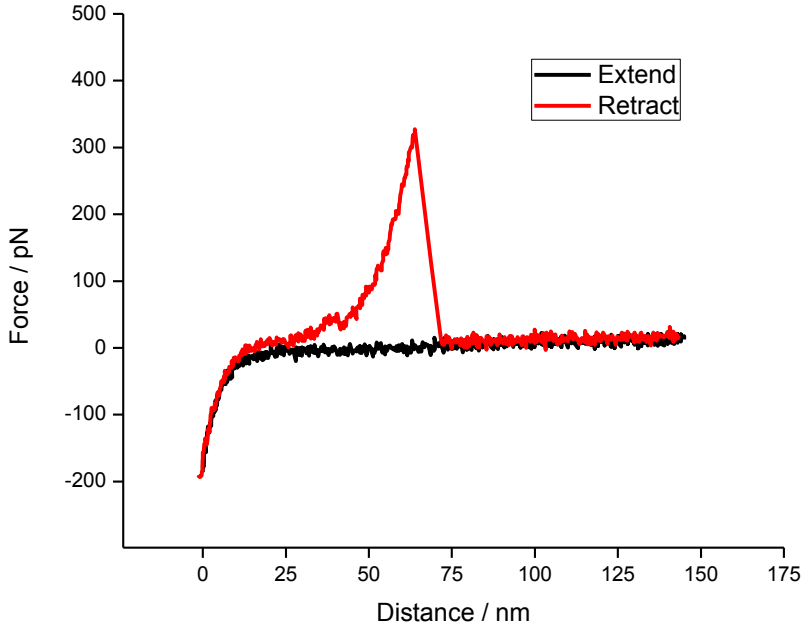

Figure 26 Typical force extension curve from a force spectroscopy experiment, representing the distance of the cantilever from the substrate (*x* axis) against any applied force (*y* axis). The extend portion (black line) represents the initial approach of the cantilever towards the substrate. The negative deflection in this line between 0 and 25 nm illustrates the force exerted on the cantilever as it strikes the opposing surface of the substrate. The retract portion (red line) represents the withdrawal of the cantilever from the substrate. The deflection between 25 and 75 nm is attributable to the stretching of an artefact that has adhered itself to the cantilever. This resistance is overcome at a force of *c*. 300 pN, whereupon the cantilever returns to its normal retract cycle. The gradient of the retract curve at the point of rupture is proportional to the rate at which the rupture force was applied (critical loading rate).

The deflection of the cantilever in the *z* axis can provide a great deal of information about the forces applied to the cantilever (Figure 26). Knowing the mechanical properties of the cantilever, it becomes possible to examine the kinetic properties of the interaction to which a force is applied by the cantilever.[86] Conceptually, understanding the relationships between bond strength and loading rates is not straightforward. In simple terms, the lifetime of a chemical bond is reduced when a force is applied directly to it, in this case the pulling force of the AFM cantilever. Higher forces reduce the thermal activation energy required to break the bond, accelerating the rate of bond dissociation. Over a range of loading rates, a relationship may be discerned between the force required to break the bond that is being stretched, and the rate at which that force was applied. This concept has been described in detail by various authors, but is commonly referred to as the Bell-Evans model.[87-88] Typical force spectra are divided into two primary regimes, at low rates an equilibrium regime

characterised by a finite force and at higher rates a kinetic regime where the force increases in a linear fashion relative to the logarithm of the rate.[89]

This concept was first demonstrated in a paper published by Merkel et al., where the authors investigated the interaction between streptavidin and biotin.[90] By varying the rate at which a force was applied to the bonds formed between these two molecules, the authors were able to deduce parameters such as the thermal off rate, k_{off}, and the distance to the energy barrier, x_t, from an understanding of the kinetic landscape of the interaction provided by the deflection of the AFM cantilever.

Dynamic force spectroscopy, utilising the apparatus of the AFM instrument, has been utilised to investigate many other binding mechanisms.[91-95] The elasticity of DNA has been studied extensively using this technique.[96-97] A common experiment, where a ssDNA anchored to a substrate is annealed in situ with its complementary strand attached to the AFM cantilever, has been used to follow the stretching and final separation of the two annealed strands of DNA.[98] Studies of this kind have revealed stages in this process, with DNA now known to undergo a transition from the canonical B form to an overstretched state approximately twice the length of the original molecule. It has even been possible to deduce an energy cost for this process, typically estimated to be in the region of 14 kcal / mol.[98]

A similar experiment, of particular interest to this study, investigated the binding of 9-aminoacridine to dsDNA.[99] By attaching the amine functionality of the ligand to the AFM prove via a PEG tether, the authors were able to measure the force required to remove the monointercalator from DNA attached to the opposing substrate. The authors of this study postulated that two separate mechanisms were occurring during the process of intercalation, attributable to different regimes within the kinetic landscape of the dynamic force spectrum that they obtained.

By attaching DNA to both the AFM probe and the substrate, Lyubchenko et al. were able to eliminate the effects that directly anchoring the ligand may have on its binding behaviour.[100] This study provided information about the binding preferences of the restriction enzyme SfiI. By introducing the enzyme, freely in solution, into the liquid cell of the AFM, the authors monitored the behaviour of the enzyme where binding had coterminously occurred to DNA strands on the cantilever and the substrate. This revealed differences in the forces required to separate the enzyme/DNA complex relative to the known binding preferences of the enzyme for different nucleotide sequences.

An understanding of the forces required to overcome certain interactions may permit characterisation of these interactions relative to known standards. It has been suggested that force spectroscopy could be used as a method for sequencing peptides.[101-102] If the forces required to move a cyclodextrin ring attached to the cantilever along a peptide chain are known, fluctuations in these forces may be attributed to known variations in the resistance provided by different regions within the peptide sequence.

The sensitivity of the AFM, in its ability to visualise molecular structures at an atomic resolution and directly manipulate single chemical bonds, makes this technique a valuable tool for any researcher. Similarly, the versatility of the AFM apparatus, with modification of the AFM probe relatively straightforward and with an array of different functionalities, means that the principles behind AFM may be readily applied to many different experimental scenarios. This does not mean to say that AFM precludes other analytical techniques. However, the volume of published research that incorporates AFM, alongside data from other methods, indicates that it is an increasingly important tool in scientific research.

Chapter 3 – Intra-molecular intercalation

Introduction

As discussed in Chapter 1, the mechanism of DNA intercalation by a variety of ligands has been investigated in considerable detail. Using the imaging facilities of AFM, supported by several other techniques, the intention of this Chapter is to investigate the DNA binding behaviour of the acridine compounds described in Chapter 1, with a view to enhancing our understanding of their mode of action. Full methods for each of the experiments described in this Chapter are provided in Chapter 7.

These particular experiments will concentrate on intramolecular mechanisms of intercalation (Type I), using well defined intercalators such as echinomycin, doxorubicin and 9-aminoacridine as models with which to compare the activity of the bisacridines. Data indicative of inter-molecular binding (Type II) will be considered briefly but examined in more detail in Chapter 4.

Despite the potent cytotoxicity of bisacridines *in vivo*, these compounds are not utilised clinically. Recently, an acridine based poison of the enzymes topoisomerase I and II was withdrawn from phase II clinical trials due to a lack of efficacy.[103-104] Greater understanding of the binding mechanism of these ligands, at the individual molecule resolution afforded by AFM, may facilitate the development of new bisacridines that find employment *in vivo*.

Agarose gel electrophoresis plasmid DNA unwinding assays

DNA intercalation is commonly associated with two changes in the physical characteristics of DNA. First, a DNA duplex is assumed to lengthen in order to accommodate the binding chromophore. Second, the separation of two base pairs, necessary to provide a hydrophobic pocket into which an intercalating chromophore might bind, results in an unwinding of the DNA helix.[28] In the case of a plasmid DNA, such a change in torsional stress is evidenced by an unwinding of the supercoiled plasmid into a fully relaxed state. Using agarose gel electrophoresis, the capacity of several intercalators to unwind a plasmid DNA was tested.

A 5386 base pair plasmid DNA (2 µl), φX174 RFI, was diluted in 70 µl of tris buffer. Eight, 9 µl aliquots were taken from this solution, to seven of which were added 1 µl of relevant concentrations of a particular ligand and to the eighth 1 µl of DMSO or water as a control. This yielded a final volume per sample of 10 µl and a DNA concentration of 7.1 nM. After an incubation period of 1 hour at room temperature, samples were transferred to a 1% agarose gel and separated via electrophoresis. The gel was stained with ethidium bromide and visualised under UV light.

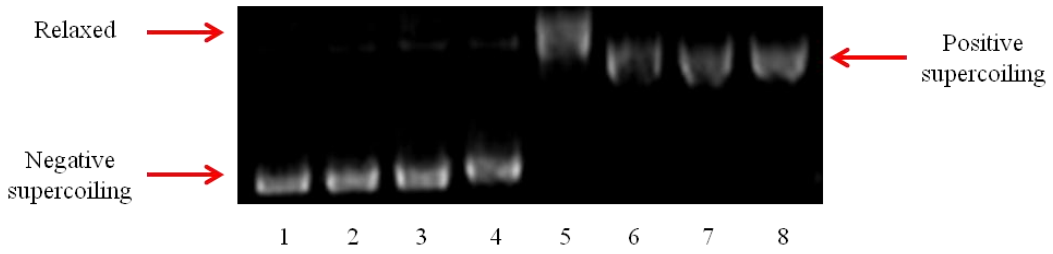

Figure 27 Agarose gel plasmid DNA unwinding assay (DNA concentration 7.1 nM), showing the unwinding of the plasmid DNA as the concentration of the ligand is increased. From lanes 1 to 8, stock concentrations of echinomycin (μM) are 0, 0.01, 0.1, 1, 10, 100, 500 and 1000. This corresponds to a ligand to base pair ratio of 0, 0.00003, 0.0003, 0.0026, 0.026, 0.26, 1.3 and 2.6.

Gel electrophoresis has been utilised to visualise the unwinding process with a large number of compounds.[105-106] Due to the topological characteristics of DNA, unwinding of the duplex at each intercalation site progressively induces left-handed supercoiling as the binding density increases, reflected in the reduced electrophoretic mobility of a plasmid DNA.[9] At a binding level where the number of right-handed supercoils is balanced by the number of left-handed supercoils, the superhelix density is considered to be at equivalence between the two species. Since the degree of helical unwinding required to reach this point of equivalence is a constant value, the helix unwinding parameter of any ligand may be determined relevant to that of the known monointercalator ethidium bromide, the helix unwinding angle of which is known independently to be 26°.[9]

Figure 27 shows a typical assay of this kind, illustrating the effects of the bisintercalator, echinomycin on supercoiled, plasmid DNA. At low concentrations, from lanes 2 to 4 of the gel, little change is observed in the electrophoretic mobility of the DNA (negative supercoiling). Between lanes 4 and 5, at ligand to base pair ratios between 0.0026 and 0.026 (or 1:384 and 1:38.4) the DNA is observed to enter a relaxed state, where the supercoiling has been removed. From lanes 5 to 6, the relaxed DNA undergoes positive supercoiling at ligand to DNA ratios between 0.026 and 0.26, at which point no further changes in the mobility of the DNA are observed.

An identical experiment was conducted with the monointercalator doxorubicin (Figure 28). In this case, unwinding of the DNA is not discernible until ligand to base pair ratios of between 0.026 and 0.26. Although the range of concentrations utilised in this assay prohibits any definitive conclusions being drawn from such an observation, this may be explained in a number of ways. First, the degree of unwinding per molecule of echinomycin is twice that of a monointercalator such as doxorubicin, with reported helix unwinding angles for quinoxaline antibiotics being in the range of 44 to 50°. Second, during the process of

electrophoresis a proportion of the bound ligand will dissociate from the DNA. Since the affinity of echinomycin for DNA is greater than that of doxorubicin, this may lead to unwinding apparently occurring at lower ligand to base pair ratios for echinomycin than for doxorubicin. Thirdly, apparent ligand to base pair ratios at which unwinding is evident may reflect the DNA sequence specificities of each ligand. The plasmid φX174 contains 5386 base pairs (2693 potential intercalation sites), and its GC content is approximately 44 %.

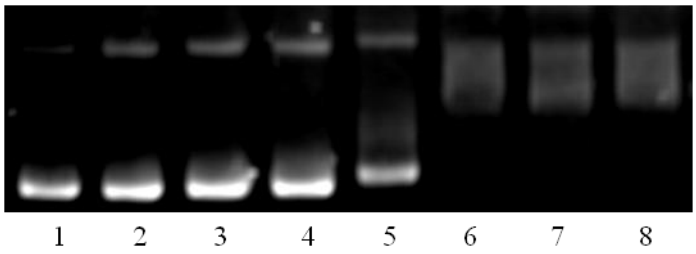

Figure 28 Agarose gel plasmid DNA unwinding assay of doxorubicin (DNA concentration 7.1 nM) showing the unwinding of the plasmid DNA as the concentration of the ligand is increased. From lanes 1 to 8, stock ligand concentrations (μM) are 0, 0.01, 0.1, 1, 10, 100, 500 and 1000. This corresponds to a ligand to base pair ratio of 0, 0, 0.0003, 0.0026, 0.026, 0.26, 1.3 and 2.6. The secondary band apparent in lanes 2 to 4 is a small amount of nicked plasmid DNA that was known to be present in the stock solution that was used for all these experiments.

Although increased ligand concentrations result in reversed supercoiling, and therefore a higher electrophoretic mobility, movement of the DNA through the gel remains less than that of the untreated DNA (see Figure 27, lanes 6 to 8). This is due to the increased contour length of the intercalated DNA, and reaches a plateau, suggesting saturation of the DNA with the ligand.

Figure 29 shows a typical unwinding assay of an acridine bisintercalator, bisacridine 2. The appearance of the gel is very similar to that obtained using echinomycin. The DNA may be observed to reach a relaxed state at concentrations of bisacridine 2 between 20 and 50 μM, corresponding to ligand to base pair ratios between 0.052 and 0.13. Saturation of the DNA with the ligand subsequently occurs at ratios between 0.13 and 0.26. A study by Wakelin et al. using the same ligand but a different plasmid DNA found that the DNA entered a relaxed state at ligand to base pair ratios of between 0.08 and 0.13, consistent with these results.[19]

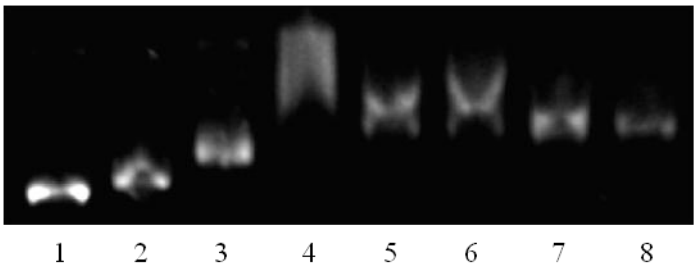

Figure 29 An agarose gel plasmid DNA unwinding assay, illustrating the binding of bisacridine 2 (DNA concentration 7.1 nM). From lanes 1 to 8 concentrations of the bisacridine are (μM) 0, 10, 20, 50, 100, 200, 500, and 1000. This corresponds to ligand to base pair ratios of 0, 0.026, 0.052, 0.13, 0.26, 0.52, 1.3 and 2.6.

Bisacridine 3 was also assessed for its capacity to unwind supercoiling in plasmid DNA (Figure 30). Given the rigidity of the inter-chromophore linker in this compound, there has been speculation as to whether the compound is able to adopt a bisintercalative Type I binding arrangement, or simply functions as a monointercalator, with one chromophore either binding to an adjacent DNA strand or remaining unbound. As may be discerned from Figure 30, the behaviour of this compound with respect to the unwinding of DNA supercoiling is very similar to that of bisacridine 2, a known Type I bisintercalator. However, at high concentrations of bisacridine 3 (exceeding ligand to base pair ratios of 1:4), there was a noticeable reduction in the intensity of the DNA bands. This is conceivably due to a degree of inter-molecular binding, causing some of the DNA to precipitate during sample incubation.

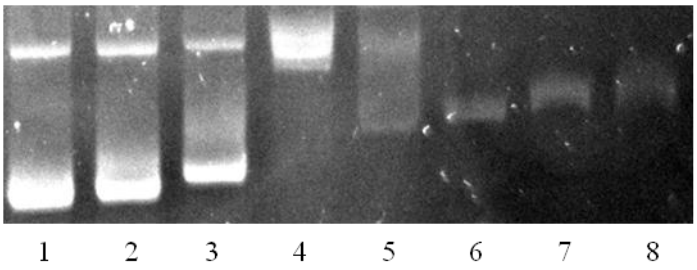

Figure 30 Plasmid unwinding assay of bisacridine 3 (DNA concentration 7.1 nM) showing the unwinding of the plasmid DNA as the concentration of the ligand is increased. From lanes 1 to 8 concentrations of the bisacridine are (μM) 0, 10, 20, 50, 100, 200, 500, and 1000. This corresponds to ligand to base pair ratios of 0, 0.026, 0.052, 0.13, 0.26, 0.52, 1.3 and 2.6.

Imaging single molecules of DNA using AFM

As discussed, two common indicators of DNA intercalation are the unwinding of DNA supercoiling, and the extension in length of the DNA strands themselves. Having ascertained the ability of bisacridines 2 and 3 to unwind the supercoiling of plasmid DNA, it remained necessary to test whether or not these compounds also cause a lengthening in DNA

sequences. Figure 31 shows the appearance of a single molecule of the plasmid DNA φX174 RF I that was utilised in the gel unwinding assays. This image was obtained via AFM imaging in air using tapping-mode. Although theoretically the length of this plasmid may be determined, it is far more straightforward, and accurate, to measure shorter, linear sections of DNA.

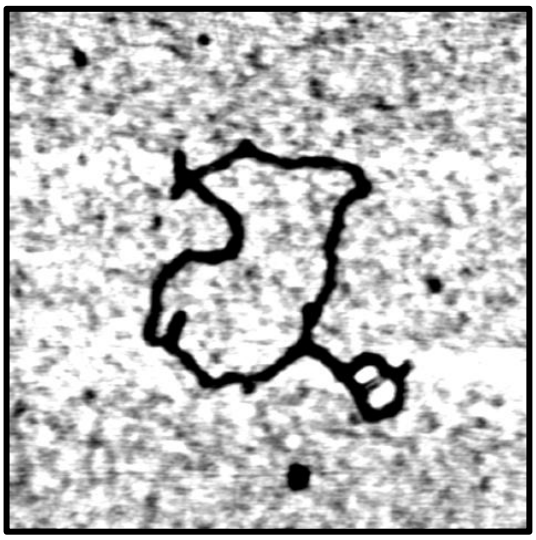

Figure 31 AFM image of the plasmid DNA, φX174 RF I, utilised in the previous gel unwinding assays. The scan size is 1 x 1 microns.

Restriction of φX174 RFI with the enzyme BfaI yielded a 771 base pair fragment of linear DNA, approximately 262 nm in length, which was ideal for obtaining reliable contour lengths. An AFM image of these linear fragments is provided in Figure 32, along with measurements of the length of these strands. To provide samples for AFM imaging, the solution of 771 base pair DNA was diluted to a concentration of 4.7 ng/µl. A volume of 5 µl of this solution was added to 5 µl of Nanopure™ water. A further 15 µl of water, or the same volume of a ligand, was then added to the DNA solution yielding a final volume of 25 µl, in which the concentration of the DNA was 1.9 nM. 25 µl of 10 mM $MgCl_2$ were subsequently added (to provide a positive counterion between the negatively charged DNA and the negatively charged surface of the mica substrate) and the complete volume of 50 µl was deposited on freshly cleaved mica and air dried under nitrogen. The mica, mounted on steel pucks, was mounted in the AFM ready for imaging.

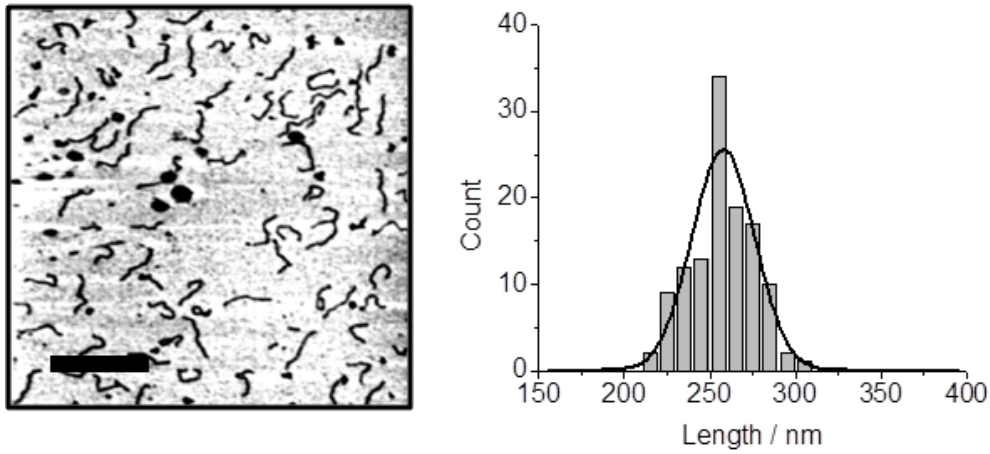

Figure 32 AFM image of the linear, 771 base pair fragment of DNA used in these experiments. The bar denotes the scale (500 nm). A mean average of 257.8 nm and standard error of 1.6 nm were derived from fitting of a gaussian distribution to the histogram (n 119).

The data presented in Figure 32 were compiled using two separate sets of data, obtained from different AFM samples of the DNA. Table 2 and Figure 33 illustrate the reproducibility of this technique, with the mean contour length of the different samples differing by only 3 nm.

Table 2 Measurements of DNA lengths, taken from various AFM images. Irrespective of the different number of measurements taken from each sample, the average length of the DNA strands was in good agreement with one another.

Sample	Mean contour length / nm (SE)	n (number of strands)
Mica sample 1	255.4 (2.2)	70
Mica sample 2	258.4 (2.6)	49

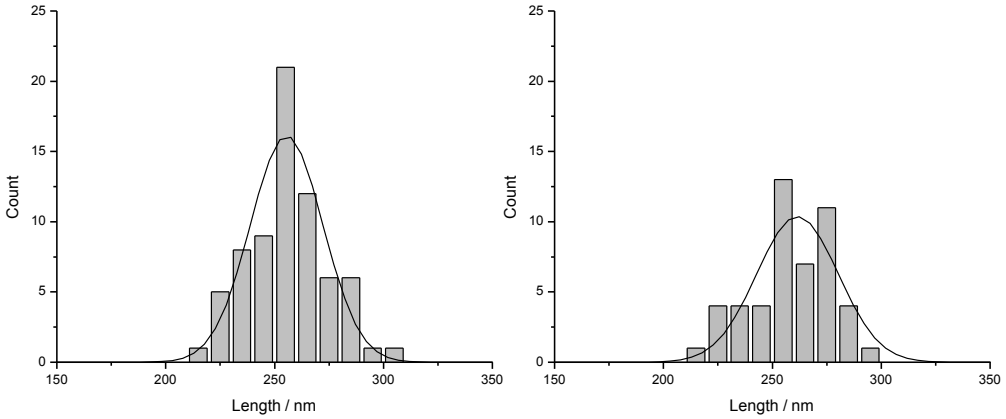

Figure 33 Histograms of contour lengths for each of the two DNA samples reported in Table 2, showing sample 1 (left) and sample 2 (right). Despite the lower number of measurements in the second histogram (right) the central tendency of each population is the same.

Although each sample had been prepared at a different time, and measurements taken independently, there was a good correlation between the mean contour lengths of each sample. Typical standard error for each sample was approximately 1% of the measured strand length.

Interpretation of histograms such as these is not always straightforward. Parametric testing of data assumes a normal, or gaussian, distribution of the data points. In the case of the second DNA control, illustrated by the right hand histogram in Figure 33, it could be argued that the distribution is in fact bimodal, that is to say that the data contains two overlapping populations, each with its own central tendency. Although a bimodal distribution may be described, there is no mathematical test to determine whether or not a distribution of data is in fact bimodal.[107] However, a data set may be tested to ascertain whether the distribution is either unimodal (i.e. normal) or multimodal.[108] Two tests for normality in a data set are the Shapiro-Wilk test and a modified version of the Kolmogorov-Smirnov test. Applying these tests to the histograms in Figure 34 using Origin Pro™ (OriginLab, ver. 8.0724) leads to the conclusion that both data sets are normally distributed (i.e. $p > 0.05$).

An important factor in the appearance of a histogram is the chosen bin width, into which the data are subdivided. A typical formula for suggesting the appropriate bin widths (k) expresses this as a function of the number of data points within a sample (n):

$$k = \sqrt{n}$$

Unfortunately, even where the bin widths of individual histograms are adjusted in this fashion, the elucidation of quantitative information from any histogram remains subjective. Certainly, it is difficult to draw meaningful conclusions about differences between different sets of data on the basis of their respective histograms alone.

A more reliable and consistent technique, for expressing the central tendency and standard deviation of data points within a data set is that of non-linear regression. The computer software used in these studies for statistical analysis, Origin Pro™ (OriginLab, ver. 8.0724), uses the Levenberg-Marquardt algorithm in curve fitting, also referred to as the damped least-squares method.[109] Simply, this algorithm estimates those parameters (such as the width of the gaussian peak) that would minimize the deviation of the theoretical gaussian curve from the experimental data. Adjusted R^2 values for the two gaussian fits presented in Figure 33 were 0.89 and 0.83, theoretically indicating that between 80 and 90 % of the data could be explained by the gaussian model.

However, the value of adjusted R^2 values in non-linear regression has recently been questioned.[110] In the context of these experiments, it should be noted that the R^2 value of the gaussian fitting in Figure 32 (n 119) was 0.89, whilst that of the distribution in Figure 25 (n 9) was 0.88. A more practical means of assessing the validity of the mean averages derived from gaussian fitting of these populations may be conducted by comparing these values to the median and arithmetic mean (sum total / n) averages of each population.

Table 3 Comparison of the gaussian mean (derived from fitting of gaussian curves to the data) and arithmetic mean (the sum total of the data divided by n) with the median average of the data presented in Figure 33. IQ stands for interquartile. The close correlation of all these averages (all within the SE) demonstrates that the data is normally distributed.

Sample	Gaussian mean (SE)	Arithmetic mean (SE)	Median (IQ range)
Mica sample 1	255.4 (2.2)	255.4 (2.2)	253.7 (24.5)
Mica sample 2	258.4 (2.6)	258.4 (2.6)	258.8 (23.5)

The excellent correlation of the gaussian mean with the arithmetic mean in the case of each separate mica sample demonstrates both the robustness and the appropriateness of the statistical analyses applied to these data sets despite the 6 % difference in their respective R^2 values of 0.89 and 0.83. The close correlation of the median with the arithmetic mean (within the standard error of the mean) provides further evidence that the data is normally distributed and not skewed.

A similar experiment was conducted to ascertain the reproducibility of measurements derived from DNA fragments treated with a ligand, the monointercalator 9-aminoacridine, at a concentration of 2 μM. After the addition of the ligand, the aqueous sample was allowed to incubate for one hour at room temperature. As for the DNA control, measurements were obtained from two separately prepared mica samples. Table 4 and Figure 34 provide a summary of these measurements, and as for the DNA controls, both measurements are virtually identical to one another and show a slight increase in the length of the strands relative to control (257.8 nm), as may be expected following binding of the intercalator.

Table 4 A comparison of the measured lengths of two separate samples of the linear DNA fragment after the addition of 2 μM 9-aminoacridine. There is a slight increase in DNA length relative to the control (257.8 nm).

Sample	Mean contour length / nm (SE)	n (number of strands)
Mica sample 1	269.5 (2.9)	66
Mica sample 2	267.0 (3.1)	37

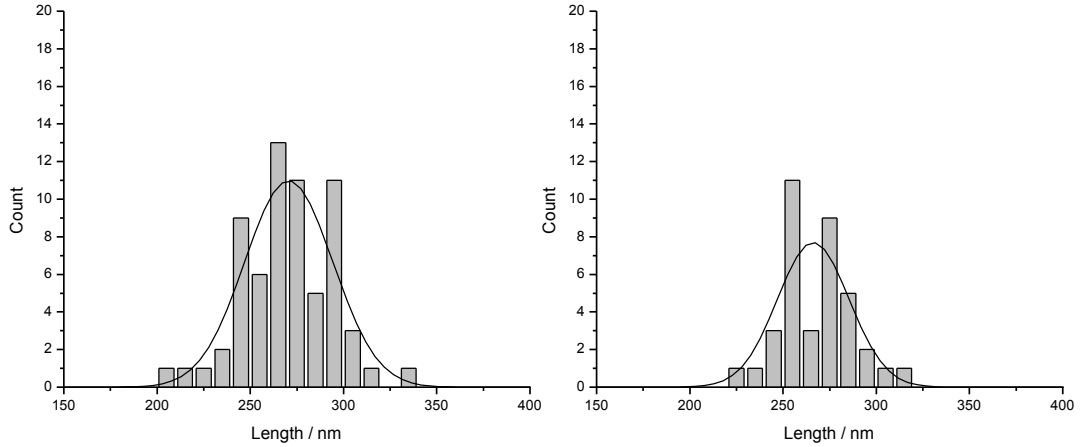

Figure 34 Histograms of contour lengths for the two DNA samples bound to 2 μM 9-aminoacridine reported in Table 4 (DNA concentration 1.9 nM), showing sample 1 (left) and sample 2 (right). Despite the larger number of measurements taken for sample 1, there is no significant change in the central tendency or distribution of measurements between the two samples.

Overall, these initial imaging experiments confirm the ability of AFM to resolve individual molecules of DNA at nanometer resolutions. Measurements derived from this technique are reproducible, demonstrated by the excellent correlation between sets of measurements derived from separately prepared samples of the same materials. This technique will be exploited further to follow the changes that occur in the physical characteristics of DNA following ligand binding over a range of ligand concentrations.

Studying ligand induced changes in DNA structure using AFM

As discussed in Chapter 2, AFM has already been utilised to investigate any changes that occur in the physical characteristics of individual DNA strands following ligand binding. The activity of several DNA intercalators, such as echinomycin and luzopeptin, has been studied using this technique.[73, 75]

Our preliminary studies focused on two well characterised intercalating agents, the bisintercalator echinomycin and the monointercalator doxorubicin. The purpose of these experiments was twofold. First, to ascertain whether or not the AFM protocol that had been adopted was sufficiently sensitive to measure the kinds of change in DNA contour length that might accompany binding of these ligands. Second, to establish if data derived from these experiments were sufficient to distinguish between the behaviors of two different ligands.

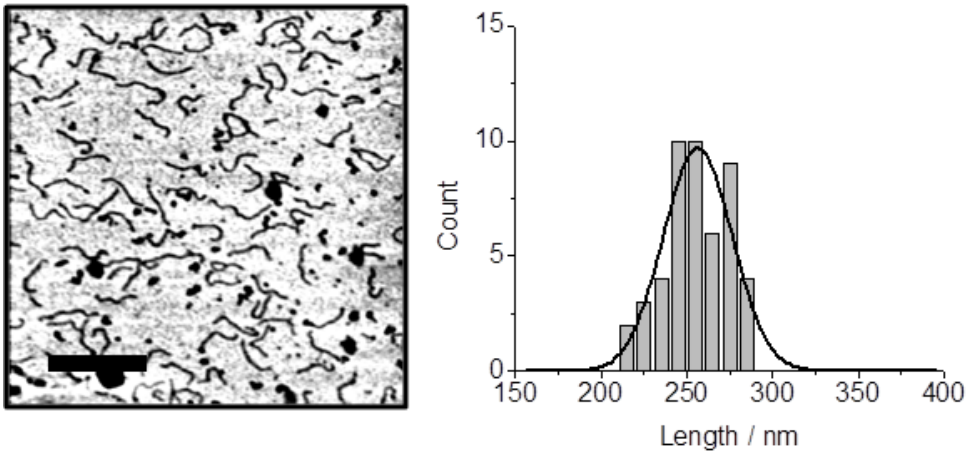

Figure 35 An AFM image of linear DNA fragments treated with 0.1% DMSO, and the corresponding histogram showing the lengths of these fragments. The scale bar denotes 500 nm. This reflects a very slight contraction relative to the aqueous control, but this is not statistically significant since each value is within the SE.

Although a control population of DNA had been defined in aqueous solution, the poor solubility of echinomycin in water necessitated the preparation of another control solution which included a small amount of DMSO (Figure 35).[75] DMSO is known to cause a slight shortening of DNA, even at low concentrations. This process was not necessary for doxorubicin, due to its greater solubility in aqueous media. To prepare this particular sample, 15 µl of an aqueous solution of 0.1% DMSO was added to the 10 µl solution of 771 base pair DNA (2.35 ng/µl), and the sample imaged via AFM as previously described.

Table 5 Comparison of DNA in aqueous solution and an aqueous solution of 0.1% DMSO. Although there is no significant difference between the mean values, changes in DNA length observed with echinomycin were considered relative to the value of 255.6 nm, and 256.9 nm for doxorubicin.

Sample	Mean contour length / nm (SE)	n (number of measured strands)
DNA (aqueous)	256.9 (2.6)	119
DNA (0.1% DMSO)	255.6 (2.6)	48

Table 5 shows the different lengths of DNA in an aqueous environment and in a solution of 0.1% DMSO. An expected shortening of the DNA in the presence of DMSO was not observed, likely due to the very low concentration of DMSO. Nevertheless, measurements for DNA bound to echinomycin will be considered relative to the DNA solution containing 0.1% DMSO, while aqueous ligands such as doxorubicin will be considered relative to the DNA in aqueous solution.

The contour length of linear DNA fragments has been shown to increase on the addition of echinomycin and doxorubicin, not only using AFM but other techniques such as gel electrophoresis and solution viscometry.[28, 111] Ideally, similar changes in DNA contour length would be observed when following our own AFM protocol. Both ligands share a preference for GC rich regions of DNA,[8] and as such the number of available binding sites within the DNA strand should be similar for each compound. Theoretically, saturation of the available binding sites should occur at a lower ratio of ligand to base pairs in the case of the bisintercalator than that of the monointercalator.

In order to preserve the same ratio of ligand to base pair ratios that were used during the plasmid unwinding assays, it was necessary to reduce the absolute concentration of the ligands since the concentration of the DNA utilised for the AFM experiments was lower than that used for gel electrophoresis (1.9 nM versus 7.1 nM). The affinity of any ligand for a receptor is defined by the dissociation constant (K_d) of that ligand, typically expressed as the concentration of the ligand at which 50 % of the ligand is bound to available binding sites. The lower the concentration at which this equilibrium occurs, the greater the affinity of the ligand for the receptor. The monointercalator 9-amino acridine has a dissociation constant in the region of 5 μM, whilst values for echinomycin and TANDEM range from 100 nM to 5 μM depending on the DNA sequence to which they are binding.[9] Dissociation constants for bisacridines are typically 10 to 15 times lower than 9-amino acridine, at approximately 100 nM. Theoretically, at ligand concentrations less than the corresponding K_d of the ligand, binding will be occurring at less than 50 % of the available binding sites even where ligand to DNA base pair ratios are preserved, rendering analysis of any data difficult. However, the ligand concentrations used in these studies cover a similar range to those used elsewhere.[19] Moreover, the correlation between results of the plasmid unwinding assays and AFM contour length assay described below, both suggesting that bisintercalator binding peaks at ligand to base pair ratios in the region of 0.25, suggest that the low initial ligand concentrations were not adversely affected by the dissociation kinetics. This observation is supported by CD experiments described later in this chapter, where significantly higher ligand concentrations were used (*c*. 3 mM) over an identical range of ligand to base pair ratios.

Data obtained for doxorubicin are presented in Figure 36 and Table 6, while data obtained for echinomycin are presented in Figure 37 and Table 7. Changes in the measured contour length of linear DNA fragments as a function of the increasing concentration of each intercalator are shown in Figure 38. For all the ligands studied herein, an exponential fit was applied to the data. There is a significant increase in DNA length on addition of either

ligand, which reaches a plateau where no further increase in the length of the DNA is observed. The change in contour length that may be derived from this plateau is approximately the same for both echinomycin and doxorubicin. However, saturation of the DNA occurs at a lower ratio of ligand to base pairs with the bisintercalator.

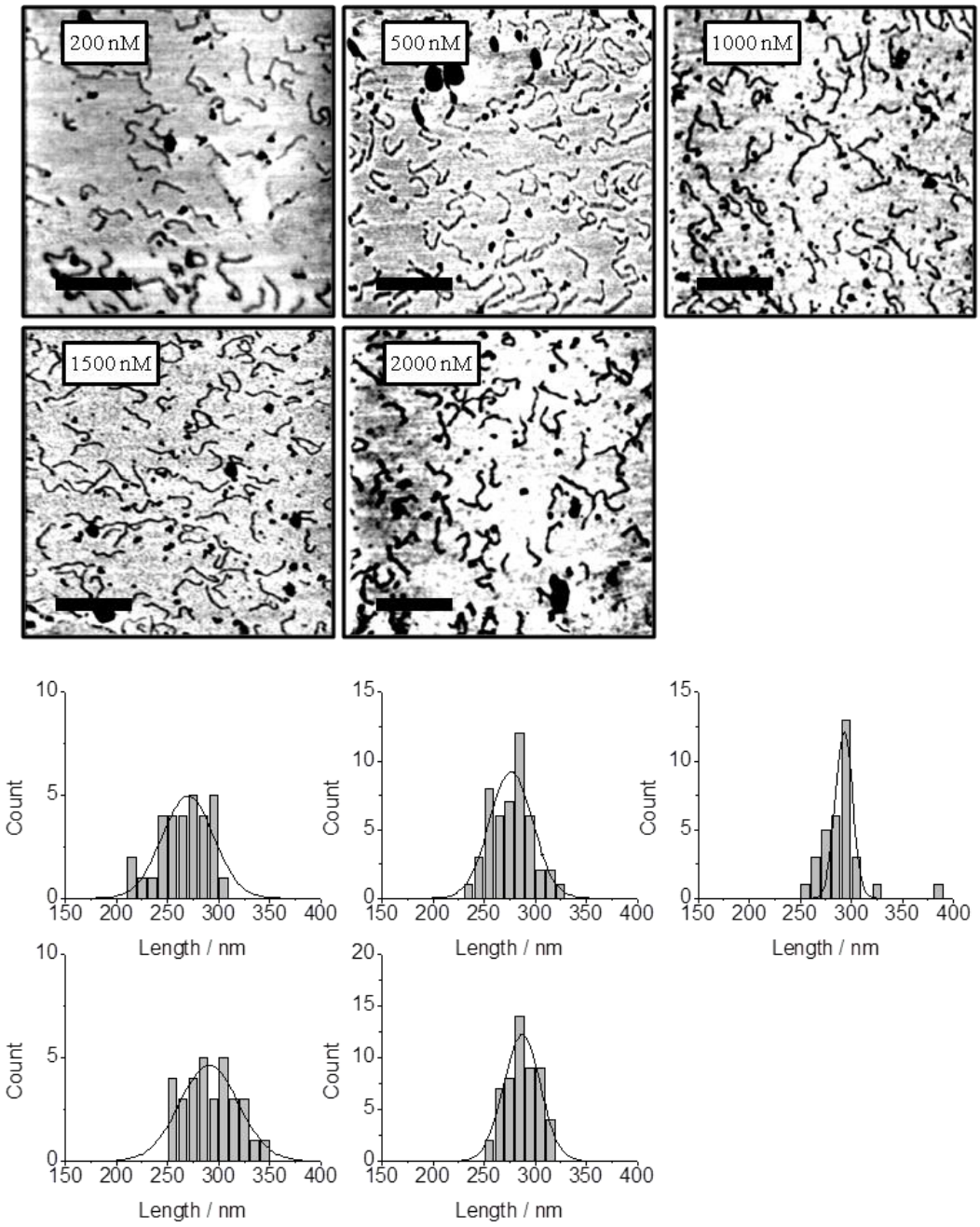

Figure 36 (above) AFM images of DNA bound to doxorubicin (DNA concentration 1.9 nM). The concentration of the ligand is shown in the figure. Scale bars denote 500 nm (below) Histograms of the lengths of the DNA within each image, showing the distributions of measured lengths and the gaussian fitting of the data.

Table 6 Mean lengths of each population of DNA strands relative to the concentration of doxorubicin. These results indicate a progressive lengthening of the DNA when the ligand concentration is increased.

Concentration / nM	Ligand to BP ratio	Mean length / nm	SE / nm	n
0	0.000	257.8	1.6	119
200	0.079	270.1	2.4	31
500	0.197	276.6	2.0	48
1000	0.394	292.7	1.0	33
1500	0.591	290.7	2.7	32
2000	0.789	287.3	1.0	53

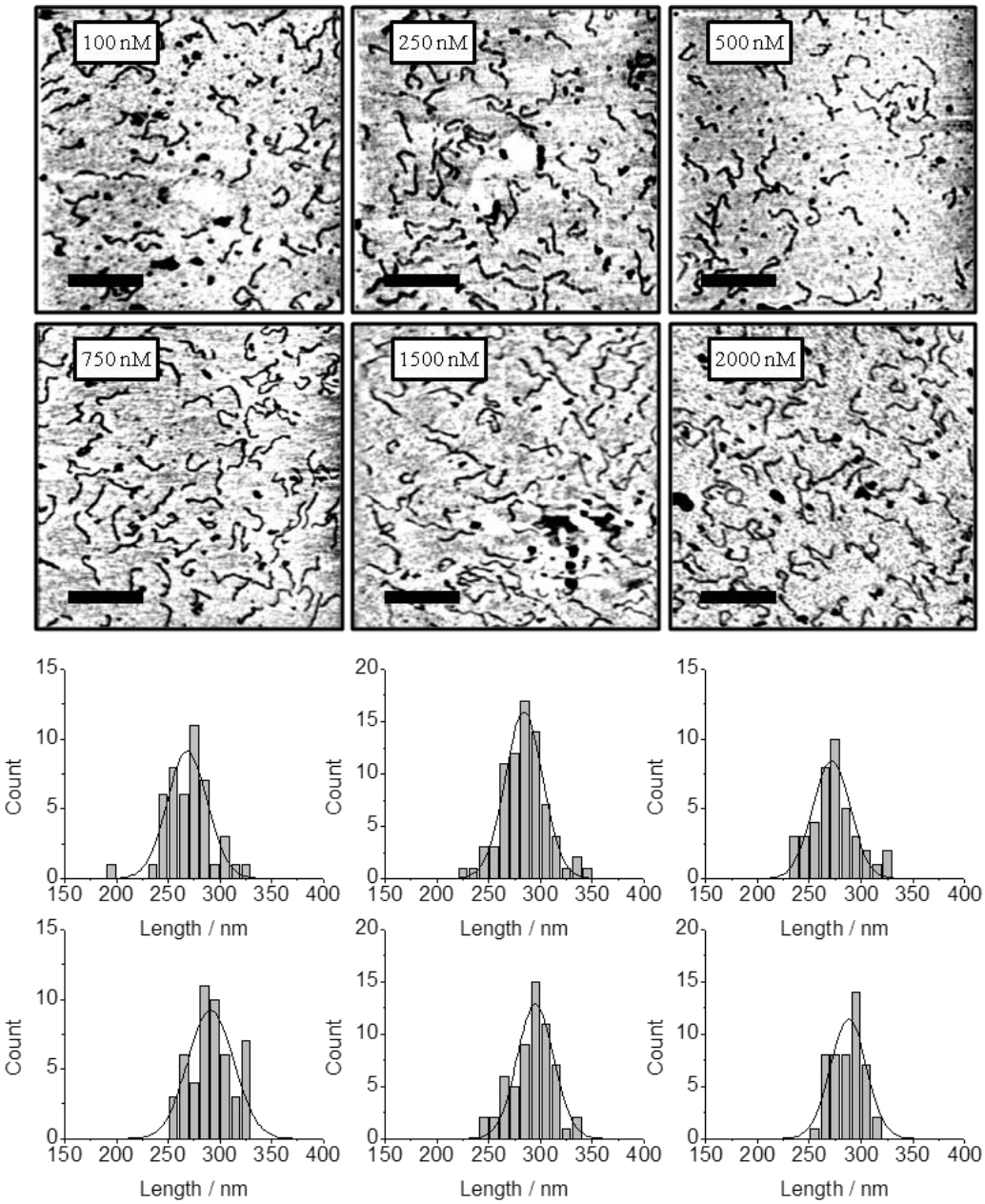

Figure 37 (above) AFM images of DNA bound to echinomycin (DNA concentration 1.9 nM). The concentration of the ligand is shown in the figure. Scale bars denote 500 nm (below) Histograms of the lengths of the DNA within each image, showing the distributions of measured lengths and the gaussian fitting of the data.

Table 7 Mean lengths of each population of DNA strands relative to the concentration of echinomycin. These results indicate a progressive lengthening of the DNA when the ligand concentration is increased.

Concentration / nM	Ligand to BP ratio	Mean length / nm	SE / nm	n
0	0.000	256.4	1.6	48
100	0.039	268.5	1.9	46
250	0.099	271.3	1.4	41
500	0.197	284.0	0.9	77
750	0.296	291.1	2.4	50
1500	0.591	295.0	1.3	61
2000	0.789	287.7	1.6	48

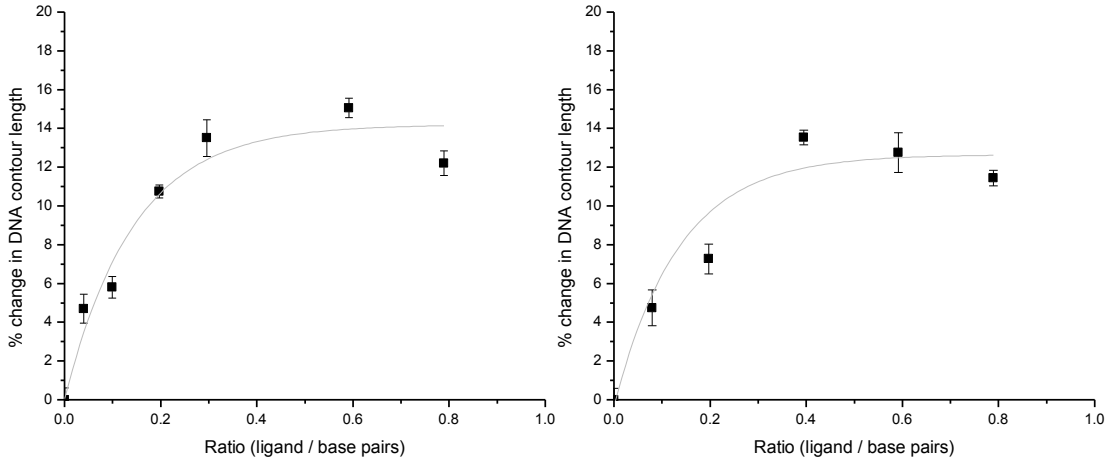

Figure 38 Plots of % change in DNA contour length versus ligand concentration (as a function of the ratio of ligand molecules to DNA base pairs) for echinomycin (left) and doxorubicin (right), using an exponential fit. The trend reflects a progressive increase in DNA length followed by a plateau. In both cases, increases in DNA length plateau at between 12 and 14%.

The presentation of data of this kind has been examined in detail. Early studies of intercalation made extensive use of viscometry, where the intercalator was bound to sonicated DNA fragments.[112] These experiments deduced a linear relationship between binding of an intercalator and the associated increase in the contour length of the DNA, accompanied by a slight curvature in the scatchard plots at high ligand concentrations.[28] Classically, non-linearity in Scatchard plots has been interpreted as being indicative of cooperative processes. After this initial increase in the length of the DNA, there is a plateau in the length of the DNA, despite further increases in ligand concentration. This suggests that at these higher ligand concentrations, the DNA is saturated with the ligand and no further binding is occurring.

Unfortunately, the simple ligand receptor model on which these assumptions were originally based may not be suitable for the complexities of intercalation, especially in the case of a

bisintercalator where one molecule is, in effect, binding conterminously to two separate receptors.[113] Although some recent studies have suggested a degree of cooperativity in some localized intercalation complexes, the consensus of opinion is that globally, intercalation is a non-cooperative process.[114] As such, initial binding of echinomycin and doxorubicin to DNA may be considered to be a linear process, where saturation is governed by the availability of energetically favourable sites for intercalation. This is demonstrated in Figure 39.

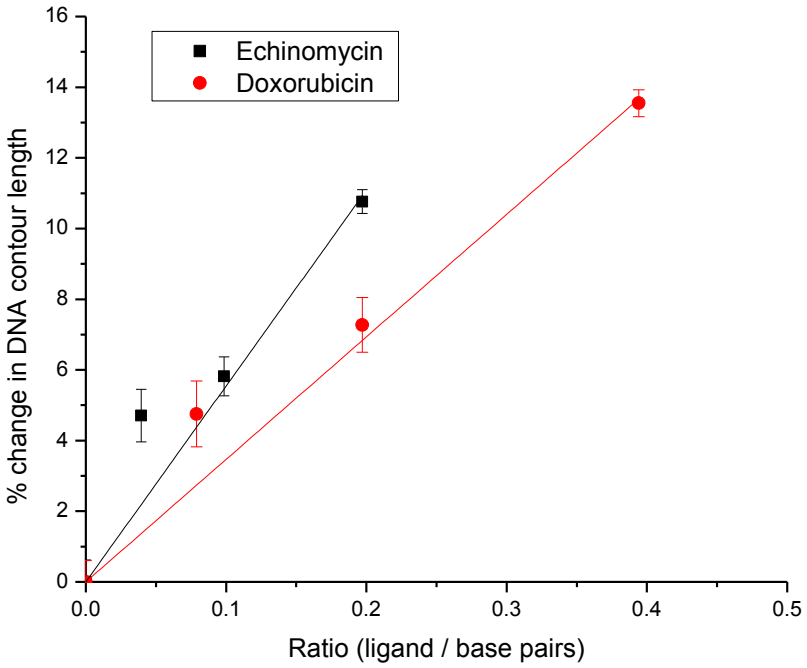

Figure 39 Plots of % change in DNA contour length versus ligand concentration (as per Figure 38), showing the increase in DNA length up to the point at which saturation occurs. As may be expected, the gradient of the line of echinomycin is greater than that of doxorubicin, suggesting that bisintercalation is occurring.

Linear regression was conducted using Origin Pro™, yielding a gradient for the slope where the intercept of the *x* and y axes was assumed to be zero. The gradient of the slope and the degree of confidence in the fitting of the linear model for each ligand are provided in Table 8.

Table 8 Values for the relationship between ligand concentration and the increase in DNA length for echinomycin and doxorubicin, showing that the trend for each ligand is significantly different to the other.

Ligand	Gradient (*x*/*y*)	SE	R^2
Echinomycin	55.4	3.3	0.99
Doxorubicin	34.7	1.2	0.99

A comparison of the data derived from Figure 38 and Figure 39 is provided in Table 9. The ratio of ligand molecules to DNA base pairs at which saturation is reached was calculated by taking the gradient of the line for the appropriate compound from Figure 39 and the value of the *y* axis at saturation from Figure 38 where,

$$y = mx + c$$

Table 9 Comparison of the changes in DNA contour length observed with echinomycin and doxorubicin and the relative number of DNA base pairs per ligand molecule. Although this highlights a difference in the ligand to base pair ratio at which the DNA ceases to increase in length, this could reflect a number of factors, such as each ligand's precise sequence selectivity and relative binding affinity for DNA.

Ligand	% change at saturation (SE)	Ligand : BP ratio at saturation	Base pairs per ligand molecule
Echinomycin	14.20 (1.05)	0.26	3.85
Doxorubicin	12.66 (1.24)	0.37	2.70

Given the similar sequence selectivities of echinomycin and doxorubicin, it is not surprising that both compounds cause a similar degree of lengthening of the DNA. The GC content of the fragment of DNA utilised in these experiments was 44% of the total number of base pairs. Theoretically, this should yield a 22% increase in the length of a DNA strand, allowing for the neighbour exclusion principle, where binding may only occur between alternate base pairs. However, estimates of this kind are not particularly helpful. The precise nucleotide specificities of any intercalating ligand are very complicated, and the preference of echinomycin and doxorubicin for GC rich regions does not preclude binding within AT rich regions. Initial binding of an intercalator can occur randomly, and only after a period of incubation with the DNA does the intercalator find binding sites from which it dissociates at a slower rate.[8] Intercalation is a reversible, non-covalent interaction between a ligand and DNA, and intercalators are known to move or 'shuffle' from one binding site to another.[9] Similarly, the arrangement of nucleotides within GC rich regions can also affect ligand binding. Echinomycin is known to bind preferentially to the nucleotide step 5'-CpG, especially where the flanking base pairs are AT.[45] Above all, theoretical assumptions regarding the change in length of the DNA assume that each intercalation event induces the same degree of lengthening within the DNA strand. Although a helix extension of 0.34 nm per intercalation event is often assumed, experimentally determined values differ considerably[11] and are strongly dependent on the characteristics of the particular ligand, the conformational arrangement of the DNA, and the conditions of the solution in which the DNA and the ligand are suspended.[115] NMR and crystal structures of short DNA sequences

may provide precise values for this parameter, but it is likely that in longer DNA stretches, the lengthening of the DNA will depend strongly on the composition of the primary sequence at the site of intercalation and the degree of ligand binding preceding the point of measurement.

Despite these considerations, some general conclusions may be drawn from this initial experiment. The overall change in the length of the DNA following intercalation is similar for both doxorubicin and echinomycin, but saturation of the DNA with each ligand occurs at different ratios of ligand to base pairs, approximately 0.26 for echinomycin and 0.37 for doxorubicin. These ratios reveal that the number of molecules in solution at the point at which saturation of the DNA is occurring is significantly higher than may be expected if binding is only occurring at GC regions, and is likely interpreted in one of two ways. First, binding is occurring at sites other than GC regions, in which case the expected rise of 0.34 nm per intercalation event is not represented by the measured percentage change in the length of the DNA strands. Second, that the number of ligand molecules in solution, or rather present in the solution of DNA and ligand, is not representative of the concentration of ligand bound to the DNA. That a very similar value was obtained from the agarose gel unwinding assay with echinomycin (saturation occurring before 0.25 ligands per DNA base pair) suggests that the higher than expected ratios are a consequence of several different factors, and not due to an irregularity of the AFM imaging experiment itself. In terms of a simple equilibrium, the concentration of bound ligand will be determined to some extent by the concentration of free ligand that remains in solution. Although, as previously discussed, the intercalation of DNA at low ligand concentrations follows a non-cooperative process, at high ligand concentrations, where many binding sites are already occupied, competition between ligands for the remaining sites may yield a degree of negative cooperativity. This phenomenon is evident in Figure 38, where the increase in DNA length slows, relative to increases in ligand concentration, as available binding sites become saturated.

Given the known preference of echinomycin for GC rich DNA, it was decided to conduct further experiments of this kind using the triostin-A analogue, TANDEM. Since this ligand has a preference for AT rich regions of DNA, parameters such as the overall change in the length of the DNA fragments observed with this ligand might be different to those observed with echinomycin. Like echinomycin, this ligand is also poorly water soluble and stock solutions were prepared in DMSO before diluting to an appropriate concentration in 0.1% DMSO. Data obtained for TANDEM via AFM imaging are provided in Figure 40.

Plots of the overall changes in DNA contour length that were observed at increasing concentrations of TANDEM are provided in Figure 41. Relative to echinomycin and doxorubicin, the value of the y axis as the change in DNA length reaches a plateau is noticeably higher in the case of TANDEM. Given the greater AT content of the DNA fragment (56%), this might suggest that the observed changes in DNA contour length for all three ligands reflect the sequence specificities of those compounds. A comparison of the changes observed for echinomycin and TANDEM is shown in Table 11.

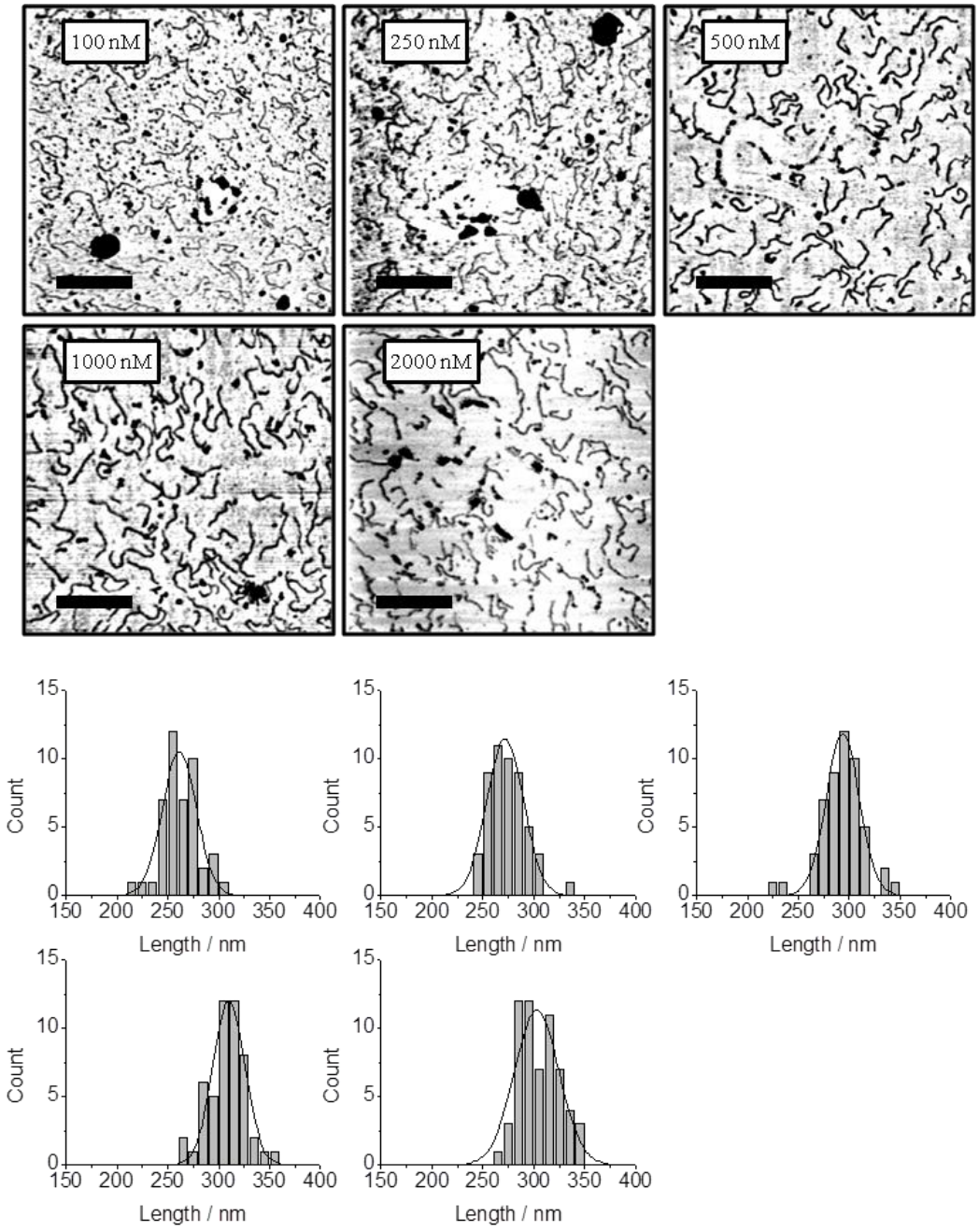

Figure 40 (above) AFM images of DNA bound to TANDEM (DNA concentration 1.9 nM). The concentration of the ligand is shown in the figure. Scale bars denote 500 nm (below) Histograms of the lengths of the DNA within each image, showing the distributions of measured lengths and the gaussian fitting of the data.

Table 10 Mean lengths of each population of DNA strands relative to the concentration of TANDEM. These results indicate a progressive lengthening of the DNA when the ligand concentration is increased.

Concentration / nM	Ligand to BP ratio	Mean length / nm	SE / nm	n
0	0.000	256.4	1.6	48
100	0.039	261.4	1.6	45
250	0.099	271.6	0.8	51
500	0.197	293.7	0.9	51
1000	0.394	310.0	1.1	50
2000	0.789	302.8	2.0	60

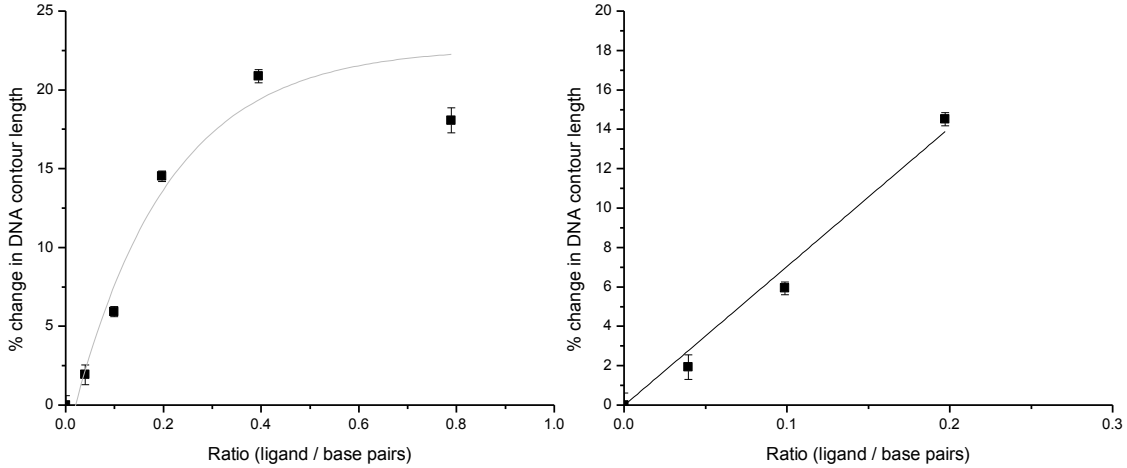

Figure 41 Changes observed in DNA contour length as a function of increasing ligand concentration for the bisintercalator TANDEM. An initial increase and subsequent plateau in the length of the DNA may be discerned (left) using an exponential fit, while non-cooperative binding at lower ligand concentrations is demonstrated (right). The gradient of the linear portion is 70.5 (x/y), with a SE of 3.4 and an R^2 value of 0.99.

Table 11 Comparison of overall changes in DNA contour length, and ligand to DNA base pair ratios at saturation for echinomycin and TANDEM. The differences between each ligand, such as the overall change in the length of the DNA likely reflect several factors, not least the different sequence specificities of these ligands.

Ligand	% change at saturation (SE)	Ligand : BP ratio at saturation	Base pairs per ligand molecule
Echinomycin	14.20 (1.05)	0.26	3.85
TANDEM	22.71 (3.90)	0.32	3.11

As with echinomycin, the expected increase in DNA contour length was not observed for TANDEM. Given an AT content of 56%, one could argue that an increase of 28% ought to be observed. However, the previous discussion of how the precise arrangement of GC base pairs could affect the number of available binding sites remains equally valid for the AT component of the DNA strand. Similarly, the slight difference in the ratio of ligand to DNA base pairs at saturation that may be discerned between echinomycin and TANDEM, 0.26 and

0.32 respectively, could be the consequence of many different factors, and cannot be considered to be significant in the context of this particular experiment. In fact, whether or not the differences between these two bisintercalators are attributable to their nucleotide preferences cannot be ascertained with the available data. Further experiments would need to be conducted, varying the nucleotide content of the DNA, before any definite conclusions may be drawn.

Despite the limitations of this experiment, some general conclusions may be drawn from these initial AFM imaging experiments that apply to all of echinomycin, doxorubicin and TANDEM. First, binding of these ligands to DNA induces a lengthening in DNA that may be detected by AFM. Lengthening of the DNA was typically in the region of 15 to 20% at ligand to base pair ratios of approximately 0.25, after which a plateau was observed in the lengthening of the DNA fragments despite further increases in ligand concentration. Second, this lengthening process followed a broadly linear, positive regime.

Investigating the binding of bisacridines to DNA using AFM

The binding of bisacridines to DNA has yet to be thoroughly investigated using AFM. Given the findings of the initial experiments with echinomycin and doxorubicin, it was decided to examine the acridine compounds described in Chapter 1 in the same manner, in order to ascertain whether or not these ligands induce a similar kind of lengthening in the DNA fragments.

Unlike echinomycin and TANDEM, where extensive studies have been conducted into their respective binding preferences, the specificities of acridine analogues have not been characterised definitively. Early studies have suggested that some bisacridines may demonstrate a preference for ApT steps under conditions of low ionic strength.[9] However, small changes to the composition of the inter-chromophore linker, such as the addition of a nitrogen atom, have been demonstrated to eliminate this slight selectivity.[9] Conversely, it has been suggested that some acridine ligands have a preference for GC rich DNA.[52]

Despite the lack of definite information as to the sequence selectivities of acridine ligands, it is not unreasonable to assume that, like echinomycin and TANDEM, these compounds will cause a progressive lengthening of DNA strands to which they are bound. The behaviour of the acridine ligands as determined by the plasmid DNA unwinding assays conducted earlier was certainly very similar to that of echinomycin and TANDEM, the acridine bisintercalators also reversing the negative supercoiling of plasmid DNA up to a ligand to base pair ratio of approximately 0.25.

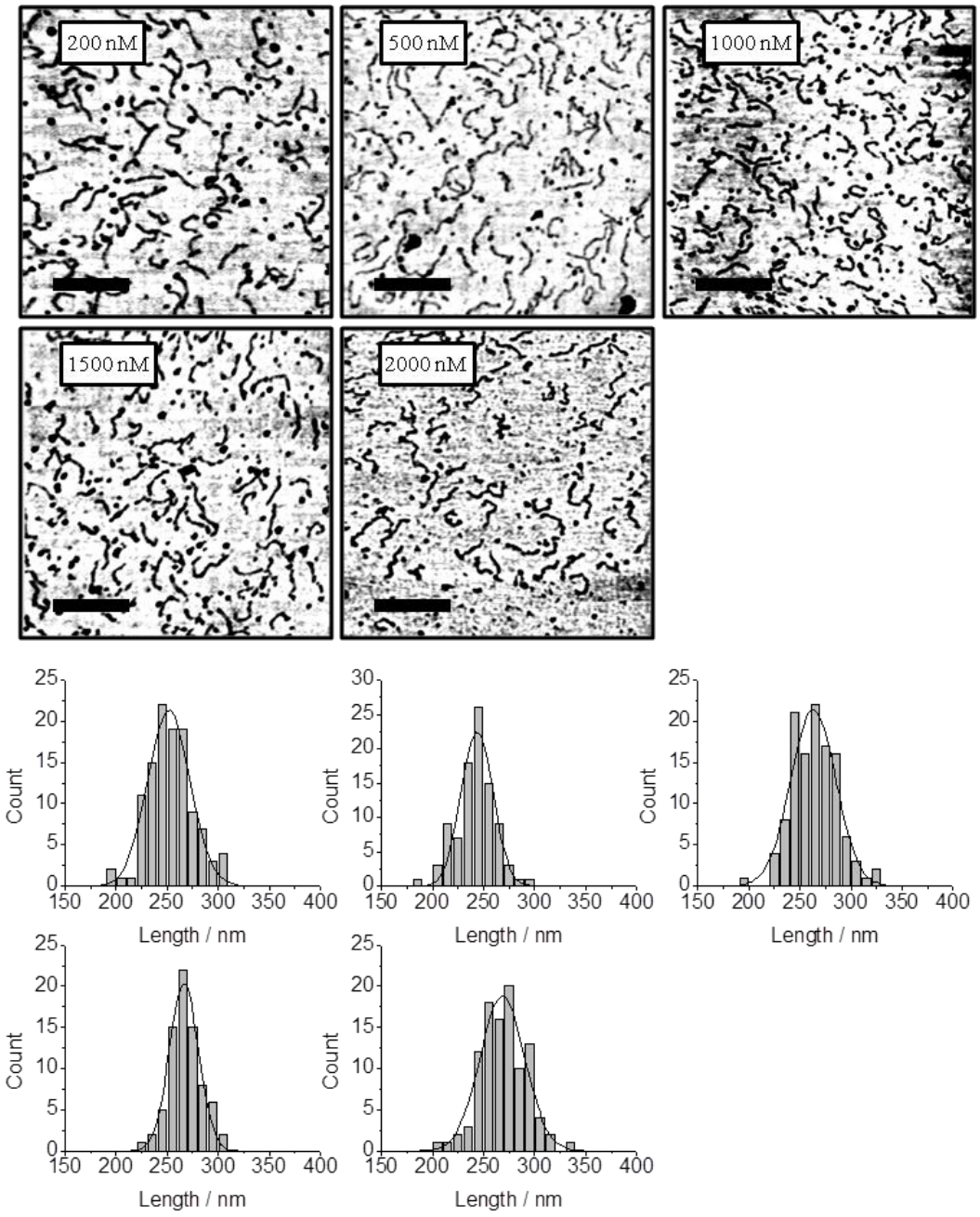

Figure 42 (above) AFM images of DNA bound to 9-aminoacridine (DNA concentration 1.9 nM). The concentration of the ligand is shown in the figure. Scale bars denote 500 nm (below) Histograms of the lengths of the DNA within each image, showing the distributions of measured lengths and the gaussian fitting of the data.

Table 12 Mean lengths of each population of DNA strands relative to the concentration of 9-aminoacridine. These results show an unexpected contraction in DNA length at 500 nM.

Concentration / nM	Ligand to BP ratio	Mean length / nm	SE / nm	n
0	0.000	257.8	1.6	119
200	0.079	251.8	0.7	113
500	0.197	243.8	0.7	93
1000	0.394	263.0	1.3	116
1500	0.591	266.4	0.7	76
2000	0.789	268.5	1.4	103

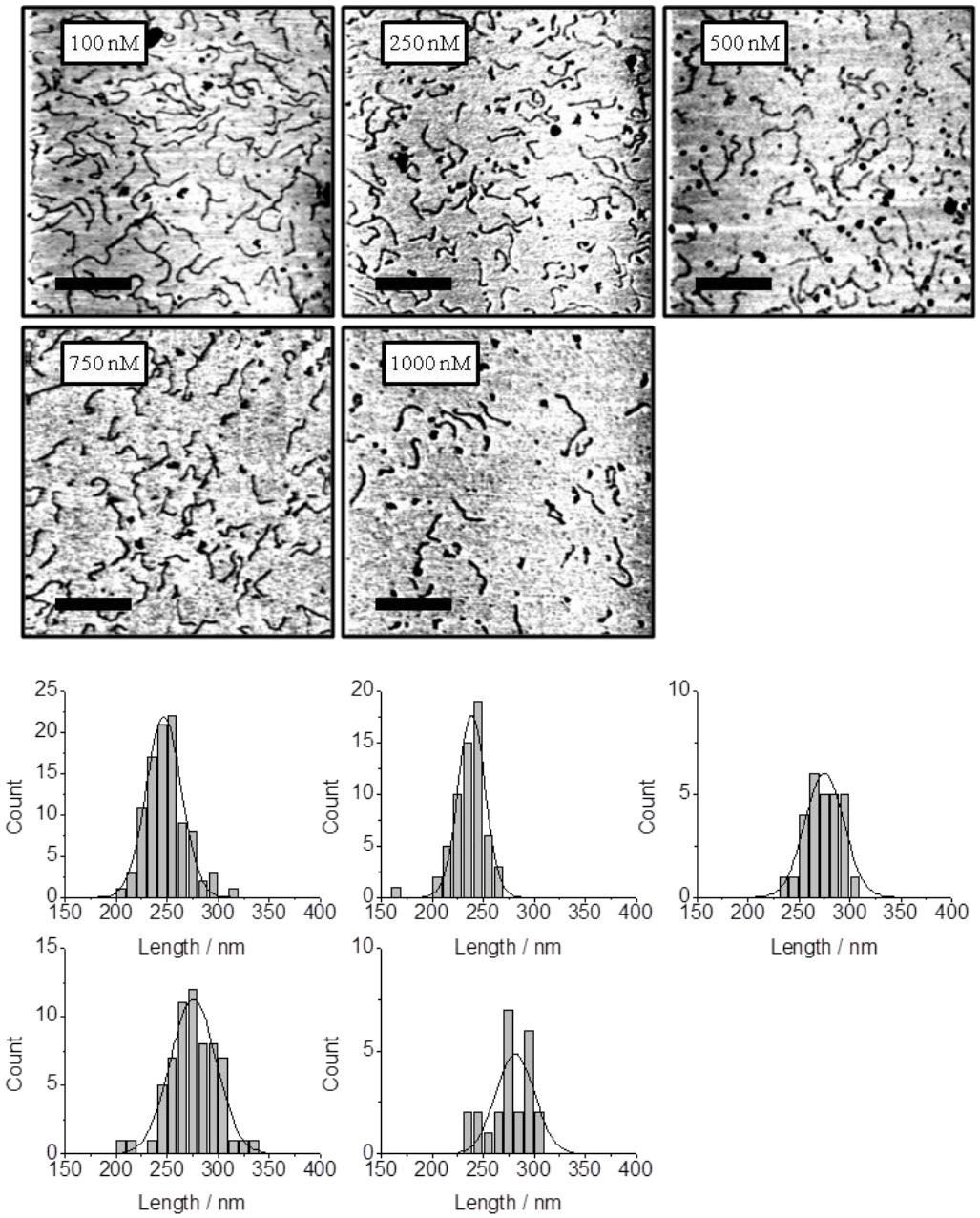

Figure 43 (above) AFM images of DNA bound to bisacridine 1 (DNA concentration 1.9 nM). The concentration of the ligand is shown in the figure. Scale bars denote 500 nm (below) Histograms of the lengths of the DNA within each image, showing the distributions of measured lengths and the gaussian fitting of the data.

Table 13 Mean lengths of each population of DNA strands relative to the concentration of bisacridine 1. These results show a similar contraction in DNA length to that observed with 9-amino acridine.

Concentration / nM	Ligand to BP ratio	Mean length / nm	SE / nm	n
0	0.000	257.8	1.6	119
100	0.039	246.8	0.8	99
250	0.099	238.9	0.7	61
500	0.197	274.8	1.3	28
750	0.296	275.7	1.3	64
1000	0.394	281.5	3.3	24

AFM imaging was first conducted using bisacridine 1 and 9-aminoacridine, a monointercalator. Data obtained for these two ligands are presented in Figure 42 and Table 12 for 9-aminoacridine, and Figure 43 and Table 13 for bisacridine 1. The overall changes that were observed in the length of DNA bound to increasing concentrations of these two compounds are shown in Figure 44. These results are somewhat surprising and reveal a contraction in the length of the DNA at low ligand concentrations that precedes lengthening.

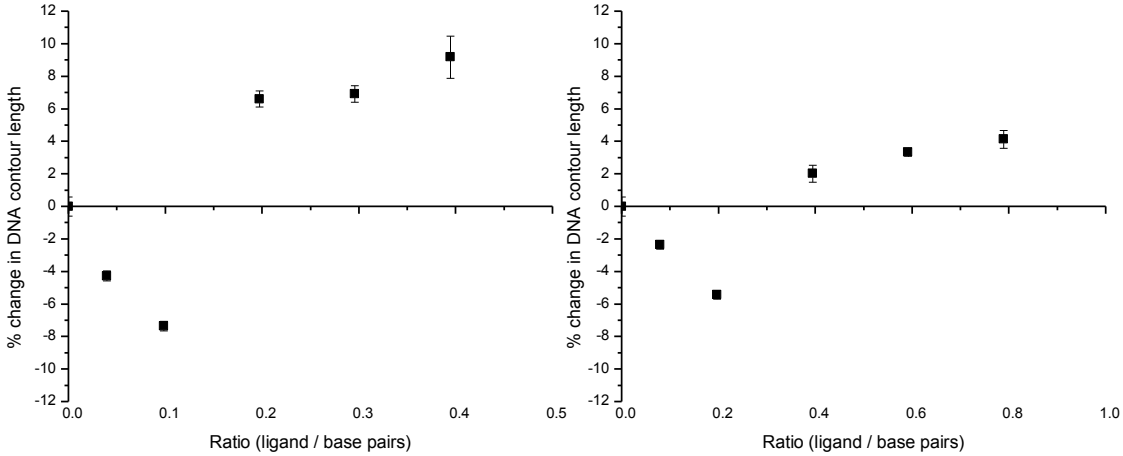

Figure 44 Comparison of the changes in DNA length observed after addition of increasing concentrations of a Bisacridine 1 (left) and 9-aminoacridine (right). Both plots show the initial contraction in DNA length that is followed by a progressive lengthening and a plateau.

As discerned from AFM imaging of experiments conducted with echinomycin and doxorubicin, there is a difference in the ratio of ligand to base pairs at which the lengthening of the DNA begins to plateau, approximately 0.2 for bisacridine 1, and 0.4 for the monointercalator. There is also a difference in the length of the DNA strands at which this plateau is observed, the length of the DNA strands bound to the bisintercalator being approximately 5% greater than those bound to the monointercalator. Given that the acridine chromophore in these compounds is identical, it may be that the inert alkyl linker of the bisacridine plays a role in determining the binding behaviour of the ligand.

Further studies were conducted using the bisintercalators that incorporated a modification to the inter-chromophore linker and a carboxamide substituent at the 4' position of the acridine. The proposed significance of these modifications to the binding mode of the ligand has been discussed in Chapter 1. Data for compounds bisacridine 2 and bisacridine 3 are presented in Figure 45 and Table 14, and Figure 46 and Table 15 respectively.

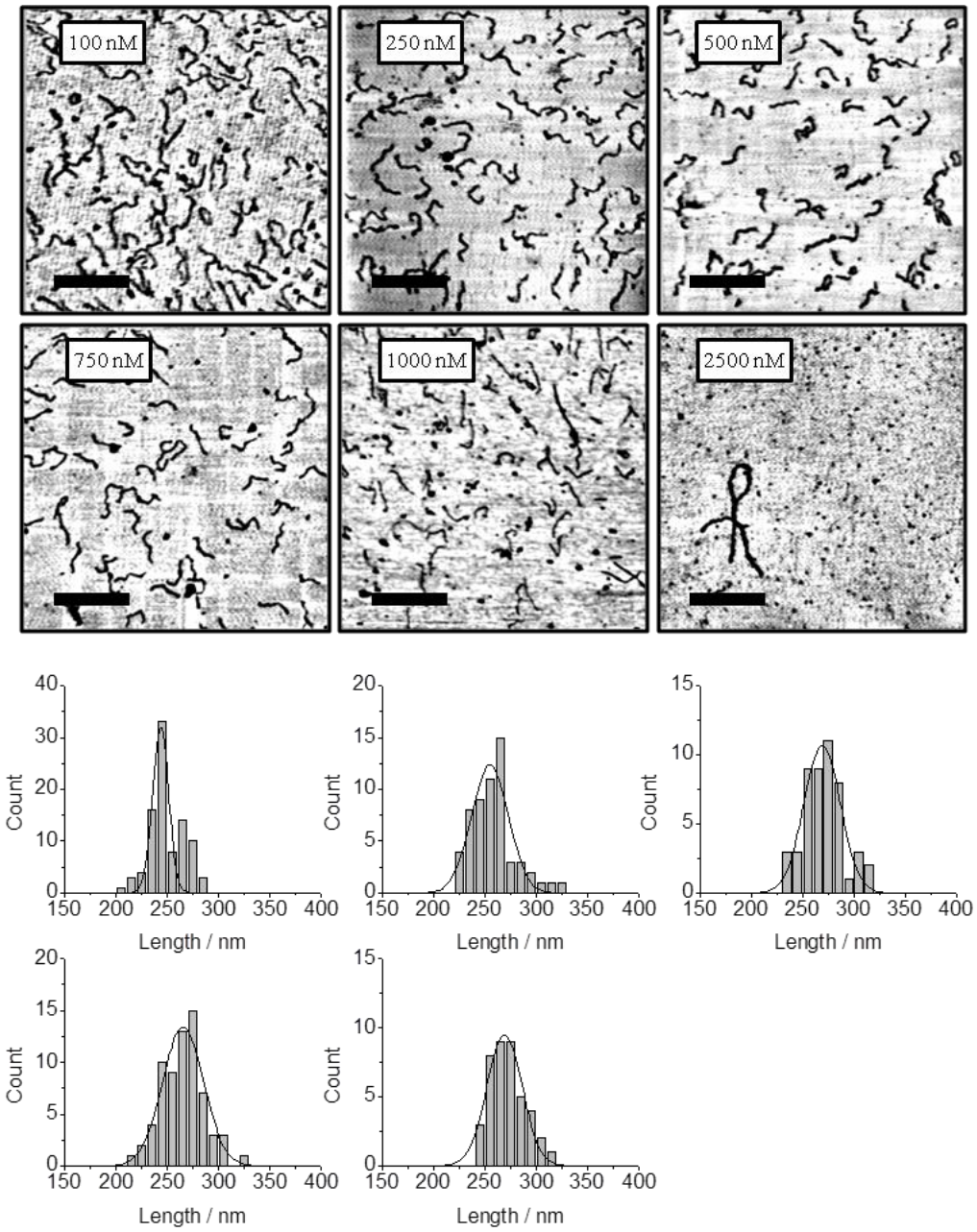

Figure 45 (above) AFM images of DNA bound to bisacridine 2 (DNA concentration 1.9 nM). The concentration of the ligand is shown in the figure. Scale bars denote 500 nm (below) Histograms of the lengths of the DNA within each image, showing the distributions of measured lengths and the gaussian fitting of the data.

Table 14 Mean lengths of each population of DNA strands relative to the concentration of bisacridine 2. Measurements were not taken at a concentration of 2500 nM.

Concentration / nM	Ligand to BP ratio	Mean length / nm	SE / nm	n
0	0.000	257.8	1.6	119
100	0.039	243.7	1.1	92
250	0.099	254.9	1.6	58
500	0.197	269.1	1.3	49
750	0.296	265.5	1.3	68
1000	0.394	269.2	0.9	41
2500	1.037	-	-	-

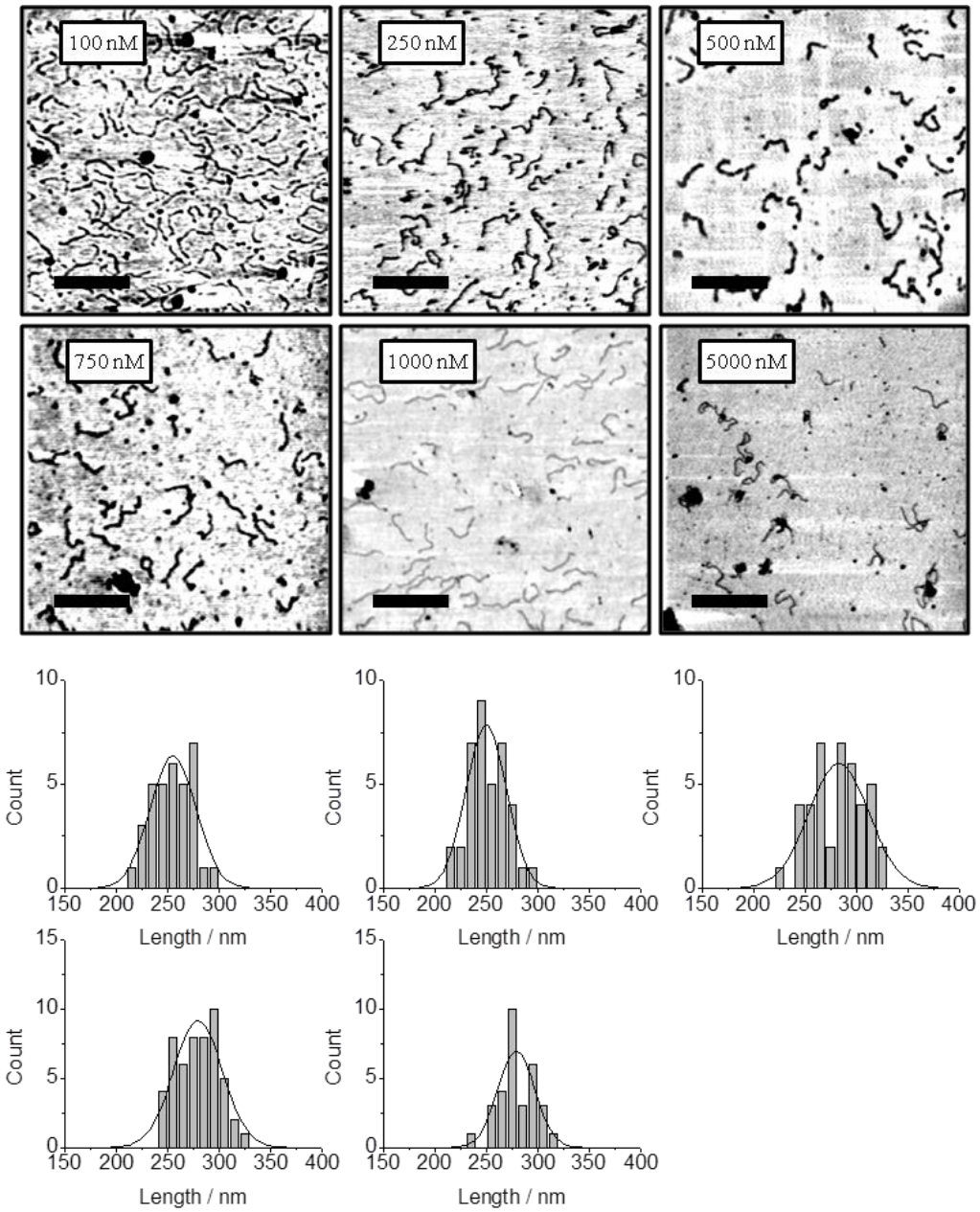

Figure 46 (above) AFM images of DNA bound to bisacridine 3 (DNA concentration 1.9 nM). The concentration of the ligand is shown in the figure. Scale bars denote 500 nm (below) Histograms of the lengths of the DNA within each image, showing the distributions of measured lengths and the gaussian fitting of the data.

Table 15 Mean lengths of each population of DNA strands relative to the concentration of bisacridine 3. Measurements were not taken at concentrations greater than 1000 nM.

Concentration / nM	Ligand to BP ratio	Mean length / nm	SE / nm	n
0	0.000	257.8	1.6	119
100	0.039	255.2	1.9	34
250	0.099	249.9	1.6	38
500	0.197	283.0	3.5	42
750	0.296	279.5	1.9	52
1000	0.394	279.2	2.3	31
5000	2.075	-	-	-

The results obtained with these acridines are provided in Figure 47. Addition of bisacridine 2 resulted in a significant contraction of the DNA at very low concentrations of the ligand, whereas the addition of bisacridine 3 produced a less marked shortening of the DNA, followed by a degree of lengthening at higher concentrations. These findings were broadly comparable to those made with bisacridine 1 and 9-aminoacridine, with subtle variations in behaviour between each ligand likely reflecting the slightly different structural chemistry of each compound.

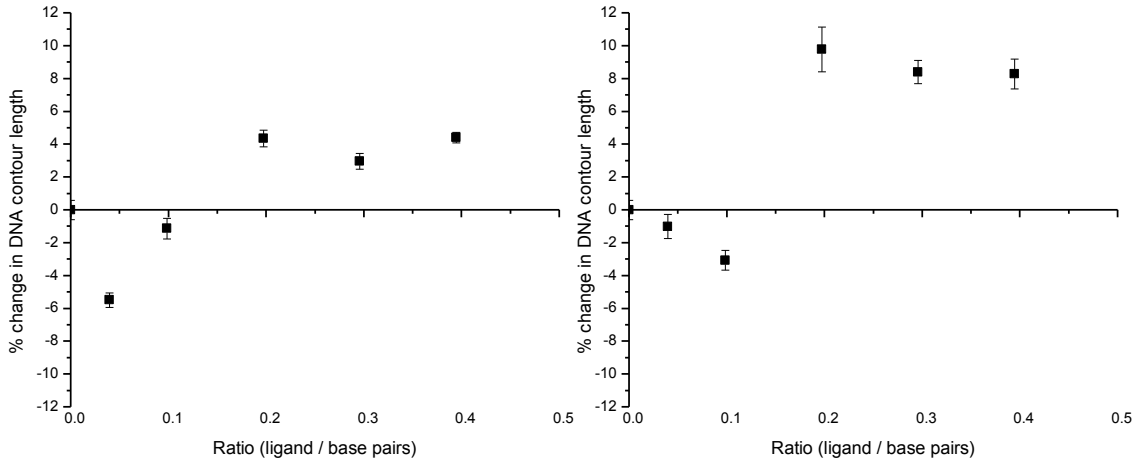

Figure 47 Comparison of the changes in contour length of DNA observed on addition of increasing concentrations of bisacridine 2 (left) and bisacridine 3 (right). As with 9-amino acridine and bisacridine 1, the initial contraction in the DNA gives way to a progressive lengthening and a plateau.

The changes observed with these acridine compounds are exceptionally difficult to compare, since there is no pharmacological model that describes the relationship between a contraction of the DNA and the corresponding increase in contour length due to intercalation of the acridine chromophore. Certainly the conventional approach of McGhee and von Hippel may not be applied directly to the data presented in Figure 44 and Figure 47. Although discrepancies between observed changes in DNA length and those calculated by theoretical approximation could be explained previously by differences in the helix extension parameters of echinomycin, doxorubicin and TANDEM from the classical value of 0.34 nm, the changes observed on binding of the acridines must incorporate a deformation of the DNA duplex. Localised changes in base stacking arrangements have been observed at intercalation sites with many different ligands.[8] The existence of Hoogsteen base pairs at some echinomycin intercalation sites has already been discussed in Chapter 2. However, given the low ratio of ligand to base pairs at which the contraction is occurring, these changes, in the case of the acridines at least, must be far more long range than had previously been thought.

A crystal structure of 9-aminoacridine, bound to an ApU residue revealed significant distortion of the arrangement of the nucleotides.[116] Although this structure may not be directly applicable to DNA since it contains a uracil nucleobase, the authors noted that the orientation of the intercalated bases did not conform to accepted structures of RNA.

The first crystal structure of an intercalated DNA complex was published in 1978.[117] Although the ligand in this study was a platinum based compound and not an acridine, the authors observed that the sugar pucker of the intercalated DNA adopted a similar pattern to that of an intercalated RNA complex. A later study of the complex between an analogue of proflavin and DNA revealed that the structure of the intercalated DNA complex shared many features with A form DNA.[118-119]

Molecular modeling studies have also suggested that acridine chromophores may induce A form character in DNA.[120] The so called ICR model, describing the structure of DNA intercalated with proflavin, exhibits many similarities with A form DNA. Here, both major and minor grooves of the intercalated DNA are significantly wider than in classical B DNA, the minor groove extending from 6 Å in its B form to 9.1 Å when intercalated (11 Å in the A form).[121] A change in the sugar pucker of the DNA was also observed, from C2' to C3'-endo, characteristic of A form DNA. Importantly, these changes occurred at low ligand concentrations, with the intercalator inducing deformations in the DNA some distance from the actual binding site. However, to date this binding model has not been corroborated by direct experimental data.

More recently, the existence of DNA in a hybrid A/B form has been demonstrated by Kypr et al.[122] Using a combination of CD and NMR, a DNA sequence where the duplex exhibited the physical characteristics of the A conformation was found to retain the C2'-endo pucker of the B conformation. Though an alternative arrangement to that described by the ICR model, both of these studies highlight the capacity of DNA to undergo transitions between conformations that are not described by the canonical categories of A, B and Z.

While the question of DNA conformation cannot be definitively resolved via AFM imaging, assuming that the binding of bisacridines to DNA induces a change from a B to an A conformation permits the data from Figure 44 and Figure 47 to be presented in a different manner. Figure 48 and Table 16 shows a reassessment of Figure 44 and Figure 47 that assumes the DNA to be in the A, as opposed to the B, conformation. Obviously such an assumption is not without its limitations. Not least, during the process of contraction that occurs during binding of low concentrations of a ligand, the DNA is most likely in a range of

different conformations. However, at a ratio of 0.1 ligands to base pairs (or 0.2 in the case of 9-aminoacridine), the extension of the DNA as a consequence of ongoing intercalation begins to outweigh any shortening of the DNA that may result from ligand induced deformation of the B-duplex.

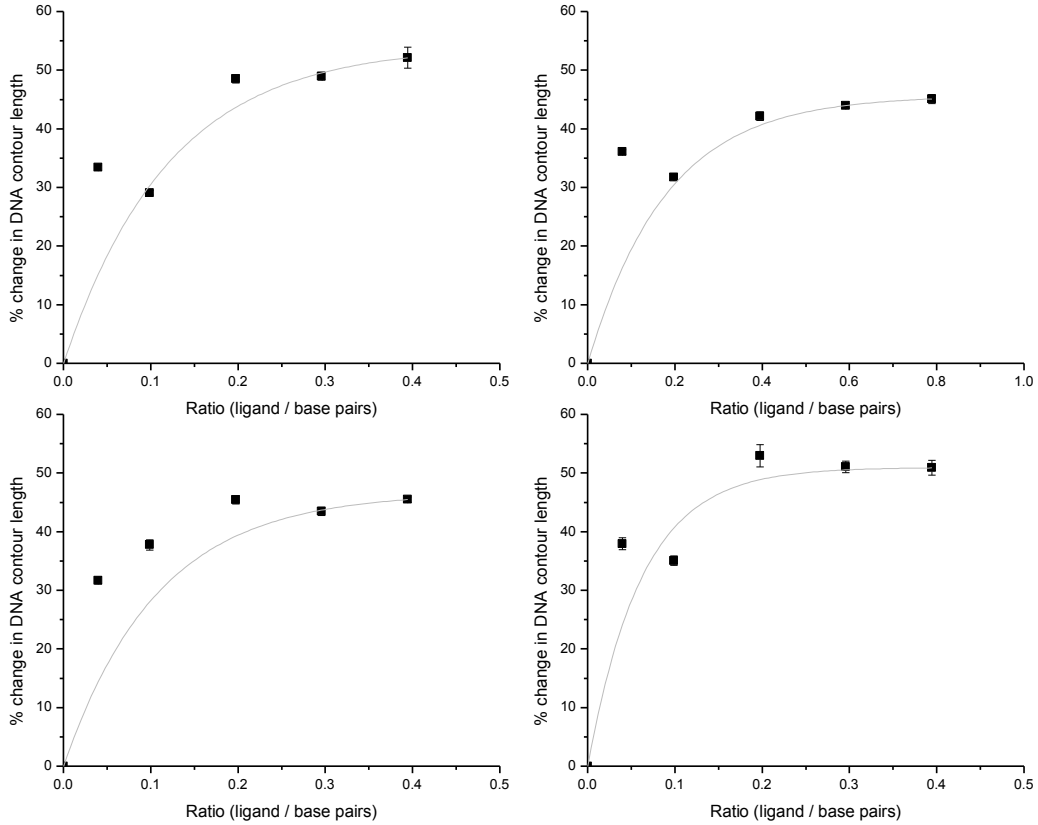

Figure 48 Comparison of changes in DNA length observed with the acridine compounds, assuming the DNA to be in the A conformation. Clockwise from top left, bisacridine 1, 9-aminoacridine, bisacridine 3, bisacridine 2. The poor fit of points at low ligand to base pair ratios reflects the likelihood that during contraction, some portions of the DNA remain in a B form. The exponential fits suggests a linear increase in strand length followed by the plateau at higher ligand concentrations that has been observed for all the ligands in this study.

Looking solely at the shape of the graphs in Figure 48, the assumed change in DNA conformation, and importantly, the change in spacing between the base pairs of the primary sequence from 0.34 nm to 0.24 nm would appear to resolve the problem of an observed contraction in the length of the DNA. However, as previously stated, a range of helix extension lengths have been reported for different compounds. That each different acridine should extend the DNA helix to the same degree, and bind to the DNA to the same extent, seems unlikely. At the same time, contraction of the DNA in itself does not necessarily constitute a change in conformation. The historical value of 0.34 nm for the distance between adjacent base pairs in the helix is an average value derived from measurements of

longer stretches of DNA, where this distance has been shown to range from 0.25 to 0.42 nm.[8]

Table 16 A comparison of the final observed increase in DNA contour length between the different acridines, highlighting the difference in these values when the DNA is assumed to enter a different configuration. Increases in strand length for the B form DNA were determined by taking a mean average of the length of the strands at ligand concentrations exceeding the point of saturation.

Ligand	% change in DNA contour length (B Form) (SE)	% change in DNA contour length (A Form) (SE)
9-aminoacridine	3.17 (0.62)	43.8 (0.9)
Bisacridine 1	7.57 (0.81)	49.9 (1.1)
Bisacridine 2	3.91 (0.47)	44.8 (0.7)
Bisacridine 3	8.82 (0.48)	51.7 (0.7)

Although unable to resolve precise helix extension parameters of individual compounds, these experiments have demonstrated AFM imaging to be sufficiently sensitive to distinguish between small changes in the length of individual molecules on a nanometer scale. This resolution has highlighted a distinction between the behaviour of sequence specific intercalators such as echinomycin and TANDEM, and a group of acridine based ligands. While echinomycin and TANDEM demonstrate a concentration dependent lengthening of the bound DNA that correlates with the particular sequence specificity of the ligand, the acridines are all observed to shorten the DNA before causing a slight lengthening at higher concentrations. Although this contraction may be explained by extensive deformation of the B duplex, leading to a reduction in the usual spacing between the base pairs, this interpretation is largely hypothetical and would need to be confirmed by further investigations.

It should be noted that the AFM protocol itself is not without limitations. Deposition of DNA on mica may, in part, be responsible for a reduction in the expected contour length of DNA molecules, although initial experiments into the reproducibility of measurements from AFM images of the kind used here would seem to allay this concern. Moreover, no shrinking was seen with either echinomycin or doxorubicin, though these compounds were analysed using the same surface preparation techniques as the acridines. Previous studies have also observed a reduction in the number of DNA molecules that may adhere to mica following binding to a ligand.[75] Although this would not explain a contraction in the length of the DNA, it would explain why DNA saturated with a ligand, and therefore (presumably) showing an extensive degree of lengthening, would not be observed during imaging since it would not have

adhered to the mica surface. The study by Tseng et al. attributed the reduction in DNA volume to variations in the GC/AT content of the particular DNA strands that they were studying, and in our case was not apparent with echinomycin or doxorubicin. However, there was a noticeable reduction in the amount of visible DNA at high concentrations of the bisacridines. This was almost certainly a consequence of inter-molecular binding activity (Figure 49), since it was not apparent with the monointercalator 9-aminoacridine or echinomycin, and may be discerned in the peculiar DNA aggregates observed at high concentrations of ligands such as bisacridine 3 (Figure 46).

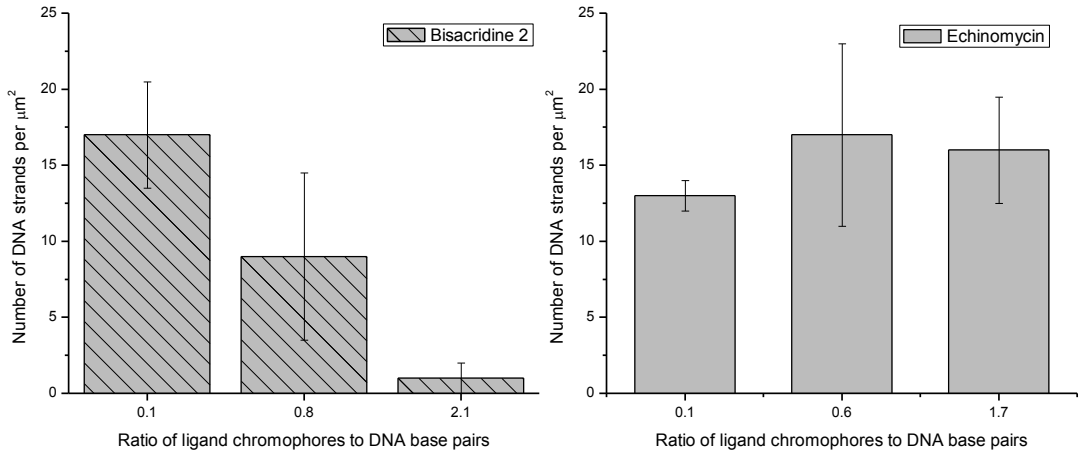

Figure 49 Comparison of the amount of DNA visible on mica at different concentrations of the two bisintercalators bisacridine 2 and echinomycin. While the average number of DNA strands per μm^2 stays roughly the same with echinomycin, there is a noticeable drop with the bisacridine.

Investigating conformational changes of DNA in air using FTIR

Although the issue of DNA conformation under the conditions of AFM imaging has been extensively discussed,[123-124] the conundrum of the observed shrinking that had been observed following binding of the DNA to acridine intercalators required further investigation. In order to ascertain whether or not a conformational change from the B to the A conformation could occur under normal laboratory conditions, experiments were conducted using FTIR. The change from B to A form DNA that occurs when DNA is allowed to dry has been followed at room temperature using FTIR and reported results would suggest that this change occurs rapidly.[125] Using this existing protocol, spectra were obtained for a sample of DNA under the same atmospheric conditions as those samples analysed by AFM.

Samples were prepared using CT-DNA (Sigma, UK), at a stock concentration of 1mg/ml. A 5 µl aliquot of the DNA solution was deposited on the ATR crystal of the FTIR apparatus and gradually allowed to dry. Spectra were obtained at 60 second intervals under standard

conditions. The FTIR signal was monitored in this way for several hours, with changes in the DNA spectra readily apparent after approximately 40 minutes.

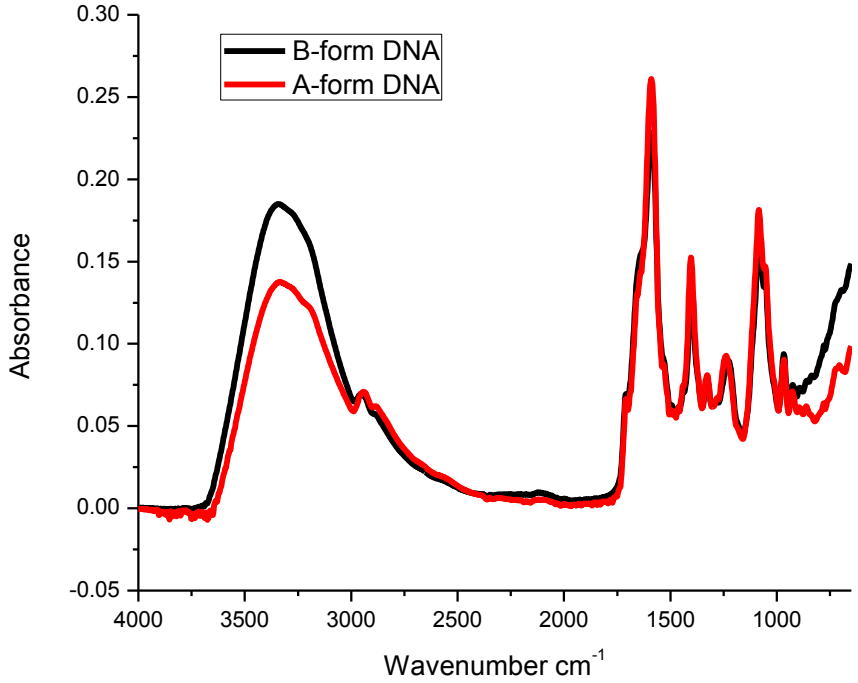

Figure 50 FTIR spectra of CT-DNA for both the B-form and the A-form. Deposition of the DNA in aqueous solution was followed over a period of time and any peak shifts observed. The large band at approximately 3250 cm^{-1} is caused by water.

Figure 50 shows the obtained spectra for CT-DNA. The spectrum of B form DNA constitutes the first in the dehydration series and that of the A form after a period of 59 minutes has elapsed, when the sample has dehydrated to equilibrium with the ambient conditions of the laboratory. No further changes in the spectra were observed after this period of time. Both spectra closely resemble those reported in the literature, and bands were assigned accordingly.[125] Figure 51 highlights the section of these spectra where differences between the A and B conformations are most readily discerned. There is a marked shift in the wavenumber of the signal at 1225cm^{-1}, indicative of the antisymmetric phosphate group in DNA in a B conformation, towards 1238cm^{-1}, typical of the A form. Similarly, the shoulder at 1185cm^{-1}, indicative of the C3' endo-sugar phosphate of A form DNA, is absent from the B form spectrum. As such, a conformational change of the DNA under standard laboratory conditions may occur.

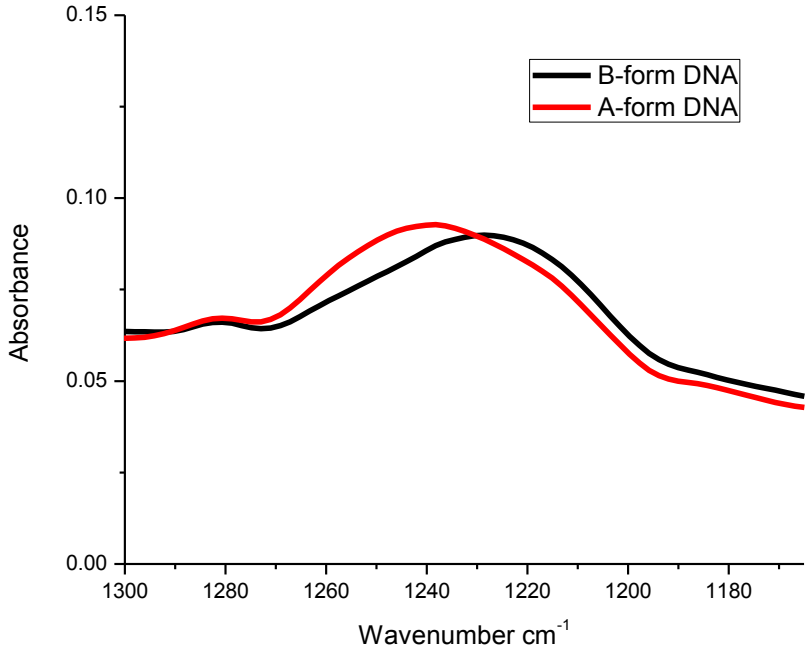

Figure 51 Enlargement of selected wavenumbers from Figure 50, where differences in the FTIR spectra of A and B DNA may be discerned, particularly the position of the peak around 1320 cm^{-1} and the shoulder at 1185cm^{-1}.

Although samples were freshly prepared and used immediately, the results of the FTIR measurements necessitated the further investigation of the stability of the DNA samples. Table 17 shows a comparison between the mean contour lengths of a freshly prepared DNA control sample of 771 base pair DNA, and the same sample after a period of twenty-four hours having been left in situ under the AFM head. As may be discerned from the table, the measured length of DNA strands from the same sample, taken after a twenty-four hour interval, is not significantly different. Both values correspond to the theoretical length of a 771 base pair fragment of DNA in a B conformation, which is 262 nm. This result suggests that once adhered to the mica, the DNA is trapped in a stable complex with the substrate and that this complex is stable for extended periods of time. Given that typical experiments with the ligands took periods of a few hours, it is therefore highly unlikely that the process of sample preparation is responsible for any observed changes in the length of the DNA.

Table 17 Comparison of the mean contour length of DNA strands taken from the same mica sample. One set of measurements were taken immediately, the other after 24 hours. There is no obvious difference in the length of either set of DNA strands.

Sample	Mean contour length / nm (SE)	n (strands measured)
DNA (t = 0)	257.8 (1.6)	119
DNA (t = + 24 hours)	258.6 (2.6)	35

Notwithstanding the results of these particular experiments, that seem to confirm that the DNA does remain in a B conformation, this issue was never really in doubt.[124] Numerous studies have confirmed that adsorption of DNA on mica does not induce a conformational change that is reflected by a shrinking of the physical length of the molecule. However, given the fact that the preparation of the DNA for AFM imaging does not appear to cause a contraction in the length of the DNA that may indicate a conformational change, and that experiments with echinomycin and TANDEM demonstrated a purely linear relationship between contour length and ligand concentration, the contraction observed with the acridine compounds would appear to be solely a consequence of the ligands themselves. In order to investigate the nature of these potential changes, further experiments were conducted using a solution based protocol.

Following conformational changes of DNA in solution using CD

One means of differentiating between the various DNA conformations is the technique of circular dichroism.[126] Changes in DNA secondary structure may be discerned by their differing effects on the rotation of a beam of polarised light. CD spectra of A and B form DNA are significantly different, permitting straightforward comparison. The intercalation of DNA with various ligands has already been followed using this technique.[127]

Experiments were conducted using the same ligands that had been analysed via AFM. Limitations to the sensitivity of the apparatus necessitated a higher concentration of DNA than had been used for the AFM imaging. Samples were prepared using CT- DNA (Sigma, UK) at a stock concentration of 1 mg/ml (3007 µM in DNA base pairs). The control was prepared by the addition of 20 µl of 200 µM NaCl to 20 µl of DNA. The volume was made up to 200 µl by the addition of tris buffer (pH 7.4). 1 µl of the appropriate concentration of each ligand was added to this volume and mixed. In the case of bisintercalators, a stock solution of 3 mM was used. To preserve the ligand to base pair ratios for direct comparison between bisintercalators and monointercalators, stock solutions of 6 mM were used for the monointercalators. The effect of the increase in volume (from 200 µl to 205 µl) on the concentrations of the DNA and the ligands was not considered to be significant.

The A form of CT-DNA was induced by the substitution of the tris buffer with ethanol. Reference spectra were obtained for both the B and the A conformations of CT-DNA and these are shown in Figure 52. The spectra obtained corresponded well to those reported in the literature.[128] The broad positive peak between 240 and 280 nm is typical of DNA in its B form, while the A form is distinguished by the larger positive peak at these wavelengths and a distinct negative peak at 210 nm.

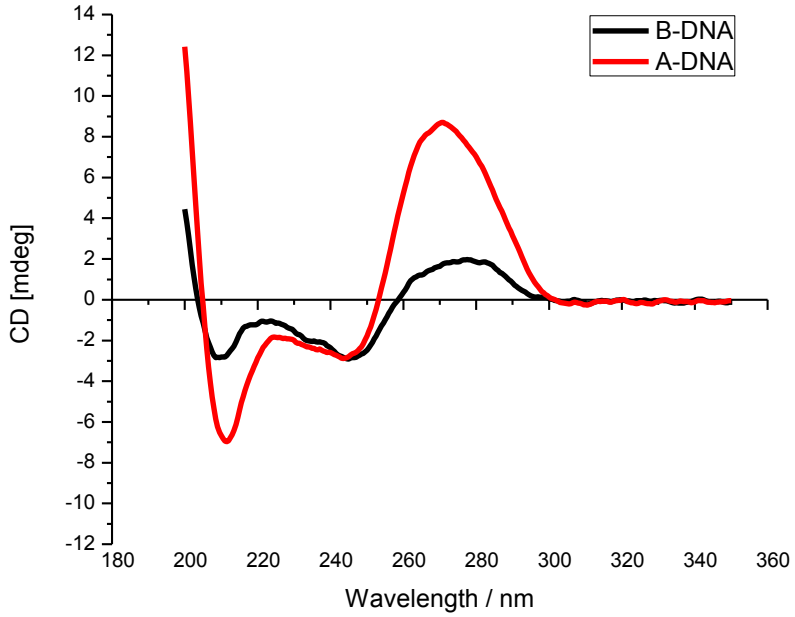

Figure 52 CD spectra of the A and B conformations of CT-DNA, showing the large negative peak at 210 nm that is typical of A-form DNA.

A control experiment was conducted where only buffer, in equivalent volumes to the ligand, was added to a solution of the DNA. This experiment confirmed that the buffer itself did not interfere with the DNA signal in any way, and even the slight increase in volume of the system following addition of the buffer, did not lead to any noticeable differences (Figure 53).

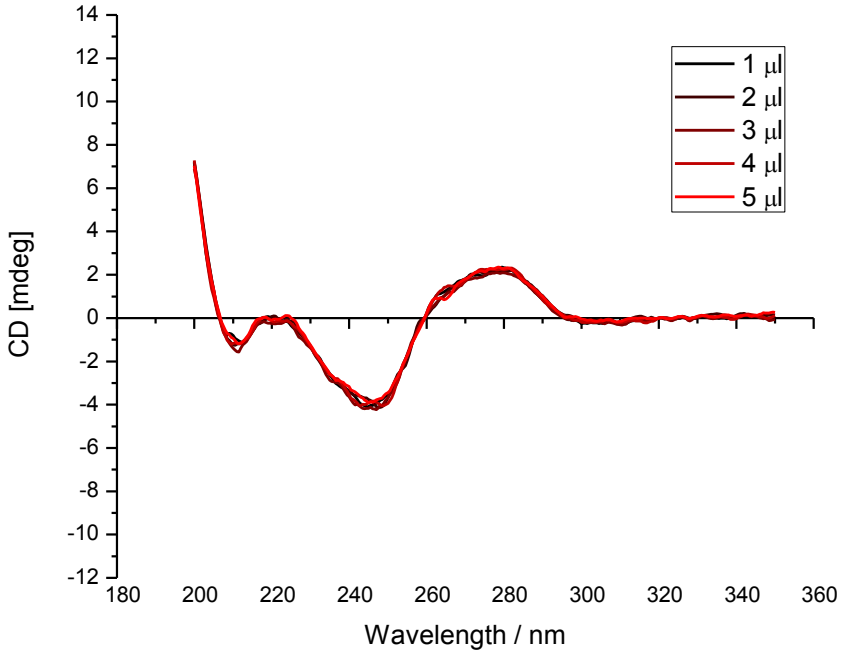

Figure 53 Addition of buffer to a solution of CT-DNA results in no changes to the spectrum. The legend denotes the volume of buffer added, each in 1 µl aliquots.

AFM imaging experiments of DNA bound to different intercalators had allowed a 1 hour incubation time after the addition of the ligand to the DNA before an experiment was conducted. Due to practical considerations regarding the use of instrumentation, such a time allowance was not possible for any experiments with CD. However, the incubation time of 1 hour that had been previously utilised was somewhat arbitrary, and different studies of intercalators have used different incubation periods of time.[33, 75] To investigate the effect that time might have on the appearance of CD spectra, a sample was prepared using bisacridine 2. Three, 1 µl aliquots of 3mM bisacridine 2 were added to the DNA solution. Spectra of the same sample were then obtained after periods of 5 minutes and 1 hour. No significant differences could be discerned between the spectra obtained after these different periods of time (Figure 54).

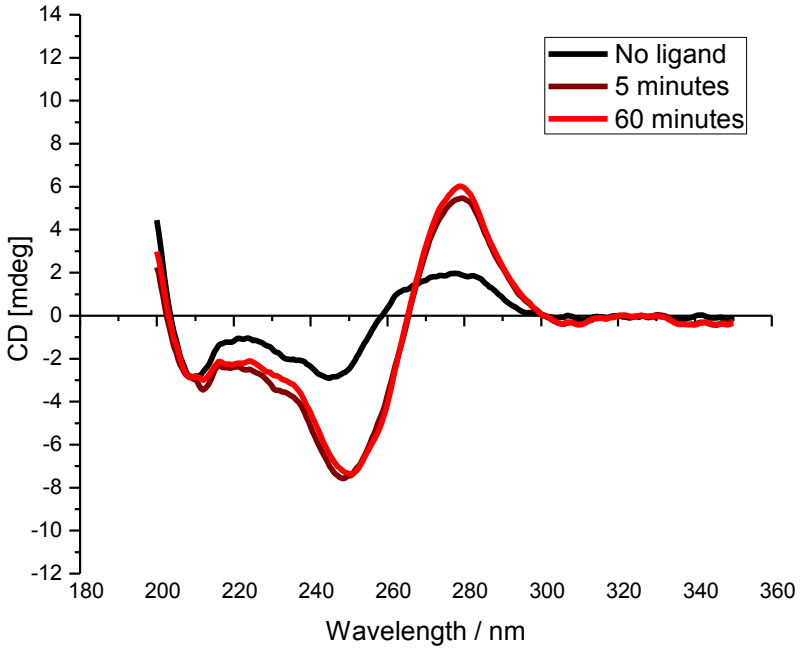

Figure 54 CD spectra of CT-DNA bound to bisacridine 2. The legend refers to the periods of time that the sample was allowed to incubate. There is a very slight divergence of the spectra at approximately 235 nm, but otherwise, relative to the DNA without ligand, the change in the DNA signal after the two incubation periods is entirely the same.

To ascertain an appropriate concentration range over which to conduct the experiments, bisacridine 2 was added to the DNA solution at increasing concentrations, over a range of chromophore to base pair ratios from 0 to 0.7. This experiment revealed stages in the binding process that would need to be considered for further studies. These data are provided in Figure 55.

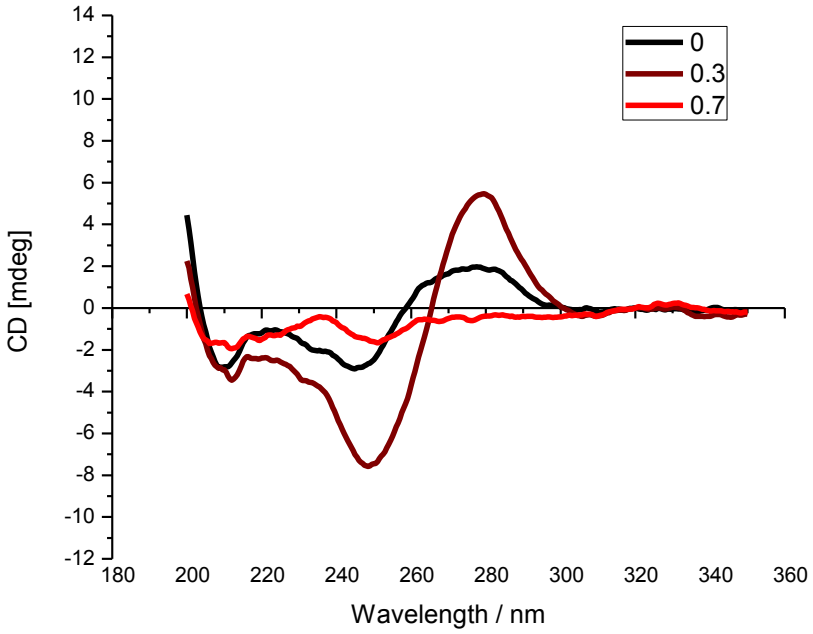

Figure 55 Addition of bisacridine 2 to CT-DNA (DNA concentration 300 µM in base pairs). Values reported in the legend correspond to the ligand chromophore to base pair ratio. At a ratio of 0.3, a marked change in intensity of the DNA signal may be observed at 280 and 250 nm. At a ratio 0f 0.7 the intensity of the signal, across the whole wavelength studied, has almost returned to zero.

At a chromophore to base pair ratio in excess of 0.5 (1 chromophore per 2 base pairs), the dramatic reduction in signal intensity is likely to be due to precipitation of the DNA. This conclusion is supported by the observation that at these high ligand concentrations, aggregated material began to appear in the cuvette that could only be removed by soaking in concentrated nitric acid. Without proper cleaning, this residue interfered with the spectra of subsequent experiments and as such, experiments were limited to a concentration range that did not exceed a chromophore to base pair ratio of 0.5. Since this ratio corresponds to the maximum degree of intercalation stipulated by the neighbour exclusion principle, experiments in excess of this value were deemed to be unnecessary.

Unfortunately, the natural products echinomycin and doxorubicin proved to be unsuitable for analysis in this fashion. Due to the chiral nature of the compounds, a signal, attributable to these compounds, was observed.[129] These signals overlapped that of the DNA, making comparison between the spectra of these compounds and the reference samples impossible. In the case of echinomycin the problem was two-fold. The DMSO content of this poorly water soluble molecule also induced a large signal at 210 nm, again overlapping the DNA signal. Spectra obtained for these compounds, in the absence of DNA, are available in Figure 56. These difficulties did not apply to the acridine compounds since none contained any chiral centres and all were soluble in water at the concentrations used.

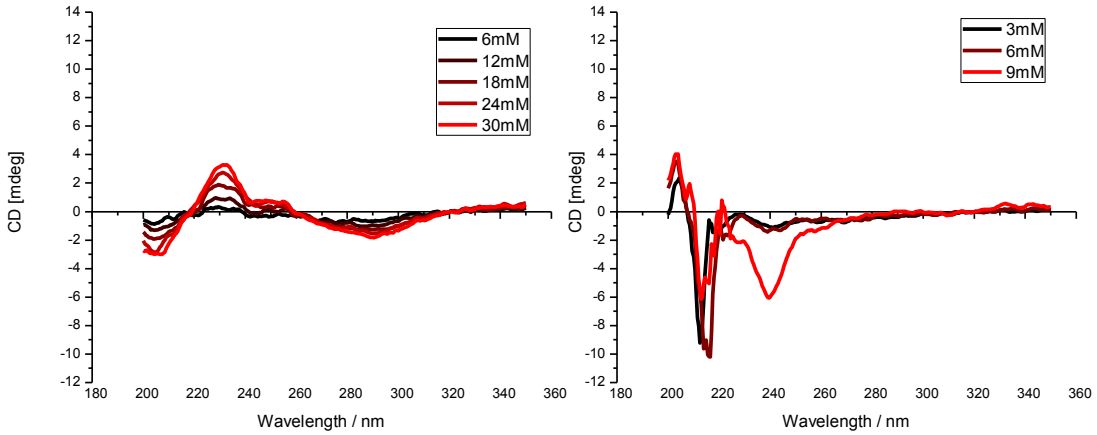

Figure 56 Comparative spectra of doxorubicin (left) and echinomycin (right). Doxorubicin shows a negative band between 260 and 300 nm, and a positive band between 220 and 240 nm. Echinomycin yields two negative bands, one at 240 and the other at 220 nm. The positive band at 210 nm is caused by the presence of DMSO. The legend refers to the concentration of the ligand that was added to the cuvette, in 1 µl aliquots.

Figure 57 illustrates the spectra obtained for the various acridine based compounds. In the case of the monointercalator 9-aminoacridine, and the alkyl linked bisacridines 1 and 2, changes are seen in the intensity of the positive band at 260 nm and the negative band at 240 nm. No meaningful change in the intensity of the band at 210 nm occurred during titration of these ligands. However, the rigid linked bisacridine 3 yielded a spectrum considerably different to those of the reference spectra and the other ligands. In the case of this compound, there is a noticeable change in the spectrum between 210 and 240 nm. Moreover, there is a significant change in the position of the peak between 260 and 280 nm, with there being a concentration dependent shift towards higher wavelengths. In the case of bisacridine 1 and bisacridine 2, the position of this peak remains unchanged over the range of ligand concentrations used, there being a distinct isodichroic point at approximately 260 nm. The loss of the isodichroic point in the case of bisacridine 3 would support the hypothesis that the DNA is undergoing a conformational change during the binding of this ligand.

The fact that none of the compounds demonstrate spectra similar to that of A form DNA suggests that the contraction observed in the length of the DNA during AFM imaging did not constitute a conformational change to the A-form. However, this may be an oversimplification. All four acridines, and noticeably bisacridine 3, show an increase in the intensity of the negative band at 210 nm as the concentration of the ligand, relative to that of the DNA, is increased. Similarly, though with the exception of bisacridine 3, there is an accompanying increase in the intensity of the band between 260 and 280 nm. Since ellipticity is derived from the precise arrangement of the nucleotides in a DNA strand, it is clear that intercalation of the DNA is causing a rearrangement of the bases. This principle is

well established, and as previously discussed, there are several elegant treatments of the precise mechanism of DNA intercalation in the literature.[51, 130-132] Although the intercalated DNA complexes do not therefore conform to the classical A form model, it is possible that they incorporate a degree of A form character. Certainly evidence from these studies demonstrates that the DNA does not remain in a strict B conformation.

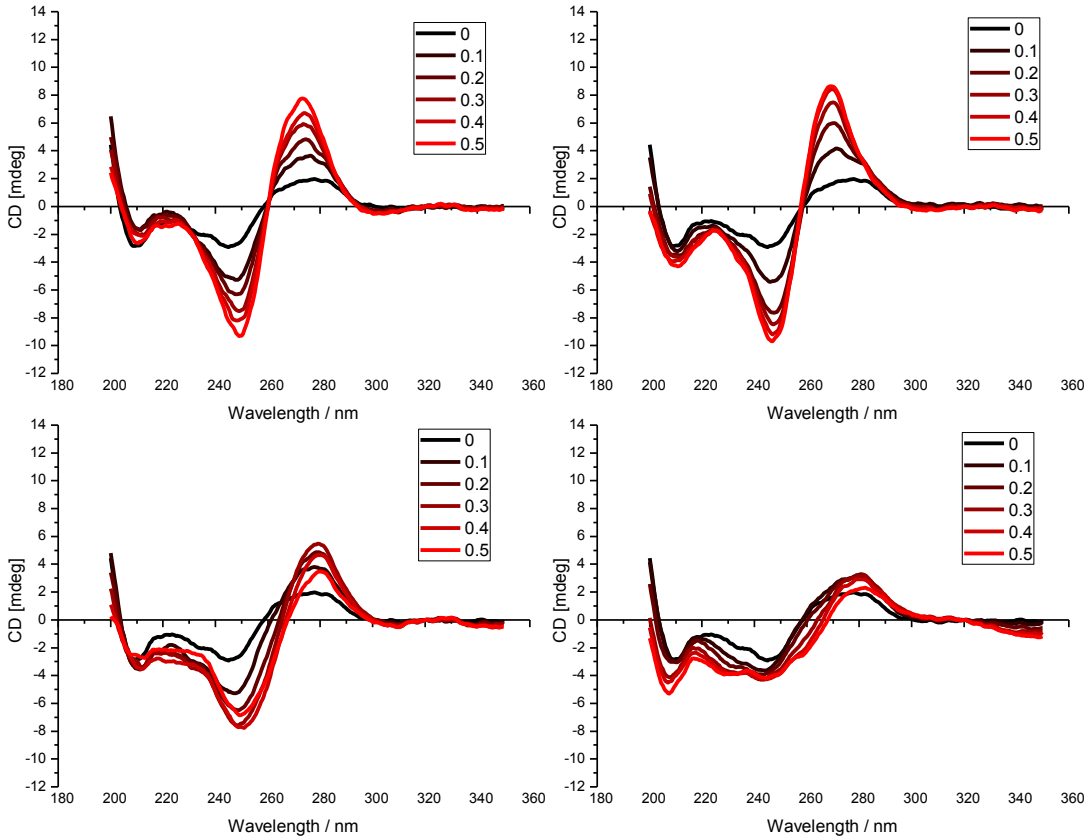

Figure 57 Spectra of CT DNA bound to four different acridine intercalators (DNA concentration 300 µM in base pairs). The legend denotes the ratio of ligand chromophores to DNA base pairs. Clockwise from top left, Bisacridine 1, 9-aminoacridine, bisacridine 3 and bisacridine 2. The spectrum for bisacridine 3 is noticeably different to those of the other compounds, and suggests that the linker in this compound is affecting the binding mode of the ligand. The induced ellipticity apparent with this compound at 340 nm, and the reduced intensity of the bands at high ligand concentrations, also suggests some precipitation of the DNA.

The sensitivity of this technique is apparent from the differences that may be observed between bisacridine 1 and bisacridine 2. While bisacridine 1 yields a spectrum remarkably similar to that of 9-aminoacridine, the bisacridine literally being a dimerised 9-aminoacridine moiety, the intensity of the changes in the bands at 260 and 240 nm is less noticeable with bisacridine 2. The band between 260 and 280 nm is also slightly shifted towards higher wave lengths in the case of the latter. Given that the only difference between bisacridine 1 and bisacridine 2 is the substitution of the acridine chromophore with a carboxamide, this

difference most likely reflects the threading nature of bisacridine 2 and its capacity to interact not only with the minor but also the major grove of the DNA duplex.

That bisacridine 3 yields a spectrum somewhat different to the other compounds requires further mention. The changes in the band at 220 nm may reveal a conformational change in the DNA that is not observed elsewhere. However, this is not the only possibility. Other studies of ligand-DNA interactions have proposed that this band may be indicative of a condensation of the DNA.[126] Although the decrease in band intensity that was highlighted in Figure 55 was considered to be indicative of precipitation, the band at 220 nm may reflect a different form of binding mechanism. While bisacridine 1 and bisacridine 2 incorporate a flexible alkyl linker, the linker in bisacridine 3 is more rigid in character and, although experimental findings are mixed, there is speculation as to whether or not bisacridines of this kind are too constrained to adopt the normal staple like conformation necessary for bisintercalation.[19] A comparison of bisacridine 3 with another rigid bisacridine, bisacridine 4, is provided in Figure 58.

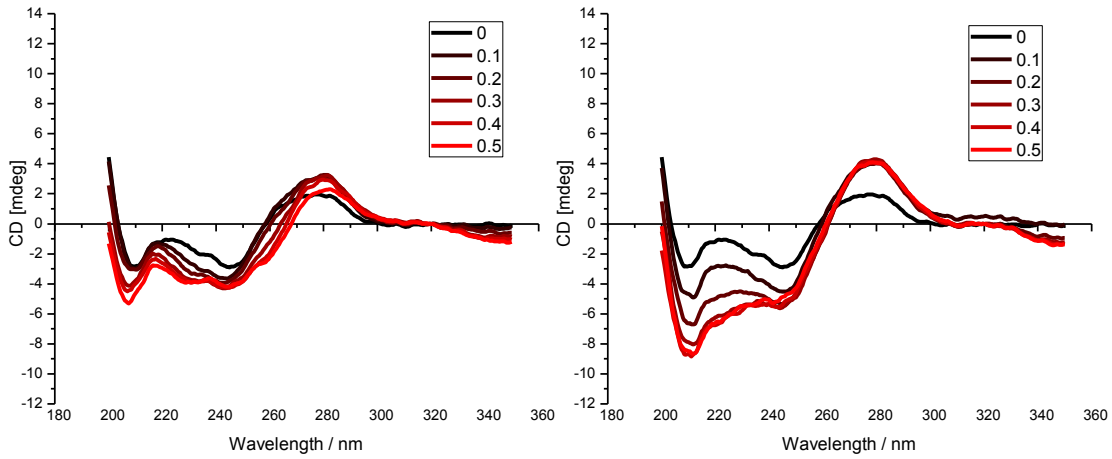

Figure 58 Comparative spectra of bisacridine 3 (left) and bisacridine 4 (right) binding to CT-DNA (DNA concentration 300 µM in base pairs). The negative peak at 210 nm, indicative of DNA in the A conformation, is apparent at higher concentrations of bisacridine 4. The legend denotes the ratio of ligand chromophores to DNA base pairs.

Although the structural difference between bisacridine 3 and bisacridine 4 is very slight, the more constrained linker of bisacridine 4 appears to cause a greater degree of change in the DNA spectrum than that of bisacridine 3. This finding would appear to support the notion that changes in the DNA spectrum at this wavelength are indeed indicative of condensation of the DNA, since the shorter rigid linker is even less likely to bind in an intra-molecular manner. Either that, or the increase in the intensity of the negative band at 210 nm, apparent with both of these compounds, reflects substantial deformation of the DNA duplex, due to

the conformational constraints imposed upon the duplex by intramolecular bisintercalation of these supposedly rigid ligands. The capability of bisacridines to bind in an intermolecular fashion will be explored in more detail in Chapter 4.

Conclusions

These experiments have revealed subtle differences between the binding mechanisms of various DNA intercalators. The quinoxaline antibiotic echinomycin, and the anthracycline doxorubicin, induce a progressive lengthening of DNA upon binding. By contrast, the binding of compounds sharing the acridine chromophore results in increases in DNA contour length that are preceded by a distinct shortening of the DNA at lower concentrations of the ligand. Interpreting this peculiarity is not straightforward, and could even be explained by these ligands adopting an alternative binding mechanism to that of intercalation at low ligand to base pair ratios such as groove binding. Although CD suggests that the different acridine ligands may bring about a conformational change in the DNA, the observed spectra of DNA bound to the compounds discussed here do not correspond exactly to the spectra of accepted DNA conformations such as A and B.[128]

Nevertheless, some conclusions may be drawn from these data that refine our understanding of the intercalative mechanism. The shortening of the DNA that is apparent at low concentrations of the acridine compounds would support the hypothesis that the DNA is undergoing some form of conformational change, and that this is dependent upon the nature of the chromophore, since this contraction occurs even with 9-aminoacridine. Despite differences in the structure of the inter-chromophore linker of the bisacridines, and the absence of the carboxamide substituent on the monointercalator 9-aminoacridine, the degree of change in the contour length of DNA fragments bound to all of these ligands is approximately the same at particular chromophore to base pair ratios. By contrast, intercalators that do not incorporate the acridine chromophore do not induce a contraction in the length of DNA at low ligand concentrations. In the cases of echinomycin and doxorubicin, a progressive and consistent lengthening of the DNA is observed until saturation of the DNA strand with the intercalator. Taken together, these findings suggest that intercalation of an acridine occurs in two phases: initial intercalation accompanied by a dramatic switch in conformation in the nucleotides surrounding the binding site, followed by a progressive lengthening of the DNA at higher ligand concentrations as more molecules bind to the DNA. Indeed, the initial contraction occurs at such low concentrations of the ligand that conformational changes must occur some distance away from the site of intercalation.[120] Hypothetically, this may reflect the relaxed nature of the unbound DNA,

able to adopt a new conformation before further intercalation renders the DNA more rigid and therefore unable to undergo further change.

This does not mean that all of the acridine compounds bind to DNA in exactly the same fashion. Although changes in the physical length of DNA were broadly similar, the length of the DNA strand itself is not an indicator of conformation. CD spectra obtained for DNA bound to the acridine based ligands reveal distinctive differences, even between structurally similar compounds. This is particularly noticeable with the acidine bisintercalators, such as bisacridine 2 and bisacridine 3. Although changes in their CD spectra, relative to the unbound B conformation of calf-thymus, are similar in the region of 240 to 260 nm, there is a noticeable change in the intensity of the band at 210 nm, indicative of A form character, in the spectrum of bisacridine 3, but not that of bisacridine 2. Given that the chromophores of these compounds are identical, it follows that the chromophore linker and its interactions in the minor groove of the DNA are to some degree responsible for the precise nature of any conformational change that the DNA undergoes. This distinction in each compound's respective CD spectra may even, as has been postulated in the case of bisacridine 3, be an indicator of intermolecular binding.

These findings themselves do not resolve the mechanism by which DNA may undergo conformational change as a consequence of intercalation. In the case of some ligands, not studied here, any conformational changes may be minimal. Interpreted alone, the data obtained from any one particular experimental protocol may be misleading. Contour length increases in DNA have been considered to be diagnostic of intercalation.[73] However, with the acridine ligands, at those chromophore to base pair ratios where the degree of contraction matches that of extension (i.e. the net change in length, in spite of ligand binding, is zero), no change in contour length may be discerned. Similarly, the results of the DNA unwinding assay conducted using gel electrophoresis do not suggest that shortening of the DNA occurs at any ligand concentration. In fact, at high acridine concentrations the mobility of the DNA is retarded in the same manner as it is for echinomycin, an observation generally attributed to lengthening of the DNA. Using a combination of techniques, peculiarities in the behaviour of individual intercalators have been identified that highlight the complexities of this particular mechanism of DNA binding. Such peculiarities may have implications for the therapeutic application of this class of compounds, including their ability to inhibit different types of intra-cellular enzymes, such as DNA topoisomerase and RNA polymerase.

.

Chapter 4 – Inter-molecular intercalation

Introduction

As discussed in Chapter 1, the capacity of bisintercalators to bind to two separate strands has been understood for some time. Initial studies utilised gel electrophoresis to demonstrate the aggregation of DNA by bisintercalators such as luzopeptin and acridine derivatives.[33-34] More recently, the interaction between separate strands of DNA and luzopeptin has been suggested by AFM imaging.[74] Full methods for each of the experiments described in this Chapter are provided in Chapter 7.

Data collected during experiments conducted in Chapter 3 suggested that binding was not always occurring in an intramolecular manner for some compounds, noticeably bisacridine 3. During the course of this Chapter, we will employ single molecule force spectroscopy to examine, quantitatively, the mechanism of intermolecular bisintercalation, and also demonstrate a novel, bulk solution approach to visualise this process using gold nanoparticles (cAuNP), functionalized with DNA.

AFM imaging of intercalated DNA reveals unusual complexes

During the course of the imaging experiments conducted in Chapter 3, unusual DNA complexes were observed when the DNA had been treated with high concentrations of a bisacridine. CD spectra of compounds bisacridine 3 and bisacridine 4 were also suggestive of the formation of inter-molecular complexes of DNA (see Chapter 3).[126] As previously stated, these compounds incorporate less flexible inter-chromophore linkers than their alkyl counterparts and, theoretically, the assumption has been that designing bisacridines in this fashion ought to encourage the kind of intermolecular binding described here.[35]

Typically, DNA adsorbed to mica from aqueous solution retained a relaxed appearance. As demonstrated in Chapter 3, the lengths of DNA derived from AFM images of this kind correspond well with the theoretical length of such DNA in its B form. Although strands may be observed to coalesce, this is unusual where the concentration of the DNA is low and simply reflects how separate strands may adhere to the same area of mica, in close proximity with one another.

A qualitative illustration of the differences between different types of intercalator is provided in Figure 59. A 1341 base pair, linear fragment of plasmid φX174, measuring 456 nm, was produced by restricting the plasmid with the enzyme BsaAI. Aliquots of this DNA solution were diluted further to 0.34 ng/ µl. A volume of 10 µl of this dilute DNA solution was combined with 15 µl of the appropriate ligand, or 15 µl of water for the control group. After

an incubation period of ten minutes, 25 µl of 10 mM $MgCl_2$ was added, yielding a total volume of 50 µl as per previous AFM imaging experiments.

The complexes observed on addition of bisacridine 3 to a 1341 base pair fragment of DNA adopt a range of morphologies. Separate strands tend to be aggregated and adopt loops and tangles that suggest that each section of DNA has been bound to another, either by an intermolecular interaction or a long-range intra-molecular mechanism.

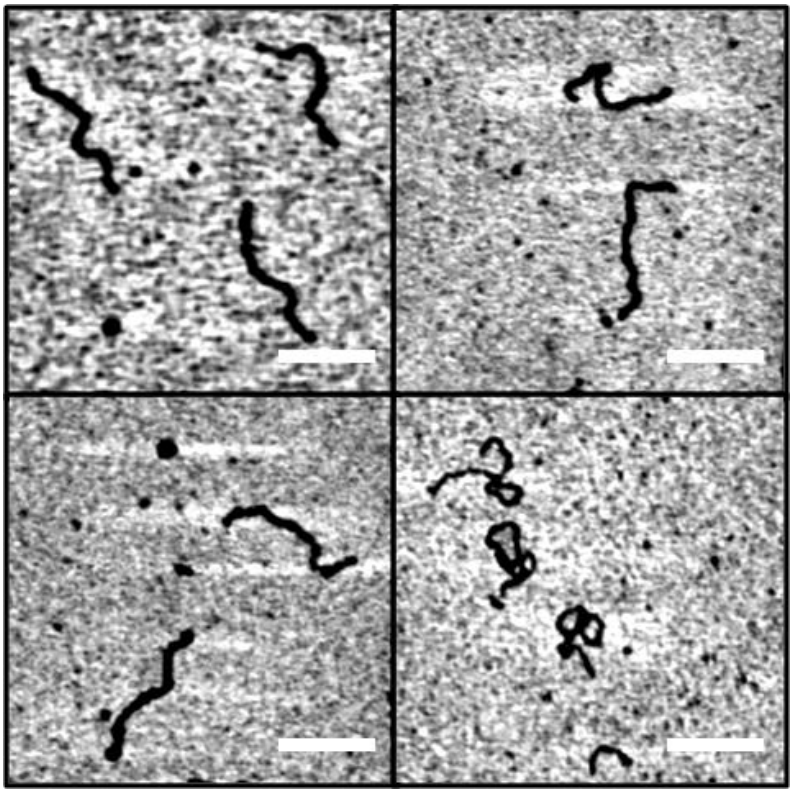

Figure 59 AFM images of DNA treated with different intercalators (scale bar denotes 250 nm). Clockwise from top left, no ligand, 10 µM echinomycin (0.1% DMSO), 10 µM bisacridine 3, 20 µM ethidium bromide. The concentration of the DNA in these samples is 0.16 nM. The appearance of the DNA bound to bisacridine 3 is very different to the other samples, losing its linear character and adopting more complex morphologies.

Complexes of this kind are not observed with the monointercalator ethidium bromide. Although intercalation of this ligand may occur throughout a DNA strand, the molecule, comprised of a single chromophore, lacks further substituents with which to bind to any adjacent DNA strands. Similarly, no aggregation of the DNA was observed with the bisintercalator echinomycin. While in theory this compound, consisting of two chromophores separated by a peptide linker, could adopt an intermolecular configuration, similar to that known to occur with luzopeptin, such a rearrangement would be highly unfavourable due to the rigid configuration of the peptide component. As such echinomycin has always been assumed to bind in a staple like configuration to DNA, via an

intramolecular mechanism.[28, 133] This hypothesis is supported by several NMR studies of DNA-echinomycin complexes,[29] and the failure of any other techniques, notably AFM, to provide any evidence of echinomycin adopting an alternative binding mode.[74]

Utilising single molecule force spectroscopy to examine intermolecular intercalation

Intercalation of an acridine monomer has been studied using force spectroscopy.[99] More broadly, this technique has been used to examine a wide range of issues, including protein binding and receptor ligand interactions, as discussed in Chapter 2. The technique has been demonstrated to be very sensitive, requiring only low concentrations and small volumes of materials. Given the lack of quantitative data surrounding the mechanism of Type II intercalation, it was decided to apply the principle of single molecule force spectroscopy to investigate this phenomenon.

A consideration of the different types of interaction that may be observed during these experiments is provided in Figure 60. The stretching events associated with a positive interaction may be analysed in a variety of ways, depending on the nature of the molecules undergoing stress. Two common models for the elastic behaviour of materials are the extensible worm-like-chain model (EWLC) and the extensible freely-jointed-chain model (EFJC). These are both mathematical models that describe the flexibility and elasticity of different types of polymer. Typically, biological materials such as DNA are best described by the EWLC, while materials such as PEG are described by the EFJC. While the EWLC envisions a semi-rigid rod that is continuously flexible, the EFJC envisions a chain that is flexible only within distinct segments. Since the PEG component constituted approximately 60 to 70 percent of the total length of the molecule that would be used in these experiments, it was decided to use the EFJC for analysis.

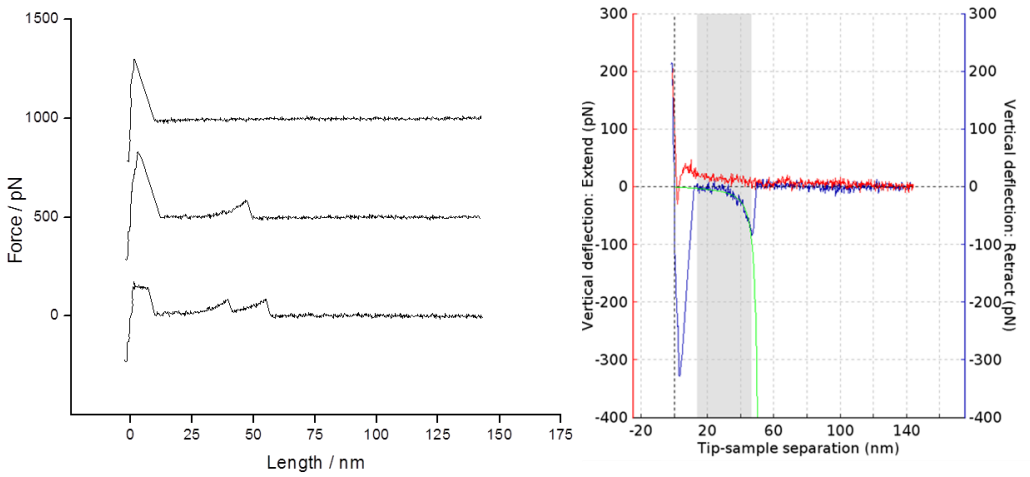

Figure 60 Typical force extension curves showing (from top to bottom) no interaction, single positive interaction, serial multiple interactions (left) and an exported image from JPK processing software, illustrating fitting of the EFJC (right). The *y* axis offset of the force curves is arbitrary for illustrative purposes and would be 0 pN in all cases.

Figure 60 highlights a difficulty often encountered with force spectroscopy, that of distinguishing between 'single' and 'multiple' stretching events. The occurrence of multiple interactions, where more than one artefact is attached to the cantilever as it is retracted from the substrate may be controlled to some degree by the surface chemistry of the substrate. By using very dilute solutions of the DNA molecule, the likelihood of more than one strand adhering to the cantilever is reduced. Multiple attachments still occur however and must be dealt with at the data analysis step. Serial multiple events of the kind illustrated in Figure 60 are easily identified. In these cases, only the final stretching event is analysed with the EFJC since preceding events are governed by the behaviour of the final event and therefore not a reliable reflection of the actual stretching event that was occurring. Parallel multiples are more commonly identified by the higher rupture forces with which they are associated, but this in itself is not sufficient to distinguish them from genuine single interactions. A protocol for separating events of this kind will be discussed in more detail later in this Chapter.

Stretching a DNA oligonucleotide

In order to characterise the functionalised substrate, an initial experiment was conducted using a bare AFM cantilever. The design of this experiment is illustrated in Figure 61. A pair of 33 base pair oligonucleotides were annealed and coupled to a 15.4 nm PEG polymer via an amine functionality at the 5' terminus of one of the oligonucleotides. In turn, the PEG was coupled to propanedithiol, leaving a free thiol group at the PEG end of the molecule. The full sequence of the DNA is as follows:

1) 5’ – NH_2 – CTACGTGGACCTGGAGAGAGGAAGGAGACTGCCTG – 3’
2) 5’ – CAGGCAGTCTCCTTCCTCTCTCCAGGTCCACGTAG – 3’

A 5 µl droplet of the PEG/DNA conjugate (60 ng/µl) was deposited on an atomically flat gold surface and placed in a humidity chamber for 20 hours, during which time coupling of the free thiol to the gold surface would occur. The surface was then passivated with a droplet of 10 mM 11-mercaptoundecanoic acid. Using a bare, gold coated cantilever (Asylum Research, BL-RC150VB) force spectroscopy was conducted in aqueous phosphate buffer by lowering and retracting the cantilever in arrays of 100 x 100 data points over areas of 10 x 10 microns on the gold surface.

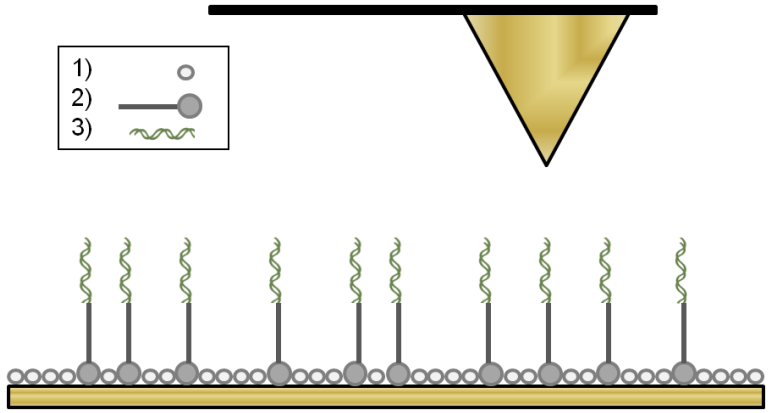

Figure 61 Illustration of the experiment, showing a passivated and functionalised substrate and the opposing bare AFM cantilever to which the DNA would adhere. Legend denotes 1) Mercaptoundecanoic acid 2) PEG 3) DNA. These experiments are conducted in liquid, where both the cantilever and the substrate are immersed in solution in a liquid cell beneath the AFM head.

Data obtained from this experiment are presented in Figure 62. Observed events, to which the EFJC could be fitted, rendered a mean breaking force of 53.2 pN and contour lengths of approximately 29.5 nm. The most probable force associated with these interactions is typical of the kinds of forces usually reported for experiments of this kind.[134] Similarly, the contour lengths of these interactions were in good agreement with the theoretical length of the oligomer that had been attached to the substrate (27.2 nm). Values for the theoretical lengths of the individual components of the oligomer, and the total calculated length of the oligomer, are provided in Table 18.

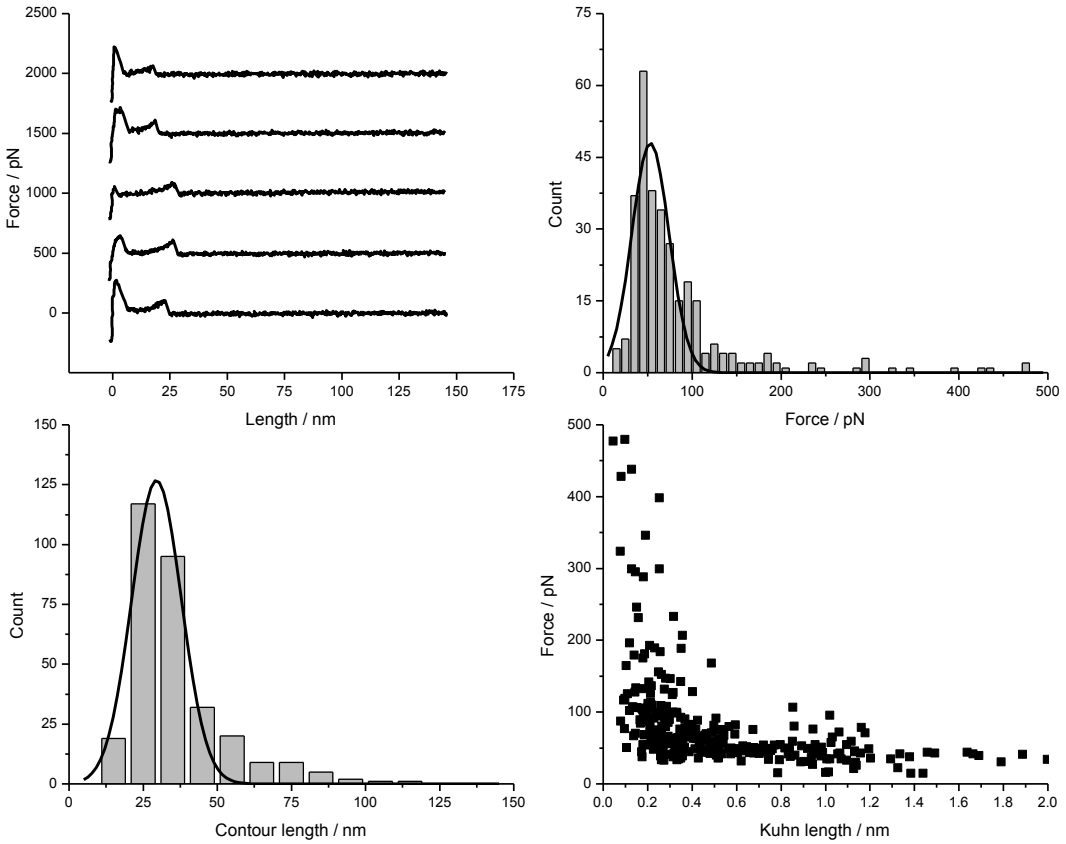

Figure 62 Data obtained from fitting of the EFJC model to observed interactions. Clockwise from top left 1) Typical force extension curves 2) Histogram of rupture forces 3) Scatter plot of rupture forces versus Kuhn length, highlighting the relationship between higher breaking forces and low Kuhn lengths 4) Histogram of contour lengths.

Table 18 Theoretical lengths of the components of the oligomer. Calculations assume a MW of the PEG of 2950 Da, and that the DNA is in a B conformation, with a mean distance between each base pair of 0.34 nm.

Molecule	Length / nm
Propanedithiol	0.6
PEG	15.4
B-DNA	11.2
Complete oligomer	27.2

The problem of multiple interactions has already been discussed earlier in this Chapter. While serial multiple interactions may be eliminated from further analysis, parallel multiple interactions are much harder to distinguish. One means for achieving this is to use the elastic character of the PEG to distinguish between single and multiple attachments.[135] Besides the rupture force and contour length of an interaction, another function of the EFJC provides a value referred to as the Kuhn length, a function of a molecule's persistence length. A recent study has established a relationship between low Kuhn lengths and higher rupture forces in PEG based systems, suggesting that lower Kuhn lengths are associated with multiple, and non-specific, attachments.[135] As may be discerned from Figure 62, these experiments

demonstrated a similar relationship, with forces greater than 100 pN typically occurring at Kuhn lengths lower than 0.6 nm. Accordingly, to reduce the impact that multiple attachments might have on the data, we applied a second filter to isolate those rupture events where the Kuhn length was greater than 0.6 nm.[135] These interactions are presented in Figure 63, along with new histograms of the lengths and forces associated with the isolated data.

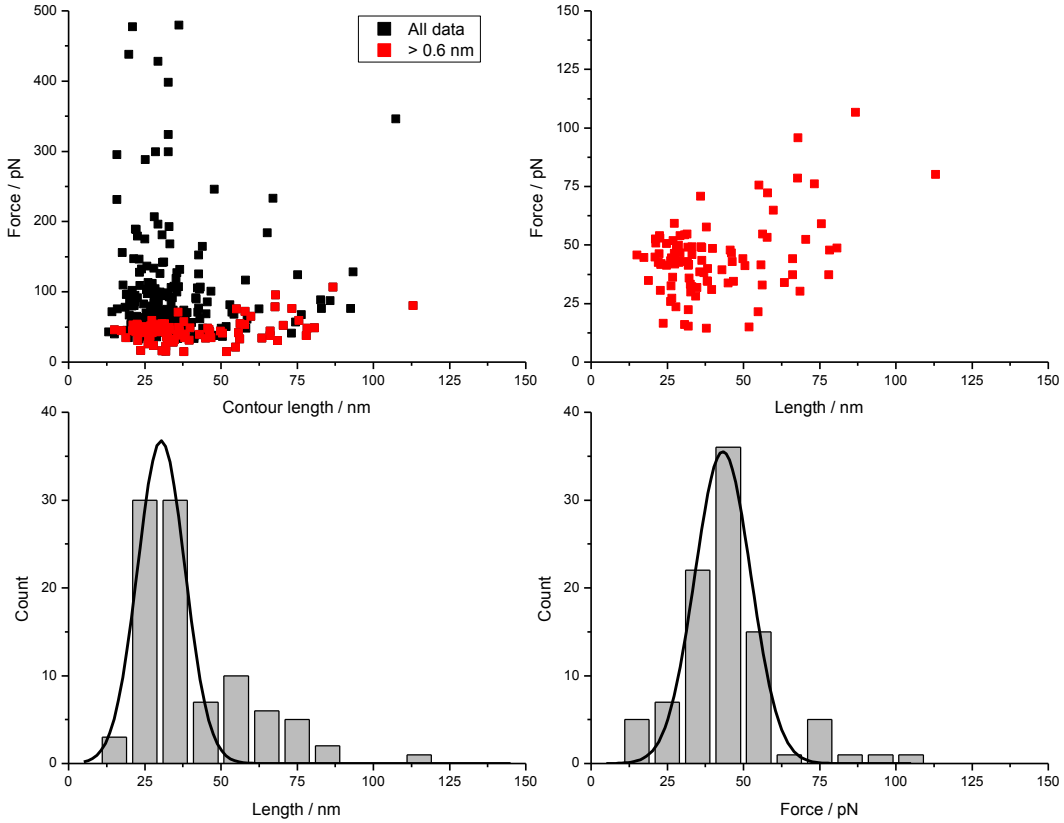

Figure 63 Clockwise from top left 1) Scatter plots of all the collected data and data where the Kuhn length was greater than 0.6 nm 2) Enlargement of the scatter plot for the selected data 3) Histogram of rupture force 4) Histogram of contour lengths.

A complete analysis of the values taken from these initial experiments is provided in Table 19. The values obtained for the contour length of the oligomer do not differ, even when the Kuhn length filter is applied to the data, and remain in good agreement with the theoretical length of 27.2 nm. There is also a 20% reduction in the mean force once interactions with Kuhn lengths of less than 0.6 nm have been removed from the analysis.

Table 19 Typical values for length and force associated with stretching of the oligomer by a bare cantilever.

Sample	Length / nm (SE)	Force / pN (SE)	n
All data	29.5 (1.4)	53.2 (3.2)	310
> 0.6 nm	30.4 (2.2)	43.3 (1.5)	94

That the observed contour lengths correspond so well with the theoretical value of 27.6 nm may be somewhat surprising, since mechanistically it seems unlikely that the AFM probe would 'pick up' the oligomer at the end of the DNA strand to which the PEG is attached. However, measurements of this kind may be subject to several variables. These include stretching of the oligomer beyond its relaxed length, the physical dimensions of the AFM probe itself, and the polydispersity of the PEG molecule to which the DNA is attached. Both the scatter plots and the histogram of length presented in Figure 63 reveal a degree of skew towards higher contour lengths, reflecting the polydispersity of the PEG molecule that was used for this study.

The question of the frequency with which these events occur is more difficult to assess. Filtering events by Kuhn length in order to eliminate those not commensurate with stretching of a single polymer chain, eliminates legitimate stretching events where more than one PEG conjugate is attached to the AFM probe. As such, the frequency of observed events may appear artificially low, especially since single stretching events are made all the more unlikely by the use of a bare cantilever, where the exposed surface area is high. However, reporting the frequency of all those events to which a freely jointed chain could be fitted is equally misleading, since this value will include a number of non-specific interactions that could be associated with a range of phenomena, such as peculiarities in the composition of the substrate and surface adhesion of the probe tip.

The relative frequency of these interactions is therefore provided both as a reflection of the number of events where the Kuhn length was greater than 0.6 nm, and of the total number of events to which the freely jointed chain model could be applied (Table 20). In reality, the frequency of events that constitute stretching of oligomers must be somewhere between these values.

Table 20 Number of interactions observed when stretching the oligomer with a bare probe, comparing the total number of force extension curves against those with Kuhn lengths greater than 0.6 nm.

Sample	n	Frequency / %	n (total force curves)
All data	310	1.03	30000
> 0.6 nm	94	0.31	30000

In order to demonstrate further that observed interactions were the result of legitimate connections between the substrate and the cantilever, a further experiment was conducted where the probe, as well as the substrate, was passivated with mercaptoundecanoic acid. By blocking the Au surface of the cantilever, it should not be possible for the DNA to adhere to

the cantilever. As such the number of interactions should be significantly reduced. Data obtained from these experiments are shown in Table 21.

Table 21 Number of interactions observed between the bare probe and a passivated probe. Only data for Kuhn lengths greater than 0.6 nm is shown.

Sample	n	Frequency / %	n (total force curves)
Passivated probe	1	0.01	20000
Bare probe	94	0.31	30000

There is a noticeable and unsurprising difference between the values reported in Table 21 and those reported in Table 20. The decline in the absolute frequency of all of the observed stretching events reflects the successful passivation of the cantilever. The fact that this value did not fall to zero may indicate two things. First, non-specific interactions always occur during any force spectroscopy experiment, since any event that causes even a slight deflection of the cantilever will be observed during the retraction of the cantilever from the substrate. Second, any parts of the probe that retain a bare gold surface could adhere to the DNA on the substrate, although, as is evident from Table 21, this eventuality appears to be very rare, if indeed it applies at all.

The binding of monointercalators with DNA

The final stage of the force spectroscopy experiments required the functionalisation of both the cantilever and the substrate with DNA. This arrangement is illustrated in Figure 64. Functionalisation and passivation of the cantilever was conducted in a similar fashion to that of the substrate, by immersing the cantilever in a droplet of the PEG/DNA solution or mercaptoundecanoic acid as appropriate. Having demonstrated the relationship between the Kuhn lengths of observed events and their associated rupture forces above, the following data will always represent only those events with Kuhn lengths greater than 0.6 nm.

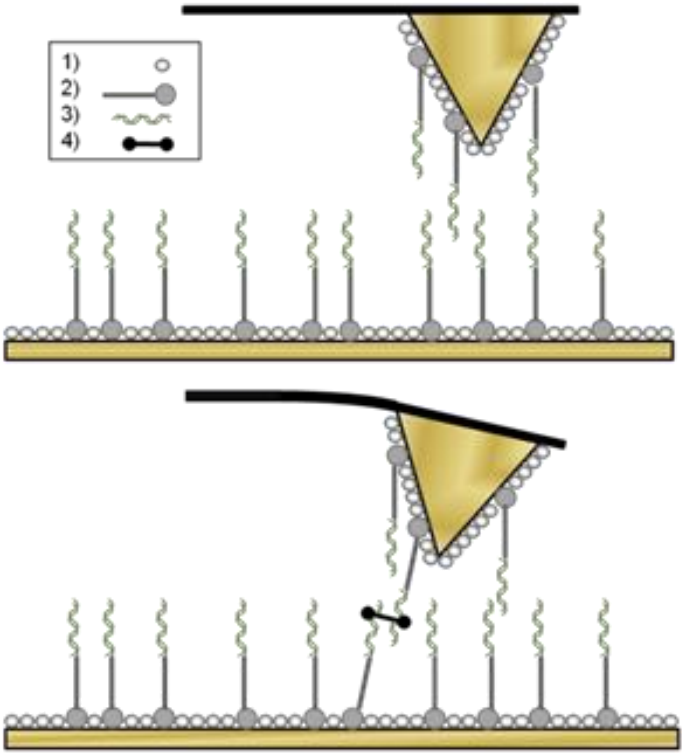

Figure 64 Experimental protocol showing setup of force spectroscopy apparatus. Legend denotes 1) Mercaptoundecanoic acid 2) PEG 3) DNA 4) Bisintercalator. The top image shows a negative interaction, where there is no connection between the substrate and the opposing cantilever. The lower image shows a positive interaction where the cantilever is deflected by the binding of a bisintercalator to two opposing DNA strands.

Figure 65 provides an illustration of the interactions that were observed when only buffer, and no ligand, was introduced to the liquid cell. Theoretically, under these conditions, no interactions should be observed, since there is no ligand in solution to bridge the opposing strands of DNA. This experiment was repeated using solutions of ethidium bromide and 9-aminoacridine, by replacing the buffer in the liquid cell of the AFM with an aqueous 200 nM solution of either of these ligands. In theory at least, since these compounds consist of a single chromophore, no events should occur.

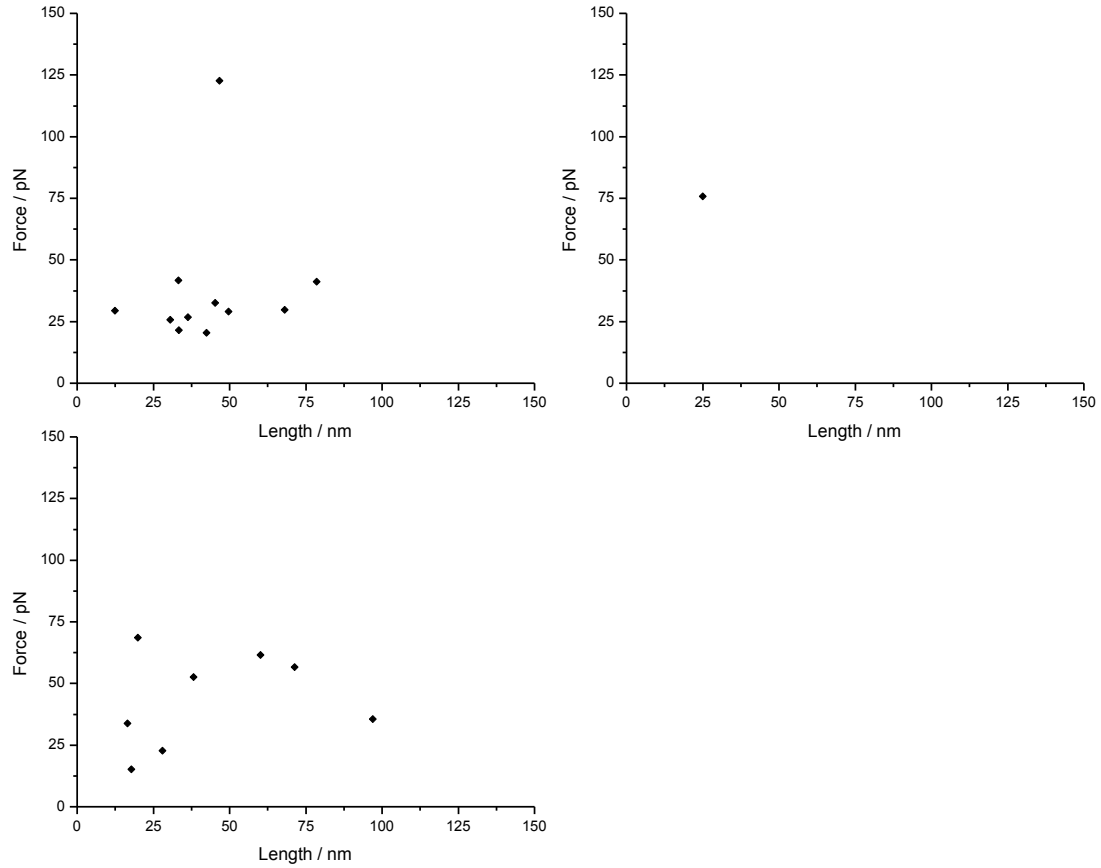

Figure 65 Data obtained from experiments conducted without a ligand (top left), and also the monointercalators 9-aminoacridine (top right) and ethidium bromide (bottom left). The frequency of stretching events in these samples was less than 0.1 %, comparable to a passivated cantilever.

Although in principle no interactions should be observed in the control (no ligand) group, a small number of interactions were observed. Interactions were also observed in the case of ethidium bromide, and a single event with 9-aminoacridine. These are almost certainly a consequence of non-specific interactions between the AFM cantilever and unwanted artefacts within the liquid cell or on the substrate, and occur very infrequently (approximately one non-specific interaction for every 2000 force extension curves generated).

Table 22 Relative frequencies of stretching events associated with different ligands. Although these ligands are known intercalators, binding is restricted to a Type I mechanism that cannot be observed using this protocol.

Sample	n	Frequency / %	n (total force curves)
No ligand	11	0.06	20000
9-aminoacridine	1	0.01	20000
Ethidium Bromide	8	0.05	15817

The binding of bisacridines with DNA

On addition of a 100 nM aqueous solution of bisacridine 3 to the AFM liquid cell there was a dramatic change in the frequency of the events that were observed, and relative to the experiments conducted with a bare AFM probe, a significant change in the lengths at which these events occurred. Typical force extension curves and histograms of the observed lengths and forces are provided in Figure 66. Data derived from these histograms are presented in Table 23, relative to the results obtained where only the substrate was functionalised.

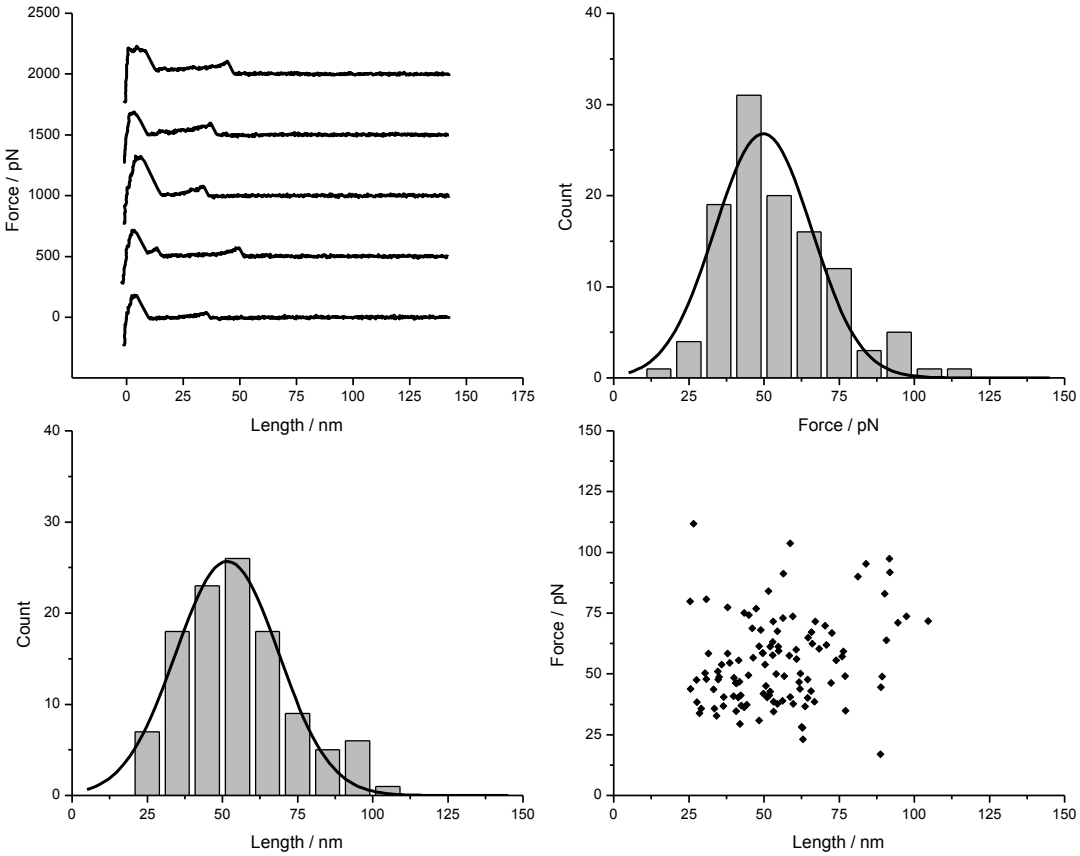

Figure 66 Clockwise from top left, typical force extension curves where bisacridine 3 has been added to the system, histogram of the force at which these events ruptured, scatter plot of the interactions, and histogram of the length at which these events occurred.

Table 23 Comparison of the lengths and forces obtained with a bare cantilever and where bisacridine 3 was introduced to a functionalised substrate and cantilever. The forces described here represent different processes; one the strength of the attachment between the AFM probe and the DNA, and the other the rupture of a bond between two separate DNA strands.

Sample	Length / nm (SE)	Force / pN (SE)	n
Bare probe	30.4 (2.2)	43.3 (1.5)	94
Bisacridine 3	51.6 (2.0)	49.7 (3.2)	113

Comparison of the contour lengths derived from the freely jointed chain that was applied to the stretching events revealed a significant increase in the length at which the events were

occurring, with the reported length of 30.4 nm for the oligomer alone rising to 51.6 nm where opposing oligomers were bridged together by the bisacridine.

Given the differences that were identified between the bisacridines in Chapter 3, these experiments were repeated with another bisacridine (bisacridine 2) with a different inter-chromophore linker (Figure 67). A comparison of the data obtained for each of the two bisacridines is provided in Table 24.

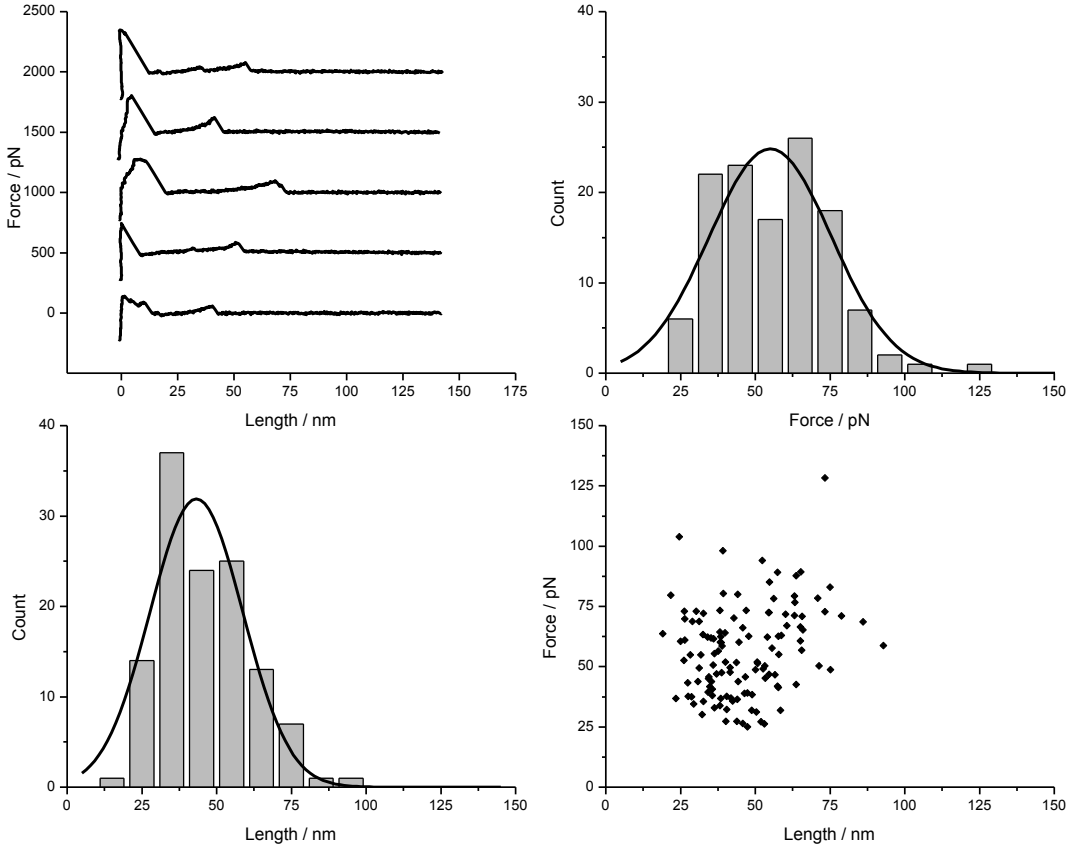

Figure 67 Clockwise from top left, typical force extension curves where bisacridine 2 has been added to the system, histogram of the force at which these events ruptured, scatter plot of the interactions, and histogram of the length at which these events occurred.

Table 24 Comparison of values for length and force obtained for the two different bisacridines 2 and 3. Although the difference in observed contour length could be considered to be statistically significant for this data, estimation of the potential length of the oligomer is very complicated.

Sample	Length / nm (SE)	Force / pN (SE)	n
Bisacridine 3	51.6 (2.0)	49.7 (3.2)	113
Bisacridine 2	43.2 (3.3)	55.0 (3.7)	123

The correlation between the observed lengths and forces for each of the bisacridines, suggests that the same interaction, a bridging of opposing DNA strands, was indeed taking place.

The relative frequencies with which these events were observed are shown in Table 25. Relative to the control and the monointercalators already discussed, there is a striking increase in the number of events that are observed when a bisacridine is added. While events observed in the absence of a ligand constituted only 0.06% of the total number of force curves, this rose to 1.13 and 0.62% in the case of bisacridine 3 and bisacridine 2 respectively.

Table 25 Comparison of the relative frequencies of events between two bisacridines, showing that the incidence of Type II events is greater in the case of bisacridine 3 than bisacridine 2.

Sample	n	Frequency / %	n (force curves)
No ligand	11	0.06	20000
Bisacridine 3	113	1.13	10000
Bisacridine 2	123	0.62	20000

The observed frequency of such interactions is governed to some degree by variations in the surface chemistry. However, the reduced frequency of interactions that were observed in the case of bisacridine 2 may also reflect the difference in the molecular structure of this compound relative to bisacridine 3. CD in Chapter 3 demonstrated that the structure of DNA intercalated with bisacridine 3 was subtly different to that of bisacridine 2, although AFM imaging demonstrated the capacity of both compounds for forming aggregates of DNA material. The rigid inter-chromophore linker of bisacridine 3 was in fact intended to restrict the ability of the compound to adopt an intra-molecular binding configuration and encourage the kind of inter-molecular activity observed via force spectroscopy. By contrast, the flexible alkane linker of bisacridine 2 permits the acridine chromophores of bisacridine 3 to adopt either a cis or a trans configuration. As such, the lower frequency of events observed for bisacridine 2 could reflect a greater degree of intra-molecular binding that would not be detected by this force spectroscopy assay. This could be tested by introducing the monointercalator 9-amino acridine to the liquid cell alongside a bisacridine. Due to competition between the monointercalator and the bisintercalator, the relative frequency of observed stretching events should decrease as the concentration of the monointercalator, relative to that of the bisintercalator, is increased.

So far the discussion has centered on the relative frequency of any observed events and the forces with which these events are associated. However, the distance between the AFM probe and the substrate at the point of bond rupture is also an important diagnostic of the events being observed. The difference in the distances observed between a non-functionalised (bare) cantilever and a cantilever functionalized with DNA has already been

discussed, and the increase in length observed with the latter supports the notion that opposing DNA strands are being coupled together. Unfortunately, the issue of length is somewhat complex in this scenario for a variety of reasons.

The issue of polydispersity in the PEG component of the oligomer has already been discussed, but there are other factors that may aggravate the range of contour lengths over which interactions are observed to be occurring. Since the oligonucleotides used to assemble the oligomer consist of more than four base pairs, it follows that more than one arrangement of two separate oligomers may be possible. In fact, applying the neighbour exclusion principle, the 33 base pair oligonucleotide consists of 16 potential intercalation sites. An attempt to reconcile some of these arrangements is illustrated in Figure 68.

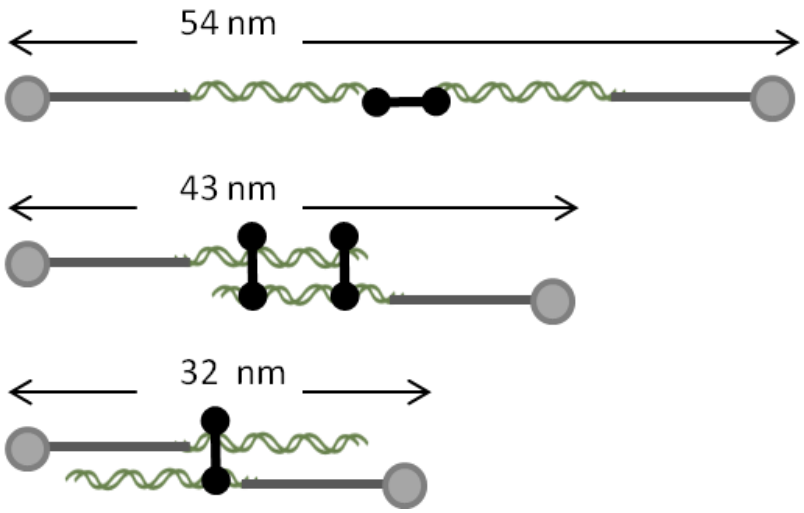

Figure 68 Potential binding arrangements of two separate oligomers with a bisacridine(s). The lengths above each molecule correspond to the contour length that may be expected for that arrangement. These arrangements are illustrative only, and the bisintercalator itself is not to scale.

Theoretically, as many as sixteen bisacridine molecules could bind simultaneously to two separate oligomers, although the chances of such an arrangement occurring in practice seem remote. Figure 68 emphasises that, even when only one bisacridine is binding, contour lengths of this coupling could vary by as much as 22 nm. In terms of observed breaking forces, binding of multiple ligands to the same strands ought to be associated with a higher observed force. However, this is not immediately obvious in the case of either of the bisacridines investigated so far.

Nevertheless, the distribution of observed rupture forces for both of the bisacridines is quite broad, as may be discerned from the relevant histograms in Figure 66 and Figure 67. That some of these forces exceed a value of 65 pN raises another issue that has not been discussed

so far, that of the overstretching of DNA, otherwise referred to as the B to S-DNA transition. Covalent attachment and in situ annealing of ssDNA in force spectroscopy experiments has been shown to be associated with a distinctive plateau in the observed forces associated with stretching of the annealed sequences.[136] At this point, the length of the DNA strand under stress may increase by as much as 70%, without a corresponding increase in force. Allowing for this mechanism, a further arrangement of the oligomers following binding of the bisacridine may be suggested Figure 69.

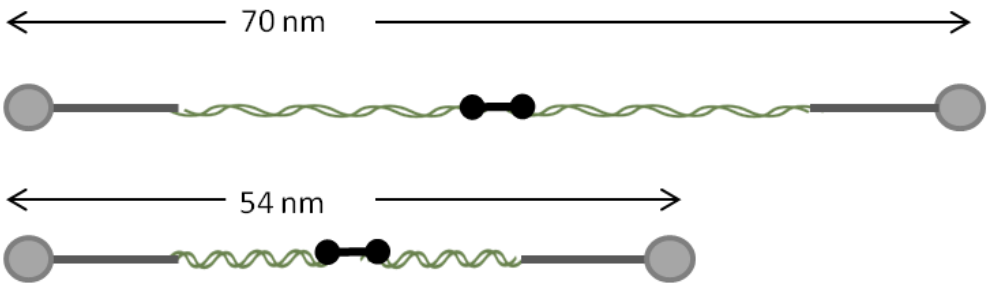

Figure 69 Graphical illustration of how the oligomer could undergo a transition from the B conformation to the overextended S conformation. Such a transition would require the application of forces exceeding that reported elsewhere for this transition, typically in the region of 65 pN.

However, the arrangement provided in Figure 69 ought to be considered unlikely. Firstly, the short length of the oligonucleotide may disguise the overstretching transition to some degree. Experiments elsewhere have utilised longer stretches of ssDNA, although admittedly the transition has been observed in sequences as short as 30 base pairs.[136] Secondly, binding of the bisacridine will not occur solely in an intermolecular fashion. Almost certainly, there will be a degree of intramolecular binding occurring, which will prevent the overstretching transition from taking place.[137] Nevertheless, since intercalation is known to be a dynamic process, with intercalating ligands effectively diffusing between a bound state and solution, it remains possible that overstretching may be occurring in some instances. Out of all of the force extension curves obtained during the course of these studies, only 2 or 3 force curves were observed to include a linear transition state at the point of rupture that may be indicative of the B to S transition. An example of one of these curves is shown in Figure 70.

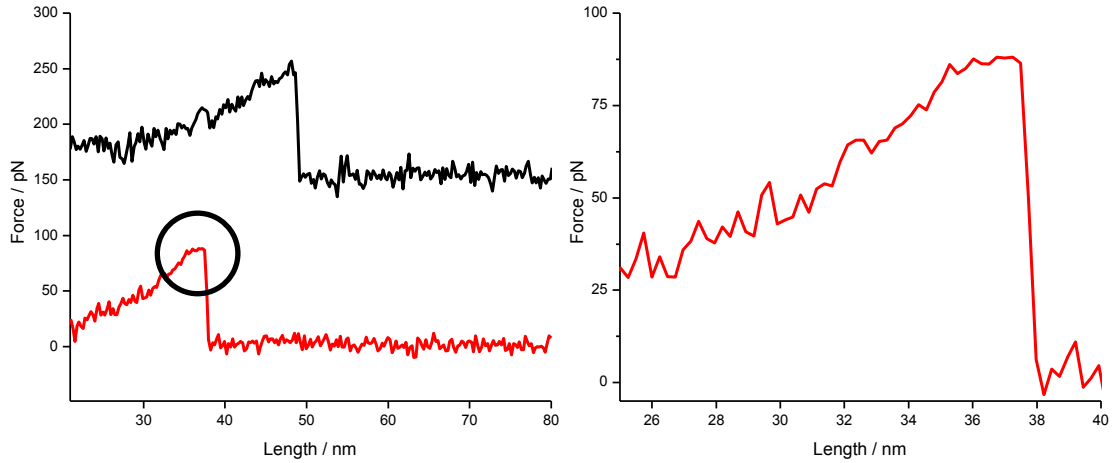

Figure 70 Example of one of a small number of force curves that demonstrated a linear phase (circled) immediately prior to the point of rupture (lower curve, left) and the same curve enlarged (right). A typical force curve that does not demonstrate the transition is provided for comparison (upper left).

The issue of the distribution of contour lengths at which events may be occurring is complicated by other factors identified in Chapter 3. Intercalation, at high degrees of DNA saturation, is associated with an increase in DNA contour length, while in the case of the bisacridines, lower concentrations of the ligand may induce a contraction in the DNA. A combination of all of these factors is likely to be responsible for the range of contour lengths over which interactions are occurring.

The binding of echinomycin and TANDEM with DNA

As previously discussed, the bisintercalator echinomycin is thought to retain a staple like, intra-molecular binding configuration. Similarly, the triostin analogue TANDEM, though having different sequence specificities to echinomycin, is thought to be unable to bind in an intermolecular fashion due to the rigidity of the molecule's interchromophore linker. As such, intermolecular binding of the kind demonstrated here by the bisacridines should not occur. To test this hypothesis, binding experiments were also undertaken using echinomycin.

Figure 71 provides clear evidence that, contrary to what may have been expected, echinomycin does indeed bind in an inter-molecular fashion. Given the rigidity of the peptide interchromophore linker, this raises questions about the precise mechanism by which binding was occurring, especially since the triostin analogue TANDEM did not demonstrate any activity at all. Since a cis to trans rearrangement of the chromophores was considered to be energetically unfavourable, it was decided to investigate the hypothesis that binding was occurring exclusively at the termini of opposing DNA strands.

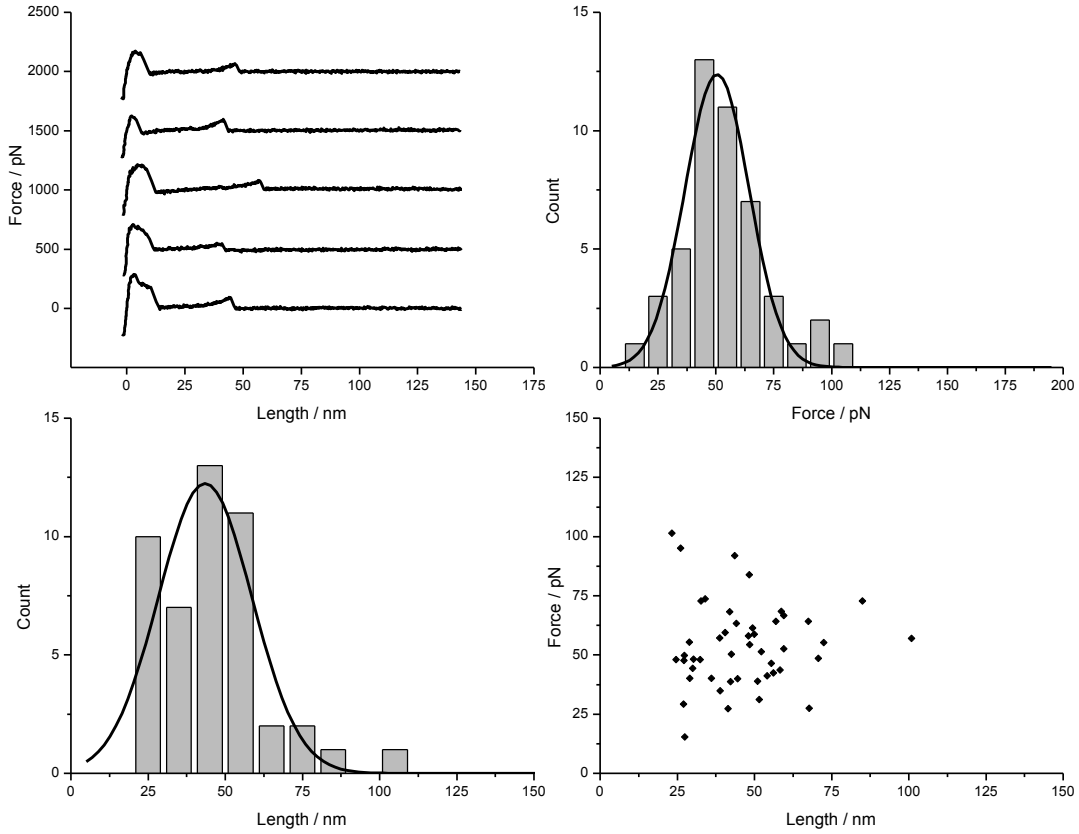

Figure 71 Data obtained for the bisintercalator echinomycin. Clockwise from top left, typical force extension curves, histogram of rupture force, scatter plot of observed interactions, histogram of contour lengths.

To test this hypothesis, the experiment was repeated with the bisintercalator TANDEM. This ligand has a known preference for AT base pairs, whereas echinomycin has a preference for GC. Another oligonucleotide was used that reflected the difference sequence specificity of TANDEM. This oligonucleotide differed from that previously used only in the composition of the terminal base pair, one being GC and the other AT. The precise sequence is provided below:

1) 5' – NH_2 – CTACGTGGACCTGGAGAGAGGAAGGAGACTGCCTA – 3'
2) 5' – TAGGCAGTCTCCTTCCTCTCTCCAGGTCCACTGAG – 3'

This sequence was annealed and prepared in exactly the same fashion as described previously. Results from experiments conducted with TANDEM, using the new oligonucleotide are shown in Figure 72.

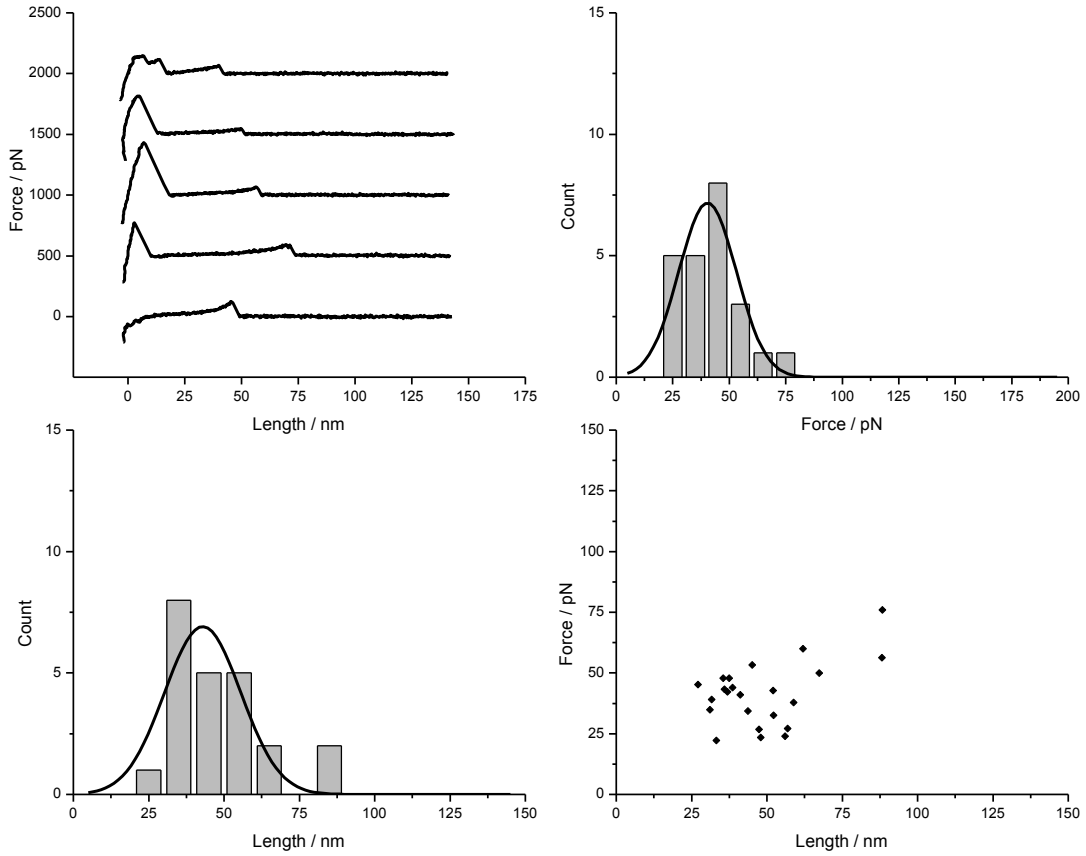

Figure 72 Data obtained for the bisintercalator TANDEM. Clockwise from top left, typical force extension curves, histogram of rupture force, scatter plot of observed interactions, histogram of contour lengths.

Having demonstrated that TANDEM exhibited similar activity to echinomycin, each compound was evaluated against the other oligonucleotide. That is to say, that echinomycin was tested against the AT terminated oligonucleotide and vice versa. Bisacridine 3 was also tested with the AT terminated oligomer.

The results of these experiments reveal that binding activity with either echinomycin or TANDEM is sensitive to the precise composition of the terminal base pairs of the oligonucleotide. While echinomycin shows activity with an oligonucleotide terminated with a GC base pair and not AT, the exact opposite applies in the case of TANDEM. By contrast, binding of a bisacridine does not appear to be sensitive to the base pair sequence of the oligonucleotide, with binding occurring in both cases (Figure 73).

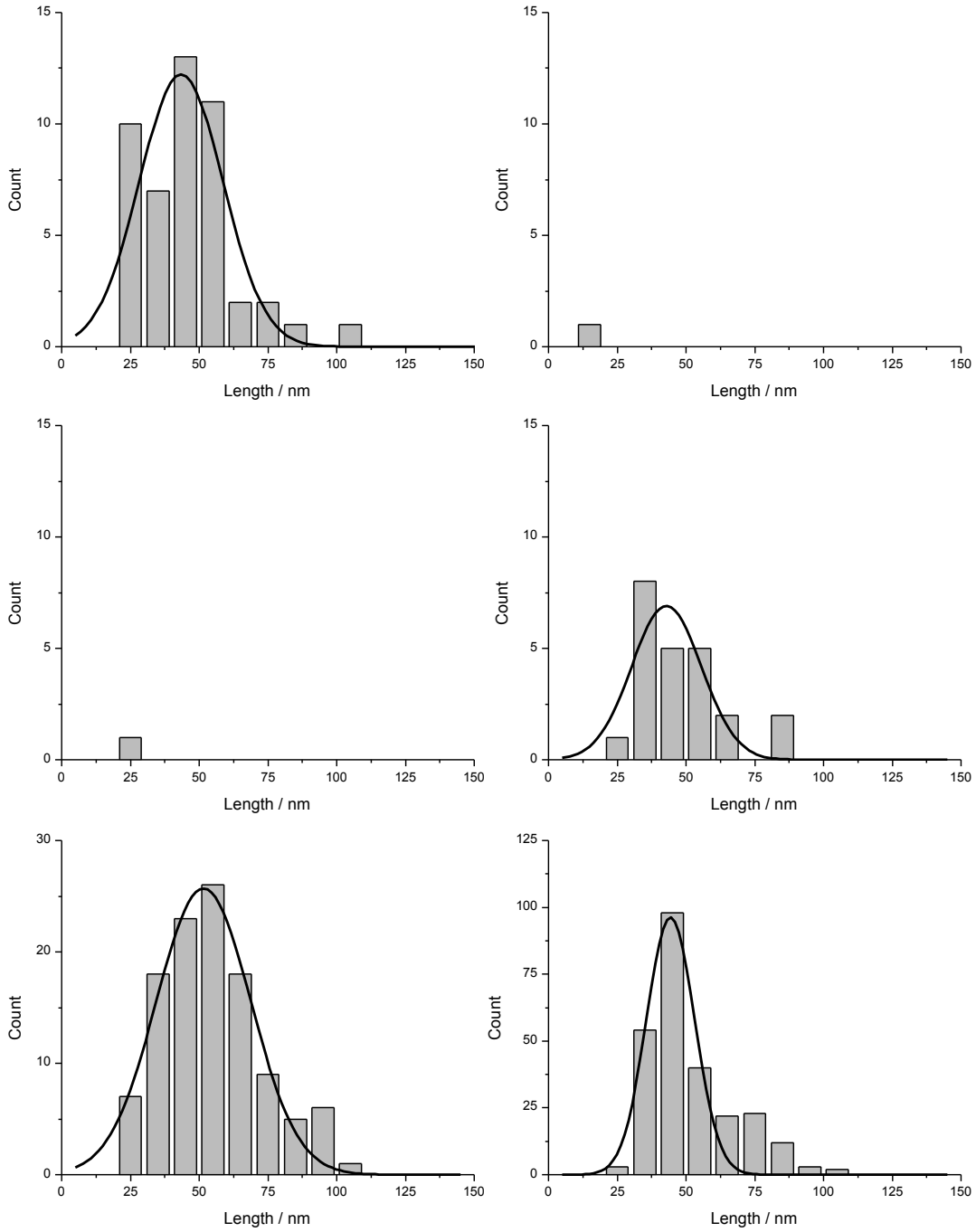

Figure 73 Histograms of contour lengths for the GC terminated oligonucleotide (left) and the AT terminated oligonucleotide (right). From top row to bottom, echinomycin, TANDEM, bisacridine 3. These histograms illustrate that in the cases of echinomycin and TANDEM, binding is dependent on the terminal base pairs of the oligonucleotides.

Importantly, the precise composition of the terminal base pairs does not reflect the optimal binding sites of either echinomycin or TANDEM. Although these ligands have, respectively, a preference for GC and AT rich regions of DNA, the arrangement of the base pairs within these areas is known to have a significant bearing on the binding of the ligand. Studies involving DNase footprinting and NMR have shown that echinomycin has a preference for 5'-CpG steps, while TANDEM binds with highest affinity to 5'-TpA.[45, 138] In the scenario

indicated in these studies, echinomycin would be binding to a 5'-GpC step, while TANDEM would be binding to a 5'-ApT step. Although a crystal structure of the TANDEM intercalator that was published in 1981 suggested that binding at ApT steps would be preferred, this interpretation has since been disproved.[139]

The fact, that the ligands would have a lower affinity for the nucleotide sequences occurring in this force spectroscopy study does not mean necessarily that binding cannot occur at all. Dissociation studies of echinomycin from DNA have demonstrated that the association rate constants for echinomycin with 5'-CpG and 5'-GpC steps differ only by a factor of 2.[43] Similarly, comprehensive DNase footprinting studies have indicated that although TANDEM does not bind to the tetranucleotide sequence 5'-AATT,[140] binding does occur at the sequence 5'-TATA and that therefore some degree of binding to ApT steps cannot be excluded.[48] All of these studies have emphasised the importance of the flanking base pairs of the nucleotide binding step. For example, although TANDEM binds to 5'-TpA steps, no binding at all is observed at the sequence 5'-CGTACG, which includes a TpA step. In this study, the tetranucleotide binding sequences would be 5'-TGCA and 5'-TATA for echinomycin and TANDEM respectively. Both of these flanking arrangements are known to support ligand binding at the central step.[45, 49] Arguably, these considerations are difficult to apply to the binding arrangement provided by a junction between the oligonucleotides used in this study. In this scenario, the nucleotides that form the central binding step are not connected by a phosphate and have complete rotational freedom with respect to one another.

Table 26 provides the most probable lengths and forces derived from these experiments with echinomycin, TANDEM and bisacridine 3. Broadly speaking, where interactions are occurring, the values for these parameters are compatible with one another, irrespective of the individual ligand under investigation. As such, these values in themselves do not reveal potential differences in the binding mechanism of a particular ligand. However, the experiment clearly demonstrates that binding of either echinomycin or TANDEM is dependent on the precise arrangement of the terminal base pairs of the DNA.

Table 26 A comparison of most probable lengths and forces for echinomycin, TANDEM and bisacridine 3 relative to each of the two different oligonucleotides.

DNA	Ligand	Length / nm (SE)	Force / pN (SE)	n
GC	Echinomycin	43.5 (3.5)	50.5 (1.7)	47
	TANDEM	-	-	1
	Bisacridine 3	51.6 (2.0)	49.7 (3.2)	113
AT	Echinomycin	-	-	1
	TANDEM	42.9 (4.0)	40.4 (2.4)	23
	Bisacridine 3	44.4 (1.8)	52.3 (3.2)	257

The relative frequency of the events observed with echinomycin and TANDEM was noticeably lower than in the case of the bisacridines (Table 27). This could reflect several different factors. Firstly, that the affinity of echinomycin and TANDEM for DNA is lower than that of the bisacridines, making binding of any kind less likely to occur. Secondly, assuming, due to the dependence of the interaction on the terminal base pairs of the oligomer, that the interaction is occurring only at one point between the two complexed oligomers, the likelihood of such an arrangement occurring is less likely than with the bisacridines where binding can occur anywhere on the DNA. Thirdly, that the complex formed between either echinomycin or TANDEM and the DNA has a shorter half-life than that formed between a bisacridine and the DNA, and that therefore it will be harder to observe.

Table 27 Relative frequencies of events occurring with echinomycin, TANDEM and bisacridine 3 relative to the composition of the terminal base pairs of the oligomer. The frequency of interactions observed in the absence of a ligand was 0.06%.

DNA	Ligand	n	Frequency / %	n (total force curves)
GC	Echinomycin	47	0.19	25127
	TANDEM	1	0.00	20355
	Bisacridine 3	113	1.13	10000
AT	Echinomycin	1	0.01	20000
	TANDEM	23	0.12	20000
	Bisacridine 3	257	1.29	20000

Since cross-linking of the DNA with echinomycin and TANDEM was dependent on the composition of the terminal base pairs of the oligomers, any proposed binding mechanism must take this into account. If the unlikely *cis* to *trans* rearrangement of each compound's chromophores is occurring, then binding could occur throughout the DNA strand as in the case of the bisacridines. As such, it must be assumed that no reconfiguration of the

molecules is taking place, and that, retaining their cis conformation, the ligands are bridging the ends of opposing DNA strands (Figure 74). In one respect, that binding is occurring at the termini of the oligonucleotides, is not without a rational foundation. Computer modeling of doxorubicin binding to various short oligonucleotide sequences revealed that the ligand would bind preferentially to the ends of the DNA. The authors proposed that this was occurring because 'the energetic and structural perturbations associated with disrupting the normal base stacking interactions are smaller for the end bases than for internal bases'.[38]

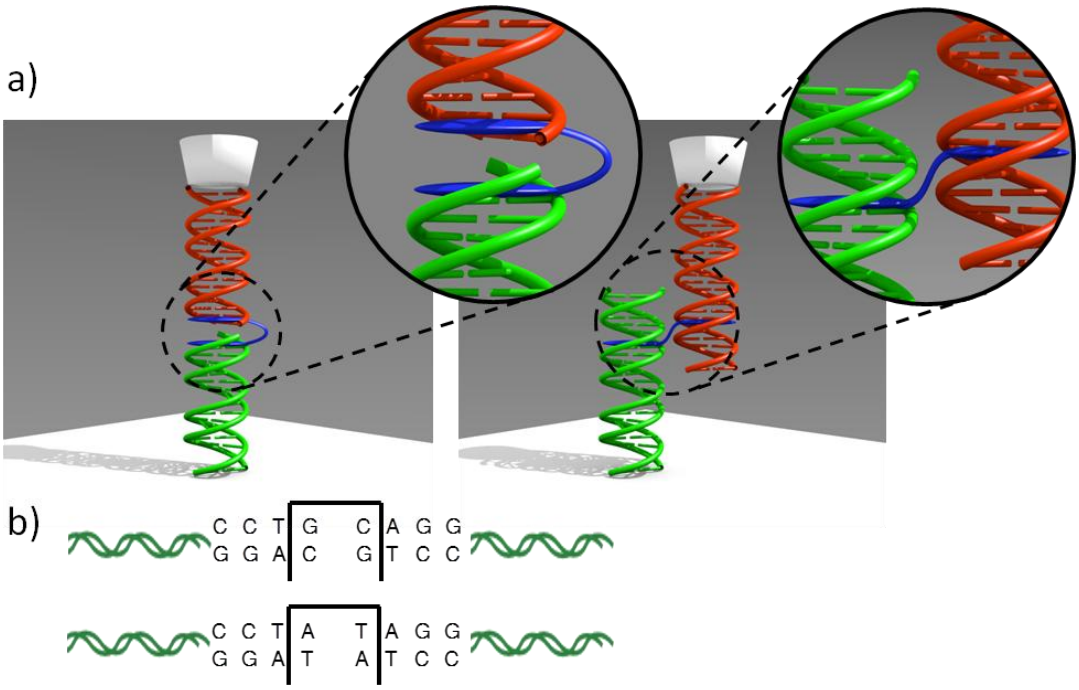

Figure 74 a) Proposed binding mechanism of echinomycin and TANDEM (left) and of the bisacridines (right). This graphic was kindly provided by Mr. Richard Steel, University of East Anglia. b) Schematic illustration of the difference in the binding site between echinomycin (top) and TANDEM (bottom).

Clearly, the mechanism proposed for echinomycin in Figure 74 could apply also to the bisacridines. However, in the case of the bisacridines, binding has been demonstrated to occur irrespective of the terminal base pairs of the oligomer and is therefore not sequence specific.

This protocol has provided quantitative information of the nature of the interaction that occurs when bisintercalators bind in an intermolecular as opposed to intramolecular manner. Although this mechanism has been observed before, it has never been extensively studied and, beyond the normal explanation of enhanced binding affinity and greater structural deformation of the bound duplex, may also be another aspect of the enhanced cellular cytotoxicity of bisintercalators relative to monointercalators.

These experiments have also identified a previously unobserved binding mode of echinomycin and TANDEM. If exploited, this mechanism could provide a means of accomplishing sequence specific, blunt-end ligation of oligonucleotides. Such a possibility could have significant implications in the application of DNA-based nanotechnologies.

Dynamic force spectroscopy of DNA bound to a bisacridine

Thus far, force spectroscopy experiments have only utilised one retraction velocity (0.5 μ/s). Although this was adequate for demonstrating whether or not Type II intercalation was occurring, more information may be obtained about the nature of a given interaction by varying the retraction speed of the AFM. A relationship between rupture forces observed via AFM and the retraction velocity at which the measurement was taken has previously been identified.[90] Combining this with an understanding of the energetics of bond formation and bond breaking permits the calculation of certain kinetic and dynamic parameters of the precise interaction that was broken at the point of rupture.[86, 88]

In order to characterise further the inter-molecular binding of a bisacridine with DNA, further experiments were conducted using the AT terminated oligonucleotide and bisacridine 2 at a range of different retraction velocities, ranging from 0.05 μ/s to 4 μ/s, covering three orders of magnitude. Slower retraction velocities were considered to be impractical, due both to the long periods of time that would be required to collect data and the effects of background noise. Similarly, although other studies have reported retraction velocities in excess of 4 μ/s,[90, 141] at these speeds hydrodynamic effects on the cantilever begin to have a significant effect on the quality of force extension curves obtained. Data collected at different retraction velocities in this fashion permitted the assembly of a dynamic force spectrum for bisacridine 2.

There is a clear relationship between the size of observed rupture forces and the critical loading rate (i.e. the loading rate at the point of bond rupture) at which the force was observed. Simply, any rupture force is proportional to the rate at which the force was applied, and as the velocity of the cantilever increases, so the measured rupture force increases. This pattern is illustrated in Figure 75, with a distinct increase in rupture forces noticeable at loading rates exceeding 1000 pN/s. Data obtained from analysis of the dynamic force spectrum are summarized in Table 28.

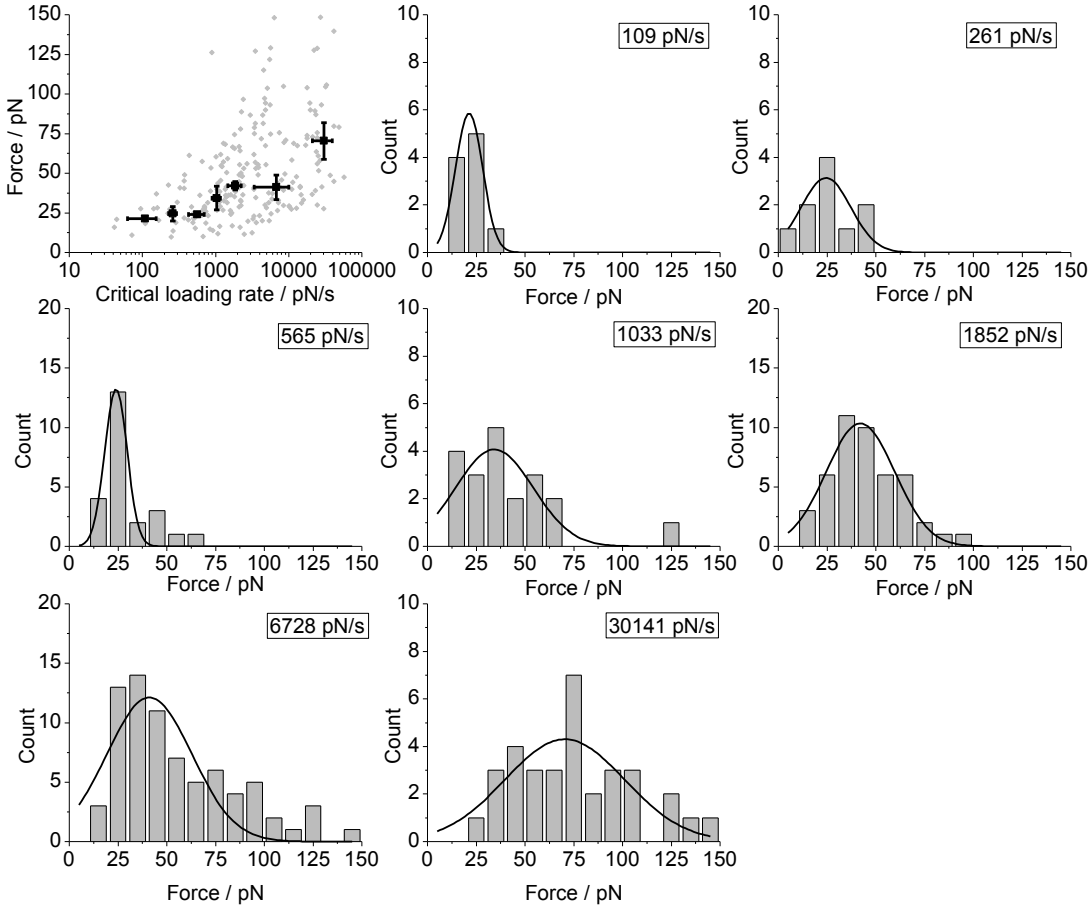

Figure 75 Top left, scatter plot of rupture force versus critical loading rate (showing the typical increase in rupture forces at higher loading rates) and histograms of forces at particular loading rates, showing the distribution of forces and gaussian fitting.

Table 28 Table of data derived from the histograms presented in Figure 75, showing the relationship between increased loading rate and increased force.

Mean critical loading rate / pN/s	SE / pN/s	Force / pN	SE / pN
108.8	46.3	21.3	0.5
261.2	32.8	24.5	4.5
564.7	134.7	23.9	1.0
1033.1	132.8	34.3	7.4
1851.8	382.8	42.1	2.6
6728.2	3342.2	41.1	7.8
30140.5	9050.8	70.4	11.6

A plot of the most probable rupture force at each subdivision of the critical loading rate is provided in Figure 76. This graph reveals the existence of two separate regimes within the dynamic force spectrum, each of which reveals different information about the nature of the interaction that is being investigated.

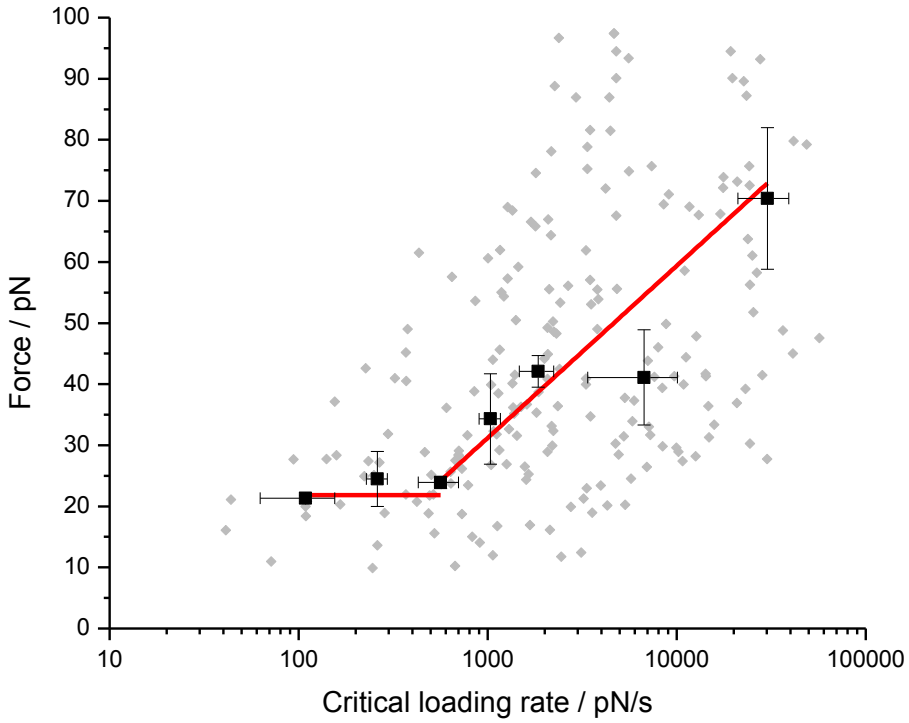

Figure 76 Plot of the most probable rupture force versus the corresponding critical loading rate (black points with error bars), overlaid against the scatter plot of the events observed during the DFS experiment. This plot highlights the existence of two separate regimes from within the dynamic force spectrum.

The sloping line at higher loading rates is representative of the kinetic regime of the bonding interaction to which a force is being applied.[89] In this region of the force spectrum, the rate at which a force is applied exceeds the rate of dissociation of the ligand from the DNA. The gradient of the slope and the value of the intercept with the *y* axis are provided in Table 29.

Table 29 Values for the gradient and the intercept of the linear regime observed at high loading rates as determined by Origin Pro™.

Bisacridine 2 (R^2 0.89)	Most probable value	SE
Gradient	28.2	4.8
y axis intercept	- 53.3	13.7

Since the slope of this line is inversely proportional to the distance to the transition state (x_t)[86] at which point rupture of the bond occurs, it is possible to determine the value of x_t using this information, using a value of 4.11 pN.nm at 24 °C (k_BT) to express the Boltzmann constant (k_B, 1.3806488 * 10^{-23} J/K) in terms of force and distance:

$$\text{Gradient} = k_BT / x_t$$

Rearranging the above formula yields a value of 1.5 Å for x_t (within a range of 1.2 to 1.8 Å). It has been suggested that values of x_t in the region of 1 Å are representative of single molecule interactions, while smaller values are indicative of the stretching of multiple bonds.[89] Certainly, values of x_t in the region of 1 to 10 Å likely represent the kinds of supramolecular reorganization and bond angle deformation liable to be occurring at the point of rupture where both the PEG tether and the DNA to which it is attached have been stretched to their full lengths.[142] Similar values for x_t have been reported in other spectroscopy studies that involve the stretching of DNA. A study utilising optical tweezers to examine the binding of actinomycin to DNA found a value of 1.1 Å (± 0.2 Å) for the distance from the bound to the unbound state of the ligand.[143]

Extrapolating the line to the critical loading rate at which the applied force is 0 pN (r_0) allows calculation of the kinetic unbinding rate of the system, according to the following equation:

$$k^0_{off} = r_0 e^{-.577 x_t / k_B T}$$

In this context, r_0 may be calculated by rearranging the typical formula of $y = mx + c$, so that:

$$r_0 = 53.3 / 28.2$$

Taking the inverse log of 53.3 / 28.2 yields a value for r^0 of 77.6 pN/s, which subsequently provides a value for k^0_{off} of 1.59 s^{-1} (within a range of 0.1 to 18.0 s^{-1}). Values for x_t and k^0_{off} are summarized in Table 30.

Table 30 Values for x_t and k^0_{off} determined from the dynamic force spectrum in Figure 76. A range for each of these values was calculated using the standard error of each parameter shown in Table 27.

	Most probable value	Range
x_t / Å	1.5	1.2 to 1.8
k^0_{off} / s^{-1}	1.6	0.1 to 18.0

The thermal off rate, k_{off}, alone does not provide an indication as to the affinity of the bisacridine for the inter-molecular binding arrangement. However, a study by Liu et al. into the binding of 9-aminoacridine to DNA, using a force spectroscopy apparatus not dissimilar to that described here, reported a similar range of values for k_{off} from 1.2 s^{-1} to 21.7 s^{-1}.[99]

The lower region of rupture forces shown in Figure 76 may be interpreted in two different ways. According to the Bell-Evans model, different regimes within a dynamic force spectrum were considered to be indicative of different barriers within the energy landscape.[86, 88] However, an alternative interpretation of the energy landscape has more recently been proposed. According to Friddle and Noy, the alternative regime observed at low critical loading rates reflects an equilibrium regime, where the rate of applied force does not exceed the rate of dissociation of the ligand from the DNA. The height of this equilibrium regime is representative of the free energy (ΔG_u) of the unbinding interaction that is being observed.[89, 144]

Assuming, as illustrated in Figure 76, that this region of the force spectrum is indeed an equilibrium state where the gradient of the fitted line is zero, it is possible to estimate a value for ΔG_u. Extrapolating this line to the point where *x* is equal to zero yields a value for *y (*or f_{eq}) of 21.84 pN (SE 0.76). The relationship between f_{eq} and ΔG_u may be described as:

$$f_{eq}^2 = 2k\,\Delta G_u$$

Applying this relationship requires the estimation of a value of k, or in this instance k_{eff} a combination of the spring constant of the cantilever and of the PEG tether that was utilised in this experiment. The nominal spring constant of the cantilever that was provided by the manufacturer was 0.027 N / m. However, the values derived from thermal tuning of the two cantilevers used to obtain the force spectrum were 0.0393 and 0.0384 N / m. Taking a mean average of these two experimentally determined spring constants yields a value for $k_{cantilever}$ of 0.0389 N/m. Assuming a typical spring constant for PEG of 150 N/m gives:

$$k_{eff} = 150*0.0389 / (0.0389 + 150)$$
$$k_{eff} = 0.0389 \text{ N / m or } 38.9 \text{ pN / nm}$$

Applying these values for k_{eff} to f_{eq} yields a value for ΔG_u of 6.13 in terms of force and distance. This value may be converted into kJ/mol:

$$(6.13 / 4.11)*2.479 = 3.70 \text{ kJ/mol}$$

Finally, converting this value of 3.70 kJ/mol into kcal yields a ΔG_u of 0.88 kcal/mol.

Data of this kind are relatively lacking, certainly from force spectroscopy investigations into the behaviour of intercalators with DNA. The study of the intra-molecular binding of

acridine with DNA by Liu et al. did not provide a value for ΔG_u. Similarly, studies of the capacity of bisacridines to form inter-molecular junctions, using agarose gel electrophoresis, did not provide any thermodynamic data for this particular binding mechanism.[33-34]

However, studies have been conducted into the intra-molecular binding of intercalators using other techniques. These studies have reported values for ΔG_u of around 7.6 kcal/mol for echinomycin and 5 kcal/mol for acridine.[145-146] The value of 0.88 kcal/mol reported here for a Type II intercalation event could be considered to be fairly consistent with these values, especially when considering that the ΔG_u for a well studied, high affinity, interaction such as that of biotin and streptavidin has been reported to be in excess of 20 kcal/mol.[147] Certainly, given the nature of a Type II intercalation event, it is not surprising that any value for ΔG_u would suggest this to be a weaker interaction than that of a Type I, intra-molecular event.

There nonetheless remain some important limitations to the value of 0.88 kcal/mol that has been obtained here. The value itself is derived from an approximate value of the effective spring constant that may not accurately reflect the elastic nature of the various components of the system, namely the combination of the cantilever, the PEG and the intercalated DNA. Moreover, the value of 0.88 kcal/mol represents an average of all of the potential binding arrangements that may occur between the two separate strands of DNA. The precise value for binding at different nucleotide steps within the DNA could be different depending on the precise arrangements of the nucleotides at the binding site.

Visualising Type II intercalation with gold nanoparticles

Gold nanoparticles are of interest in several fields, notably as a means of detecting contamination of water by mercury, forensic science, drug delivery and in the development of conducting materials.[148-151] The particles themselves are very versatile, and can be functionalised in a number of ways with proteins or DNA, typically via thiol chemistry.

Disperse suspensions of gold nanoparticles have a characteristic red colour that becomes colourless when the particles aggregate. Precipitated gold nanoparticles are typically blue in colour. Controlled aggregation of gold nanoparticles has been demonstrated in a number of ways, including by the addition of sodium chloride, or the annealing of particles functionalised with ssDNA.[152-154]

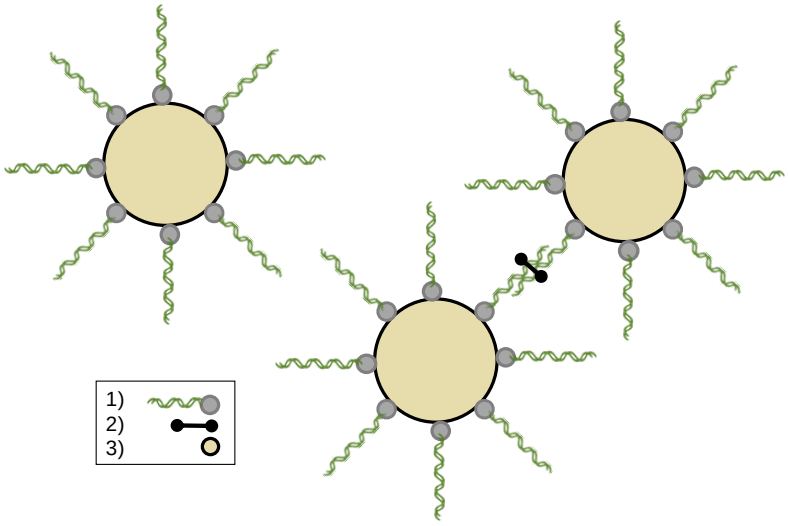

Figure 77 Graphical illustration of the experimental concept, showing how aggregation of the particles occurs on addition of a bisintercalator. The legend denotes 1) DNA 2) Bisintercalator 3) Gold nanoparticle.

Theoretically, cross-linking of DNA by bisintercalators should yield the typical red to colourless change in a solution of these particles functionalised with dsDNA. A schematic of the experiment is provided in Figure 77. Although the cross-linking of DNA by bisintercalators has been demonstrated using force spectroscopy, these experiments were relatively slow and required complex analysis in order to interpret the data. The simple colour change associated with aggregation of the gold nanoparticles would provide a simple assay for determining, instantly, whether or not cross-linking of DNA is occurring.

A 3 nM stock solution of gold nanoparticles was prepared by mixing separate solutions of gold (III) chloride trihydrate (32 µM) and trisodium citrate (170 µM) at 85°C for two and a half hours.[155] Two complementary oligonucleotides, with the same sequence as used in the force spectroscopy experiments were annealed. One of these oligonucleotides incorporated a thiol group at the 5' terminus. The sequences of the DNA are as follows:

1) 5' – [ThiC6] – CTACGTGGACCTGGAGAGAGGAAGGAGACTGCCTG – 3'
2) 5' – CAGGCAGTCTCCTTCCTCTCTCCAGGTCCACGTAG – 3'

In order to attach the DNA to the gold nanoparticles, 31.5 µl of a 25 µM solution of the thiolated DNA was added to 1.5 ml of the gold nanoparticles along with a volume of 30 µl of 500 µM trisodium citrate (pH 3.0). After mixing, the solution was left standing for 10 minutes before 52.5 µl of 2 M sodium chloride was added, whereupon the solution was left in a rotary mixer for 20 minutes. A further 150 µl of 2 M sodium chloride were subsequently added to the solution, and the system returned to the rotary mixer for 40 minutes. In order to

remove unbound nanoparticles and DNA, the solution was centrifuged at 8000 rpm for 30 minutes. The supernatant was decanted, and the red aggregate resuspended in 10 mM phosphate buffer (pH 7.4). Successful attachment of the DNA to the nanoparticles was confirmed by UV spectrophotometry. Gold nanoparticles have a characteristic absorption band at 520 nm, which shifts to 525 nm when DNA is coupled to the particle surface.

Adding intercalators to solutions of gold nanoparticles

In order to ascertain whether or not cross-linking of the DNA on the nanoparticles occurs when a bisintercalator is added to the solution, experiments were conducted using UV spectrophotometry. A volume of 570 µl of the gold nanoparticle and DNA solution was transferred to a cuvette, to which 1 µl aliquots of the relevant ligand were then added. Spectra were obtained after each addition.

Addition of either an increased volume of PBS buffer or sequential addition of a 2 mM solution of 9-aminoacridine caused no change to the position of the peak at 525 nm, indicating that under these conditions the gold nanoparticles remained stable. On addition of increasing concentrations of the acridine monointercalator, a new peak was observed around 400 nm, typical of UV absorbance by an acridine (Figure 78). At the same time, no change in the colour of the solution could be observed following the addition of the acridine, with both the control, and the solution remaining a brick red colour.

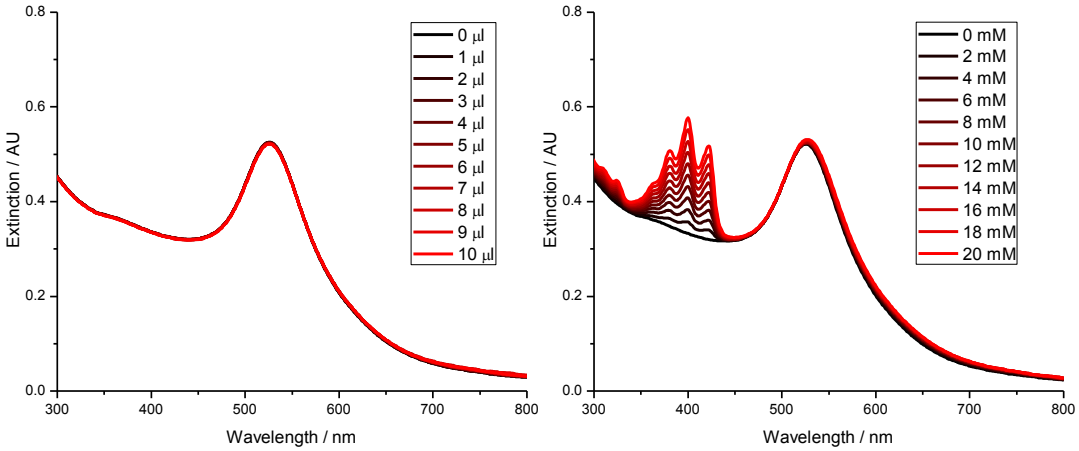

Figure 78 UV absorbance spectra of gold nanoparticles functionalised with dsDNA. Stepwise addition of 10, 1 µl aliquots of PBS buffer did not change the appearance of the spectra in any way (left). Addition of 10, 2 µl aliquots of 2 mM 9-aminoacridine did not cause a change in the peak at 525 nm, but did result in the appearance of a new peak at 400 nm.

Addition of the bisacridines to the nanoparticle solution produced a measurable change in the position of the peak at 525 nm that is characteristic of the aggregation of gold particles. A

colour change from red to colourless was also observed with the two bisacridines, bisacridine 2 and bisacridine 3.

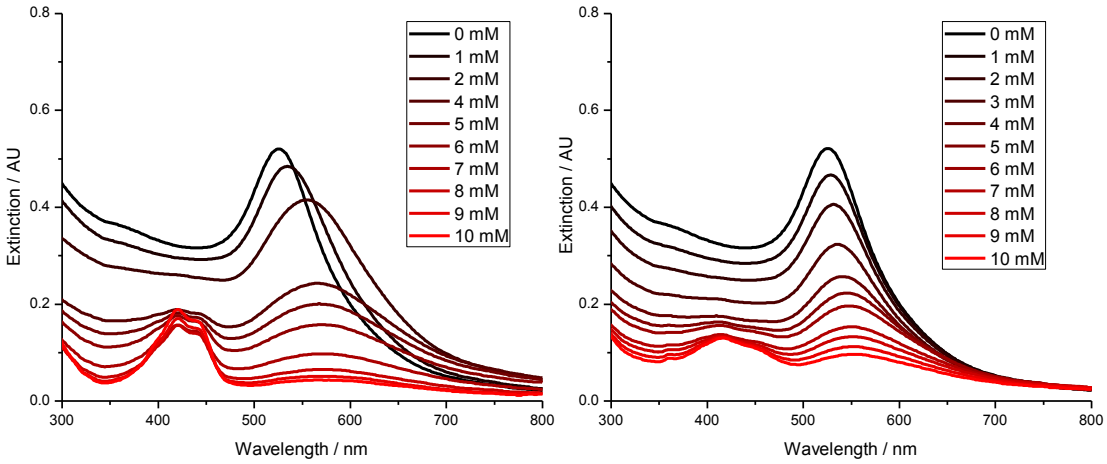

Figure 79 Spectra of the bisacridines bisacridine 2 (left) and bisacridine 3 (right). With bisacridine 2, there is a rapid change in the position of the peak at 525 nm, accompanied by a shoulder in the wavelengths around 600 nm, indicative of aggregation. The fall in intensity of this peak reflects a degree of precipitation. The characteristic absorbance peak of the acridine may also be seen at 400 nm. With bisacridine 3 the peak shift occurs more gradually, and there is no shoulder at 600 nm, suggesting that here, aggregation of the gold particles is following a different mechanism.

A comparison of the colour of the solutions, following addition of the monointercalator and the bisintercalators, also demonstrates the differences between the various compounds. This change from red to colourless is shown in Figure 80.

Figure 80 Solutions of gold nanoparticles. From left, control (no ligand), 10 mM bisacridine 2, 20 mM 9-aminoacridine, 10 mM bisacridine 3. The colour change from red to colourless is typical of gold nanoparticle aggregation caused by the bisacridines.

Since the oligonucleotide utilised in these experiments was identical to the GC terminated oligonucleotide used in the force spectroscopy experiments, it was hoped that binding may also be observed with echinomycin. Due to the poor aqueous solubility of echinomycin, it

was necessary to suspend the compound in DMSO. This was further diluted to an aqueous solution of 10% DMSO in PBS. Stepwise addition of DMSO to the gold nanoparticles without the ligand was conducted in order to ascertain if the solvent might cause the particles to aggregate.

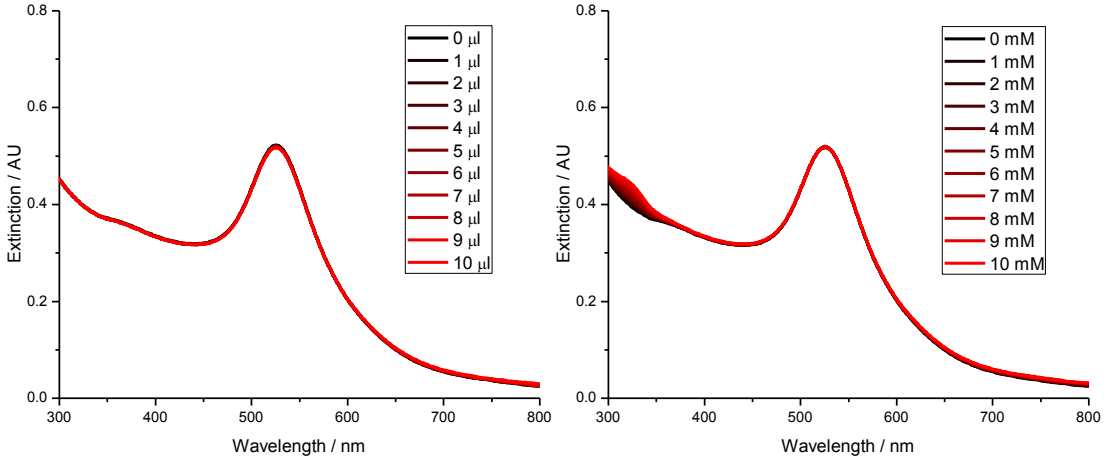

Figure 81 Spectra showing stepwise addition of 1 µl aliquots of DMSO (left) and addition of 1 µl aliquots of a 1mM solution of echinomycin in 10% DMSO (right). The bands evident at 320 nm in the echinomycin sample are likely indicative of the presence of echinomycin, which absorbs UV at 243 and 320 nm.

Figure 81 demonstrates that no change in the peak at 525 nm was observed, either with DMSO or echinomycin. A comparison of the colours of the gold nanoparticle solution after the addition of each of the ligands is provided in Figure 82. Addition of echinomycin to the gold nanoparticles did not result in a change from red to colourless. Given the results of the force spectroscopy experiments, this was somewhat disappointing. However, this may be attributable to several factors, which should be considered in turn. First, force spectroscopy experiments were conducted at a much lower echinomycin concentration than experiments with the gold nanoparticles (100 nM and 1 to 10 mM respectively). At nanomolar concentrations, echinomycin is water soluble and hence it was possible to reduce the DMSO content of the solution to only 0.1%. DMSO has been shown to cause changes in DNA secondary structure, typically a slight contraction, which may inhibit the attachment of a ligand. Second, the frequency of the events observed via force spectroscopy was, in the case of echinomycin and TANDEM, significantly lower than with the bisacridines. Furthermore, by lowering the AFM cantilever towards the substrate, connections of this kind would have been more likely to occur due to the increased proximity of the oligomers, whereas the gold nanoparticles are moving freely in solution. Third, it has not been possible to quantify the amount of DNA attached to any of the gold nanoparticles. Although studies elsewhere are attempting to address this issue, there does not currently exist an accessible protocol capable

of rendering an accurate concentration for the DNA on the surface of the gold nanoparticles.[152] As such it is not possible to determine the ratio between the ligands and the DNA. Since Type II intercalation is known to occur at high ligand to DNA base pair ratios, it is possible that, at the concentrations utilised in these experiments, the ratio of echinomycin to DNA was not sufficiently high to give way to cross-linking of separate DNA strands.

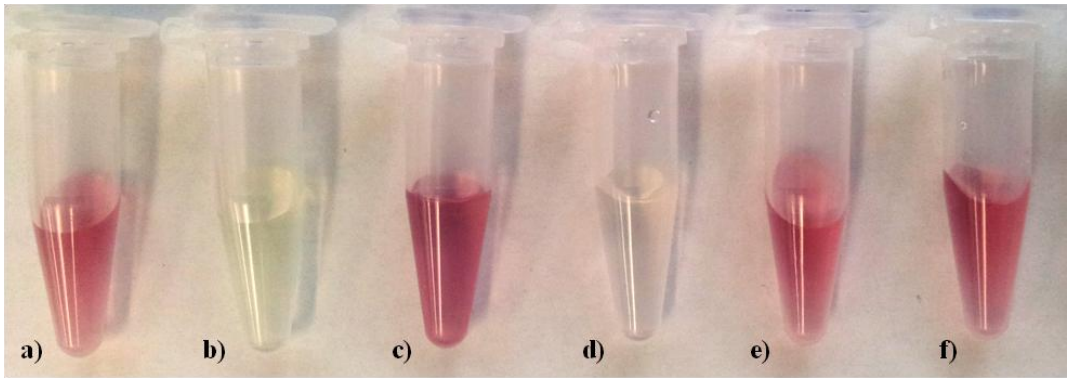

Figure 82 Solutions of gold nanoparticles containing different ligands. a) no ligand b) 10 mM bisacridine 2 c) 20 mM 9-aminoacridine d) 10 mM bisacridine 3 e) DMSO f) 10 mM echinomycin. Colour changes with the bisacridines reveal the Type II binding mechanism, which is not observed with echinomycin.

Reversing ligand induced aggregation of gold nanoparticles

The binding activity of intercalators has been demonstrated previously via sequestration with the surface active agent sodium dodecyl sulphate (SDS).[156] Simply, by changing the binding equilibrium between the ligand and the DNA, SDS will remove bound ligand from DNA, reversing the process of intercalation. In order to ascertain whether or not the process of nanoparticle aggregation could be reversed via this mechanism, SDS was added to solutions of gold nanoparticles that had been aggregated with the bisacridines.

In order to establish whether or not the SDS itself would change the stability of the nanoparticle suspension, 1 µl aliquots of 20 mM SDS (10 mM phosphate buffer, pH 7.4) were added to a solution of 570 µl of the nanoparticles and no changes were observed (Figure 83).

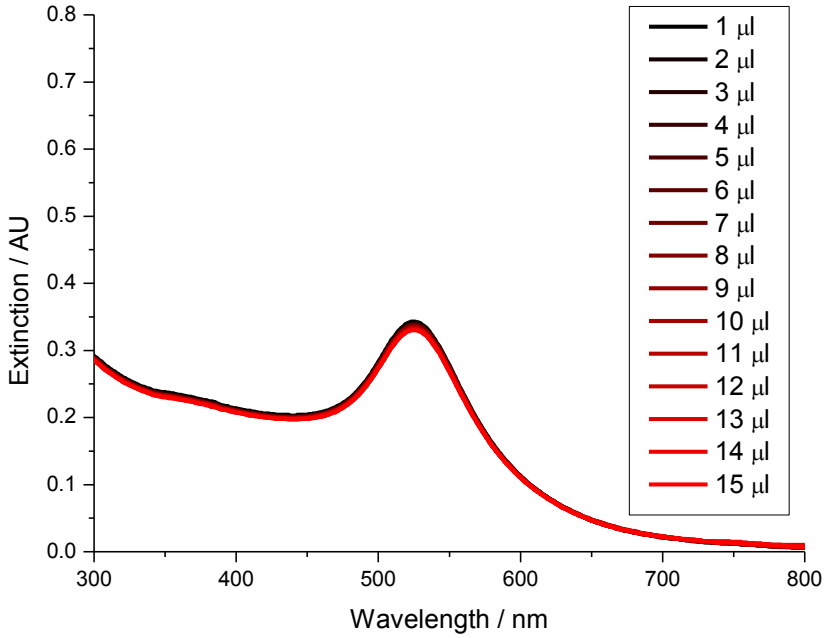

Figure 83 Addition of 1 µl aliquots of SDS to the gold nanoparticle solution. No changes to the appearance of the spectrum are observed.

In order to test the reversibility of the aggregation process following the addition of a ligand, aliquots of bisacridine 2 were added to the gold nanoparticle solution until a change in the spectrum was observed that indicated that aggregation of the nanoparticles was occurring. At this point, successive quantities of SDS were added to the aggregated solution until the spectrum had returned to that of the gold nanoparticle solution prior to aggregation (Figure 84).

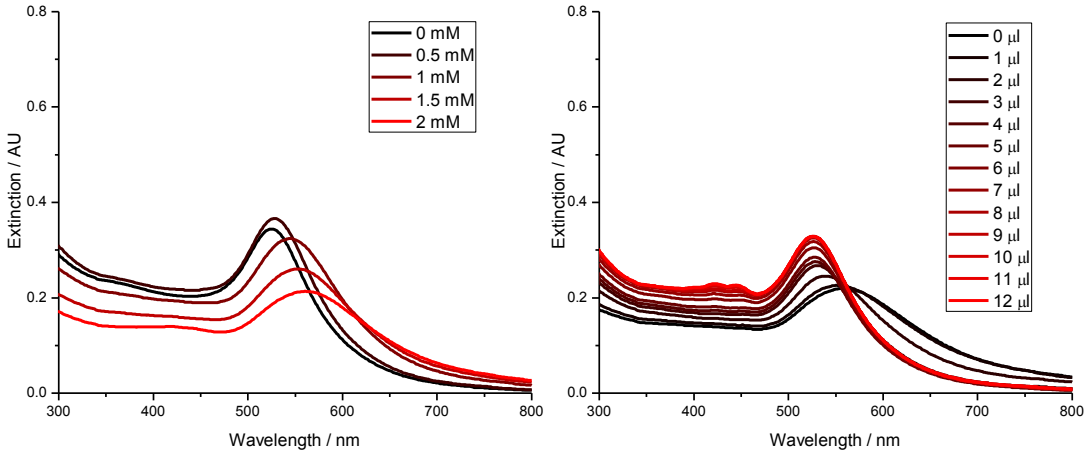

Figure 84 Spectra of gold nanoparticles binding to increasing concentrations of bisacridine 2 (left) and reversal of DNA-ligand binding by addition of an increasing concentration of SDS (right).

This experiment was repeated using another bisacridine, bisacridine 3, and similar results were obtained (Figure 85).

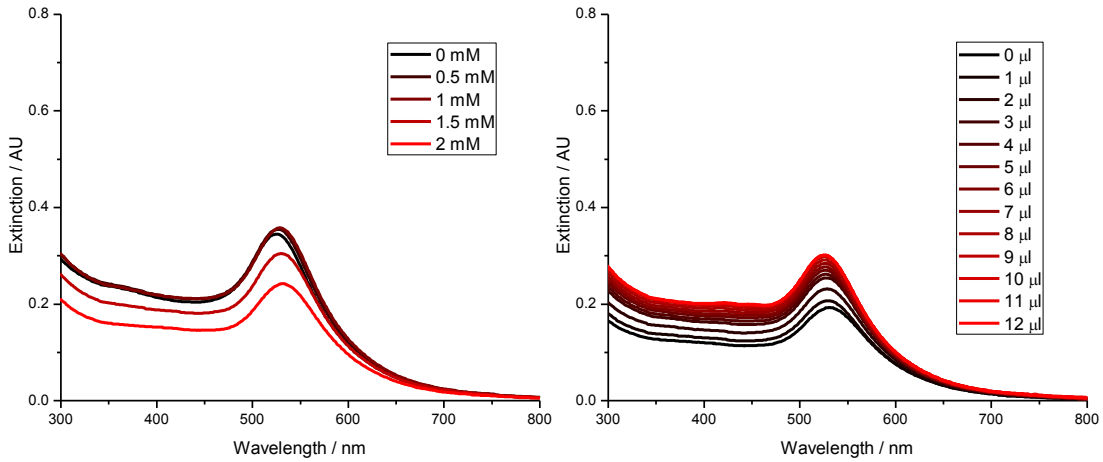

Figure 85 Spectra of gold nanoparticles binding to increasing concentrations of bisacridine 3 (left) and reversal of DNA-ligand binding by addition of an increasing concentration of SDS (right).

Both Figure 84 and Figure 85 illustrate that aggregation of gold nanoparticles by bisacridines is a reversible process. There is also an associated colour change, from colourless to red (Figure 86).

Figure 86 Solutions of gold nanoparticles containing 2mM bisacridine 2. A change from red to colourless corresponding to the change in peak position in Figure 84 is shown (left) alongside the same solution after the addition of 12 µl of 20 mM SDS (right). In each case, the left hand eppendorf contains a solution of gold nanoparticles and DNA.

An alternative means of demonstrating the reversibility of the intercalation of DNA with a ligand is via the use of CT-DNA in place of SDS. Whereas the surfactant removes bound ligand from the DNA attached to the gold nanoparticles, addition of further quantities of DNA, freely in solution, effectively reduces the ratio of ligand molecules to available DNA base pairs (Figure 87). Addition of calf-thymus DNA to the aggregated solutions of gold nanoparticles caused a reversal of the aggregation. In all cases, a colour change was observed from colourless to red.

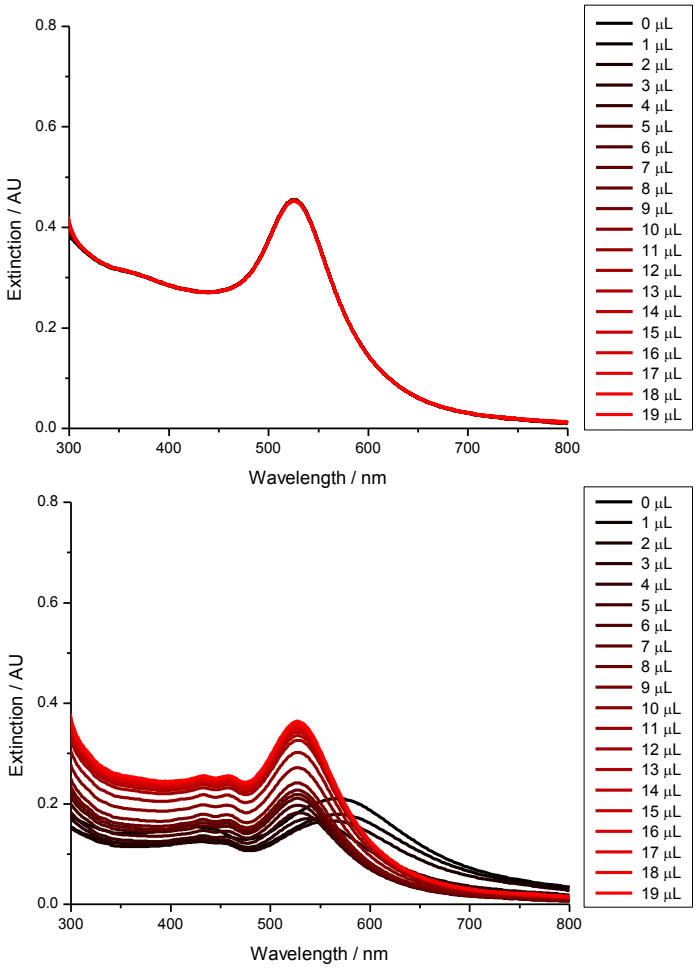

Figure 87 UV absorbance spectra of gold nanoparticles, showing that the addition of successive, 1 µl aliquots of CT-DNA does not affect the spectrum (top) but that increasing the amount of free DNA in solution can reverse the aggregation process after the addition of bisacridine 2 (bottom).

Measuring the aggregation of gold nanoparticles via DLS

An alternative means of demonstrating the reversible aggregation of gold nanoparticles is that of dynamic light scattering (DLS). Not only the colour and UV absorbance spectra of solutions of gold nanoparticles may be diagnostic of aggregation, but also the size of individual or aggregated particles within the solution.

Experiments were conducted in order to ascertain whether or not a difference in the diameter of any aggregated material within the solution could be found after the addition of a bisintercalator. Experiments were also conducted to confirm whether or not these aggregates were broken down by the process of surfactant sequestration as suggested by the colour change of the solution from colourless to red. Data obtained from these experiments are provided in Table 31. Particle size analysis of the nanoparticles was performed in a 1.5 ml plastic UV-visible absorbance cuvette using a Malvern Zetasizer Nano-ZS. Measurements

for the ligands were taken after the addition of 4 µl of 500 µM solutions of the bisacridines bisacridine 2 and bisacridine 3, each to an initial volume of 570 µl of the gold nanoparticles. Measurements involving SDS were taken after the addition of 12 µl of 20mM SDS to an aggregated solution of the gold nanoparticles, containing 4 µl of either of the bisacridine ligands.

Table 31 Mean diameters for different solutions of gold nanoparticles obtained via DLS. Note that addition of SDS to a solution of gold nanoparticles functionalised with DNA results in a change in mean diameter from 31 to 56 nm. Addition of the bisacridines yields a large increase in mean particle diameter.

	Mean diameter / nm	λmax / nm
cAuNP	24.17	519 – 520
cAuNP + DNA	31.30	523 – 527
cAuNP(DNA) + SDS	55.86	523 - 527
cAuNP(DNA) + bisacridine2	645.03	560 – 561
cAuNP(DNA) + bisacridine 2 + SDS	48.26	525 – 527
cAuNP(DNA) + bisacridine 3	113.47	530 - 533
cAuNP(DNA) + bisacridine 3 + SDS	50.94	524 – 528

These experiments confirm the results obtained via UV absorbance. The mean diameter of the gold nanoparticles following the addition of both a bisacridine ligand and SDS is approximately the same as the diameter of the particles prior to the addition of SDS, around 50 nm. However, on addition of bisacridine 2, there is a significant change in the mean diameter of the particles present in solution from 24.17 nm to 645.03 nm.

The DLS data also highlight a significant difference between particle sizes observed with bisacridine 2 and bisacridine 3. While the mean diameter of aggregates observed on binding of bisacridine 2 is 645 nm, that of those bound to bisacridine 3 is 113 nm. Whether or not this difference is actually significant is open to question, since the values for particle sizes determined by DLS are averages of the entire range of particle sizes present in solution. However, the UV spectra presented in Figure 79 showed a difference in the spectral changes that could be observed with bisacridine 2 and bisacridine 3. If this difference is indeed significant, it might be explained in a number of ways. Firstly, aggregation of the gold nanoparticles may be occurring in a different way with each compound. Although the chromophore of each of these bisacridines is identical, the structure of their interchromophore linkers is very different. This may lead to differences in their respective modes of intercalation. Secondly, the affinity of each compound for binding of this kind may

be different. Monitoring the Type II binding of these compounds via force spectroscopy revealed a higher incidence of interactions with bisacridine 3 relative to bisacridine 2.

Visualising the aggregation of gold nanoparticles using TEM

Further evidence that bisintercalators are cross-linking DNA attached to the gold nanoparticles is provided by TEM. Samples of gold nanoparticle solutions, before and after the addition of a ligand, were deposited on carbon films and pictures were obtained that reveal the clusters of gold nanoparticles that have formed as a result of the presence of the bisintercalator in the solution.

Pictures of two TEM samples are provided in Figure 88. While the gold nanoparticle solution provided a uniform coverage of the carbon scaffold demonstrating individual or clusters of 2 or 3 separate gold nanoparticles, the ligand sample was very different. Addition of bisacridine 2 yielded large clusters of gold nanoparticles due to the inter-molecular DNA binding mechanism of this compound.

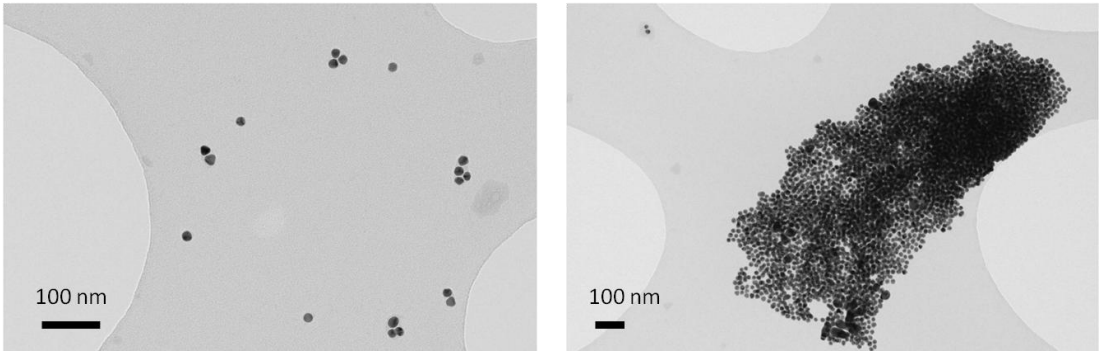

Figure 88 TEM images of gold nanoparticles functionalised with DNA (left) and the same nanoparticles after the addition of bisacridine 2 (right), showing the kinds of large nanoparticle aggregates formed by Type II intercalation.

Conclusions

These experiments have demonstrated conclusively that bisintercalators are capable of binding to DNA in two different ways; via the intra-molecular mechanism referred to as Type I intercalation, and via the inter-molecular mechanism referred to as Type II intercalation. Type II intercalation by luzopeptin and some bisacridine analogues has already been shown elsewhere as discussed, however, the force spectroscopy study described here constitutes the first attempt to characterise the strength of this particular binding interaction. Further work will be required in order to ascertain whether or not Type II intercalation of DNA may have a chemotherapeutic application.

The force spectroscopy assay used for investigating Type II intercalation also revealed an unexpected binding mode of the bisintercalators echinomycin and TANDEM.[157] The sequence-specific Type II intercalation of the termini of opposing strands that is suggested by these experiments has never been revealed in any other studies involving the DNA binding behaviour of these two compounds. This particular finding is unlikely to find an application in the treatment of cancers, and so far has only been visualised using short stretches of DNA under the idealized conditions described above. However, in theory such a binding mechanism could be of considerable value in the field of the nanosciences. Reversible, controlled coupling of the termini of different DNA strands would enable the construction of longer DNA sequences, a process that is currently only possible by enzyme ligation.

The results of the force spectroscopy experiments with the bisacridines are supported by a gold-nanoparticle aggregation assay. When functionalised with DNA, gold nanoparticles aggregate readily on addition of a bisintercalator. There are a number of ways in which this experiment could be adjusted to provide more information about the cross-linking process. For example, by changing the nucleotide composition of the DNA, the sequence specificity of the intercalating ligand could be examined. Alternatively, the DNA could be replaced with an alternative structure such as RNA. Although the assay is restricted to ligands that bind in an inter-molecular fashion, there are many ways in which this assay could be adjusted to provide further information about the binding behaviour of such a compound.

Chapter 5 – Targeting secondary structures of DNA

Introduction

Ligands that bind to DNA are known cytotoxics, some of which have proven to be clinically useful (such as amsacrine), but the binding behaviour of small ligands such as intercalators does not demonstrate a high degree of specificity. The preference of some intercalators, such as echinomycin, for DNA sequences rich in particular nucleotides in the context of the extensive DNA sequences present in the nucleus of a cell, does not afford a means for effectively controlling the delivery of a cytotoxic agent to a patient.

This kind of relatively indiscriminate binding results in many ligands currently in clinical use, such as doxorubicin or cisplatin, suffering from narrow therapeutic indices where the margin between a therapeutic or a toxic dose is very small.[36] Ideally, it would be possible to deliver a ligand exclusively to the preferred site of action, thereby avoiding any dose related toxicities caused by indiscriminate binding activity. This problem has been approached in a number of ways, including through the development of pro-drugs that are activated by endogenous metabolic pathways (e.g. cyclophosphamide and 5-fluorouracil) to drug delivery systems or techniques that ensure the release of a ligand only at the desired site of action.[158]

Another approach to targeted drug delivery stems from more sophisticated understanding of particular disease states. Discovery of the genetic components of certain kinds of breast cancer led to the design of the monoclonal antibody trastuzumab (Herceptin™), a therapy which has revolutionized the treatment of HER2 positive metastatic breast cancer. Classically, the specificity of many chemotherapies has stemmed from the accelerated rate of cell division that occurs in most tumours. Targeting particular cellular processes associated with cell division offers a means of refining specificity of this kind.

Higher order DNA structures have been of interest for some time, offering a means of directing ligand binding towards DNA in a more controlled fashion than the simple primary sequence of the DNA itself.[159-160] These higher order structures are often prominent in the promoter regions of oncogenes and telomeres, suggesting a relationship between such secondary structures and the uncontrolled cell division associated with a tumour.[161] Specific examples of DNA secondary structures are G-quadruplex, associated with guanine rich regions, I-motif (associated with cytosine rich regions) and three or four-way DNA junctions such as the Holliday junction. The following experiments will examine two of these secondary structures, the Holliday junction and the I-motif. Full methods for each of the experiments described in this Chapter are provided in Chapter 7.

AFM imaging of the Holliday junction

In 2007 the crystal structure of an acridine binding at the cross-over region of a Holliday junction was published.[160, 162] In theory at least, stabilizing a Holliday junction via a small ligand should interrupt homologous recombination and thereby induce apoptosis. Techniques for studying the Holliday junction have hitherto tended to be indirect, such as gel electrophoresis, fluorescence titrations and CD.[163-164] However, a few papers have been published that have utilised AFM to provide direct visualization of the Holliday junction, as well as other secondary structures such as G-quadruplex.[165-166] One particular study used AFM to follow the branch migration of the Holliday junction, from initial formation of the cruciform structure (in its open conformation), to resolution where the DNA strands separate.[167] Borrowing the techniques of some of these earlier studies, our intention was to use AFM to provide direct evidence of the stabilization of the Holliday junction by an acridine.

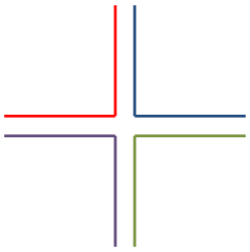

Figure 89 Cartoon of a four-way DNA structure, the Holliday junction.[168] Each of the separately coloured strands represents a strand of ssDNA.

Four separate oligonucleotides, capable of forming a four-way cruciform structure, were purchased (New England Biolabs, UK). The arrangement of the four separate oligonucleotides in a HJ structure is illustrated in Figure 89. The four oligonucleotides constituted two pairs of hemi-junctions. Each pair of oligonucleotides from each hemi-junction was annealed to its complementary strand, one strand being 39 base pairs in length, the other 35. The four base pair overhang permitted the attachment of a longer DNA tether, a 428 base pair linear fragment of DNA restricted from the plasmid pcDNA3.1/Hygro (+) (Invitrogen, UK). After ligation of the oligonucleotides to the longer DNA tether, the two separate hemi-junctions were annealed at equimolar ratios in TNM buffer for 4 minutes at a temperature of 50°C. The annealed material was then added to 45 µl of a solution of 10 mM $MgCl_2$ and immediately transferred to freshly cleaved mica for AFM imaging.

Unfortunately, repeated scans did not reveal any homogeneity in the surface features. Broadly speaking, DNA structures fell into one of three categories (Figure 90). First, and by far the most extensive, were linear DNA structures very similar to those observed prior to annealing. Second, were linear DNA structures approximately twice the length of those

structures that fell into the previous category. Finally, a very small number of potential cruciform structures were also identified (Figure 92).

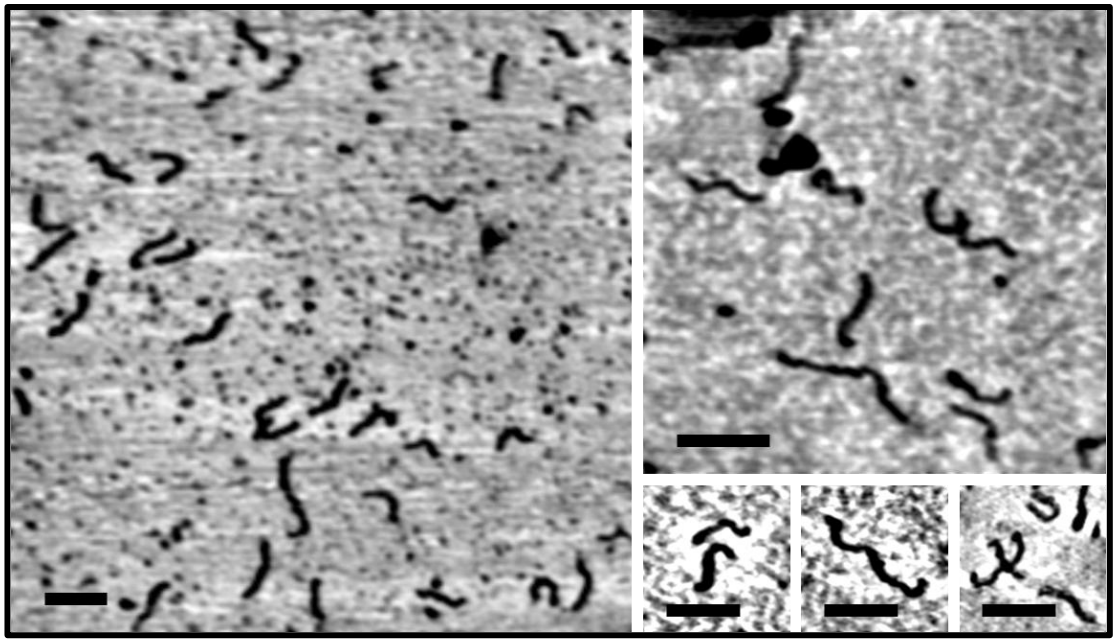

Figure 90 AFM images of the annealed Holliday junction hemi-junctions. The enlargements show the three typical types of features that were isolated from these images. The scale bars denote 200 nm.

Those DNA structures that were similar in conformation and physical dimensions to the original 427 base pair DNA fragments may be considered in three ways. First, they could be 427 base pair fragments of DNA that had failed to ligate to the oligonucleotides. Second, they may have been fragments that had failed to join together during the annealing process. Third, these particular DNA strands may have annealed, forming unstable cruciform structures that had resolved and separated before the samples were transferred to mica. The longer DNA strands, measuring approximately twice the length of the other linear DNA strands could be another product of the earlier ligation step. However, this is unlikely since the ligation products had been separated via electrophoresis, where the respective bands were clearly defined from one another. The effectiveness of this technique is supported by data collected from this experiment and the previous AFM experiment with a 771 base pair DNA fragment, where larger strands were not observed in the control groups. More likely, these linear structures are separate hemi-junctions that have successfully annealed, but where branch migration of the junction is not apparent.

Obviously, the original intention of this experiment was to identify cruciform structures typical of the open conformation of the Holliday junction. The few cruciform structures that were observed need not necessarily have been partially resolved Holliday junctions and

despite the low concentration of DNA material that was adsorbed onto the mica these structures may in fact be separate strands lying either on top of or next to one another. The possibility that these strands are lying on top of one another may be eliminated in individual cases by considering a cross-sectional profile the *z* axis of an image (Figure 91).[169]

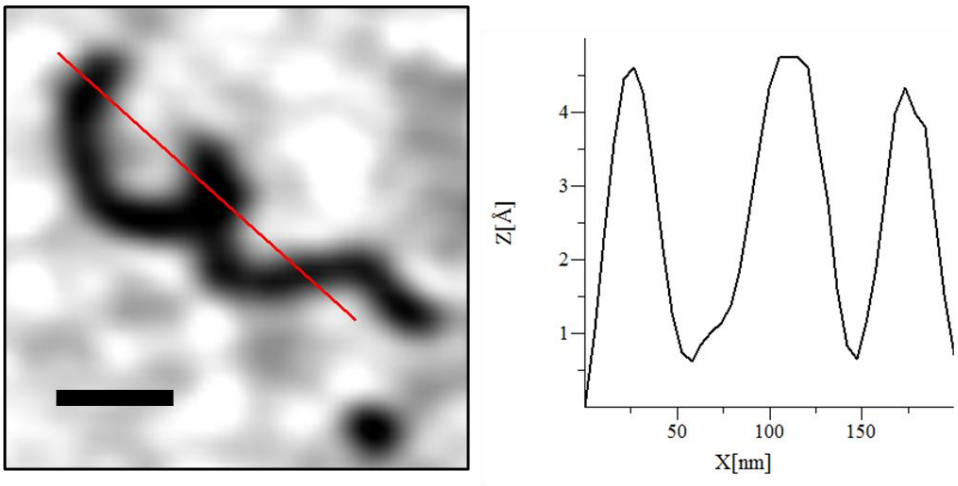

Figure 91 AFM image of an isolated DNA cruciform structure (left). The scale bar denotes 50 nm. The red line corresponds to a cross section of the image which is illustrated (right). This illustration demonstrates that there is no increase in the value of the *z* axis where the two strands meet, proving that these strands are not overlapping.

Furthermore, of the few cruciform structures that were isolated, in some cases the arms of the structures were equal in length. In the case of a situation where two strands had collided on the mica, it is probable that one arm would be longer or shorter than the other three, reflecting the random nature of the process. It therefore remains possible that these structures are indeed Holliday junctions showing varying degrees of branch migration.[167]

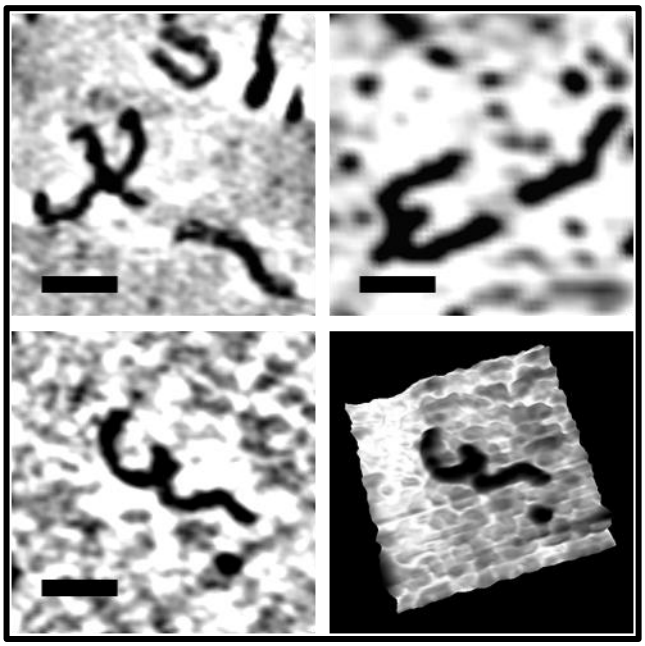

Figure 92 Cruciform structures isolated during AFM scanning of the annealed Holliday junction material. Clockwise from top left 1) A probable random arrangement of DNA, where one arm of the cruciform is noticeably shorter than the others 2 + 4) Potential Holliday junctions 3) 3 dimensional representation of the cruciform structure identified in 4. The scale bars denote 100 nm.

In an attempt to increase the number of cruciform structures, the annealing process was adjusted in a number of ways. Annealing was conducted in a range of buffers, including TBE, sodium cocodylate and HEPES, while the temperature of the heat block was also adjusted over a range from 40 to 60°C and periods of time from two to ten minutes. None of these adjustments yielded an increase in the number of potential Holliday junctions that were observed.

Force spectroscopy of the I-Motif

The binding of a bisacridine to another DNA secondary structure, the I-motif (Figure 93), has also been suggested.[170] Although the biological significance of this structure remains uncertain, its association with G-quadruplex, known to be associated with the enzyme telomerase and a large number of cancers, suggests that this structure may also be a viable target for chemotherapies.[171]

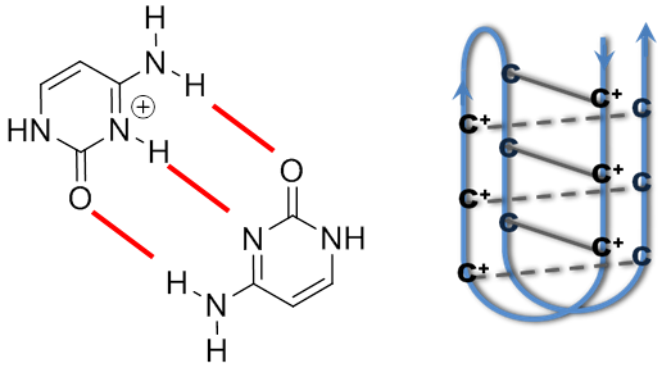

Figure 93 Graphical illustration of the I-motif structure, showing the H-bonding arrangement with a protonated cytosine base.[172]

The unfolding of a G-quadruplex has been examined using force spectroscopy, a technique that could be readily applied to monitoring the unfolding of the I-motif.[173] Using apparatus similar to that employed earlier in this study to explore inter-molecular intercalation (Figure 94), an oligonucleotide containing I-motif forming regions was stretched between the substrate to which it was attached and the opposing, bare AFM cantilever. The sequence of the oligonucleotide is as follows:

1) 5' – [NH_2] – TAACCCTAACCCTAACCCTAACCC – 3'

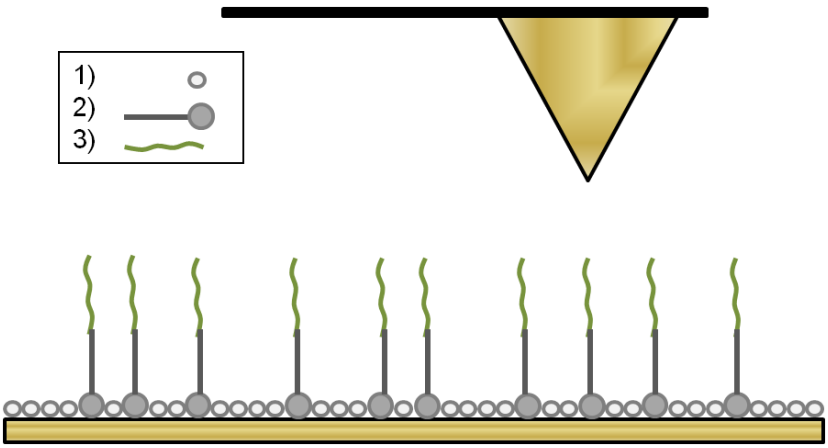

Figure 94 Illustration of the experimental design for stretching a ssDNA molecule. The surface of the AFM probe is bare and as such is able to adhere to the DNA attached to the substrate. The legend denotes 1) mercaptoundecanoic acid 2) PEG 3) ssDNA.

The preparation of the PEG tether and the passivation of the substrate were conducted in the same manner as previously described for the DNA cross-linking experiments. This experiment was conducted under three different sets of buffer conditions: at pH 7, where the I-motif is not believed to occur; pH 5, where the protonated cytosine regions of the oligonucleotide should form an I-motif; and at pH 7 in the presence of silver ions which are believed to induce I-motif formation even at neutral pH.[172] Using a bare, gold coated

cantilever (Asylum Research, BL-RC150VB) force spectroscopy was conducted in liquid by lowering and retracting the cantilever in arrays of 100 x 100 data points over areas of 10 x 10 microns on the gold surface.

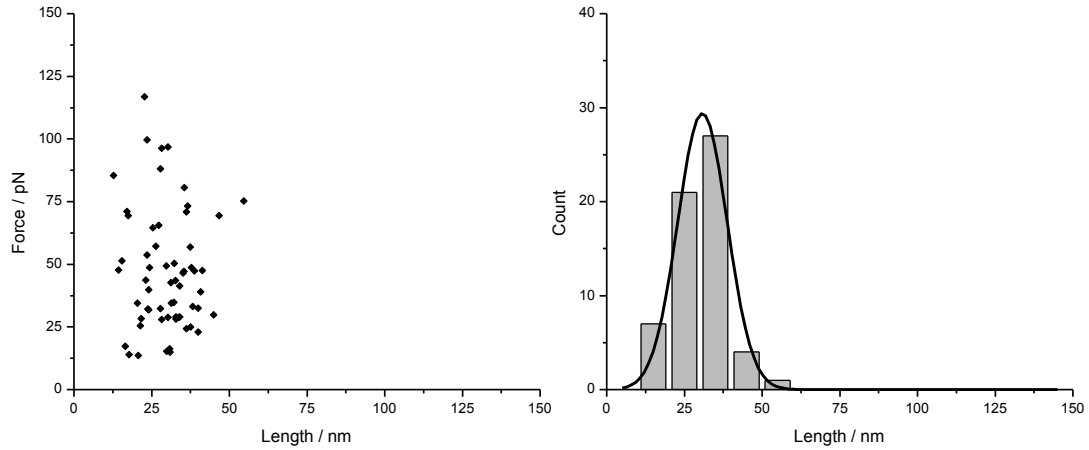

Figure 95 Scatter plot of observed interactions with Kuhn lengths greater than 0.6 nm (left) and histogram of lengths (right). These data were collected at pH 7.

An initial experiment to explore the range of lengths and forces that would be encountered yielded the data presented in Figure 95. Although events covered a fairly wide range of forces, gaussian fitting of the observed lengths provided a contour length for the oligonucleotide of 30.8 nm (SE 0.9 nm). Given that the oligonucleotide utilised here was 24 bases in length, and that the rise per base pair in ssDNA is 0.68 nm, the experimentally determined value corresponded well with the theoretical length of the molecule of 31.72 nm for the ssDNA coupled to the 15.4 nm PEG tether.

This same experiment was repeated under the other two sets of conditions. Firstly, the pH 7 buffer was substituted with 10 mM sodium cacodylate buffer pH 5.5. Secondly, the buffer was substituted with 10mM sodium cacodylate buffer pH 7.4 containing 100 µM $AgNO_3$. Figure 96 provides a comparison of the forces observed under each set of conditions and the data are tabulated in Table 32.

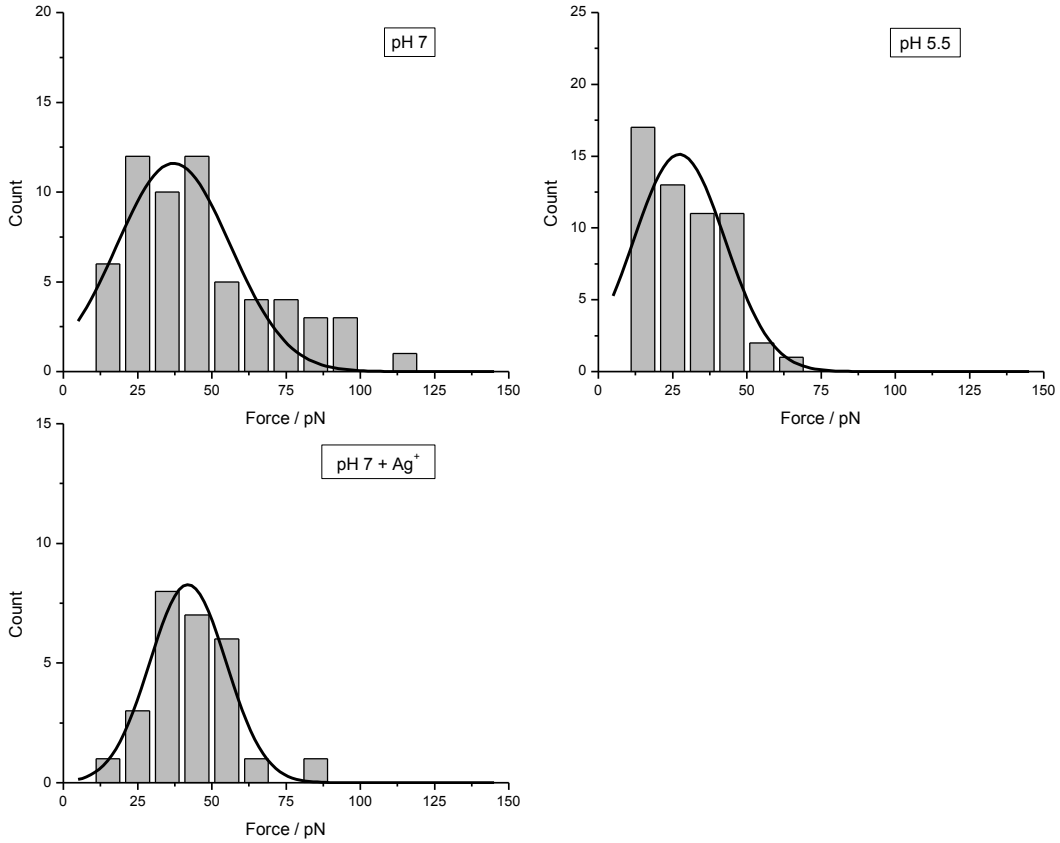

Figure 96 Histograms of force for stretching of the I-motif forming oligonucleotide sequence under different conditions of pH and buffer ion content. These histograms do not reveal any significant differences in observed forces under the different conditions of buffer and pH.

Although the distribution of observed forces is greater at pH 7, and mean observed forces for each set of conditions are different from one another, these observations are unlikely to be significant. It is important to note that, at a single retraction velocity, the precise numerical value of the most probable rupture force is a meaningless figure.[89]

Table 32 Comparison of the different forces obtained from the histograms in Figure 96 for each pH and buffer, showing the similarities in observed rupture forces.

	Mean force / pN (SE)	n
pH 7	37.1 (5.2)	60
pH 5.5	27.3 (5.1)	55
pH 7 + Ag^+	41.9 (1.8)	27

Conclusions

The failure of the Holliday junction binding assay may be attributed to several different factors. Primarily, the DNA preparation techniques yielded insufficient DNA material for extensive adjustment of the final annealing step. The initial cleavage of the plasmid DNA resulted in a considerable loss of DNA, the 427 base pair fragment constituting only 8% of

the 5428 base pair plasmid. Separation of the DNA following digestion and ligation reduced yields further, with the separation of the DNA from the agarose gel inherently inefficient.

The AFM imaging of the DNA hemi-junctions after annealing suggests that the complementary halves of the expected Holliday junction were aligning. If a more efficient means of generating the requisite DNA starting materials was utilised, theoretically the Holliday junction structure could be separated from other DNA material after the annealing process, thereby increasing the number of cruciform structures that may be visualized and also providing a secondary means of verifying that such cruciform structures are indeed true DNA secondary structures and not simply the result of separate strands lying in close proximity to one another.

Such an approach has already been demonstrated elsewhere using PCR to generate the hemi-junctions and agarose gel electrophoresis at 4°C to separate annealed Holliday junctions from non-annealed material.[167] This approach also resolves another problem with the experimental approach that was utilised here, specifically that of the annealing buffer. Successful annealing is dependent on the presence of metal ions such as magnesium, to facilitate the alignment of complementary nucleotide base pairs. Unfortunately, these same ions also stabilize the Holliday junction and prevent, or significantly slow, branch migration. Gel electrophoresis offers a means of removing the annealing buffer and subsequently replacing it with another such as TE buffer, under which conditions branch migration may occur.

That aside, this procedure did re-emphasize the capability of AFM as a means for providing direct evidence of activity at a single molecule level. The products of the DNA annealing process could be separated from one another using quantities of material that would be below the sensitivities of other commonly used processes such as gel electrophoresis. If the experimental procedure could be refined in the ways previously suggested, there is no doubt that AFM imaging would be capable of providing direct evidence of ligand-induced stabilization of a Holliday junction.

The results of efforts to discern differences in a short oligonucleotide capable of forming an I-motif structure were equally disappointing. Although the preliminary results demonstrated the capability of the AFM apparatus to resolve even a short oligonucleotide sequence such as that utilised here, the protocol would need to be developed if the unfolding of an I-motif structure is to be observed in this fashion. The next step, potentially, would be to attach a

functional group to the 3’ end of the oligonucleotide, perhaps a biotin bead, which could be trapped by a streptavidin coating on the AFM probe (Figure 97).

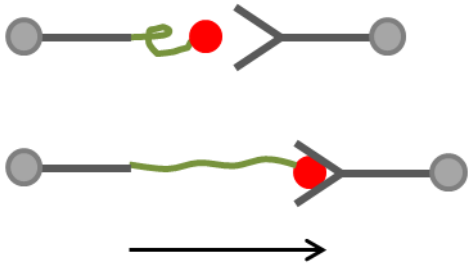

Figure 97 Conceptual arrangement of a ssDNA (green) coupled to a biotin bead (red). By lowering the streptavidin functionalised PEG attached to the AFM probe towards the substrate, coupling of the biotin and streptavidin will occur. The arrow demonstrates the direction of retraction after coupling has occurred.

Under the arrangement described in Figure 97, the oligonucleotide could be stretched over a range of loading rates, between the covalent gold-thiol linkage of the 5’ terminus, and the streptavidin-biotin complex at the 3’ terminus. However, given the small size of the I-motif, effectively spanning only four, tri-nucleotide cytosine regions, the oligonucleotide sequence may also require modification. Lengthening the sequence to incorporate multiple I-motif forming regions might facilitate the observation of unfolding of these regions as serial multiple events within a given force extension curve, so revealing the transition from the folded to the unfolded state of the I-motif.

Chapter 6 – Conclusions

Conclusions and future work

Despite advances in the diagnosis and treatment of cancer, there remains a pressing need for new chemotherapeutic agents. Although an improved medical understanding of specific cancers, such as those of the lung or prostate, has improved patient outcomes in certain cases there is no doubt that cancer will continue to be one of the leading causes of death in the human population.[174-176] As such, the discovery of new lines of treatment, whatever their nature, is of considerable importance.

Although a considerable period of time has elapsed since amsacrine was licensed for clinical use in the UK, research has continued into this class of ligand and the acridine analogues examined in these studies offer various advantages relative to other ligands.[177-179] First, these compounds are relatively straightforward to synthesize. Second, unlike the larger peptide bisintercalator echinomycin, all of the acridine dimers used in this study are water soluble. The failure to translate the in-vitro cytotoxicity of bisintercalators to a clinical environment does not necessarily preclude them from being chemotherapeutic agents of the future. Many of the limitations of small DNA binding ligands, such as a relative lack of specificity, could potentially be overcome by innovations in formulation and drug delivery.

These studies have confirmed previous theoretical assumptions that the acridine chromophore induces wide ranging deformation of the DNA duplex, the intercalated structure akin to that of the dehydrated A form of the classical Watson-Crick duplex.[120] Given the sensitivity of many intra-cellular enzymes, not only topoisomerase II, the ability of the acridines to induce a conformational switch in DNA sequences may yet find a chemotherapeutic application.

The capacity of bisintercalators to bind to DNA in an inter-molecular fashion has attracted considerably less attention than the mechanism of intra-molecular intercalation. Although previous studies have demonstrated the coalescence of DNA bound to luzopeptin and various bisacridine analogues,[33-34] the importance of this mechanism, as a factor either of the enhanced *in vitro* cytotoxicity of bisintercalators or of their narrow *in vivo* therapeutic window, has never been fully explored.

Given the success of agents such as cisplatin, it is perhaps surprising that inter-molecular binding of a ligand to separate DNA strands has attracted so little attention. Although the inter-molecular binding of a platinating agent occurs between adjacent strands of ssDNA within a double stranded duplex, the cytotoxic effect would presumably be similar. Physical knots and tangles within DNA would provide a physical barrier to transcription, interfering

with strand separation and thereby inducing apoptosis. Such an occurrence must be considered all the more likely when DNA is packed tightly in the nucleus of the cell.[55]

Advances have been made in refining the chemistry of intercalators in order to enhance the specificity of these ligands for particular DNA structures.[180] Although efforts in this study to visualise a Holliday junction using AFM were not entirely successful, the binding of a bisacridine at a four way Holliday junction has been demonstrated via crystallography.[160, 162] An improved understanding of the role that higher order structures such as the Holliday junction and the G-quadruplex play in DNA replication and repair will doubtless facilitate the use of ligand binding in these regions for oncological purposes.[161]

These studies have also revealed a previously unobserved intercalative mechanism that has implications for the employment of bisintercalators, not as medical agents, but nano-engineering tools. Sequence specific, blunt-end, inter-molecular binding of DNA by echinomycin and TANDEM could be exploited in a number of ways.[157] In recent years there has been considerable interest in the creation of nanoscale structures using short oligonucleotide sequences.[181] Although initially a novelty, the ability to manipulate biological material in a controlled fashion could have profound implications for both medical technologies and materials' science. Current techniques, involving ligase enzymes, are hampered by the inefficiency of blunt-end ligations, particularly with short oligonucleotide sequences.[182] A recent paper has demonstrated the use of intercalators as molecular chaperones.[183] Since intercalation is a non-covalent interaction, use of these ligands in this context is ideal since the process is non-destructive and the ligand is easily removed via surfactant sequestration.

In view of the application of intercalators in a chemotherapeutic context, it is possible to overlook the other areas where intercalators have been shown to be medically useful agents. The quinoxalines, such as echinomycin and echinoserine, have been evaluated for their antibacterial properties.[17] Similarly, artemisinin-acridine conjugates have been examined not only for their *anti*-tumour activity but also for their potential in combating malaria.[178] There is also a report of the quinomycin antibiotic, quinaldopeptin, having *anti*-viral properties.[184] Even if the mechanism of DNA intercalation itself is found to have little direct application in other therapeutic areas, intercalators may function as a scaffold, anchoring an additional functionality or a pro-drug within nucleosomal DNA.

These experiments have utilised the technique of AFM to gain an insight into the behaviour of intercalating ligands with DNA. This technique has been demonstrated to offer numerous

advantages to alternative analytical techniques that have previously been used for studies of this kind. Although some expertise is required on the part of the operator, in order to obtain AFM images of reasonable clarity, samples are relatively straightforward to prepare and may be obtained in a short period of time. The assay of DNA contour lengths conducted in this study has revealed some aspects of DNA intercalation with acridines that had hitherto only been suggested by theoretical models. In this case, direct examination of the physical characteristics of individual molecules has revealed a phenomenon that may have been disguised by bulk techniques such as flow viscometry and gel electrophoresis. Although greater resolution may be obtained via NMR and X-ray crystallography, experiments of this kind can be difficult to conduct, reflected in the paucity of any crystal structures for DNA-acridine complexes.[118]

Similarly, despite a significant body of published literature surrounding the intra-molecular binding of echinomycin, no evidence has been reported to suggest that this molecule is capable of binding to separate DNA strands.[75] Clearly, the nature of the inter-molecular mechanism suggested herein would prohibit its detection; the event occurs at low frequencies and only where blunt-end fragments of DNA are in close proximity with one another. This would automatically preclude its detection via, for example, a plasmid unwinding assay. This in itself demonstrates the remarkable sensitivity of single molecule force spectroscopy.

Continued advances in AFM technology, such as faster scan rates, and improvements in AFM probe design, are likely to ensure that AFM becomes a more accessible and even more sensitive technique. Given that AFM images of benzene rings have already been reported elsewhere,[185] it is not difficult to envisage that AFM may yet prove to be capable of distinguishing individual ligands bound to a DNA structure. Data derived from AFM experiments are now available in a growing number of publications, and this is certain to continue in the future.

Chapter 7 – Experimental methods

Plasmid DNA unwinding assay

A protocol for visualizing the unwinding of plasmid DNA was modeled on the protocol described by Wakelin et al.[19] Agarose gels (1%) were prepared using 1 g of agarose in 100 ml of 1xTAE buffer (pH 8). The solution was heated until all of the agarose had dissolved. After being allowed to cool for a period of a few minutes, the solution was transferred to an electrophoresis tank (10 by 6.5 cm) and allowed to set. The gel was then covered in an appropriate volume of 1xTAE buffer.

Samples were prepared by the addition of 2 µl of φX174 RFI plasmid DNA (New England Biolabs, UK, concentration 1 mg/ml), to 70 µl of 10 mM tris HCl buffer (pH 7), yielding a final volume of 72 µl. A total of 8, 9 µl aliquots were taken from this solution, to 7 of which were added 1 µl of relevant concentrations of a particular ligand and to the eighth 1 µl of DMSO or water as a control. This yielded a final volume per sample of 10 µl. Assuming a molecular weight of 650 g/mol for each nucleotide, and knowing that the plasmid consisted of 5386 base pairs, the concentration of the DNA in each 10 µl sample was determined to be 7.1 nM.

After an incubation period of one hour, 2 µl of loading buffer were added to each sample and the samples were transferred to separate wells on the agarose gel. A power pack was connected to the electrophoresis chamber and set at 70 V for a period of approximately two and a half hours.

After this period of time, the gel was removed from the electrophoresis chamber and transferred to a plastic container. The gel was covered with a 1 µg/ml solution of ethidium bromide for ten minutes and then rinsed with 1xTAE buffer. The gel was exposed to a UV light source and images of the gel were obtained for analysis. All images were processed using GeneSnap© (Synoptics, UK) and adjusted for brightness and contrast.

Synthesis of bisacridine 1

Bisacridines 2, 3, and 4 were synthesized by Dr. L. A. Howell at the University of East Anglia.[50] The bisacridine N-(6-(acridin-9-ylamino)octyl)acridine-9-amine was synthesized from acridone and 1,8 diaminooctane using procedures that have been described elsewhere.[54] Acridone (1 g, 5.15 mmol) was hearted to reflux in $SOCl_2$ (10 ml) with 2 drops of DMF for 1 hour. $SOCl_2$ was removed under vacuum and the residue dissolved in dry phenol (10 g) which was then heated to 110°C. After 15 minutes, the temperature was reduced to 55°C and 1,8 - diaminooctane (0.38 g, 2.56 mmol, 0.5 equivalents) was added. The mixture was stirred for 2 hours and an aqueous solution of NaOH (2 M, 20 ml) was added. The resulting solution

was extracted with DCM (15 ml) which was dried ($MgSO_4$) and evaporated to give the crude product. Purification by flash column chromatography was followed by dissolution in 1.25 M HCl in MeOH to give the final product. After removing the methanol under vacuum, the final product was dissolved in water and stored at -20°C.

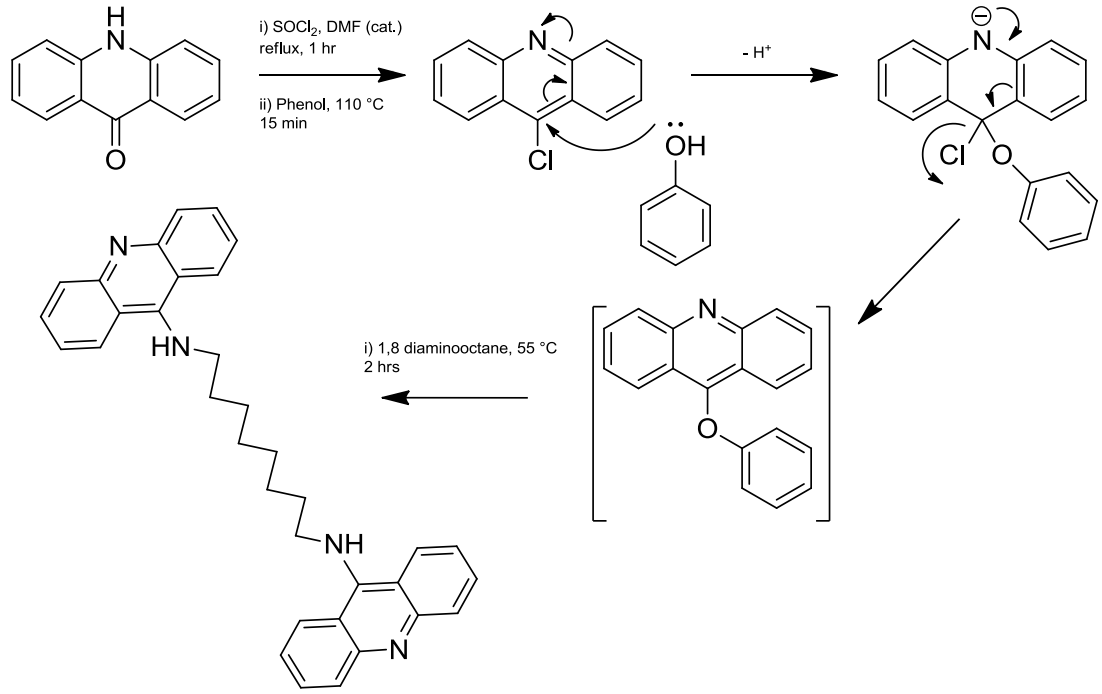

Figure 98 Synthesis of bisacridine 1, showing the Meisenheimer complex that is generated by the interaction between phenol and 9-chloroacridine.

Generation of the product was confirmed by ^{1}H NMR (400 MHz, CD_3OD). Due to the symmetrical nature of the compound each signal in the ^{1}H NMR spectrum equated to double the number of protons in that environment. There were four signals in the aromatic region of the spectrum, corresponding to the 16 acridine protons at 8.5 (d), 7.97 – 7.93 (m), 7.81 (d) and 7.55 ppm (t). In the aliphatic region of the spectrum there were three signals, excluding the solvent, at 4.14 (t), 2 – 1.97 (m) and 1.49 – 1.45 (m) ppm, attributable to the 8 methylene groups of the inter-chromophore linker.

DNA contour length assay

This protocol was modeled on that described by Tseng et al.[75] A plasmid DNA, φX174 RF I, was obtained from New England Biolabs (UK) in a concentration of 1 mg/ml. A portion of this was restricted using the enzyme BfaI (NEB, UK). 5 µl of the stock solution of DNA was added to 35 µl of water and 5 µl of restriction buffer in an eppendorf tube (New England Biolabs Buffer 4). Finally, 5 µl (25 units) of the enzyme BfaI was added to the solution, giving a final volume of 50 µl, and it was mixed thoroughly before being incubated at 37°C.

After one hour, the solution was removed from the incubation chamber and the restriction digestion was stopped by the addition of 10 µl of loading buffer.

Aliquots of this solution were loaded onto a 1% agarose gel, prepared as previously described. A power pack was connected to the gel and allowed to run for a period of approximately two hours at 70 volts. This was found to provide adequate separation of the three fragments yielded by the digest. The gel was then removed from the electrophoresis chamber, and stained with 0.1% ethidium bromide solution for ten minutes. The gel was visualised by exposure to UV light.

The band corresponding to the 771 base pair fragment (Figure 99) was excised and then purified using a QIA Quick Kit© (QIAGEN, UK) following the supplier's instructions. The concentration of the derived DNA solution was determined via NanoDrop© instrument at a wavelength of 260 nm (ThermoScientific, UK), and the solution stored at -20°C until used.

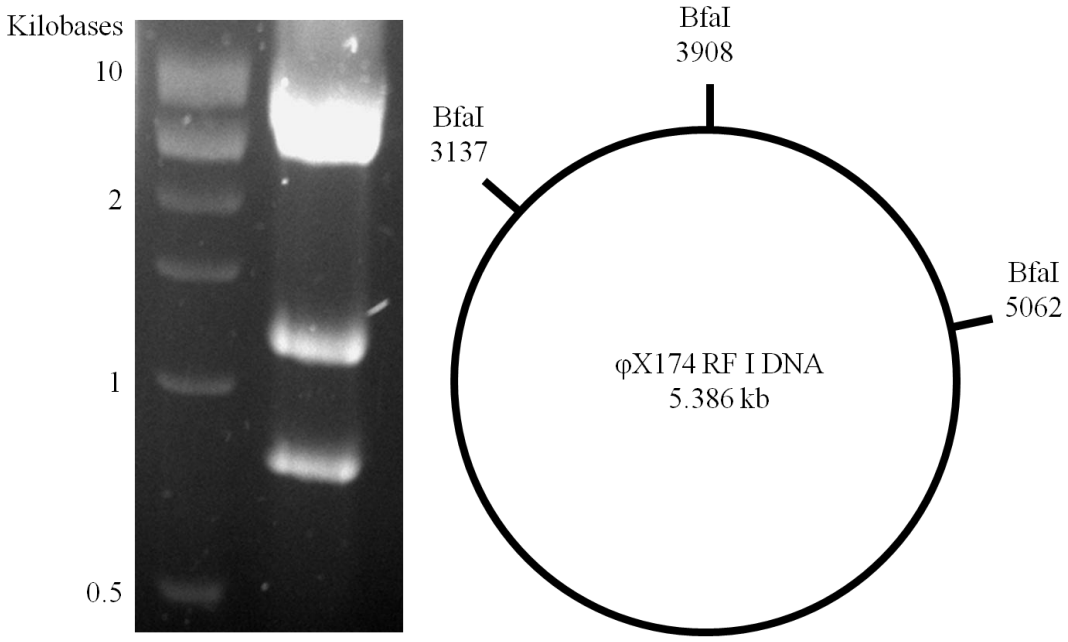

Figure 99 Agarose gel showing the three products of BfaI digestion of φX174 (left). The lowest of the three bands was the one excised, and is seen part way between the bands at 500 and 1000 base pairs on the ladder (lane 1, New England Biolabs 1 kb DNA ladder). The restriction map shows the precise locations of cleavage by the enzyme.

Samples for DNA imaging were prepared by the addition of 15 µl of Nanopure™ water to 10 µl of a solution of the 771 base pair fragment of φX174 DNA (concentration 2.35 ng/µl). 25 µl of 10 mM $MgCl_2$ were then added, giving a final system volume of 50 µl. Assuming a molecular weight of 650 g/mol, the concentration of DNA in the initial solution volume of 25 µl was found to be 1.9 nM. The entire volume of 50 µl was transferred to freshly cleaved

mica that had been mounted on a metallic AFM disc. Cleaving of the mica was performed by peeling with adhesive tape. After a period of 10 minutes to allow DNA strands to adhere to the mica, the disc was rinsed using 10, 1 ml drops of distilled water and then air-dried under nitrogen.

Samples prepared to test particular ligands were prepared by the addition of 15 µl of an appropriate concentration of the ligand to 10 µl of a solution of the 771 base pair fragment of φX174 DNA. Controls were prepared using water in place of the ligand. Following an incubation period of one hour, 25 µl of 10 mM $MgCl_2$ were added, giving a final system volume of 50 µl. The system was then transferred to freshly cleaved mica, mounted on a metallic AFM disc as before.

Imaging was conducted in tapping-mode in air using a CPII© AFM (Veeco Instruments, USA), equipped with a small area scanner. Calibration of the instrument in the *x* and *y* dimensions was conducted according to the manufacturer's instructions using commercially available calibration grids. Commercially available cantilevers were used (Veeco Instruments, models RTESPA-CP and TESP as appropriate), with images captured in height mode. In order to minimize the forces between the cantilever and the substrate, the set-point was increased until contact with the surface was lost and then gradually decreased until a surface trace was again visible. Gains were adjusted to optimise image clarity as required.

Using the seven hundred and seventy-one base pair fragment of φx174, it was found that images conducted at speeds of approximately two hertz, over a region of two by two microns yielded images of sufficient sharpness and contrast to ensure reproducible measurement of the fragments adsorbed to the mica surface. A pixel resolution of 1024 by 1024 pixels provided a physical resolution of 1.9 nm per pixel versus 3.9 nm for scans conducted at 512 pixels. Assuming a helical rise of 0.34 nm per intercalation event according to the classical principle of intercalation, this corresponded to an experimental sensitivity of 5.5 intercalation events at the former resolution versus 11 at the latter. To ensure consistency of calibration, measurements of DNA length were only taken from images obtained using the CPII AFM.

Collected images were processed and examined using WSxM (Nanotec) and adjusted as required for brightness and contrast.[186] Contour length measurements of DNA strands were made manually using the 'segmented line' tool in the programme ImageJ© (NIH, public domain). Statistical analyses were conducted using OriginPro© (OriginLab Corporation, USA). Measurements of individual DNA strands were tabulated and plotted as a histogram of contour lengths. Mean values and standard error for each population were derived from

the peak of a gaussian curve fitted to the histogram. Measurements of the contour lengths of DNA treated with the acridines were expressed as a percentage change in the length of the DNA fragments.

Fourier transform infrared spectroscopy

Experiments were conducted using a Bruker IFS 66/S Spectrometer (Bruker Optics UK, United Kingdom) fitted with a Specac (Orpington, UK) Golden Gate Single Reflection Diamond ATR, using a method described by Whelan et al.[125] Samples were prepared using CT-DNA (Sigma, UK), at a stock concentration of 1mg/ml. A 5 µl aliquot of the DNA solution was deposited on the diamond, and spectra collected over various periods of time under standard conditions, at wavelengths between 4000 and 550 cm^{-1}. Scans were repeated, at a scan time of 40 scans and intervals of 60 seconds for one hour at a resolution of 2 cm^{-1}. Spectra were analysed using OPUS (Bruker Optik, version 6).

Circular dichroism

CD was conducted using a Jasco J-810 spectropolarimeter, adapting a methodology described by Ivanov et al.[128] All experiments used a quartz cuvette with a path length of 1 mm. Spectra were collected over a wavelength from 350 to 200 nm at a data pitch of 0.5 nm in continuous scanning mode at room temperature. The scanning speed was set at 200 nm / minute with a response of 1 second at a band width of 2 nm. Spectra were accumulated in triplicate and averaged. Samples were prepared using CT-DNA (Sigma, UK) at a stock concentration of 1mg/ml (3007 µM in DNA base pairs). The control was prepared by the addition of 20 µl of 200 µM NaCl to 20 µl of DNA. The volume was made up to 200 µl by the addition of 10 mM tris HCL buffer (pH 7). 1 µl of the appropriate concentration of each ligand was added to this volume and mixed. In the case of bisintercalators, a stock solution of 3 mM was used. To preserve the ligand to base pair ratios for direct comparison between bisintercalators and monointercalators, stock solutions of 6 mM were used for the monointercalators. The A form of CT-DNA was induced by the substitution of the tris buffer with ethanol. After subtracting the buffer from the signal, each spectrum was zero corrected at 320 nm and processed using OriginPro™ (OriginLab, ver. 8.0724).

Visual DNA cross-linking assay

A 1341 base pair, linear fragment of plasmid φX174, measuring 456 nm, was produced by restricting the plasmid with the enzyme BsaAI. This restriction enzyme yields two fragments, one of 1341 base pairs and the other of 4045 base pairs.

Fragments were separated via agarose gel electrophoresis and purified using a Qiagen agarose removal kit in the manner previously described. A stock solution of DNA was prepared and the concentration determined via NanoDrop©.

Aliquots of this DNA solution were diluted further to 0.34 ng/µl. 10 µl of this dilute DNA solution was combined with 15 µl of the appropriate ligand, or 15 µl of water for the control group. The concentration of DNA in this solution, assuming a molecular weight per base pair of 650 g/mole, was calculated to be 0.16 nM. After an incubation period of ten minutes, 25 µl of 10 mM $MgCl_2$ was added, yielding a total volume of 50 µl, and the solution deposited on freshly cleaved mica for a period of 10 minutes. Samples were then rinsed with Nanopure™ water and dried under nitrogen.

Imaging was conducted using a Veeco Instruments CPII. Data were collected in intermittent-contact mode at 512x512 over regions of 2x2 microns at a scan rate of 2 Hz. Cantilevers were purchased from Asylum Research UK (AC160TS). Images were collated and processed using WSxM (Nanotec).[186]

Force spectroscopy of DNA

Force spectroscopy was conducted using a NanoWizard 2™ AFM fitted with a liquid cell (JPK, DE) containing 3 mM phosphate buffer (Fisher Scientific, UK, pH 7) or the appropriate concentration of a ligand. In order to maintain the same ratio of ligand chromophores to DNA base pairs, bisintercalating compounds were used at half the concentration (100 nM) of the monointercalators (200 nM). Solutions were prepared in phosphate buffer and filtered using syringe filters with a 0.2 µm PTFE membrane and used immediately.

Gold coated cantilevers were purchased from Asylum Research (BL-RC150VB) and used as received (nominal spring constant 0.027 N/m). Cantilevers were calibrated using the thermal tune method (range 0.016 N/m to 0.058 N/m).[187] Experiments were conducted in contact mode, at a relative setpoint of 0.2 nN. The z-length for all experiments was 150 nm and the approach and retract speeds set at 0.5 microns per second and a resolution of 2048 Hz. Force spectra were collected in arrays of 100 x 100 data points over areas of 10 x 10 microns. Dynamic force spectroscopy was conducted by adjusting the retraction velocity over a range of speeds from 0.05 to 4 microns per second. Spectra were exported and analysed using JPK's data processing software (JPK instruments, DE, ver. 4.0.0). Data sets were exported and analysed using OriginPro™ (OriginLab, ver. 8.0724).

Designing a tether for force spectroscopy experiments

In order to conduct stretching experiments with DNA, it is essential for the DNA to be attached securely to another surface. Although DNA may be attached directly to another surface such as gold, it is also advisable to incorporate a spacer molecule in the arrangement, in order to keep the DNA clear of any non-specific attachments with the gold surface to which it is attached.

Two pairs of 33 base pair oligonucleotides, with an amine functionality at the 5' position, and their complementary sequences were purchased from Sigma UK. The sequences of the oligonucleotides were:

1) 5' – NH_2 – CTACGTGGACCTGGAGAGAGGAAGGAGACTGCCTG – 3'
   5' – CAGGCAGTCTCCTTCCTCTCTCCAGGTCCACGTAG – 3'

2) 5' – NH_2 – CTACGTGGACCTGGAGAGAGGAAGGAGACTGCCTA – 3'
   5' – TAGGCAGTCTCCTTCCTCTCTCCAGGTCCACGTAG – 3'

These sequences were annealed according to the protocol provided by the manufacturer and purified using a Qiagen nucleotide clean up kit. A 25 nm, 2950 Da PEG with a polydispersity index of 1.03 (Iris Biotech, DE) was coupled to the oligonucleotide via a hydroxysuccinimide functionality using a literature protocol and purified via ethanol precipitation (Figure 100).[188]

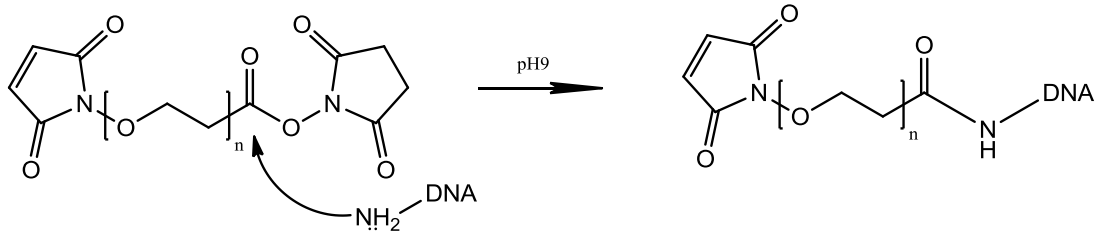

Figure 100 Coupling of the amine terminated DNA to PEG.

The successful coupling of PEG with the DNA was confirmed by gel permeation chromatography (Table 33) using a 30 cm TSKgel 3000PW column (Sigma, UK) at a flow rate of 0.8 ml/min. A significant shift in the retention time of the DNA was observed after the attachment of the PEG (Figure 101).

Table 33 Retention times (minutes) for the separate components and for the coupled PEG / DNA tether, showing an increase in retention time for the PEG/DNA conjugate relative to the DNA alone.

	DNA	PEG	PEG / DNA
MW / g/mol	20457	2950	23407
Run 1	22.66	29.26	22.54
Run 2	22.63	29.38	22.57
Run 3	22.62	29.38	22.56
Mean time	22.63	29.34	22.56
σ	0.02	0.07	0.01

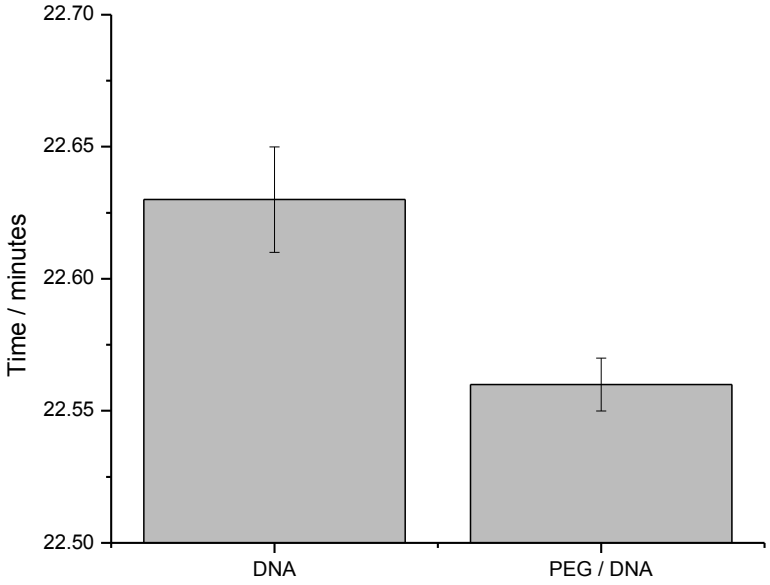

Figure 101 Difference in the mean retention time, as determined by GPC, of the DNA alone and the DNA after attachment to the PEG, confirming attachment of the DNA to the PEG.

A thiol termination was added to the oligonucleotide and PEG conjugate by the addition of propanedithiol (Figure 102) and purified again via ethanol precipitation. The final solution was diluted to a concentration of 60 ng/µl with phosphate buffer and stored at -20°C until used.

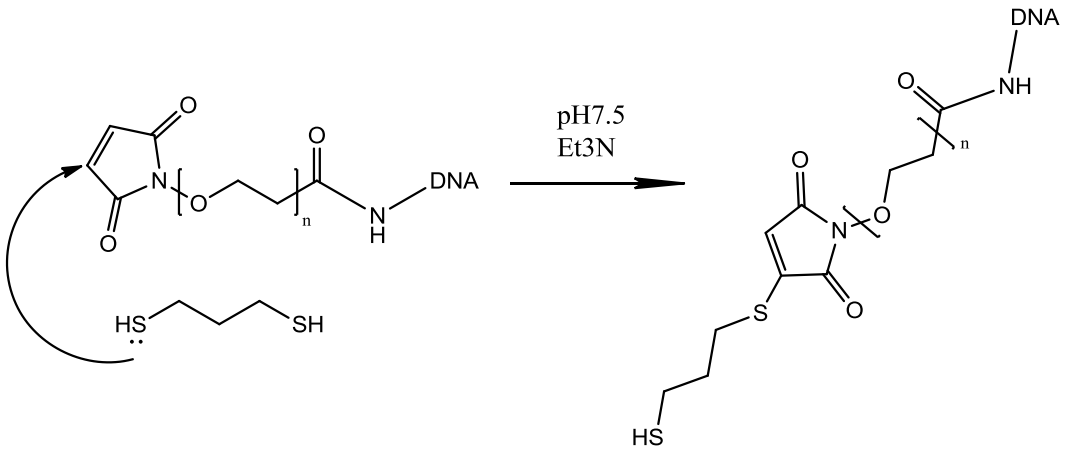

Figure 102 Attachment of propanedithiol to maleimide.

Preparing a substrate for force spectroscopy experiments

Successful AFM experiments are dependent on the quality of the surface underneath the AFM cantilever.[189] In order to provide a flat gold surface to which the thiol functionality of the PEG and DNA could be attached, freshly cleaved mica was coated with gold using an Auto306 vacuum coater (Edwards), according to the manufacturer's instructions. Deposition was stopped once the gold layer had reached a thickness of 50 nm. The gold-coated mica was then glued to microscope slides using a thin layer of Araldite™ glue, sandwiching the gold between the mica and the glass. The slides were stored at room temperature until used. The gold surface was exposed for use by peeling away the mica layer with adhesive tape which was then disposed of, leaving the gold attached to the glass slide.[190]

Gold coated cantilevers were purchased from Asylum Research (BL-RC150VB) and used as received (nominal spring constant 0.027 N/m). Functionalisation was performed by depositing a 5 µl droplet of the PEG and DNA conjugate on an exposed gold surface, and by immersing a clean cantilever in a droplet of the same solution (Figure 103).

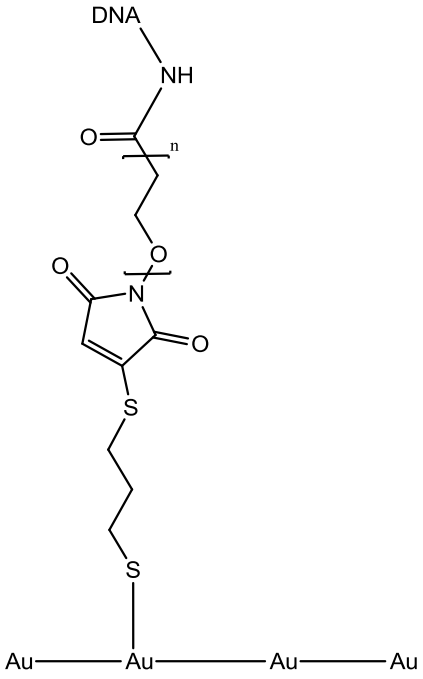

Figure 103 Schematic illustration of sulphur co-coordinating with a gold surface.

The mechanism by which a thiol interacts with gold is not fully understood.[191-192] It has been suggested that the thiol proton is lost as hydrogen gas.[193] Importantly, the strength of the coupling has been ascertained, and reported to be approximately 45 kcal/mol.[191] Although the bond between gold and sulphur is semi-covalent, with both electrons donated by the sulphur, the strength of this bond significantly exceeds that of the typical interactions, such as hydrogen bonds, that may be investigated using AFM and thus provides a suitable anchor. The substrates and the cantilevers were placed in a humidity chamber at 6°C and left for 20 hours.[194] The reaction was terminated by rinsing with Nanopure™ water. Passivation of substrates and cantilevers was performed immediately using a 10 mM solution of 11-mercaptoundecanoic acid (Figure 104) in a fifty percent solution of DMSO in water for a period of one hour. Passivation was terminated by rinsing with Nanopure™ water.

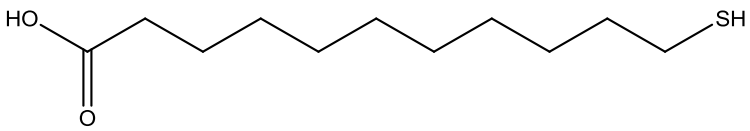

Figure 104 The molecular structure of 11-mercaptoundecanoic acid.

The effects of 11-mercaptoundecanoic acid on the substrate are two-fold. Firstly, non-specific adhesion between bare gold surfaces, on the substrate and the opposing cantilever, is eliminated by successful blockade of these areas. Secondly, hydrophobic interactions between neighbouring chains of 11-mercaptoundecanoic acid and the PEG/DNA tether promote the formation of a monolayer of these chains, where the body of the chain is

perpendicular to the anchoring surface. This facilitates the 'pick-up' of molecules by the AFM cantilever.[195]

Synthesis of gold nanoparticles

Separate solutions of gold (III) chloride trihydrate (32 μM) and trisodium citrate (170 μM) were heated to 60°C. The trisodium citrate was mixed with the gold (III) chloride under rapid stirring, and the temperature increased to 85°C for two and a half hours, yielding a transparent, red solution of gold nanoparticles of approximately 3 nM concentration.[155]

A 33 base pair oligonucleotide, with a thiol functionality at the 5' position, and its complementary sequence were purchased from Sigma UK. The sequences of the oligonucleotides were:

1) 5' – [ThiC6] – CTACGTGGACCTGGAGAGAGGAAGGAGACTGCCTG – 3'
2) 5' – CAGGCAGTCTCCTTCCTCTCTCCAGGTCCACGTAG – 3'

Stock solutions of each oligonucleotide were prepared according to the manufacturer's instructions. Annealing was conducted using equimolar quantities of each oligonucleotide in 10 mM trisodium citrate and 5 mM HEPES buffer. The solution was heated to 95°C for five minutes in a standard heat block and then allowed to cool to room temperature over a period of one hour. The solution was stored at -20°C until required.

For some time, DNA has been attached to gold nanoparticles using a salt aging process described by Mirkin et al.[196] This approach requires the introduction, gradually, of high concentrations of sodium chloride to the suspension of gold nanoparticles. After repeated attempts, the authors were unable to replicate this approach due to the instability of the nanoparticles in NaCl.

Recently, an alternative method has been published for attaching DNA to gold nanoparticles that reduces the need for sodium chloride.[197] Instead, the functionalisation is conducted under acidic pH. In order to attach the DNA to the gold nanoparticles, 31.5 μl of a 25 μM solution of the thiolated DNA was added to 1.5 ml of the gold nanoparticles along with a volume of 30 μl of 500 μM trisodium citrate (pH 3.0). After mixing, the solution was left standing for ten minutes before 52.5 μl of 2 M NaCl was added, whereupon the solution was left in a rotary mixer for 20 minutes. After this period of time, a further 150 μl of 2 M NaCl were added to the solution, and the system returned to the rotary mixer for 40 minutes.

In order to remove unbound nanoparticles and DNA, the solution was centrifuged at 8000 rpm for 30 minutes. The supernatant was decanted, and the red aggregate resuspended in 10 mM phosphate buffer (pH 7.4) before being centrifuged for a further 30 minutes. This step was repeated three times in order to remove as much unbound material as possible. After the final rinsing step, the gold nanoparticles were resuspended in 1.5 ml of phosphate buffer.

Successful attachment of the DNA to the gold nanoparticles was initially confirmed by agarose gel electrophoresis. Solutions of gold nanoparticles are very unstable, causing them to precipitate on electrophoresis. Successful attachment of DNA to gold particles may therefore be demonstrated by the movement of properly functionalised particles through an agarose gel (Figure 105).

Figure 105 Agarose gel comparing the electrophoretic character of a solution of gold citrate nanoparticles (left lane) and a solution of the same nanoparticles functionalised with DNA (right lane). The blue colour apparent in the left lane is typical of precipitated gold nanoparticles. The stability of the functionalised nanoparticles under these conditions confirms the attachment of the DNA.

The addition of DNA to gold nanoparticles may be also be followed quantitatively by changes in the UV absorbance spectra of the solutions. Gold nanoparticles have a typical peak in absorbance at a wavelength of 520 nm. Functionalisation of the particles with dsDNA results in a shift in the position of this peak from 520 to 525 nm (Figure 106).

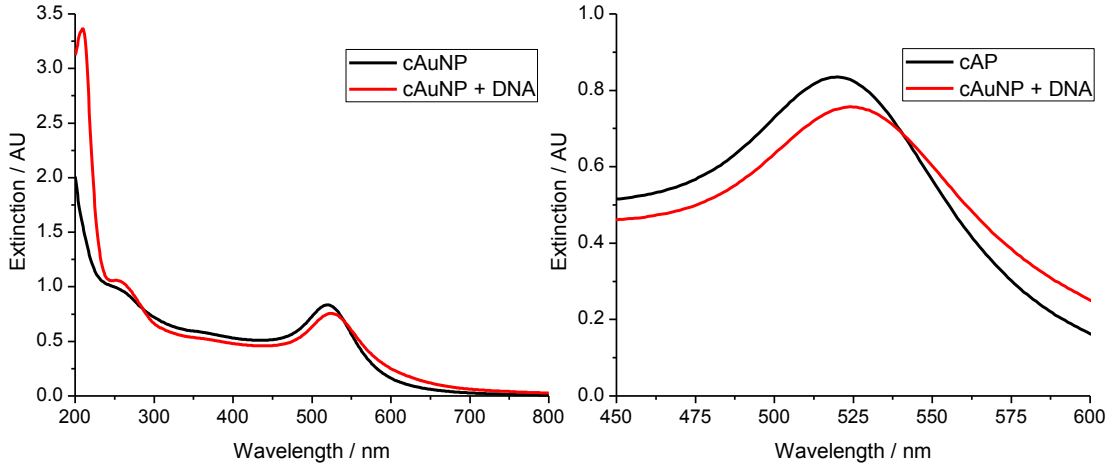

Figure 106 Complete spectra for gold nanoparticles and gold nanoparticles functionalised with DNA (left). The peaks between 500 and 550 nm correspond to the gold particles themselves, while the appearance of a peak at 260 nm with the functionalised particles

reflects the presence of DNA. An enlargement of these spectra, showing a restricted wavelength range, shows the shift in the peak of the gold particles from 520 to 525 nm.

Ultraviolet spectroscopy

Ultraviolet-visible (UV-Vis) spectra were recorded using a Hitachi U-3000 spectrophotometer at room temperature. A quartz cuvette with a 1 cm path length was used for all experiments.

To an initial volume of 570 µl of the gold nanoparticle and DNA solution, the relevant ligand was added in 1 µl aliquots and the cuvette shaken gently by hand for a period of one minute. After each addition, the UV absorbance of the solution was measured. Spectra were exported for analysis using OriginPro™ (OriginLab, ver. 8.0724).

Dynamic light scattering

Particle size analysis of the nanoparticles was performed in a 1.5 ml plastic UV-visible absorbance cuvette using a Malvern Zetasizer Nano-ZS. Particle sizes were obtained for both the gold nanoparticles, and gold nanoparticles functionalized with DNA. Measurements for the ligands were taken after the addition of 4 µl of 500 µM solutions of the bisacridines bisacridine 2 and bisacridine 3, each to an initial volume of 570 µl of the gold nanoparticles. Measurements involving SDS were taken after the addition of 12 µl of 20mM SDS to an aggregated solution of the gold nanoparticles, containing 4 µl of either of the bisacridine ligands.

Transmission electron microscopy

One drop of a solution of gold nanoparticles functionalised with DNA was added to a copper TEM grid incorporating a holey carbon film. A second sample was prepared using a volume of 570 µl of a solution of the same gold nanoparticles after the addition of 4 µl of 500 µM bisacridine 2. Images were obtained using a FEI Tecnai G2 20 Twin transmission electron microscope (John Innes Centre, Norwich, UK) operating at 200.0 kV.

Holliday junction assay

Firstly, four oligonucleotides capable of forming a cruciform junction were purchased from Sigma, UK. Each pair of oligonucleotides was annealed according to the manufacturer's instructions, forming a hemi-junction that incorporated a 4 base pair overhang that could be ligated to another complementary DNA sequence (Figure 107).[165] In order to provide structures of sufficient size to visualise via AFM, each hemi-junction was ligated to a longer stretch of duplex DNA. A quantity of a plasmid DNA, pcDNA3.1/Hygro (+) (Invitrogen,

UK), was transformed and then separated using a QIAGEN plasmid purification kit (QIAGEN, UK). The DNA was purified via ethanol precipitation, and the concentration confirmed via NanoDrop. The initial concentration of the DNA stock solution was 1.6 mg/ml.

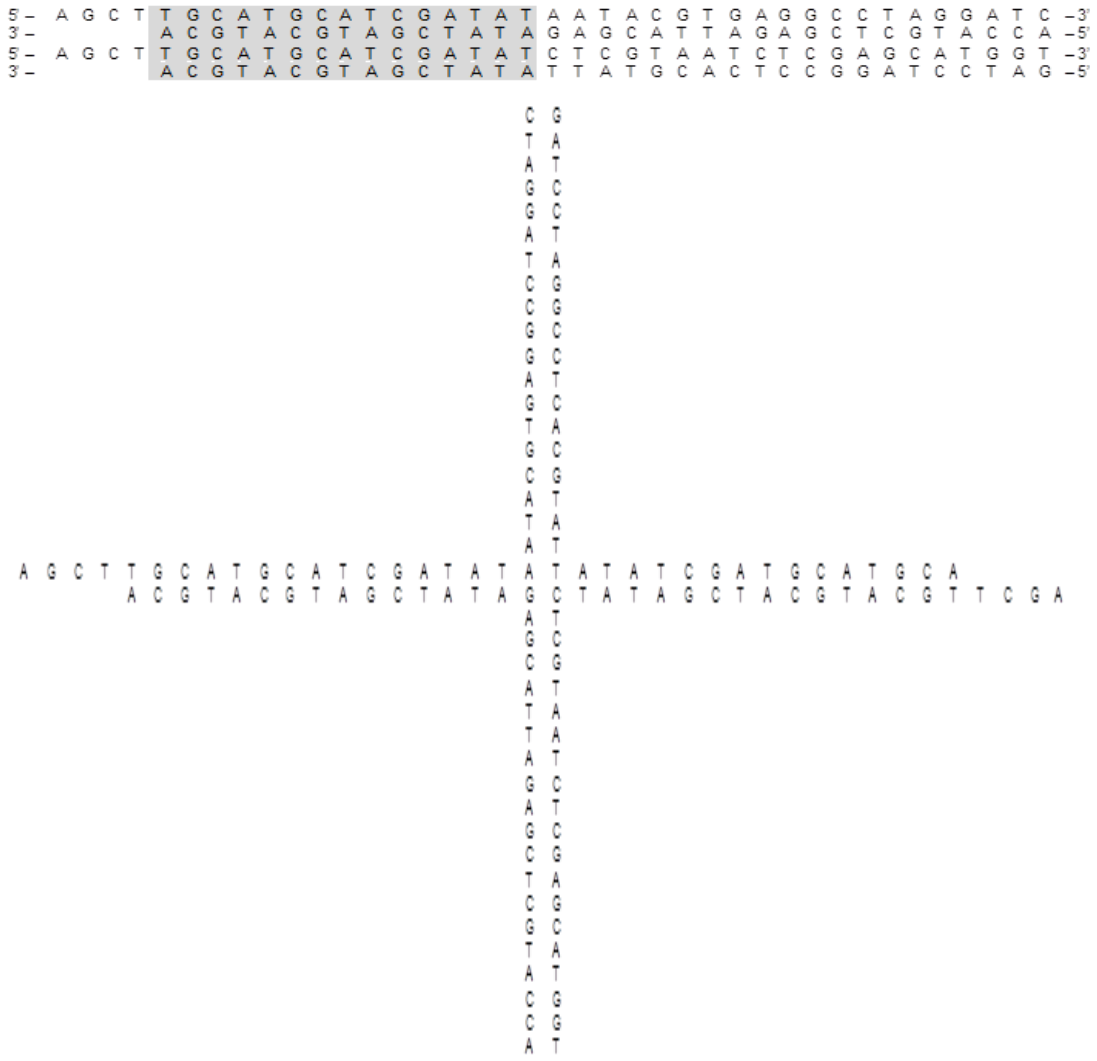

Figure 107 Sequences of the four oligonucleotides (top) used to construct a Holliday junction. The highlighted area shows the complementary region between each of the pairs of oligonucleotides. The lower half of the figure illustrates how the two separate hemi-junctions would align after annealing.

The extracted plasmids were digested with the enzyme NdeI (New England Biolabs, UK), generating linear DNA. In order to eliminate the accumulation of unwanted ligation products, the linear DNA sequences were treated with calf-alkaline phosphatase (Invitrogen, UK). This process removed the terminal phosphate groups from the end termini of the DNA, which are essential for covalent attachment of one DNA sequence to another. The processed DNA was then restricted with the enzyme HindIII (Invitrogen, UK), yielding a 427 base pair

DNA duplex with a 4 base pair sticky overhang complementary to that of the oligonucleotide hemi-junctions. This fragment was separated from the remaining DNA via agarose gel electrophoresis and purified using a QIAGEN gel purification kit (Figure 108).

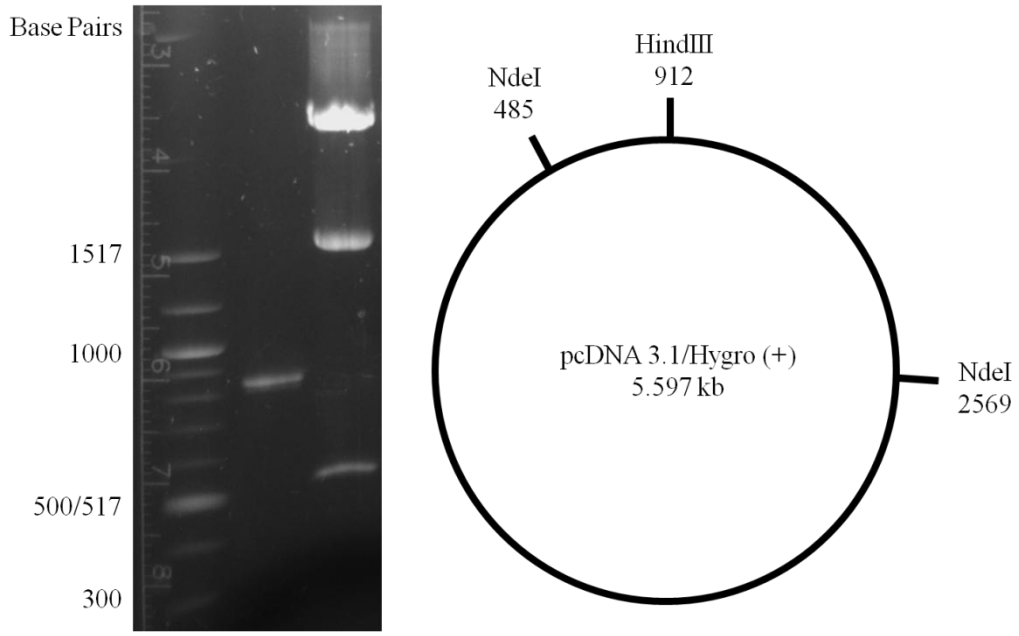

Figure 108 Digestion of pcDNA 3.1/Hygro (+) with enzymes NdeI and HindIII. The agarose gel shows the three digestion fragments (lane 3) relative to a 100 base pair DNA ladder (New England Biolabs, lane 1). Lane 2 shows an 842 base pair DNA fragment from an alternative digest that was included as an additional reference standard. The schematic illustration of the plasmid pcDNA 3.1 shows the locations of the restriction sites.

The processed DNA was analysed using AFM in order to ascertain whether or not the separation of the 427 base pair fragment from other products of the digestion had been effective and that the length of the DNA correlated with the expected size of the fragment (Figure 109). This experiment was conducted in the same manner as had previously been used when measuring the 771 base pair fragments of DNA from the plasmid φX174, substituting the DNA.

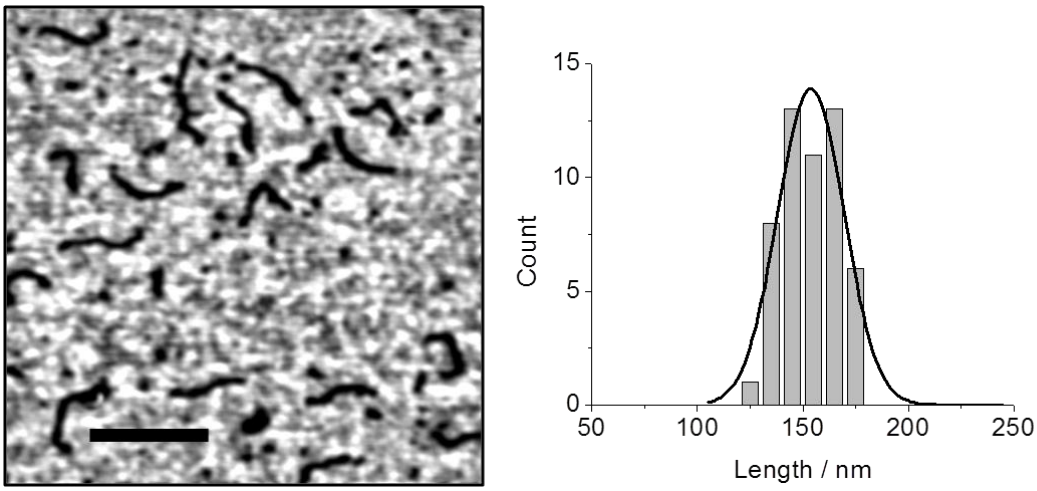

Figure 109 AFM image of the 427 base pair fragment of pcDNA 3.1/Hygro (+) and the corresponding histogram of the contour lengths of isolated DNA strands from the image. The scale bar denotes 250 nm.

Assuming that the DNA remains in a B-conformation, with a helical rise of 0.34 nm per base pair, the theoretical length of the 427 base pair fragment would be 145 nm. This corresponds well with the value of 154 nm obtained by direct measurement of DNA contour lengths from AFM images.

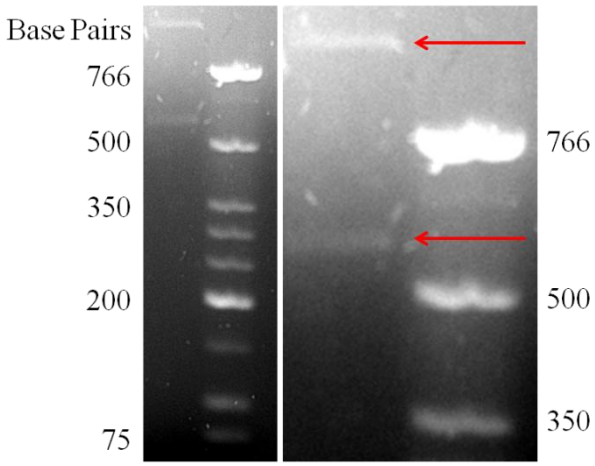

Figure 110 Agarose gel showing the products of the ligation of the 427 base pair DNA fragment and the corresponding oligonucleotides (lane 1) versus a low molecular weight DNA ladder (New England Biolabs, lane 2). The enlargement highlights two of the three products of the ligation, the third being smaller than the 75 base pair marker on the ladder and not visible on the gel.

Each hemi-junction was ligated to the 427 base pair duplex using T4 ligase (New England Biolabs, UK). This procedure yielded three potential products, these being two hemi-junctions, two 427 base pair duplexes, or the desired hemi-junction/427 base pair conjugate (Figure 110). The hemi-junction/427 base pair conjugate was separated from the other products via agarose gel electrophoresis and purified using a QIAGEN kit. The concentration

of the final product in aqueous solution was confirmed via NanoDrop, and was typically in the region of 5 ng/µl.

In order to form a Holliday junction, or rather a solution of Holliday junctions that could be analysed using AFM, the separate pairs of hemi-junctions were annealed at equimolar ratios in TNM buffer for 4 minutes at a temperature of 50°C. Typically, the volumes of material used were 1 µl of each HJ hemi-junction (at a concentration of 5 ng/µl) and 3 µl of TNM buffer (10 mM tris-HCl, pH 7.9, 50 mM NaCl, 10 mM $MgCl_2$). The annealed material was then added to 45 µl of a solution of 10 mM $MgCl_2$ and immediately transferred to freshly cleaved mica. AFM imaging was conducted in tapping mode at a scan rate of 2 Hz and a resolution of 512 pixels.

Force spectroscopy of the I-motif

Force spectroscopy was conducted using a NanoWizard 2™ AFM fitted with a liquid cell (JPK, DE). Preparation of the substrate was conducted in the same manner, and used the same materials, as the force spectroscopy DNA cross-linking assay. The only difference between these two protocols was the composition of the DNA sequence, in this case a ssDNA sequence of 24 bases with an amine functionality at the 5' terminus. The sequence of this DNA is as follows:

1) 5' – [NH_2] – TAACCCTAACCCTAACCCTAACCC – 3'

Gold coated cantilevers were purchased from Asylum Research (BL-RC150VB) and used as received (nominal spring constant 0.027 N/m). Cantilevers were calibrated using the thermal tune method (range 0.016 N/m to 0.058 N/m). Experiments were conducted in contact mode, at a setpoint of 0.6 nN and a relative setpoint of 0.2 nN. The z-length for all experiments was 150 nm and the approach and retract speeds set at 0.5 microns per second and a resolution of 2048 Hz. Force spectra were collected in arrays of 100 x 100 data points over areas of 10 x 10 microns. Spectra were exported and analysed using JPK's data processing software (JPK instruments, DE, ver. 4.0.0). Data sets were exported and analysed using OriginPro™ (OriginLab, ver. 8.0724).

The experiment was repeated under three different sets of conditions, using three different buffers to fill the liquid cell. These buffers were 3mM phosphate buffer pH 7, 10 mM sodium cacodylate buffer pH 5.5 and 10mM sodium cacodylate buffer pH 7.4 containing 100 µM $AgNO_3$.

References

1. R. G. Blanks, S. M. Moss, C. E. McGahan, M. J. Quinn, P. J. Babb, Effect of NHS breast screening programme on mortality from breast cancer in England and Wales, 1990-8: comparison of observed with predicted mortality *BMJ* **2000**, *321*, 665-669.
2. J. Boda-Heggemann, S. Mai, J. Fleckenstein, K. Siebenlist, A. Simeonova, M. Ehmann, V. Steil, F. Wenz, F. Lohr, F. Stieler, Flattening-filter-free intensity modulated breath-hold image-guided SABR (Stereotactic Ablative Radiotherapy) can be applied in a 15-min treatment slot *Radiother. Oncol.* **2013**, *109*, 505 - 509.
3. L. Zhou, S. Zhang, X. Zhen, H. Yu, G. Zhang, R. Wang, Validation of an improved 'diffeomorphic demons' algorithm for deformable image registration in image-guided radiation therapy *Biomed. Mater. Eng.* **2013**, *23*, S383-392.
4. M. Fukuchi, K. Ishibashi, Y. Tajima, N. Okada, M. Yokoyama, N. Chika, S. Hatano, T. Matsuzawa, K. Kumamoto, Y. Kumagai, H. Baba, E. Mochiki, H. Ishida, Oxaliplatin-based Chemotherapy in Patients Aged 75 Years or Older with Metastatic Colorectal Cancer *Anticancer Res.* **2013**, *33*, 4627-4630.
5. G. Galizia, F. De Vita, E. Lieto, A. Zamboli, F. Morgillo, P. Castellano, A. Mabilia, A. Auricchio, A. Renda, F. Ciardiello, M. Orditura, Conversion chemotherapy followed by hepatic resection in colorectal cancer with initially unresectable liver-limited metastases *Oncol. Rep.* **2013**.
6. L. Kelland, The resurgence of platinum-based cancer chemotherapy *Nat. Rev. Cancer* **2007**, *7*, 573-584.
7. C. A. Hudis, Trastuzumab--mechanism of action and use in clinical practice *N. Engl. J. Med.* **2007**, *357*, 39-51.
8. S. Neidle, M. J. Waring, *Molecular aspects of anticancer drug-DNA interactions*, Macmillan, Basingstoke, **1993**.
9. L. P. Wakelin, Polyfunctional DNA intercalating agents *Med. Res. Rev.* **1986**, *6*, 275-340.
10. M. J. Waring, *Sequence-specific DNA binding agents*, RSC Publishing, Cambridge, **2006**.
11. M. J. Waring, DNA modification and cancer *Annu. Rev. Biochem.* **1981**, *50*, 159-192.
12. B. J. Foster, K. Clagett-Carr, D. D. Shoemaker, M. Suffness, J. Plowman, L. A. Trissel, C. K. Grieshaber, B. Leyland-Jones, Echinomycin: the first bifunctional intercalating agent in clinical trials *Invest. New Drugs* **1985**, *3*, 403-410.
13. V. Luzzati, F. Masson, L. S. Lerman, Interaction of DNA and proflavine: a small-angle x-ray scattering study *J. Mol. Biol.* **1961**, *3*, 634-639.
14. L. S. Lerman, The structure of the DNA-acridine complex *Proc. Natl. Acad. Sci. USA* **1963**, *49*, 94-102.
15. S. Wadler, L. Tenteromano, L. Cazenave, J. A. Sparano, E. S. Greenwald, A. Rozenblit, R. Kaleya, P. H. Wiernik, Phase II trial of echinomycin in patients with advanced or recurrent colorectal cancer *Cancer Chemother. Pharmacol.* **1994**, *34*, 266-269.
16. W. J. Gradishar, N. J. Vogelzang, L. J. Kilton, S. J. Leibach, A. W. Rademaker, S. French, A. B. Benson, 3rd, A phase II clinical trial of echinomycin in metastatic soft tissue sarcoma. An Illinois Cancer Center Study *Invest. New Drugs* **1995**, *13*, 171-174.
17. S. Blum, H. P. Fielder, I. Groth, C. Kempter, H. Stephan, G. Nicholson, J. W. Metzger, G. Jung, Biosynthetic capacities of actinomycetes. 4. Echinoserine, a new member of the quinoxaline group, produced by Streptomyces tendae *J. Antibiot.* **1995**, *48*, 619-625.
18. Y. B. Kim, Y. H. Kim, J. Y. Park, S. K. Kim, Synthesis and biological activity of new quinoxaline antibiotics of echinomycin analogues *Bioorg. Med. Chem. Lett.* **2004**, *14*, 541-544.

19. L. P. Wakelin, X. Bu, A. Eleftheriou, A. Parmar, C. Hayek, B. W. Stewart, Bisintercalating threading diacridines: relationships between DNA binding, cytotoxicity, and cell cycle arrest *J. Med. Chem.* **2003**, *46*, 5790-5802.
20. J. D. Watson, F. H. Crick, Molecular structure of nucleic acids; a structure for deoxyribose nucleic acid *Nature* **1953**, *171*, 737-738.
21. D. L. Nelson, M. M. Cox, *Lehninger principles of biochemistry*, 3rd ed., Worth Publishers, New York, **2000**.
22. M. H. Wilkins, W. E. Seeds, A. R. Stokes, H. R. Wilson, Helical structure of crystalline deoxypentose nucleic acid *Nature* **1953**, *172*, 759-762.
23. R. E. Franklin, R. G. Gosling, Evidence for 2-chain helix in crystalline structure of sodium deoxyribonucleate *Nature* **1953**, *172*, 156-157.
24. A. H. Wang, G. J. Quigley, F. J. Kolpak, J. L. Crawford, J. H. van Boom, G. van der Marel, A. Rich, Molecular structure of a left-handed double helical DNA fragment at atomic resolution *Nature* **1979**, *282*, 680-686.
25. A. D. Bates, A. Maxwell, *DNA topology*, 2nd ed. ed., Oxford University Press, Oxford, **2005**.
26. A. Bodley, L. F. Liu, M. Israel, R. Seshadri, Y. Koseki, F. C. Giuliani, S. Kirschenbaum, R. Silber, M. Potmesil, DNA topoisomerase II-mediated interaction of doxorubicin and daunorubicin congeners with DNA *Cancer Res.* **1989**, *49*, 5969-5978.
27. S. Neidle, C. M. Nunn, Crystal structures of nucleic acids and their drug complexes *Nat. Prod. Rep.* **1998**, *15*, 1-15.
28. S. P. Wakelin, M. J. Waring, The binding of echinomycin to deoxyribonucleic acid *Biochem. J.* **1976**, *157*, 721-740.
29. K. J. Addess, J. Feigon, NMR investigation of Hoogsteen base pairing in quinoxaline antibiotic--DNA complexes: comparison of 2:1 echinomycin, triostin A and [N-MeCys3,N-MeCys7] TANDEM complexes with DNA oligonucleotides *Nuc. Acids Res.* **1994**, *22*, 5484-5491.
30. D. Mendel, P. B. Dervan, Hoogsteen base pairs proximal and distal to echinomycin binding sites on DNA *Proc. Natl. Acad. Sci. USA* **1987**, *84*, 910-914.
31. G. J. Quigley, G. Ughetto, G. A. van der Marel, J. H. van Boom, A. H. Wang, A. Rich, Non-Watson-Crick G.C and A.T base pairs in a DNA-antibiotic complex *Science* **1986**, *232*, 1255-1258.
32. M. M. Murr, M. T. Harting, V. Guelev, J. Ren, J. B. Chaires, B. L. Iverson, An octakis-intercalating molecule *Bioorg. Med. Chem.* **2001**, *9*, 1141-1148.
33. C. H. Huang, C. K. Mirabelli, S. Mong, S. T. Crooke, Intermolecular cross-linking of DNA through bifunctional intercalation of an antitumor antibiotic, luzopeptin A (BBM-928A) *Cancer Res.* **1983**, *43*, 2718-2724.
34. N. K. Annan, P. R. Cook, S. T. Mullins, G. Lowe, Evidence for cross-linking DNA by bis-intercalators with rigid and extended linkers is provided by knotting and catenation *Nuc. Acids Res.* **1992**, *20*, 983-990.
35. S. T. Mullins, N. K. Annan, P. R. Cook, G. Lowe, Bisintercalators of DNA with a rigid linker in an extended configuration *Biochemistry* **1992**, *31*, 842-849.
36. H. G. Keizer, H. M. Pinedo, G. J. Schuurhuis, H. Joenje, Doxorubicin (adriamycin): a critical review of free radical-dependent mechanisms of cytotoxicity *Pharmacol. Ther.* **1990**, *47*, 219-231.
37. W. C. Tse, D. L. Boger, Sequence-selective DNA recognition: natural products and nature's lessons *Chem. Biol.* **2004**, *11*, 1607-1617.
38. G. E. Kellogg, J. N. Scarsdale, F. A. Fornari, Jr., Identification and hydropathic characterization of structural features affecting sequence specificity for doxorubicin intercalation into DNA double-stranded polynucleotides *Nuc. Acids Res.* **1998**, *26*, 4721-4732.
39. I. Lasnitzki, J. H. Wilkinson, The Effect of Acridine Derivatives on Growth and Mitoses of Cells In Vitro *Br. J. Cancer* **1948**, *2*, 369-375.

40. P. R. Young, N. R. Kallenbach, Site exclusion and sequence specificity in binding of 9-aminoacridine to the deoxytetranucleotide dpApGpCpT *Proc. Natl. Acad. Sci. USA* **1980**, *77*, 6453-6457.
41. T. I. Watkins, G. Woolfe, Effect of changing the quaternizing group on the trypanocidal activity of dimidium bromide *Nature* **1952**, *169*, 506-507.
42. D. J. Patel, L. L. Canuel, Ethidium bromide-(dC-dG-dC-dG)2 complex in solution: intercalation and sequence specificity of drug binding at the tetranucleotide duplex level *Proc. Natl. Acad. Sci. USA* **1976**, *73*, 3343-3347.
43. K. R. Fox, M. J. Waring, Stopped-flow kinetic studies on the interaction between echinomycin and DNA *Biochemistry* **1984**, *23*, 2627-2633.
44. M. C. Fletcher, K. R. Fox, Visualising the dissociation of sequence selective ligands from individual binding sites on DNA *FEBS Lett.* **1996**, *380*, 118-122.
45. M. C. Fletcher, K. R. Fox, Dissociation kinetics of echinomycin from CpG binding sites in different sequence environments *Biochemistry* **1996**, *35*, 1064-1075.
46. C. Marchand, C. Bailly, M. J. McLean, S. E. Moroney, M. J. Waring, The 2-amino group of guanine is absolutely required for specific binding of the anti-cancer antibiotic echinomycin to DNA *Nuc. Acids Res.* **1992**, *20*, 5601-5606.
47. J. P. Malkinson, M. K. Anim, M. Zloh, M. Searcey, A. J. Hampshire, K. R. Fox, Efficient solid-phase-based total synthesis of the bisintercalator TANDEM *J. Org. Chem.* **2005**, *70*, 7654-7661.
48. C. M. Low, K. R. Fox, R. K. Olsen, M. J. Waring, DNA sequence recognition by under-methylated analogues of triostin A *Nuc. Acids Res.* **1986**, *14*, 2015-2033.
49. A. J. Hampshire, K. R. Fox, Preferred binding sites for the bifunctional intercalator TANDEM determined using DNA fragments that contain every symmetrical hexanucleotide sequence *Anal. Biochem.* **2008**, *374*, 298-303.
50. L. A. Howell, Design, synthesis and biological evalulation of 9-aminoacridines that target the holiday junction *PhD thesis*, University of East Anglia **2009**.
51. R. M. Acheson, E. C. Constable, R. G. M. Wright, G. N. Taylor, The Synthesis of Linked Acridines as Intercalating and Anti-Tumor Agents *J. Chem. Res-S.* **1983**, 2-3.
52. A. Adams, J. M. Guss, C. A. Collyer, W. A. Denny, L. P. Wakelin, Crystal structure of the topoisomerase II poison 9-amino-[N-(2-dimethylamino)ethyl]acridine-4-carboxamide bound to the DNA hexanucleotide d(CGTACG)2 *Biochemistry* **1999**, *38*, 9221-9233.
53. A. Adams, J. M. Guss, C. A. Collyer, W. A. Denny, A. S. Prakash, L. P. Wakelin, Acridinecarboxamide topoisomerase poisons: structural and kinetic studies of the DNA complexes of 5-substituted 9-amino-(N-(2-dimethylamino)ethyl)acridine-4-carboxamides *Mol. Pharmacol.* **2000**, *58*, 649-658.
54. G. J. Atwell, B. F. Cain, B. C. Baguley, G. J. Finlay, W. A. Denny, Potential antitumor agents. 43. Synthesis and biological activity of dibasic 9-aminoacridine-4-carboxamides, a new class of antitumor agent *J. Med. Chem.* **1984**, *27*, 1481-1485.
55. M. J. Marin, B. D. Rackham, A. N. Round, L. A. Howell, D. A. Russell, M. Searcey, A rapid screen for molecules that form duplex to duplex crosslinks in DNA *Chem. Commun.* **2013**, *49*, 9113-9115.
56. A. Bogner, P. H. Jouneau, G. Thollet, D. Basset, C. Gauthier, A history of scanning electron microscopy developments: towards "wet-STEM" imaging *Micron* **2007**, *38*, 390-401.
57. G. Binnig, H. Rohrer, C. Gerber, E. Weibel, Tunneling through a controllable vacuum gap *Appl. Phys. Lett.* **1982**, *40*, 178 - 180.
58. G. Binnig, C. F. Quate, C. Gerber, Atomic force microscope *Phys. Rev. Lett.* **1986**, *56*, 930-933.
59. H. G. Hansma, D. E. Laney, M. Bezanilla, R. L. Sinsheimer, P. K. Hansma, Applications for atomic force microscopy of DNA *Biophys. J.* **1995**, *68*, 1672-1677.
60. JPK_Instruments, NanoWizard AFM Handbook **2012**, 1-54.

61. Y. L. Lyubchenko, L. S. Shlyakhtenko, T. Ando, Imaging of nucleic acids with atomic force microscopy *Methods* **2011**, *54*, 274-283.
62. C. Bustamante, J. Vesenka, C. L. Tang, W. Rees, M. Guthold, R. Keller, Circular DNA molecules imaged in air by scanning force microscopy *Biochemistry* **1992**, *31*, 22-26.
63. P. G. Royall, D. Q. Craig, D. M. Price, M. Reading, T. J. Lever, An investigation into the use of micro-thermal analysis for the solid state characterisation of an HPMC tablet formulation *Int. J. Pharm.* **1999**, *192*, 97-103.
64. P. G. Royall, D. Q. M. Craig, D. B. Grandy, The use of micro-thermal analysis as a means of in situ characterisation of a pharmaceutical tablet coat *Thermochim. Acta* **2001**, *380*, 165 - 173
65. H. G. Hansma, I. Revenko, K. Kim, D. E. Laney, Atomic force microscopy of long and short double-stranded, single-stranded and triple-stranded nucleic acids *Nuc. Acids Res.* **1996**, *24*, 713-720.
66. Y. Martin, C. C. Williams, H. K. Wickramasinghe, Atomic force microscope–force mapping and profiling on a sub 100 Å scale *J. Appl. Phys.* **1987**, *61*, 4723-4730.
67. N. H. Thomson, Atomic Force Microscopy of DNA Structure and Interactions, in *Applied scanning probe methods VI : characterization* (Eds.: B. Bhushan, S. Kawata), Springer, Berlin, **2007**, pp. 127 - 164.
68. L. Gross, F. Mohn, N. Moll, P. Liljeroth, G. Meyer, The chemical structure of a molecule resolved by atomic force microscopy *Science* **2009**, *325*, 1110-1114.
69. D. G. de Oteyza, P. Gorman, Y. C. Chen, S. Wickenburg, A. Riss, D. J. Mowbray, G. Etkin, Z. Pedramrazi, H. Z. Tsai, A. Rubio, M. F. Crommie, F. R. Fischer, Direct imaging of covalent bond structure in single-molecule chemical reactions *Science* **2013**, *340*, 1434-1437.
70. G. C. Ratcliff, D. A. Erie, A novel single-molecule study to determine protein-protein association constants *J. Am. Chem. Soc.* **2001**, *123*, 5632-5635.
71. A. Henn, O. Medalia, S. P. Shi, M. Steinberg, F. Franceschi, I. Sagi, Visualization of unwinding activity of duplex RNA by DbpA, a DEAD box helicase, at single-molecule resolution by atomic force microscopy *Proc. Natl. Acad. Sci. USA* **2001**, *98*, 5007-5012.
72. K. Nakano, Y. Katsumi, N. Soh, T. Imato, An Atomic Force Microscopy Assay of Intercalation Binding, Unwinding, and Elongation of DNA, Using a Water-Soluble Psoralen Derivative as a Covalent Binding Probe Molecule *Bull. Chem. Soc. Jpn.* **2010**, *83*, 273 - 275
73. J. E. Coury, L. McFail-Isom, L. D. Williams, L. A. Bottomley, A novel assay for drug-DNA binding mode, affinity, and exclusion number: scanning force microscopy *Proc. Natl. Acad. Sci. USA* **1996**, *93*, 12283-12286.
74. T. Berge, E. L. Haken, M. J. Waring, R. M. Henderson, The binding mode of the DNA bisintercalator luzopeptin investigated using atomic force microscopy *J. Struct. Biol.* **2003**, *142*, 241-246.
75. Y. D. Tseng, H. Ge, X. Wang, J. M. Edwardson, M. J. Waring, W. J. Fitzgerald, R. M. Henderson, Atomic force microscopy study of the structural effects induced by echinomycin binding to DNA *J. Mol. Biol.* **2005**, *345*, 745-758.
76. A. V. Bolshakova, O. I. Kiselyova, A. S. Filonov, O. Y. Frolova, Y. L. Lyubchenko, I. V. Yaminsky, Comparative studies of bacteria with an atomic force microscopy operating in different modes *Ultramicroscopy* **2001**, *86*, 121-128.
77. I. Sokolov, Atomic Force Microscopy in Cancer Cell Research *Cancer Nanotechnology* **2007**, 1-17.
78. M. E. Nunez, M. O. Martin, P. H. Chan, L. K. Duong, A. R. Sindhurakar, E. M. Spain, Atomic force microscopy of bacterial communities *Methods Enzymol.* **2005**, *397*, 256-268.
79. G. Popescu, Quantitative phase imaging of nanoscale cell structure and dynamics *Methods Cell. Biol.* **2008**, *90*, 87-115.

80. S. Asif, K. Wahla, R. Colton, O. Warren, Quantitative imaging of nanoscale mechanical properties using hybrid nanoindentation and force modulation *J. Appl. Phys.* **2001**, *3*, 1192-1200.
81. L. Chopinet, C. Formosa, M. P. Rols, R. E. Duval, E. Dague, Imaging living cells surface and quantifying its properties at high resolution using AFM in QI mode *Micron* **2013**, *48*, 26-33.
82. D. Xu, G. D. Watt, J. N. Harb, R. C. Davis, Electrical conductivity of ferritin proteins by conductive AFM *Nano Lett.* **2005**, *5*, 571-577.
83. L. Fonseca, F. Perez-Murano, C. Calaza, R. Rubio, J. Santander, E. Figueras, I. Gracia, C. Cane, M. Moreno, S. Marco, Thermal AFM: a thermopile case study *Ultramicroscopy* **2004**, *101*, 153-159.
84. A. Hammiche, M. Reading, H. M. Pollock, M. Song, D. J. Hourston, Localized thermal analysis using a miniaturized resistive probe *Rev. Sci. Instrum.* **1996**, *67*, 4268.
85. P. G. Royall, V. Kett, C. S. Andrews, D. Q. M. Craig, Identification of Crystalline and Amorphous Regions in Low Molecular Weight Materials by Micro-thermal Analysis *J. Phys. Chem.* **2001**, *105*, 7021-7026.
86. E. Evans, Probing the relation between force--lifetime--and chemistry in single molecular bonds *Annu. Rev. Biophys. Biomol. Struct.* **2001**, *30*, 105-128.
87. G. I. Bell, Models for the specific adhesion of cells to cells *Science* **1978**, *200*, 618-627.
88. E. Evans, K. Ritchie, Strength of a weak bond connecting flexible polymer chains *Biophys. J.* **1999**, *76*, 2439-2447.
89. R. W. Friddle, A. Noy, J. J. De Yoreo, Interpreting the widespread nonlinear force spectra of intermolecular bonds *Proc. Natl. Acad. Sci. USA* **2012**, *109*, 13573-13578.
90. R. Merkel, P. Nassoy, A. Leung, K. Ritchie, E. Evans, Energy landscapes of receptor-ligand bonds explored with dynamic force spectroscopy *Nature* **1999**, *397*, 50-53.
91. O. Otto, S. Sturm, N. Laohakunakorn, U. F. Keyser, K. Kroy, Rapid internal contraction boosts DNA friction *Nat. Commun.* **2013**, *4*, 1780.
92. T. A. Sulchek, R. W. Friddle, K. Langry, E. Y. Lau, H. Albrecht, T. V. Ratto, S. J. DeNardo, M. E. Colvin, A. Noy, Dynamic force spectroscopy of parallel individual Mucin1-antibody bonds *Proc. Natl. Acad. Sci. USA* **2005**, *102*, 16638-16643.
93. M. Sletmoen, G. Skjak-Braek, B. T. Stokke, Mapping enzymatic functionalities of mannuronan C-5 epimerases and their modular units by dynamic force spectroscopy *Carbohyd. Res.* **2005**, *340*, 2782-2795.
94. M. Raible, M. Evstigneev, P. Reimann, F. W. Bartels, R. Ros, Theoretical analysis of dynamic force spectroscopy experiments on ligand-receptor complexes *J. Biotechnol.* **2004**, *112*, 13-23.
95. T. Strunz, K. Oroszlan, R. Schafer, H. J. Guntherodt, Dynamic force spectroscopy of single DNA molecules *Proc. Natl. Acad. Sci. USA* **1999**, *96*, 11277-11282.
96. D. Kim, N. K. Chung, J. S. Kim, J. W. Park, Immobilizing a single DNA molecule at the apex of AFM tips through picking and ligation *Soft Matter* **2010**, *6*, 3979-3984.
97. K. R. Chaurasiya, T. Paramanathan, M. J. McCauley, M. C. Williams, Biophysical characterization of DNA binding from single molecule force measurements *Phys. Life Rev.* **2010**, *7*, 299-341.
98. L. H. Pope, M. C. Davies, C. A. Laughton, C. J. Roberts, S. J. Tendler, P. M. Williams, Force-induced melting of a short DNA double helix *Eur. Biophys. J.* **2001**, *30*, 53-62.
99. C. Liu, Z. Jiang, Y. Zhang, Z. Wang, X. Zhang, F. Feng, S. Wang, Intercalation interactions between dsDNA and acridine studied by single molecule force spectroscopy *Langmuir* **2007**, *23*, 9140-9142.
100. A. V. Krasnoslobodtsev, L. S. Shlyakhtenko, Y. L. Lyubchenko, Probing interactions within the synaptic DNA-Sfil complex by AFM force spectroscopy *J. Mol. Biol.* **2007**, *365*, 1407-1416.

101. B. A. Ashcroft, Q. Spadola, S. Qamar, P. Zhang, G. Kada, R. Bension, S. Lindsay, An AFM/rotaxane molecular reading head for sequence-dependent DNA structures *Small.* **2008**, *4*, 1468-1475.
102. A. Dunlop, J. Wattoom, E. A. Hasan, T. Cosgrove, A. N. Round, Mapping the positions of beads on a string: dethreading rotaxanes by molecular force spectroscopy *Nanotechnology* **2008**, *19*, 345706.
103. F. Caponigro, C. Dittrich, J. B. Sorensen, J. H. Schellens, F. Duffaud, L. Paz Ares, D. Lacombe, C. de Balincourt, P. Fumoleau, Phase II study of XR 5000, an inhibitor of topoisomerases I and II, in advanced colorectal cancer *Eur. J. Cancer* **2002**, *38*, 70-74.
104. C. Dittrich, B. Coudert, L. Paz-Ares, F. Caponigro, M. Salzberg, T. Gamucci, X. Paoletti, C. Hermans, D. Lacombe, P. Fumoleau, Phase II study of XR 5000 (DACA), an inhibitor of topoisomerase I and II, administered as a 120-h infusion in patients with non-small cell lung cancer *Eur. J. Cancer* **2003**, *39*, 330-334.
105. I. Antonini, P. Polucci, A. Magnano, B. Gatto, M. Palumbo, E. Menta, N. Pescalli, S. Martelli, Design, synthesis, and biological properties of new bis(acridine-4-carboxamides) as anticancer agents *J. Med. Chem.* **2003**, *46*, 3109-3115.
106. G. Dougherty, The unwinding of circular DNA by intercalating agents as determined by gel electrophoresis *Biosci. Rep.* **1983**, *3*, 453-460.
107. P. R. Jackson, G. T. Tucker, H. F. Woods, Testing for bimodality in frequency distributions of data suggesting polymorphisms of drug metabolism--hypothesis testing *Br. J. Clin. Pharmacol.* **1989**, *28*, 655-662.
108. C. Zhang, B. E. Mapes, B. J. Soden, Bimodality in tropical water vapour *Q. J. Roy. Meteor. Soc.* **2003**, *129*, 2847 - 2866.
109. K. Levenberg, A method for the solution of certain non-linear problems in least squares **1944**, *2*, 164 - 168.
110. A. N. Spiess, N. Neumeyer, An evaluation of R2 as an inadequate measure for nonlinear models in pharmacological and biochemical research: a Monte Carlo approach **2010**, *10*, 6.
111. V. Cassina, D. Seruggia, G. L. Beretta, D. Salerno, D. Brogioli, S. Manzini, F. Zunino, F. Mantegazza, Atomic force microscopy study of DNA conformation in the presence of drugs *Eur. Biophys. J.* **2011**, *40*, 59-68.
112. K. Geller, K. E. Reinert, Evidence for an increase of DNA contour length at low ionic strength *Nuc. Acids Res.* **1980**, *8*, 2807-2822.
113. J. D. McGhee, P. H. von Hippel, Theoretical aspects of DNA-protein interactions: co-operative and non-co-operative binding of large ligands to a one-dimensional homogeneous lattice *J. Mol. Biol.* **1974**, *86*, 469-489.
114. M. Hossain, G. Suresh Kumar, DNA intercalation of methylene blue and quinacrine: new insights into base and sequence specificity from structural and thermodynamic studies with polynucleotides *Mol. Biosyst.* **2009**, *5*, 1311-1322.
115. F. Barcelo, J. Martorell, F. Gavilanes, J. M. Gonzalez-Ros, Equilibrium binding of daunomycin and adriamycin to calf thymus DNA. Temperature and ionic strength dependence of thermodynamic parameters *Biochem. Pharmacol.* **1988**, *37*, 2133-2138.
116. N. C. Seeman, R. O. Day, A. Rich, Nucleic acid-mutagen interactions: crystal structure of adenylyl-3',5'-uridine plus 9-aminoacridine *Nature* **1975**, *253*, 324-327.
117. A. H. Wang, J. Nathans, G. van der Marel, J. H. van Boom, A. Rich, Molecular structure of a double helical DNA fragment intercalator complex between deoxy CpG and a terpyridine platinum compound *Nature* **1978**, *276*, 471-474.
118. A. Adams, Crystal structures of acridines complexed with nucleic acids *Curr. Med. Chem.* **2002**, *9*, 1667-1675.
119. T. D. Sakore, K. K. Bhandary, H. M. Sobell, Visualization of drug-nucleic acid interactions at atomic resolution. X. Structure of a N,N-dimethylproflavine: deoxycytidylyl(3'-5')deoxyguanosine crystalline complex *J. Biomol. Struct. Dyn.* **1984**, *1*, 1219-1227.

120. S. Neidle, L. H. Pearl, P. Herzyk, H. M. Berman, A molecular model for proflavine-DNA intercalation *Nuc. Acids Res.* **1988**, *16*, 8999-9016.
121. S. Neidle, T. C. Jenkins, Molecular modeling to study DNA intercalation by anti-tumor drugs *Methods Enzymol.* **1991**, *203*, 433-458.
122. L. Trantirek, R. Stefl, M. Vorlickova, J. Koca, V. Sklenar, J. Kypr, An A-type double helix of DNA having B-type puckering of the deoxyribose rings *J. Mol. Biol.* **2000**, *297*, 907-922.
123. Y. Fang, T. S. Spisz, J. H. Hoh, Ethanol-induced structural transitions of DNA on mica *Nuc. Acids Res.* **1999**, *27*, 1943-1949.
124. N. H. Thomson, S. Kasas, B. Smith, H. G. Hansma, P. K. Hansma, Reversible binding of DNA to mica for AFM imaging *Langmuir* **1996**, *12*, 5905-5908.
125. D. R. Whelan, K. R. Bambery, P. Heraud, M. J. Tobin, M. Diem, D. McNaughton, B. R. Wood, Monitoring the reversible B to A-like transition of DNA in eukaryotic cells using Fourier transform infrared spectroscopy *Nuc. Acids Res.* **2011**, *39*, 5439-5448.
126. J. Kypr, I. Kejnovska, D. Renciuk, M. Vorlickova, Circular dichroism and conformational polymorphism of DNA *Nuc. Acids Res.* **2009**, *37*, 1713-1725.
127. G. Chirico, L. Lunelli, G. Baldini, Conformation of intercalated DNA plasmids investigated by circular dichroism and dynamic light scattering *Biophys. Chem.* **1990**, *38*, 201-211.
128. V. I. Ivanov, L. E. Minchenkova, E. E. Minyat, M. D. Frank-Kamenetskii, A. K. Schyolkina, The B to A transition of DNA in solution *J. Mol. Biol.* **1974**, *87*, 817-833.
129. P. Costantino, P. De Santis, G. Ughetto, Circular dichroism studies on the echinomycin--DNA complex *FEBS Lett.* **1978**, *88*, 349-352.
130. E. Marco, A. Negri, F. J. Luque, F. Gago, Role of stacking interactions in the binding sequence preferences of DNA bis-intercalators: insight from thermodynamic integration free energy simulations *Nuc. Acids Res.* **2005**, *33*, 6214-6224.
131. S. Nafisi, A. A. Saboury, N. Keramat, J. F. Neault, H. A. Tajmir-Riahi, Stability and structural features of DNA intercalation with ethidium bromide, acridine orange and methylene blue *J. Mol. Struct.* **2007**, *827*, 35-43.
132. D. Reha, M. Kabelac, F. Ryjacek, J. Sponer, J. E. Sponer, M. Elstner, S. Suhai, P. Hobza, Intercalators. 1. Nature of stacking interactions between intercalators (ethidium, daunomycin, ellipticine, and 4',6-diaminide-2-phenylindole) and DNA base pairs. Ab initio quantum chemical, density functional theory, and empirical potential study *J. Am. Chem. Soc.* **2002**, *124*, 3366-3376.
133. G. Ughetto, A. H. Wang, G. J. Quigley, G. A. van der Marel, J. H. van Boom, A. Rich, A comparison of the structure of echinomycin and triostin A complexed to a DNA fragment *Nuc. Acids Res.* **1985**, *13*, 2305-2323.
134. J. Zlatanova, S. M. Lindsay, S. H. Leuba, Single molecule force spectroscopy in biology using the atomic force microscope *Prog. Biophys. Mol. Biol.* **2000**, *74*, 37-61.
135. S. L. Guo, N. Li, N. Lad, S. Desai, B. B. Akhremitchev, Distributions of Parameters and Features of Multiple Bond Ruptures in Force Spectroscopy by Atomic Force Microscopy *J. Phys. Chem. C.* **2010**, *114*, 8755-8765.
136. J. Morfill, F. Kuhner, K. Blank, R. A. Lugmaier, J. Sedlmair, H. E. Gaub, B-S transition in short oligonucleotides *Biophys. J.* **2007**, *93*, 2400-2409.
137. R. Krautbauer, L. H. Pope, T. E. Schrader, S. Allen, H. E. Gaub, Discriminating small molecule DNA binding modes by single molecule force spectroscopy *FEBS Lett.* **2002**, *510*, 154-158.
138. M. C. Fletcher, R. K. Olsen, K. R. Fox, Dissociation of the AT-specific bifunctional intercalator [N-MeCys3,N-MeCys7]TANDEM from TpA sites in DNA *Biochem. J.* **1995**, *306 (Pt 1)*, 15-19.

139. M. A. Viswamitra, O. Kennard, W. B. Cruse, E. Egert, G. M. Sheldrick, P. G. Jones, M. J. Waring, L. P. Wakelin, R. K. Olsen, Structure of TANDEM and its implication for bifunctional intercalation into DNA *Nature* **1981**, *289*, 817-819.
140. M. Lavesa, R. K. Olsen, K. R. Fox, Sequence-specific binding of [N-MeCys3,N-MeCys7]TANDEM to TpA *Biochem. J.* **1993**, *289 (Pt 2)*, 605-607.
141. M. Sletmoen, G. Skjak-Braek, B. T. Stokke, Single-molecular pair unbinding studies of mannuronan C-5 epimerase AlgE4 and its polymer substrate *Biomacromol.* **2004**, *5*, 1288-1295.
142. H. Clausen-Schaumann, M. Seitz, R. Krautbauer, H. E. Gaub, Force spectroscopy with single bio-molecules *Curr. Opin. Chem. Biol.* **2000**, *4*, 524-530.
143. T. Paramanathan, I. Vladescu, M. J. McCauley, I. Rouzina, M. C. Williams, Force spectroscopy reveals the DNA structural dynamics that govern the slow binding of Actinomycin D *Nuc. Acids Res.* **2012**, *40*, 4925-4932.
144. A. Noy, R. W. Friddle, Practical single molecule force spectroscopy: How to determine fundamental thermodynamic parameters of intermolecular bonds with an atomic force microscope *Methods* **2013**, *60*, 142-150.
145. W. Adam, P. Groer, K. Mielke, C. R. Saha-Moller, R. Hutterer, W. Kiefer, V. Nagel, F. W. Schneider, D. Ballmaier, Y. Schleger, B. Epe, Photochemical and photobiological studies with acridine and phenanthridine hydroperoxides in cell-free DNA *Photochem. Photobiol.* **1997**, *66*, 26-33.
146. F. Leng, J. B. Chaires, M. J. Waring, Energetics of echinomycin binding to DNA *Nuc. Acids Res.* **2003**, *31*, 6191-6197.
147. S. Allen, J. Davies, A. C. Dawkes, M. C. Davies, J. C. Edwards, M. C. Parker, C. J. Roberts, J. Sefton, S. J. Tendler, P. M. Williams, In situ observation of streptavidin-biotin binding on an immunoassay well surface using an atomic force microscope *FEBS Lett.* **1996**, *390*, 161-164.
148. M. P. Bui, T. J. Baek, G. H. Seong, Gold nanoparticle aggregation-based highly sensitive DNA detection using atomic force microscopy *Anal. Bioanal. Chem.* **2007**, *388*, 1185-1190.
149. J. S. Lee, M. S. Han, C. A. Mirkin, Colorimetric detection of mercuric ion (Hg2+) in aqueous media using DNA-functionalized gold nanoparticles *Angew. Chem. Int. Ed.* **2007**, *46*, 4093-4096.
150. D. Liu, W. Chen, K. Sun, K. Deng, W. Zhang, Z. Wang, X. Jiang, Resettable, multi-readout logic gates based on controllably reversible aggregation of gold nanoparticles *Angew. Chem. Int. Ed.* **2011**, *50*, 4103-4107.
151. H. Tang, N. Zhang, Z. Z. Chen, K. H. Xu, L. G. Zhuo, L. G. An, G. W. Yang, Probing hydroxyl radicals and their imaging in living cells by use of FAM-DNA-Au nanoparticles *Chem. Eur. J.* **2008**, *14*, 522-528.
152. J. A. Milton, S. Patole, H. Yin, Q. Xiao, T. Brown, T. Melvin, Efficient self-assembly of DNA-functionalized fluorophores and gold nanoparticles with DNA functionalized silicon surfaces: the effect of oligomer spacers *Nuc. Acids Res.* **2013**, *41*, e80.
153. K. Sato, K. Hosokawa, M. Maeda, Rapid aggregation of gold nanoparticles induced by non-cross-linking DNA hybridization *J. Am. Chem. Soc.* **2003**, *125*, 8102-8103.
154. J. Y. Shim, V. K. Gupta, Reversible aggregation of gold nanoparticles induced by pH dependent conformational transitions of a self-assembled polypeptide *J. Colloid Interface Sci.* **2007**, *316*, 977-983.
155. J. Turkevich, P. C. Stevenson, J. Hillier, A study of the nucleation and growth processes in the synthesis of colloidal gold *Discussions of the Faraday Soc.* **1951**, *11*, 55 - 75.
156. K. R. Fox, L. P. Wakelin, M. J. Waring, Kinetics of the interaction between echinomycin and deoxyribonucleic acid *Biochemistry* **1981**, *20*, 5768-5779.
157. B. D. Rackham, L. A. Howell, A. N. Round, M. Searcey, Non-covalent duplex to duplex crosslinking of DNA in solution revealed by single molecule force spectroscopy *Org. Biomol. Chem.* **2013**, *11*, 8340-8347.

158. R. Tong, H. D. Hemmati, R. Langer, D. S. Kohane, Photoswitchable Nanoparticles for Triggered Tissue Penetration and Drug Delivery *J. Am. Chem. Soc.* **2012**.
159. B. F. Eichman, B. H. Mooers, M. Alberti, J. E. Hearst, P. S. Ho, The crystal structures of psoralen cross-linked DNAs: drug-dependent formation of Holliday junctions *J. Mol. Biol.* **2001**, *308*, 15-26.
160. A. L. Brogden, N. H. Hopcroft, M. Searcey, C. J. Cardin, Ligand bridging of the DNA Holliday junction: molecular recognition of a stacked-X four-way junction by a small molecule *Angew. Chem.* **2007**, *119*, 3924-3928.
161. T. A. Brooks, S. Kendrick, L. Hurley, Making sense of G-quadruplex and i-motif functions in oncogene promoters *FEBS J.* **2010**, *277*, 3459-3469.
162. A. L. Brogden, N. H. Hopcroft, M. Searcey, C. J. Cardin, Ligand bridging of the DNA Holliday junction: molecular recognition of a stacked-X four-way junction by a small molecule *Angew. Chem. Int. Ed.* **2007**, *46*, 3850-3854.
163. D. H. Evans, R. Kolodner, Construction of a synthetic Holliday junction analog and characterization of its interaction with a Saccharomyces cerevisiae endonuclease that cleaves Holliday junctions *J. Biol. Chem.* **1987**, *262*, 9160-9165.
164. D. M. Lilley, All change at Holliday junction *Proc. Natl. Acad. Sci. USA* **1997**, *94*, 9513-9515.
165. A. Y. Lushnikov, A. Bogdanov, Y. L. Lyubchenko, DNA recombination: holliday junctions dynamics and branch migration *J. Biol. Chem.* **2003**, *278*, 43130-43134.
166. C. D. Mao, W. Q. Sun, N. C. Seeman, Designed two-dimensional DNA Holliday junction arrays visualized by atomic force microscopy *J. Am. Chem. Soc.* **1999**, *121*, 5437-5443.
167. M. Karymov, D. Daniel, O. F. Sankey, Y. L. Lyubchenko, Holliday junction dynamics and branch migration: single-molecule analysis *Proc. Natl. Acad. Sci. USA* **2005**, *102*, 8186-8191.
168. F. A. Hays, J. Watson, P. S. Ho, Caution! DNA crossing: crystal structures of Holliday junctions *J. Biol. Chem.* **2003**, *278*, 49663-49666.
169. A. N. Round, Atomic force microscopy of plant cell wall polysaccharides *PhD thesis*, University of East Anglia **1999**.
170. P. Alberti, J. Ren, M. P. Teulade-Fichou, L. Guittat, J. F. Riou, J. Chaires, C. Helene, J. P. Vigneron, J. M. Lehn, J. L. Mergny, Interaction of an acridine dimer with DNA quadruplex structures *J. of Biomol. Struct. & Dyn.* **2001**, *19*, 505-513.
171. J. A. Brazier, A. Shah, G. D. Brown, I-Motif formation in gene promoters: unusually stable formation in sequences complementary to known G-quadruplexes *Chem. Commun.* **2012**, *48*, 10739-10741.
172. H. A. Day, C. Huguin, Z. A. E. Waller, Silver cations fold i-motif at neutral pH *Chem. Commun.* **2013**, *49*, 7696-7698.
173. X. Q. Zhao, J. Wu, J. H. Liang, J. W. Yan, Z. Zhu, C. J. Yang, B. W. Mao, Single-molecule force spectroscopic studies on intra- and intermolecular interactions of g-quadruplex aptamer with target shp2 protein *J. Phys. Chem. B.* **2012**, *116*, 11397-11404.
174. S. R. Alberts, A. Cervantes, C. J. van de Velde, Gastric cancer: epidemiology, pathology and treatment *Ann. Oncol.* **2003**, *14 Suppl 2*, ii31-36.
175. L. E. Coate, F. A. Shepherd, Maintenance therapy in advanced non-small cell lung cancer: evolution, tolerability and outcomes **2011**, *3*, 139-157.
176. A. Sita-Lumsden, D. A. Dart, J. Waxman, C. L. Bevan, Circulating microRNAs as potential new biomarkers for prostate cancer *Br. J. Cancer* **2013**, *108*, 1925-1930.
177. J. R. Goodell, A. V. Ougolkov, H. Hiasa, H. Kaur, R. Remmel, D. D. Billadeau, D. M. Ferguson, Acridine-based agents with topoisomerase II activity inhibit pancreatic cancer cell proliferation and induce apoptosis *J. Med. Chem.* **2008**, *51*, 179-182.
178. M. Jones, A. E. Mercer, P. A. Stocks, L. J. La Pensee, R. Cosstick, B. K. Park, M. E. Kennedy, I. Piantanida, S. A. Ward, J. Davies, P. G. Bray, S. L. Rawe, J. Baird, T. Charidza, O. Janneh, P. M. O'Neill, Antitumour and antimalarial activity of artemisinin-acridine hybrids *Bioorg. Med. Chem. Lett.* **2009**, *19*, 2033-2037.

179. A. F. Valdes, Acridine and acridinones: old and new structures with antimalarial activity *O. Med. Chem. J.* **2011**, *5*, 11-20.
180. L. A. Howell, R. A. Bowater, M. A. O'Connell, A. P. Reszka, S. Neidle, M. Searcey, Synthesis of small molecules targeting multiple DNA structures using click chemistry *ChemMedChem* **2012**, *7*, 792-804.
181. P. W. Rothemund, Folding DNA to create nanoscale shapes and patterns *Nature* **2006**, *440*, 297-302.
182. D. R. Horspool, R. J. Coope, R. A. Holt, Efficient assembly of very short oligonucleotides using T4 DNA Ligase *BMC Res. Notes* **2010**, *3*, 291.
183. A. A. Greschner, K. E. Bujold, H. F. Sleiman, Intercalators as Molecular Chaperones in DNA Self-Assembly *J. Am. Chem. Soc.* **2013**, *135*, 11283 - 11288.
184. S. Toda, K. Sugawara, Y. Nishiyama, M. Ohbayashi, N. Ohkusa, H. Yamamoto, M. Konishi, T. Oki, Quinaldopeptin, a novel antibiotic of the quinomycin family *J. Antibiot.* **1990**, *43*, 796-808.
185. M. Endo, Y. Yang, Y. Suzuki, K. Hidaka, H. Sugiyama, Single-molecule visualization of the hybridization and dissociation of photoresponsive oligonucleotides and their reversible switching behavior in a DNA nanostructure *Angew. Chem. Int. Ed.* **2012**, *51*, 10518-10522.
186. I. Horcas, R. Fernandez, J. M. Gomez-Rodriguez, J. Colchero, J. Gomez-Herrero, A. M. Baro, WSXM: a software for scanning probe microscopy and a tool for nanotechnology *Rev. Sci. Instrum.* **2007**, *78*, 013705.
187. J. L. Hutter, J. Bechhoefer, Calibration of Atomic Force Microscope tips **1993**, *64*, 1868 - 1873.
188. G. T. Hermanson, *Bioconjugate techniques*, 2nd ed. ed., Academic, London, **2008**.
189. Y. L. Lyubchenko, L. S. Shlyakhtenko, AFM for analysis of structure and dynamics of DNA and protein-DNA complexes *Methods* **2009**, *47*, 206-213.
190. M. Hegner, P. Wagner, G. Semenza, Ultralarge Atomically Flat Template-Stripped Au Surfaces for Scanning Probe Microscopy *Surf. Sci.* **1993**, *291*, 39-46.
191. H. Gronbeck, A. Curioni, W. Andreoni, Thiols and disulfides on the Au(111) surface: The headgroup-gold interaction *J. Am. Chem. Soc.* **2000**, *122*, 3839-3842.
192. A. Ladik, Immobilization of DNA onto Gold and Dehybridization of Surface-Bound DNA on glass *Nanoscape* **2010**, *7*, 5.
193. J. C. Love, L. A. Estroff, J. K. Kriebel, R. G. Nuzzo, G. M. Whitesides, Self-assembled monolayers of thiolates on metals as a form of nanotechnology *Chem. Rev.* **2005**, *105*, 1103-1169.
194. W. Zhang, R. Barbagallo, C. Madden, C. J. Roberts, A. Woolford, S. Allen, Progressing single biomolecule force spectroscopy measurements for the screening of DNA binding agents *Nanotechnology* **2005**, *16*, 2325-2333.
195. N. H. Green, P. M. Williams, O. Wahab, M. C. Davies, C. J. Roberts, S. J. B. Tendler, S. Allen, Single-molecule investigations of RNA dissociation *Biophys. J.* **2004**, *86*, 3811-3821.
196. C. A. Mirkin, R. L. Letsinger, R. C. Mucic, J. J. Storhoff, A DNA-based method for rationally assembling nanoparticles into macroscopic materials *Nature* **1996**, *382*, 607-609.
197. X. Zhang, M. R. Servos, J. Liu, Instantaneous and quantitative functionalization of gold nanoparticles with thiolated DNA using a pH-assisted and surfactant-free route *J. Am. Chem. Soc.* **2012**, *134*, 7266-7269.

List of figures

List of tables

Appendix 1

ChemComm

RSC Publishing

COMMUNICATION

View Article Online
View Journal | View Issue

Cite this: *Chem. Commun.*, 2013, **49**, 9113

Received 23rd July 2013,
Accepted 22nd August 2013

DOI: 10.1039/c3cc45600e

www.rsc.org/chemcomm

A rapid screen for molecules that form duplex to duplex crosslinks in DNA†

María J. Marín,‡[a] Benjamin D. Rackham,‡[b] Andrew N. Round,[b] Lesley A. Howell,[b] David A. Russell*[a] and Mark Searcey*[b]

We describe a gold nanoparticle based assay that can rapidly determine the crosslinking of DNA duplexes by ligands. Such compounds have potential in targeting highly compacted DNA such as that found in the nucleosome.

Studies of ligand–DNA interactions tend to focus on naked structures either through gel techniques[1] or, more recently, through single molecule studies.[2] In cells, DNA is tightly compacted into the nucleosome, where it is closely associated with the histone proteins and where it is tightly wound so that one duplex structure lies close to another.[3] There are few studies of ligands binding to nucleosomal DNA, in part due to the complexity in forming the core particle and also due to the requirement for techniques such as footprinting[4] and crystallography[5] that allow the assessment of the results.

Surrogate techniques, that allow the study of histone–DNA and DNA–DNA interactions and the effects of these on molecule binding have not been disclosed and yet have the potential to change the way ligand–DNA interactions are viewed and new therapeutics are designed. One simple example is how small molecules with multiple functions are affected by the presence of both protein and other DNA strands when binding to a duplex sequence. There have been several recent descriptions of multinuclear platinum complexes, one of which has progressed into clinical trial[6] and which could potentially have crosslinked protein to DNA or DNA duplex to DNA duplex.[7] Pyrrolobenzodiazepine dimers such as the clinically tested SJG-136[8] could potentially form crosslinks within the nucleosome that run along a minor groove from one duplex strand to another. These studies suggest that a simple test for this novel higher order interaction is required. Gold nanoparticles (*ca.* 16 nm in diameter) exhibit an intense red colour in aqueous solution that changes upon aggregation of the particles.[9] The colour change is due to the coupling interactions between the surface plasmon fields of the particles. Various studies have focussed on the combination of single stranded DNA with gold nanoparticles to investigate sequence recognition properties[10] and even the ability of small molecules to stabilise the duplex.[11] However, to our knowledge, there are no studies of double stranded DNA (dsDNA) on nanoparticles to investigate duplex to duplex interactions that may be crucial in nucleosome targeting. In this paper, we describe a rapid colorimetric technique based on the aggregation of dsDNA functionalised gold nanoparticles that allows the identification of ligands that can crosslink two duplex strands – a DNA to DNA crosslink (Fig. 1a). We have applied this technique to the identification of a classical bisintercalator that has previously only been shown to bind in a two base pair sandwich fashion (bisacridine **1**, Fig. 1b)[12] and to a second molecule designed to form DNA to DNA crosslinks (bisacridine **2**, Fig. 1b).[13] The monointercalator 9-aminoacridine (9-AA, Fig. 1b) was used as a control since it does not have the ability to crosslink the duplex and therefore, it should not produce aggregation of the dsDNA functionalised gold nanoparticles (Fig. 1a).

Water soluble gold nanoparticles were prepared *via* the citrate reduction method[14] and were functionalised with thiolated DNA using a pH-assisted method.[15] The thiolated DNA was added as a pre-formed duplex. The dsDNA functionalised nanoparticles formed a red suspension in phosphate buffer (10 mM, pH 7.4) (Fig. 2) and were stable in the presence of NaCl as compared with non-functionalised nanoparticles (Fig. S1 in ESI†).

9-Aminoacridine-4-carboxamides, such as compounds **1** and **2**, are known DNA intercalating agents. The bisintercalator linked through an eight methylene chain, compound **1**, has previously been shown to bind to and unwind supercoiled DNA and to have a potent antiproliferative effect on tumour cells in culture.[12] We have previously shown that the compound with a six methylene linker is able to crosslink DNA duplexes,[16] but the longer chain allows for bisintercalation as a "staple" like structure similar to natural products such as echinomycin.[17] 9-Aminoacridine-4-carboxamide exhibits some sequence selectivity, with a preference

[a] *School of Chemistry, University of East Anglia, Norwich Research Park, Norwich NR4 7TJ, UK. E-mail: d.russell@uea.ac.uk*
[b] *School of Pharmacy, University of East Anglia, Norwich Research Park, Norwich NR4 7TJ, UK. E-mail: m.searcey@uea.ac.uk; Fax: +44 (0)1603 592009; Tel: +44 (0)1603 592026*

† Electronic supplementary information (ESI) available: Experimental details for this work. See DOI: 10.1039/c3cc45600e

‡ These two authors contributed equally to this work.

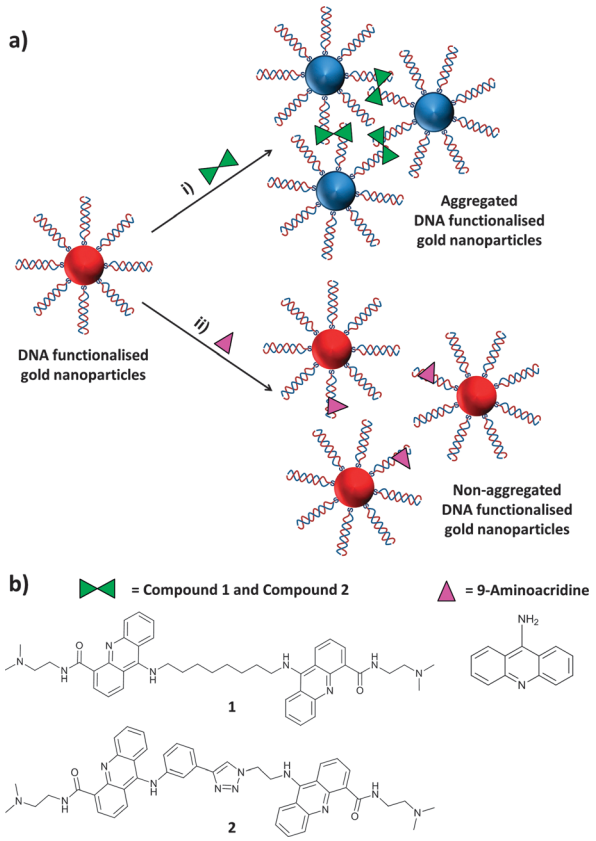

Fig. 1 (a) Schematic representation of: (i) the aggregation of the dsDNA functionalised gold nanoparticles in the presence of a bisintercalator and (ii) non-aggregation of the dsDNA functionalised gold nanoparticles in the presence of the monointercalator; (b) chemical structure of compound **1**, compound **2** and 9-aminoacridine.

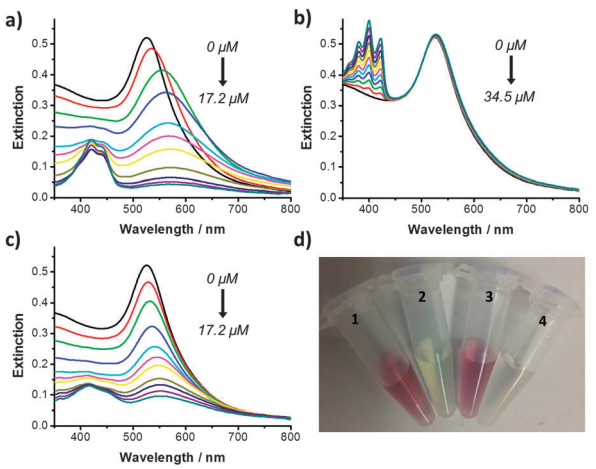

Fig. 2 UV-Vis extinction spectrum of dsDNA functionalised gold nanoparticles (PB 10 mM, pH 7.4) after addition of increasing concentrations of: (a) **1**; (b) 9-AA; and (c) **2** and (d) Eppendorf tubes containing dsDNA functionalised gold nanoparticles after addition of: (1) no compound; (2) **1** (17.2 μM); (3) 9-AA (34.5 μM); and (4) **2** (17.2 μM). All of the samples were shaken by hand for 1 min prior to measurement.

for GC rich sequences.[18] The double stranded oligonucleotide used to functionalise the gold nanoparticles (5′-CTACGTGGACCT-GGAGAGAGGAAGGAGACTGCCTG) contains multiple sites for intercalation with compounds **1** and **2**. Increasing concentrations of compound **1** (from 0 to 17.2 μM) were added to a sample of the dsDNA functionalised gold nanoparticles. The samples were slowly shaken by hand for 1 min. The UV-Vis extinction spectrum of the functionalised gold nanoparticle solution was measured before and after addition of the corresponding compound **1** concentration (Fig. 2a). Upon addition of increasing concentrations of **1**, the surface plasmon absorption band showed a significant red shift from 525 to 578 nm and a decrease in intensity. Incubation of the gold nanoparticles with **1** led to a rapid (<1 min) disappearance of the red colour (Fig. 2d). These results suggest that the bisintercalator **1** is causing aggregation of the dsDNA functionalised gold nanoparticles through duplex to duplex crosslinking. A similar titration was performed with phosphate buffer (PB) and no colour change was observed (Fig. S2a in ESI†). The increase in the extinction seen at 400–500 nm in Fig. 2a is due to the addition of increasing concentrations of **1** (Fig. S2b in ESI†).

The observed colour change could be a consequence of simple intercalation rather than crosslinking. In order to elucidate whether crosslinking between **1** and the DNA was taking place, the dsDNA functionalised gold nanoparticles were incubated with 9-AA. Titration with 9-AA from 0 to 34.5 μM (*i.e.* twice the final concentration of the bisintercalator) led to neither a change in the UV-Vis extinction spectrum of the nanoparticles (Fig. 2b) nor in the colour of the solution (Fig. 2d), suggesting that the aggregation of the nanoparticles in the presence of **1** is not simply a consequence of intercalation but rather a crosslinking. The increase in extinction seen at 350–450 nm is due to the addition of increasing concentrations of 9-AA (Fig. S2c in ESI†).

In a recent study, we described the use of click chemistry to generate bisintercalators designed to bind to higher order DNA structures.[13] Some of these compounds were designed to direct the second chromophore away from the duplex, one such molecule being the bisintercalator compound **2**. When the dsDNA functionalised gold nanoparticles were incubated with increasing concentrations of **2** (0 to 17.2 μM) a red shift (from 525 to 554 nm) in the surface plasmon absorption band was observed accompanied by a decrease in the extinction intensity (Fig. 2c). The changes in the surface plasmon band led to the disappearance of the red colour (Fig. 2d). The increase in the extinction seen at 400–500 nm is due to the addition of increasing concentrations of **2** (Fig. S2d in ESI†). A summary of how the addition of compound **1**, **2** and 9-AA affects the intensity of the extinction maxima can be seen in Fig. S3 in ESI.†

The surfactant sequestration technique has been utilised in kinetic studies of drug–DNA interactions in order to assess dissociation kinetics of ligands from the duplex.[19] Surfactant sequestration was applied to demonstrate the reversibility of the ligand–DNA binding and, therefore, the reversibility of the aggregation of the dsDNA functionalised gold nanoparticles. In an initial step, dsDNA functionalised gold nanoparticles were treated with **1** (3.5 μM) to induce aggregation of the particles. A red shift in the surface plasmon absorption band of the nanoparticles from 525 to 560 nm (Fig. 3a) and a change in the colour of the solution (Fig. 3b) were observed upon addition of **1**. Increasing concentrations of sodium dodecylsulfate (SDS) (from 34.8 to 442.9 μM) were added to the solution of gold nanoparticles containing **1**.

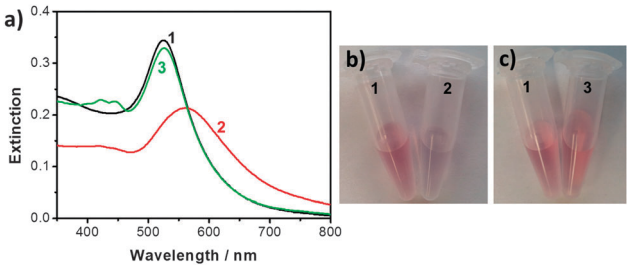

Fig. 3 (a) UV-Vis extinction spectrum of dsDNA functionalised gold nanoparticles (PB 10 mM, pH 7.4): (1) alone; (2) after addition of **1** (3.5 μM); and (3) after addition of **1** (3.5 μM) and SDS (442.9 μM). (b) and (c) Eppendorf tubes containing dsDNA functionalised gold nanoparticles (PB 10 mM, pH 7.4): (1) alone; (2) after addition of **1** (3.5 μM); and (3) after addition of **1** (3.5 μM) and SDS (442.9 μM). All of the samples were shaken by hand for 1 min prior to measurement.

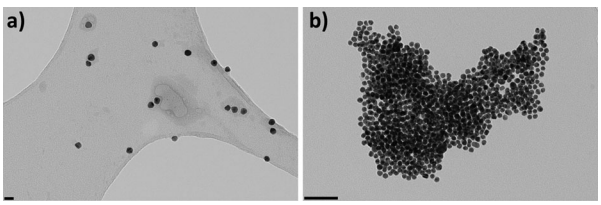

Fig. 4 TEM images of dsDNA functionalised gold nanoparticles (a) before and (b) after addition of **1** (3.5 μM). Scale bars: (a) 20 nm and (b) 100 nm.

The samples were shaken by hand for 1 min and the UV-Vis extinction spectrum was recorded (Fig. 3a). After addition of SDS (442.9 μM), the extinction maximum shifted back to 525 nm (Fig. 3a) and the colour of the solution turned to the initial deep red (Fig. 3c). These results clearly demonstrate the reversibility of the DNA-compound **1** crosslinking reaction. Addition of increasing concentrations of SDS to a solution of DNA functionalised gold nanoparticles without compound **1** had no effect on the surface plasmon absorption band of the solution (Fig. S4 in ESI†). The reversibility process was also confirmed by dynamic light scattering that showed an increase in the hydrodynamic diameter of the dsDNA functionalised gold nanoparticles after addition of compound **1**. The diameter of the aggregated particles decreased when SDS was added to the solution containing **1**, *i.e.*, when the aggregation was reversed (Table S1 in ESI†).

Further verification of the reversibility of the crosslinking between the DNA and compound **1** came from the titration of a solution of dsDNA functionalised gold nanoparticles containing **1** (3.5 μM, aggregated nanoparticles) with non-immobilised calf thymus DNA (CT-DNA). When the CT-DNA is in excess, it competes with the gold nanoparticles for ligand binding and should lead to disaggregation as **1** is sequestered onto the non-immobilised DNA. Upon addition of CT-DNA (97 μM base pairs), the surface plasmon absorption band shifted back to 525 nm and the extinction intensity increased (Fig. S5a in ESI†) confirming the reversibility of the ligand–DNA crosslinking. Addition of the same concentrations of CT-DNA to a solution of dsDNA functionalised nanoparticles without **1** produced no changes in the surface plasmon absorption band (Fig. S5b in ESI†).

Transmission electron microscopy (TEM) was used to further confirm the crosslinking between dsDNA functionalised gold nanoparticles and compound **1**. TEM images of the dsDNA functionalised particles showed dispersed gold nanoparticles (Fig. 4a). In the presence of compound **1** the nanoparticles aggregated forming large clusters as observed in Fig. 4b.

The ability of small molecules to crosslink duplex DNA (from strand to strand) is well documented and studied – it forms the basis for the clinically used antitumour agents such as cyclophosphamide – whereas duplex to duplex crosslinking is largely unexplored and remains difficult to visualise by macroscopic means, such as gel electrophoresis. As the move towards personalised medicine and gene targeting continues, the ability to target DNA that is compacted into the nucleosome and to study its susceptibility to drugs and ligands is an imperative. In this paper, we have shown that a compound previously demonstrated to bind to one duplex structure is also able to form duplex to duplex crosslinks. We have also demonstrated that it is possible to design molecules with rigid linkers that can reach across from one DNA strand to another, a potential benefit in a compact structure in the cell. The use of gold nanoparticle conjugates to demonstrate duplex to duplex crosslinking is a rapid colorimetric approach to detection which could be extended to other molecules.

We thank the School of Chemistry (UEA) for the post-doctoral fellowship of M.J.M. and the School of Pharmacy (UEA) for a studentship for B.D.R. The authors are grateful to Dr Kim Find (John Innes Centre, Norwich) for assistance with the TEM.

Notes and references

1 A. J. Hampshire, D. A. Rusling, V. J. Broughton-Head and K. R. Fox, *Methods*, 2007, **42**, 128.
2 I. Mela, R. Kranaster, R. M. Henderson, S. Balasubramanian and J. M. Edwardson, *Biochemistry*, 2012, **51**, 578.
3 (*a*) D. M. Lilley and J. F. Pardon, *Annu. Rev. Genet.*, 1979, **13**, 197; (*b*) O. J. Rando and K. Ahmad, *Curr. Opin. Cell Biol.*, 2007, **19**, 250.
4 P. M. Brown and K. R. Fox, *Methods Mol. Biol.*, 1997, **90**, 81.
5 R. K. Suto, R. S. Edayathumangalam, C. L. White, C. Melander, J. M. Gottesfeld, P. B. Dervan and K. Luger, *J. Mol. Biol.*, 2003, **326**, 371.
6 D. I. Jodrell, T. R. Evans, W. Steward, D. Cameron, J. Prendiville, C. Aschele, C. Noberasco, M. Lind, J. Carmichael, N. Dobbs, G. Camboni, B. Gatti and F. De Braud, *Eur. J. Cancer*, 2004, **40**, 1872.
7 T. Muchova, S. M. Quintel, N. P. Farrell, V. Brabec and J. Kasparkova, *JBIC, J. Biol. Inorg. Chem.*, 2012, **17**, 239.
8 J. A. Hartley, *Expert Opin. Invest. Drugs*, 2011, **20**, 733.
9 (*a*) C. L. Schofield, A. H. Haines, R. A. Field and D. A. Russell, *Langmuir*, 2006, **22**, 6707; (*b*) C. L. Schofield, R. A. Field and D. A. Russell, *Anal. Chem.*, 2007, **79**, 1356.
10 (*a*) C. A. Mirkin, R. L. Letsinger, R. C. Mucic and J. J. Storhoff, *Nature*, 1996, **382**, 607; (*b*) D. A. Giljohann, D. S. Seferos, W. L. Daniel, M. D. Massich, P. C. Patel and C. A. Mirkin, *Angew. Chem., Int. Ed. Engl.*, 2010, **49**, 3280; (*c*) K. Saha, S. S. Agasti, C. Kim, X. Li and V. M. Rotello, *Chem. Rev.*, 2012, **112**, 2739.
11 S. J. Hurst, M. S. Han, A. K. Lytton-Jean and C. A. Mirkin, *Anal. Chem.*, 2007, **79**, 7201.
12 L. P. G. Wakelin, X. Bu, A. Eleftheriou, A. Parmar, C. Hayek and B. W. Stewart, *J. Med. Chem.*, 2003, **46**, 5790.
13 L. A. Howell, R. A. Bowater, M. A. O'Connell, A. P. Reszka, S. Neidle and M. Searcey, *ChemMedChem*, 2012, **7**, 792.
14 B. V. Enüstün and J. Turkevich, *J. Am. Chem. Soc.*, 1963, **85**, 3317.
15 X. Zhang, M. R. Servos and J. Liu, *J. Am. Chem. Soc.*, 2012, **134**, 7266.
16 N. H. Hopcroft, A. L. Brogden, M. Searcey and C. J. Cardin, *Nucleic Acids Res.*, 2006, **34**, 6663.
17 M. J. Waring and L. P. G. Wakelin, *Nature*, 1974, **252**, 653.
18 M. Searcey, S. McClean, B. Madden, A. T. McGown and L. P. G. Wakelin, *Anti-Cancer Drug Des.*, 1998, **13**, 837.
19 L. P. G. Wakelin, P. Chetcuti and W. A. Denny, *J. Med. Chem.*, 1990, **33**, 2039.

Organic & Biomolecular Chemistry

RSC Publishing

PAPER

View Article Online
View Journal | View Issue

Cite this: *Org. Biomol. Chem.*, 2013, **11**, 8340

Non-covalent duplex to duplex crosslinking of DNA in solution revealed by single molecule force spectroscopy†

Benjamin D. Rackham, Lesley A. Howell, Andrew N. Round* and Mark Searcey*

Received 26th July 2013,
Accepted 14th October 2013

DOI: 10.1039/c3ob42009d

www.rsc.org/obc

Small molecules that interact with DNA, disrupting the binding of transcription factors or crosslinking DNA into larger structures, have significant potential as cancer therapies and in nanotechnology. Bisintercalators, including natural products such as echinomycin and rationally designed molecules such as the bis-9-aminoacridine-4-carboxamides, are key examples. There is little knowledge of the propensity of these molecules to crosslink duplex DNA. Here we use single molecule force spectroscopy to assay the crosslinking capabilities of bisintercalators. We show that bis-9-aminoacridine-4-carboxamides with both rigid and flexible linkers are able to crosslink duplex strands of DNA, and estimate the equilibrium free energy of a 9-aminoacridine-4-carboxamide bisintercalator from DNA at 5.03 kJ mol^{-1}. Unexpectedly, we find that echinomycin and its synthetic analogue TANDEM are capable of sequence-specific crosslinking of the terminal base pairs of two duplex DNA strands. In the crowded environment of the nucleosome, small molecules that crosslink neighbouring DNA strands may be expected to have significant effects on transcription, while a small molecule that facilitates sequence-specific blunt-end ligation of DNA may find applications in the developing field of DNA nanotechnology.

Introduction

DNA binding molecules are used extensively in the treatment of cancer and yet molecules that can bind to and crosslink multiple strands of DNA are relatively unexplored. The nitrogen mustards exert their effects through the formation of interstrand covalent crosslinks on a single duplex strand that inhibit DNA processing in proliferative cells.[1] Adriamycin (doxorubicin) is a natural product that forms a non-covalent interaction with DNA in which a planar aromatic chromophore is inserted between the base pairs, forming a complex that inhibits the enzyme topoisomerase II.[2] This is an example of a monointercalating compound. Echinomycin is a bisintercalator, in which two chromophores are inserted into the helix,[3] again leading to inhibition of DNA processing and cell death. Although it has advanced into clinical trials, echinomycin is not clinically utilised.

In a cell, DNA is tightly compacted into the nucleosome and it is likely bifunctional molecules that can bind in the nucleus will interact with more than one strand of DNA. Several years ago, a gel based technique was used to demonstrate that luzopeptin A had the ability to form duplex to duplex crosslinks through bisintercalation,[4] although this conclusion was challenged.[5] Intercalators have also been specifically designed to favour crosslinking.[6] These threading acridines are also potent cytotoxins and it is possible that the ability to crosslink duplex strands in the nucleosome, preventing unpacking during replication, is contributing to this activity.

The sequence recognition properties of DNA also make it a powerful tool for the preparation of devices on the nanoscale. This has been demonstrated by disclosures of "smiley" faces, DNA walkers and nanoscale frameworks to study reactivity.[7–9] DNA has also been exploited for its ability to act as a molecular wire, with the insertion of ruthenium complexes into sequences up to 100 base pairs in length.[10] Nanoscale structures often rely on large circular plasmid DNA that is then stitched together using smaller sequences that are designed to make the plasmid fold into unusual shapes.[7] Smaller oligonucleotides could be built up to longer stretches using enzyme based ligation, although the efficiency of this process is dependent on the size of the ligation site.[11]

The effects of small molecules on the assembly of DNA structures in the nanotechnology arena have been less well studied. Small molecules can crosslink four-way junctions, bind to three-way junctions and even promote the assembly of

School of Pharmacy, University of East Anglia, Norwich Research Park, Norwich NR4 7TJ, UK. E-mail: m.searcey@uea.ac.uk, a.round@uea.ac.uk; Fax: +44 (0)1603 592009; Tel: +44 (0)1603 592026

†Electronic supplementary information (ESI) available. See DOI: 10.1039/c3ob42009d

higher order DNA structures at room temperature.[12–14] If (i) it is possible to crosslink duplex DNA in solution and (ii) the binding site is properly defined, the potential to build up DNA nanostructures arises.[4,15] However, to build linear DNA structures would require an end-to-end non-covalent ligation, which is hard to demonstrate with these compounds.

The 9-aminoacridine-4-carboxamide bisintercalators demonstrate little sequence selectivity, with a reported preference for 5′-GC sequences.[16,17] By contrast, the binding modes of the natural product echinomycin and the synthetic analogue of triostin-A, TANDEM, are more clearly defined. NMR and crystallographic studies demonstrate that both echinomycin and TANDEM adopt a staple-like conformation on binding to DNA.[18,19] Echinomycin has a pronounced sequence selectivity for a four base pair sequence with a central CpG step, whereas TANDEM prefers to bind to a sequence with a central TpA.[20,21]

Other than by crystallography, the phenomenon of duplex to duplex crosslinks is difficult to study.[22] The use of an atomic force microscope (AFM) in force spectroscopy mode allows the study of molecular interactions at a single molecule level.[23–25] By tethering oligonucleotides to the cantilever probe and to a gold-coated surface, it is possible to study the interactions between the two DNA strands. Here, we report on our force spectroscopy study of the crosslinking abilities of several bisintercalators. We find that in the absence of ligand, the DNA strands do not interact, whereas in the presence of a bisintercalator such as a bisacridine, we observe the crosslinking of the two DNA strands. In the presence of echinomycin and TANDEM, this crosslinking interaction is dependent upon the identity of the terminal nucleotide; when the final base is changed to fit the sequence selectivity of the ligand, we observe events that indicate the rupture of end-to-end crosslinking interactions. Thus we demonstrate that bisintercalators based upon 9-aminoacridine-4-carboxamides can crosslink one duplex DNA strand to another, and show that echinomycin and TANDEM non-covalently link two DNA strands in a sequence specific manner.

Results and discussion

The synthesis of bisacridine **1** was recently described.[26] Modelling (data not shown) suggests that the two chromophores are unable to stack well on each other due to the rigid linker between them, suggesting a possible mode of intercalation with DNA that differs from the classical 'Type I' intercalation interaction. We assessed the ability of bisacridine **1** to crosslink DNA duplexes. Crosslinking of duplex DNA strands by bisintercalators has previously been proposed by the group of Henderson as an explanation for the observation of compact, coiled and crossed DNA structures in AFM images.[27] When we use AFM to image duplex DNA to which bisacridine **1** has been added, we observe increases (from 14–19% to 30%; see ESI†) in the proportion of DNA strands that overlie each other and that adopt more compact, coiled conformations, in comparison to the same DNA sequences imaged with the monointercalator ethidium bromide, the rigidly-linked bisintercalator echinomycin and without any intercalator (Fig. 1). The proportion of coils and crossovers in the DNA-only control reflects the way the DNA is adsorbed to the mica surface.

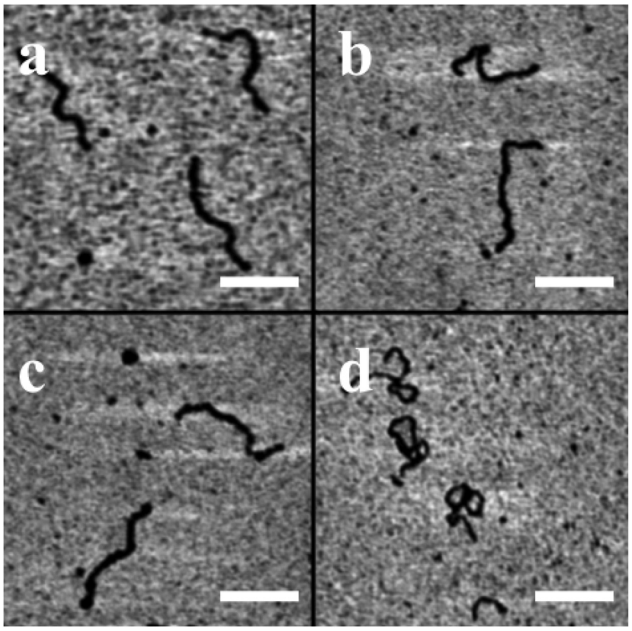

Fig. 1 AFM images of (a) 1341 bp dsDNA control, (b) DNA + echinomycin, (c) DNA + ethidium bromide, (d) DNA + bisacridine **1**. In all cases the scale bar denotes 250 nm.

In order to establish that bisintercalator **1** crosslinks DNA, we use force spectroscopy, following the experimental setup represented in Fig. 2a. With DNA covalently bound to both probe and substrate surfaces, an interaction between the opposing duplex DNA strands is recorded as a peak in the force *vs*. distance plot (Fig. 2b), at a force representing the resistance of the bond to stretching and at a distance reflecting the separation of probe and surface at which the interaction is ruptured. Fig. 2c shows the distribution of forces arising from rupture events in this experiment when bisacridine **1** is added into solution while DNA-functionalised probe and substrate surfaces are cyclically brought together and separated. In more than 4% of these cycles a rupture event is recorded on separation. In the absence of the bisintercalator less than 0.3% of cycles show rupture events. A low level of non-specific events between probe and surface is expected in such an experiment. Similarly, no cross-linking is observed on the introduction of a monointercalator (9-aminoacridine, ethidium bromide – see Table 1). By contrast, addition of bisintercalator **2**, a flexibly linked bisintercalator, gives rise to an increase in the number of observed rupture events (Fig. 2d) in a similar way to that seen for bisintercalator **1**. Table 1 presents the frequencies of rupture events observed, as well as the mean forces and lengths recorded for the crosslinking interactions. The relative frequencies of unbinding events for the systems described above demonstrate that the two bisintercalators do crosslink

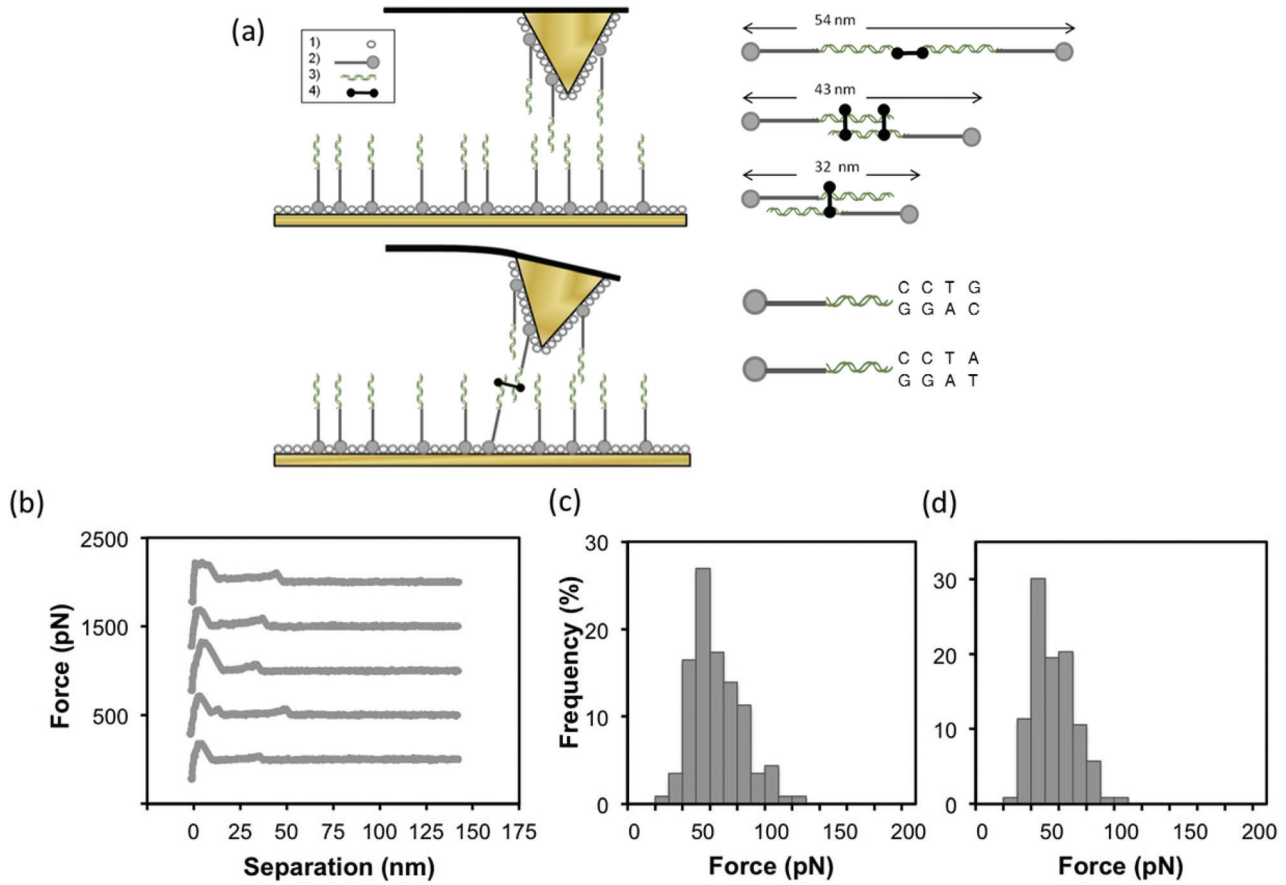

Fig. 2 (a) (left) Schematic illustration of the experimental setup: AFM cantilever and opposing substrate showing no interaction (top) and a positive interaction (bottom). The legend denotes (1) 11-mercaptoundecanoic acid, (2) PEG, (3) DNA, (4) bisintercalator. (right) Predicted binding arrangements and theoretical lengths of the bound complexes and enlargement of the terminal base pairs of each of the two DNA sequences. The only difference is the composition of the terminal base pair, being either GC or AT. (b) Typical force-extension curves for the interaction between bisintercalator **1** and GC-terminated DNA. (c) Distribution of forces for the interaction between bisintercalator **1** and GC-terminated DNA at a retract velocity of 0.5 μm s^{-1}. (d) Distribution of forces for the interaction between bisintercalator **2** and GC-terminated DNA at a retract velocity of 0.5 μm s^{-1}.

Table 1 Comparison of most probable contour lengths and rupture forces for each intercalator (at a retract velocity of 0.5 μm s^{-1}). Frequencies were calculated as a function of the total number of observed events relative to the total number of collected force curves. Values in brackets are standard errors for the length and force columns, and total number of force–distance cycles in the number of observed events column

Terminal base pair	Ligand	Rupture length/nm	Rupture force/pN	Number of events with Kuhn length ≥0.6 nm	Number of observed eFJC events
GC	Bisacridine **1**	51.6 (2.0)	49.7 (3.2)	113	438 (10 000)
AT	Bisacridine **1**	44.4 (1.8)	52.3 (3.2)	257	551 (20 000)
GC	Bisacridine **2**	43.2 (2.6)	55.0 (3.7)	123	502 (20 000)
AT	Bisacridine **2**	46.0 (2.2)	57.3 (3.7)	135	427 (20 000)
GC	9-Amino acridine	—	—	1	45 (20 000)
GC	Ethidium bromide	—	—	8	16 (15 817)
GC	—	—	—	11	56 (20 000)
GC	Echinomycin	43.5 (3.5)	50.5 (1.7)	47	367 (25 127)
AT	Echinomycin	—	—	1	12 (20 000)
GC	TANDEM	—	—	1	8 (20 355)
AT	TANDEM	42.9 (4.0)	40.4 (2.4)	23	92 (20 000)

duplex DNA strands, in agreement with the AFM image analysis presented above.

Unexpectedly, we observed a smaller but significant number of crosslinking interactions between the two G/C-terminated surfaces when echinomycin was present in solution (Fig. 3). Echinomycin has a rigid structure linking the two chromophores, imposing a staple-like conformation on the molecule and strongly favouring Type 1 intercalation. Such a conformation does not allow crosslinking unless the intercalated sites are the terminal sequences of two different strands.

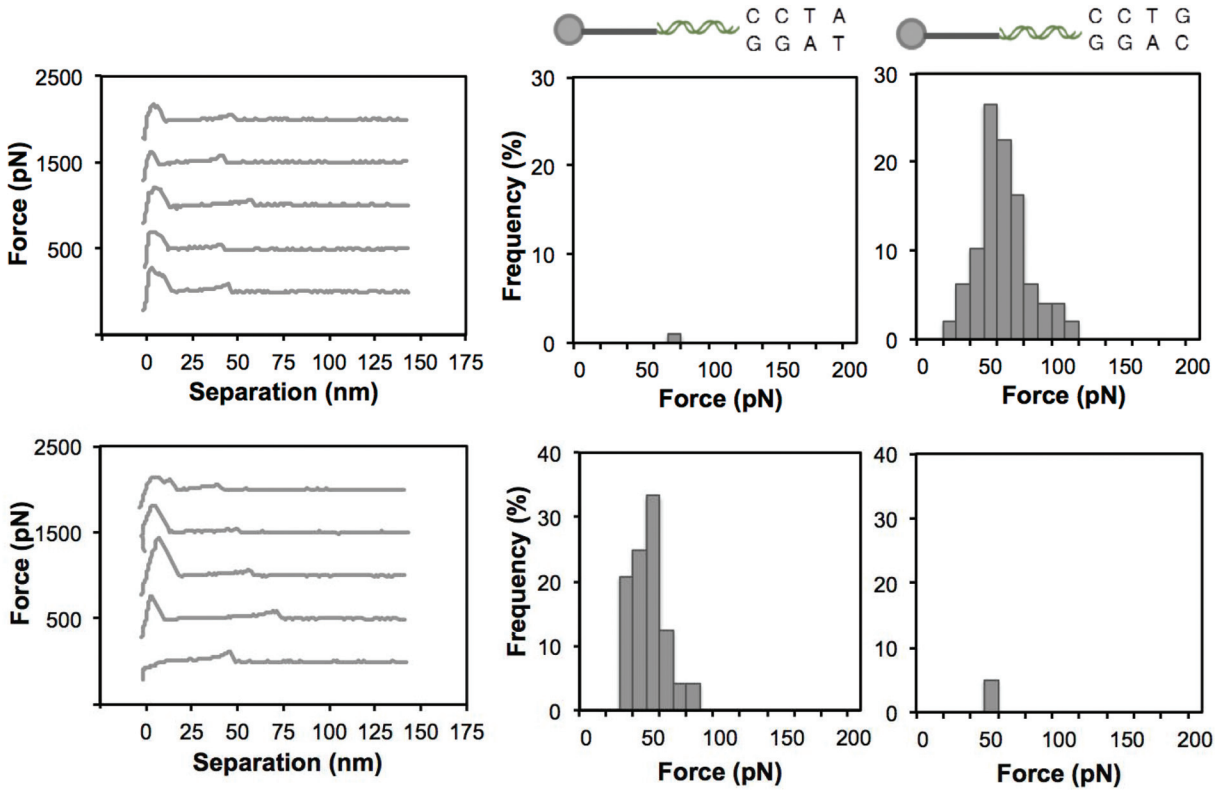

Fig. 3 Comparative force curves and histograms of rupture force for echinomycin (top) and TANDEM (bottom). The central column applies to binding activity with the AT terminated DNA, and the right hand column with the GC terminated DNA.

Echinomycin has a pronounced preference for a CpG binding sequence, and the DNA oligos used in this experiment would form a GC pair if their termini were brought together (5′-TG linking to 5′-CA, giving a TGCA sequence). We tested whether we were observing Type 1 intercalation crosslinking the two DNA strands by varying the terminal base pairing. With A/T termini, crosslinking by echinomycin was abolished (Fig. 3, Table 1). While the sequence formed by the two joined strands is not the most favoured binding site for echinomycin,[20] previous work found binding by echinomycin to this sequence.[28] This suggests that crosslinking is occurring *via* Type 1 intercalation between the two terminal base pairs. We also tested a synthetic analogue of Triostin A, TANDEM, with a similarly constrained rigid linker structure between its chromophores but a strong preference for binding to AT sequences. In this case we find crosslinking between AT-terminated strands (5′-TA linking to 5′-TA, giving a TATA sequence) and none between GC-terminated strands (Fig. 3, Table 1). Since the terminal bases are the only difference between the two sequences used, these results taken together suggest that echinomycin and TANDEM are indeed binding in a staple-like manner at the end of the sequence, crosslinking the blunt ends of the DNA duplexes. It is notable that we do not observe crosslinking by echinomycin in the AFM images (Fig. 1b), which in this case would be manifest as longer polymers where two or more sequences are joined at their terminal ends. We attribute this to two factors: the lower concentration of free ends in much longer polymers and their concomitant decrease in likelihood of meeting in dilute solution, and the lower rate of end-to-end crosslinking observed in the force spectroscopy data compared to the bisacridines (Table 1).

In order to understand something about the energetics of the crosslinking interactions, it is necessary to construct a dynamic force spectrum and apply a suitable model in order to extract the parameters k_{off} and x_β, the intrinsic unbinding rate of the bond and the distance to the transition state, respectively. Recently Friddle and Noy introduced a new model[29,30] that describes both the equilibrium (at low loading rates) and non-equilibrium (at high loading rates) regimes of the dynamic force spectrum. In cases where the equilibrium regime is reached in the force spectrum, a third parameter, the equilibrium force f_{eq} (the minimum force required to move the binding pair apart by the distance x_β, beyond which they can no longer instantaneously rebind) may be obtained and from it ΔG_u, the equilibrium free energy, for the bond. We describe our implementation of the Friddle–Noy model in ESI.† Before applying the model we follow Akhremitchev's method[31] of using the fitted Kuhn lengths to distinguish between single and multiple polymer stretches, selecting only single polymer stretches (those with Kuhn lengths greater than 0.6 nm) for further analysis. When we apply the Friddle–Noy model to the dynamic force spectrum for the crosslinking interaction

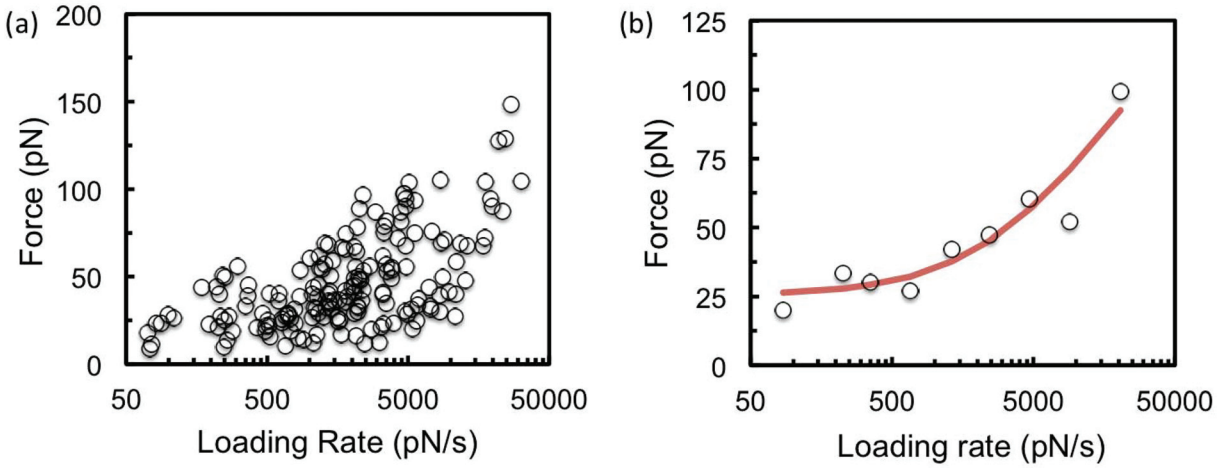

Fig. 4 (a) Scatter plot showing the distribution of rupture forces relative to critical loading rate (left). (b) Linear plot of the relationship between rupture force and critical loading rate, from which x_β, k_{off} and f_{eq} are determined.

Table 2 Table of values for x_β and k_{off} for the four bisintercalators used in this study

Ligand/terminal BP	x_β/nm (±SE)	k_{off}/s^{-1} (±SE)	f_{eq}/pN (±SE)
Bisacridine **1**/AT	0.137 (0.26)	9.52 (1.92)	—
Bisacridine **1**/GC	0.148 (0.22)	9.02 (1.1)	—
Bisacridine **2**/AT	0.130 (0.80)	22.45 (18.9)	25.5 (6.8)
Bisacridine **2**/GC	0.154 (0.12)	10.31 (0.96)	—
Echinomycin/GC	0.149 (0.10)	7.88 (0.65)	—
TANDEM/AT	0.137 (0.16)	7.32 (0.65)	—

between A/T-terminated DNA and bisacridine **2** for loading rates in the range 70–39 000 pN s^{-1} we get the results depicted in Fig. 4 and Table 2. The dynamic force spectrum shows a clear transition from non-equilibrium to equilibrium regime, giving rise to estimates for the values of x_β and k_{off} of 0.13 nm and 22.4 s^{-1} respectively, and a value of 25.5 pN for f_{eq}, leading to a equilibrium free energy, ΔG_u, value of 5.03 kJ mol^{-1}. This value is lower than the range of free energies of association reported for type I intercalation by echinomycin (32 kJ mol^{-1})[32] and other intercalators (16–44 kJ mol^{-1}),[33] likely reflecting the constraints imposed on the binding conformation by the bridging of the linker between two DNA strands. For the crosslinking interactions of bisacridine **1**, echinomycin and TANDEM, and for bisacridine **2** with the G/C-terminated DNA, the recorded rupture events did not reach far enough into the low loading rate regime for reliable values of f_{eq} and ΔG_u to be estimated. The values of x_β and k_{off} for each of these interactions are presented in Table 2. In all the bisintercalators studied, the values of x_β and k_{off} fall within the ranges 0.13 to 0.16 nm and 7.3 to 22.4 s^{-1} respectively, suggesting that the crosslinking interactions being explored for the two bisacridines, for echinomycin and for TANDEM are similar to each other, as well as to other high-affinity non-covalent interactions such as the digoxigenin–antidigoxigenin complex.[34] In particular, a value of x_β of around 1 Ångström typically signifies the measurement of a single bond, whereas values below 0.1 Å usually result from the measurement of multiple bonds breaking.[29]

There have been few previous single molecule force spectroscopy studies of the interaction between acridine intercalators and DNA. Liu *et al.*[25] investigated the dynamic force spectrum of the interaction between acridine tethered to an AFM probe and duplex DNA tethered to a substrate. The dynamic force spectrum presented by Liu *et al.* covers a similar range of loading rates to the work presented here. Using the Bell–Evans model[35] they found two distinct linear regimes in the force *vs.* ln(loading rate) plot, leading them to propose the existence of two energy barriers to the disassociation of the acridine–DNA bond. The second barrier, associated with higher forces and loading rates, is characterised by x_β and k_{off} values similar to those found in this study (0.28 nm and 21.7 s^{-1} respectively). The Bell–Evans model and the Friddle–Noy model suggest very different origins for the observation of different linear regimes in the dynamic force spectrum. In the Bell–Evans model, each distinct linear regime is attributed to a different energy barrier in the rupture of the bond. In the Friddle–Noy model, a single energy barrier is generally assumed and a maximum of two distinct linear regimes may be observed: an asymptotically flat regime at low loading rates tending towards the value of f_{eq}, the minimum equilibrium unbinding force, and a regime at higher loading rates that represents the single energy barrier in much the same way as the Bell–Evans model. Thus, while in the present work we use the Friddle–Noy method to find f_{eq} from the low loading rate regime, the Bell–Evans model requires the assertion of a second, long range (x_β = 1.18 nm), interaction to fit Liu *et al.*'s data. To the best of our knowledge there are no other reports of such a long range interaction in the unbinding of acridine intercalators from DNA. In the dynamic force spectra for the other bisintercalators studied, in which the low loading rate regime is under-represented, the data is best fit by a single energy barrier.

Experimental

Intercalating ligands

The acridine ligands and TANDEM were synthesised as previously described.[26,36,37] Echinomycin and 9-amino acridine (Sigma, UK) and ethidium bromide (Fisher Scientific, UK) were purchased and used as received. Solutions were prepared in pH 7 phosphate buffer (Fisher Scientific UK, Cat. no. B/4765/77), filtered using syringe filters with a 0.2 μm PTFE membrane and used immediately. Scheme 1 shows the structures of all intercalators used in this study.

AFM imaging

φX174 RF I plasmid DNA (1 mg mL^{-1}) was obtained from New England Biolabs (UK) and restricted using the enzyme BsaAI (NEB, UK). Fragments were separated *via* agarose gel electrophoresis. The band corresponding to a 1341 bp fragment was excised and then purified using a QIA Quick Kit (QIAGEN, UK) following the supplier's instructions. The final concentration of the DNA fragment in 10 mM Tris HCl (pH 8.5) was determined *via* NanoDrop instrument (ThermoScientific, UK), and the solution stored at −20 °C until used.

Experimental samples were prepared by the addition of 15 μL of an appropriate concentration of the ligand (10 μM echinomycin (in 0.1% DMSO) or bisacridine **1**, 20 μM ethidium bromide (in water), in order to maintain the same ratio of intercalator chromophores to DNA base pairs) to 10 μL of a solution of the 1341 bp fragment of φX174 DNA (concentration 0.34 ng μL^{-1}). This ratio corresponds to an intercalator to base pair ratio of approximately 25 : 1, within the range of ratios explored previously using this technique.[27] Controls were prepared using water in place of the ligand. Following an incubation period of 1 h, 25 μL of 10 mM $MgCl_2$ were added, giving a final system volume of 50 μL. The system was then transferred to freshly cleaved mica, mounted on a metallic AFM disc. After a period of 10 min to allow incubated DNA strands to adhere to the mica, the disc was rinsed using Nanopure™ water and dried under nitrogen.

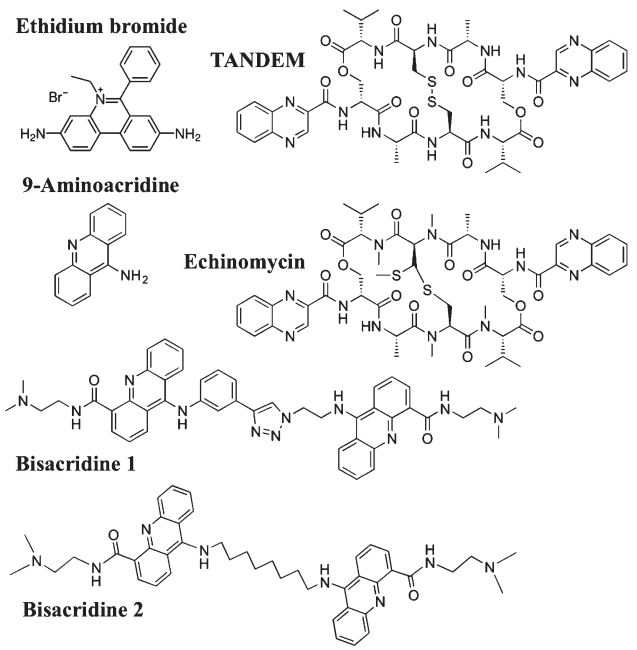

Scheme 1 Structures of the intercalators used in this study.

Imaging was conducted in tapping-mode in air using a CPII atomic force microscope (Veeco Instruments, USA), equipped with a small area scanner. Commercially available cantilevers were used, with images captured in height mode at a scan rate of 2 Hz in a 512 × 512 pixel format over areas of 2 × 2 μm. The set-point was increased until contact with the surface was lost and then gradually decreased until a surface trace was again visible. Collected images were processed and examined using commercially available image editing software and adjusted as required for brightness and contrast.

Single molecule force spectroscopy

Two pairs of 33 base pair oligonucleotides were purchased from Sigma (UK). The sequences of the oligonucleotides yielding the GC termination are (1) 5′-NH_2-CTACGTGGACCTGGAGAGAGGAAGGAGACTGCCTG-3′ (2) 5′-CAGGCAGTCTCCTTCCTCTCTCCAGGTCCACGTAG-3′ and those yielding the AT termination are (1) 5′-NH_2-CTACGTGGACCTGGAGAGAGGAAGGAGACTGCCTA-3′ (2) 5′-TAGGCAGTCTCCTTCCTCTCTCCAGGTCCACTGAG-3′. The oligonucleotides were annealed according to the protocol provided by the manufacturer and purified using a Qiagen (UK) nucleotide clean-up kit. A 15.4 nm, 3000 Da PEG (Iris Biotech, DE) was coupled to the oligonucleotide *via* a hydroxysuccinimide functionality and a thiol termination was added to the oligonucleotide and PEG conjugate by the addition of propanedithiol using a published protocol.[38] The final solution was diluted to a concentration of 60 ng μL^{-1} with pH 7 phosphate buffer (Fisher Scientific, UK) and stored at −20 °C until used.

Substrate gold deposition was performed using an Auto306 vacuum coater (Edwards) onto freshly cleaved mica. Deposition was stopped once the gold layer had reached a thickness of 50 nm. Coated mica was then glued to microscope slides using a thin layer of Araldite™ glue, and stored at room temperature until used. The gold surface was exposed for use by peeling with adhesive tape.

Gold-coated cantilevers (serial code BL-RC150VB, typical spring constant 0.027 N m^{-1}) were purchased from Asylum Research (UK) and used as received. Functionalisation was performed by depositing a 5 μL droplet of the PEG and DNA conjugate on an exposed gold surface, and by immersing a clean cantilever in a droplet of the same solution. The substrates and the cantilevers were placed in a humidity chamber at 6 °C for 24 h.[39] The reaction was terminated by rinsing with Nanopure™ water. Passivation of substrates and cantilevers was performed immediately using a 10 mM solution of 11-mercaptoundecanoic acid in a 50% solution of DMSO in water for 1 h. Passivation was terminated by rinsing with Nanopure™ water.

Force spectroscopy was conducted using a NanoWizard 3™ AFM fitted with a liquid cell (JPK, DE). Either pH 7 phosphate buffer (Fisher Scientific, UK) or the appropriate concentration of a ligand (100 nM for bisintercalators and 200 nM for monointercalators) in either water (acridines) or 0.1% DMSO (echinomycin, TANDEM) was introduced to the cell. Cantilevers, as described above, were calibrated using the thermal tune method. Experiments were conducted in contact mode, at a setpoint of 0.6 nN and a relative setpoint of 0.2 nN. The *z*-length for all experiments was 150 nm and the approach and retract speeds set at 0.5 microns per second and a resolution of 2048 Hz. For the dynamic force spectroscopy study, retraction speeds were varied from 0.05 to 4 microns per second, and the resolution adjusted as required. Force spectra were collected in arrays of 100 × 100 data points over areas of 10 × 10 microns. Force spectra were exported and analysed using JPK's data processing software (JPK instruments, DE, ver. 4.2.23). Observed events were fitted with an extended freely-jointed chain model and the compiled data was analysed using OriginPro™ (OriginLab, ver. 8.0724).

Conclusions

We have developed a highly sensitive probe for examining the crosslinking properties of bisintercalators. Besides crystallography, a method for unambiguously identifying crosslinking of duplex DNA by intercalators has been lacking, leading to the current situation where the interactions we report here have not been observed before. This situation is now changing,[40] opening a new avenue in exploration of the properties of bisintercalators. Echinomycin and TANDEM are known to bind to DNA in a staple-like conformation and to have sequence selectivity for a CpG and TpA respectively in the centre of the four base pair binding site. We have now demonstrated using single molecule force spectroscopy that these properties can be exploited to join DNA sequences in an end-to-end fashion. The differences in binding exhibited by the two compounds are entirely consistent with the changes in sequence at the ends of the two oligonucleotides. The binding mode for echinomycin and its analogue TANDEM differ from the acridine bisintercalators examined here in that, while the latter may form end-to-end crosslinks as well, they are also able to form duplex-to-duplex crosslinks of the type previously shown and described as type II bisintercalation (see Fig. 5), and this second binding mode is likely to be more common.

In the environment of the nucleosome, the close proximity of multiple strands of DNA is likely to facilitate the crosslinking of duplexes upon exposure to the acridine bisintercalators and this mechanism may represent a significant factor in the activity of these molecules. The novel end-to-end linking mechanism disclosed here for echinomycin and TANDEM, conversely, may have little opportunity to manifest itself *in nucleo* due to the relative paucity of free ends of DNA. However, the ability to assemble DNA strands in this end-to-end, sequence-specific fashion has implications for the use of rationally designed DNA sequences in nanoscale self-assembly. The application of small molecules that promote the formation of higher order structures in DNA (including intercalators[41]) may be combined with those that non-covalently ligate sequences in order to build structures that are accessible from the "bottom up" of small oligonucleotide sequences rather than the "top-down" approach using large plasmid structures. The discovery of further small molecules that specifically target DNA ends in a sequence specific fashion is a major goal for future research.

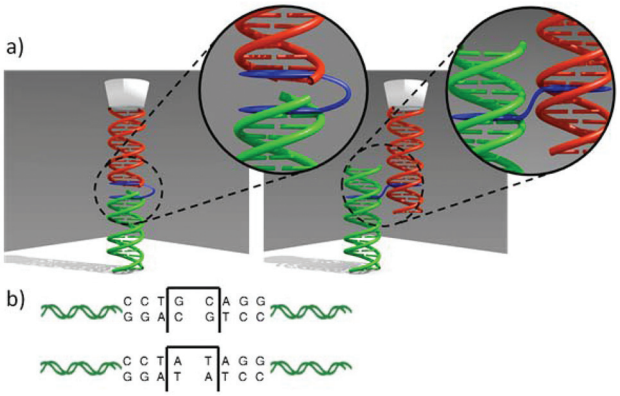

Fig. 5 (a) Schematic illustration of the proposed difference in binding modes between echinomycin and TANDEM (left) and the bisacridines (right). (b) Illustration of the binding arrangements of echinomycin (top) and TANDEM (bottom) at the termini of the DNA strands.

Acknowledgements

The authors would like to acknowledge the assistance of Dr Richard Steele in the production of Fig. 5, and BR would like to acknowledge the University of East Anglia for funding his studentship.

References

1 A. Guainazzi, A. J. Campbell, T. Angelov, C. Simmerling and O. D. Schärer, *Chemistry*, 2010, **16**, 12100.
2 J. L. Nitiss, *Nat. Rev. Cancer*, 2009, **9**, 338.
3 M. M. Van Dyke and P. B. Dervan, *Science*, 1984, **225**, 1122.
4 C. H. Huang, C. K. Mirabelli, S. Mong and S. T. Crooke, *Cancer Res.*, 1983, **43**, 2718.
5 K. R. Fox and C. Woolley, *Biochem. Pharmacol.*, 1990, **39**, 941.
6 S. T. Mullins, N. K. Annan, P. R. Cook and G. Lowe, *Biochemistry*, 1992, **31**, 842.
7 P. W. K. Rothemund, *Nature*, 2006, **440**, 297.
8 Y. Sannohe, M. Endo, Y. Katsuda, K. Hidaka and H. Sugiyama, *J. Am. Chem. Soc.*, 2010, **132**, 16311.
9 M. von Delius and D. A. Leigh, *Chem. Soc. Rev.*, 2011, **40**, 3656.

10 H. Song, J. T. Kaiser and J. K. Barton, *Nat. Chem.*, 2012, **4**, 615.
11 D. R. Horspool, R. J. Coope and R. A. Holt, *BMC Res. Notes*, 2010, **3**, 291.
12 D. R. Boer, J. M. C. A. Kerckhoffs, Y. Parajo, M. Pascu, I. Usón, P. Lincoln, M. J. Hannon and M. Coll, *Angew. Chem.*, 2010, **49**, 2336.
13 A. L. Brogden, N. H. Hopcroft, M. Searcey and C. J. Cardin, *Angew. Chem.*, 2007, **46**, 3850.
14 L. A. Howell, Z. A. E. Waller, R. Bowater, M. O'Connell and M. Searcey, *Chem. Commun.*, 2011, **47**, 8262.
15 N. H. Hopcroft, A. L. Brogden, M. Searcey and C. J. Cardin, *Nucleic Acids Res.*, 2006, **34**, 6663.
16 A. K. Todd, A. Adams, J. H. Thorpe, W. A. Denny, L. P. Wakelin and C. J. Cardin, *J. Med. Chem.*, 1999, **42**, 536.
17 A. Adams, J. M. Guss, C. A. Collyer, W. A. Denny and L. P. Wakelin, *Biochemistry*, 1999, **38**, 9221.
18 K. J. Addess and J. Feigon, *Nucleic Acids Res.*, 1994, **22**, 5484.
19 G. Ughetto, A. H. Wang, G. J. Quigley, G. A. van der Marel, J. H. van Boom and A. Rich, *Nucleic Acids Res.*, 1985, **13**, 2305.
20 A. J. Hampshire and K. R. Fox, *Anal. Biochem.*, 2008, **374**, 298.
21 C. M. Low, H. R. Drew and M. J. Waring, *Nucleic Acids Res.*, 1984, **12**, 4865.
22 N. K. Annan, P. R. Cook, S. T. Mullins and G. Lowe, *Nucleic Acids Res.*, 1992, **20**, 983.
23 K. R. Chaurasiya, T. Paramanathan, M. J. McCauley and M. C. Williams, *Phys. Life Rev.*, 2010, **7**, 299.
24 R. Eckel, R. Ros, A. Ros, S. Wilking, N. Sewald and D. Anselmetti, *Biophys. J.*, 2003, **85**, 1968.
25 C. Liu, Z. Jiang, Y. Zhang, Z. Wang, X. Zhang, F. Feng and S. Wang, *Langmuir*, 2007, **23**, 9140.
26 L. A. Howell, R. A. Bowater, M. A. O'Connell, A. P. Reszka, S. Neidle and M. Searcey, *ChemMedChem*, 2012, **7**, 792.
27 T. Berge, E. L. Haken, M. J. Waring and R. M. Henderson, *J. Struct. Biol.*, 2003, **142**, 241.
28 C. Bailly, D. Gentle, F. Hamy, M. Purcell and M. J. Waring, *Biochem. J.*, 1994, **300**, 165.
29 R. W. Friddle, A. Noy and J. J. De Yoreo, *Proc Natl. Acad. Sci. U. S. A.*, 2012, **109**, 13573.
30 A. Noy and R. W. Friddle, *Methods*, 2013, **60**, 142.
31 S. Guo, N. Li, N. Lad, S. Desai and B. B. Akhremitchev, *J. Phys. Chem. C*, 2010, **114**, 8755.
32 F. Leng, J. B. Chaires and M. J. Waring, *Nucleic Acids Res.*, 2003, **31**, 6191.
33 J. Mazerski, *Task Q.*, 2001, **5**, 301.
34 G. Neuert, C. Albrecht, E. Pamir and H. E. Gaub, *FEBS Lett.*, 2006, **580**, 505.
35 E. Evans, *Annu. Rev. Biophys. Biomol. Struct.*, 2001, **30**, 105.
36 L. P. G. Wakelin, X. Y. Bu, A. Eleftheriou, A. Parmar, C. Hayek and B. W. Stewart, *J. Med. Chem.*, 2003, **46**, 5970.
37 J. P. Malkinson, M. K. Anim, M. Zloh, M. Searcey, A. J. Hampshire and K. R. Fox, *J. Org. Chem.*, 2005, **70**, 7654.
38 G. T. Hermanson, *Bioconjugate Techniques*, Academic Press, 2nd edn, 2010.
39 W. Zhang, R. Barbagallo, C. Madden, C. J. Roberts, A. Woolford and S. Allen, *Nanotechnology*, 2005, **16**, 2325.
40 M. J. Marín, B. D. Rackham, A. N. Round, L. A. Howell, D. A. Russell and M. Searcey, *Chem. Commun.*, 2013, **49**, 9113.
41 A. A. Greschner, K. E. Bujold and H. F. Sleiman, *J. Am. Chem. Soc.*, 2013, **135**, 11283.

Appendix 2

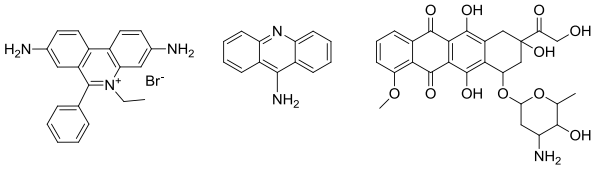

Figure 1 – Ethidium bromide, 9-amino acridine, doxorubicin

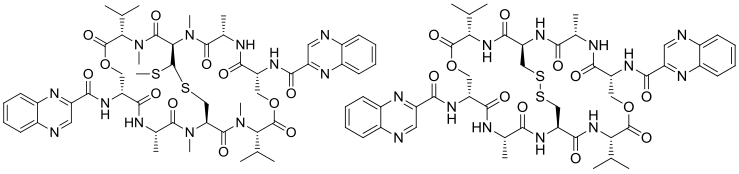

Figure 2 – Echinomycin, TANDEM

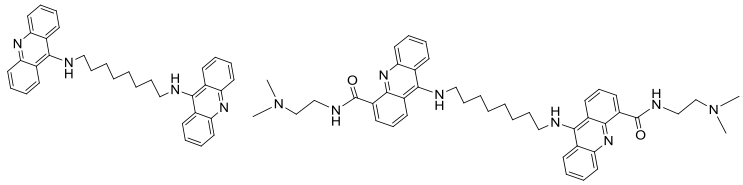

Figure 3 – Bisacridine 1, bisacridine 2

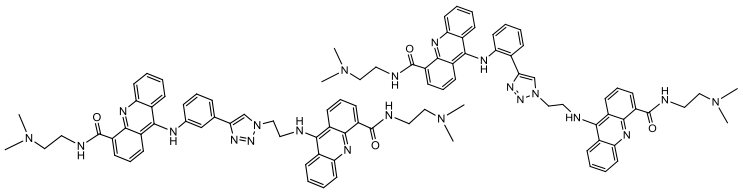

Figure 4 – Bisacridine 3, bisacridine 4